PROCEEDINGS
Of The
ELECTRON BEAM SYMPOSIUM
FIFTH ANNUAL MEETING
March 28-29, 1963
Boston, Massachusetts

EDITOR — J. R. MORLEY

alloyd electronics corporation
CAMBRIDGE 42, MASSACHUSETTS

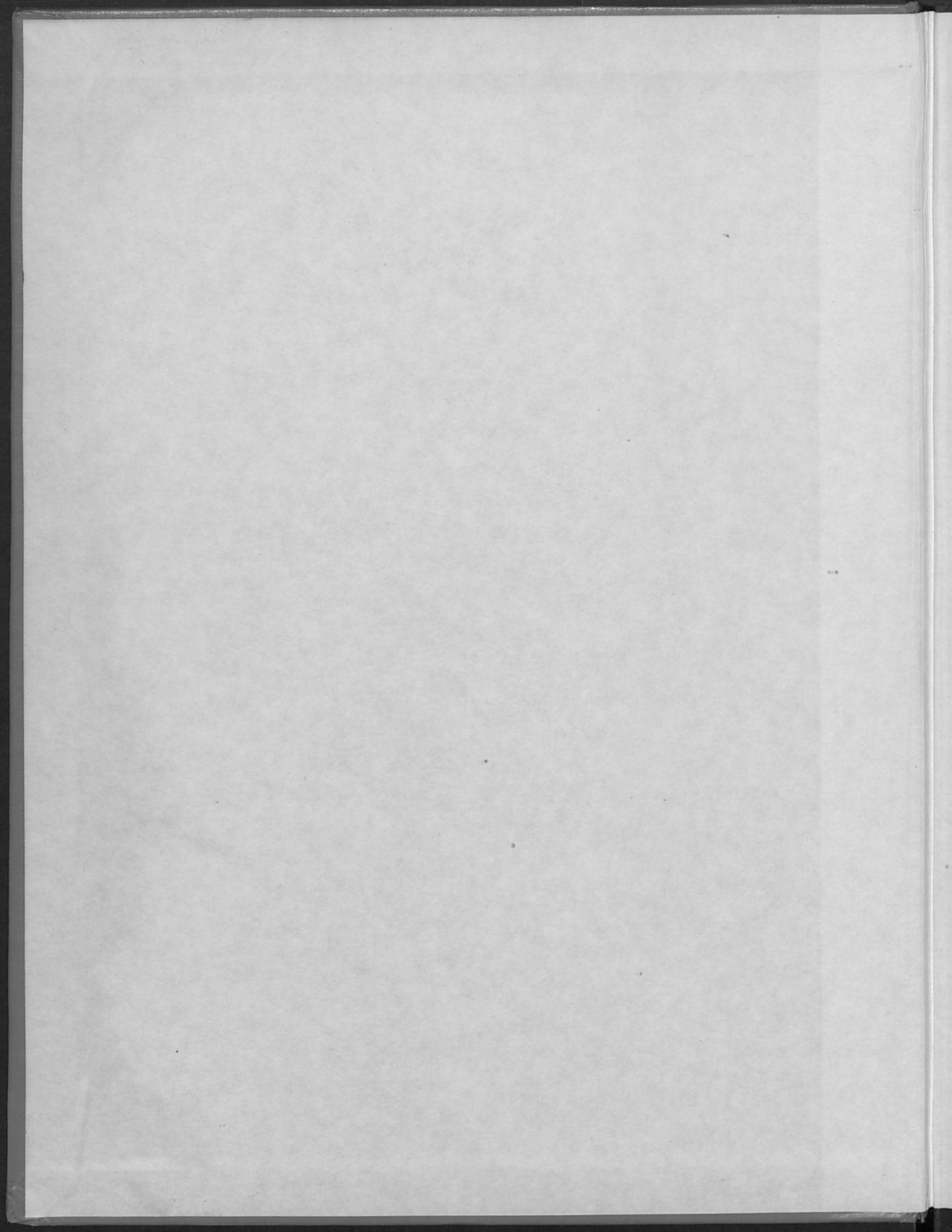

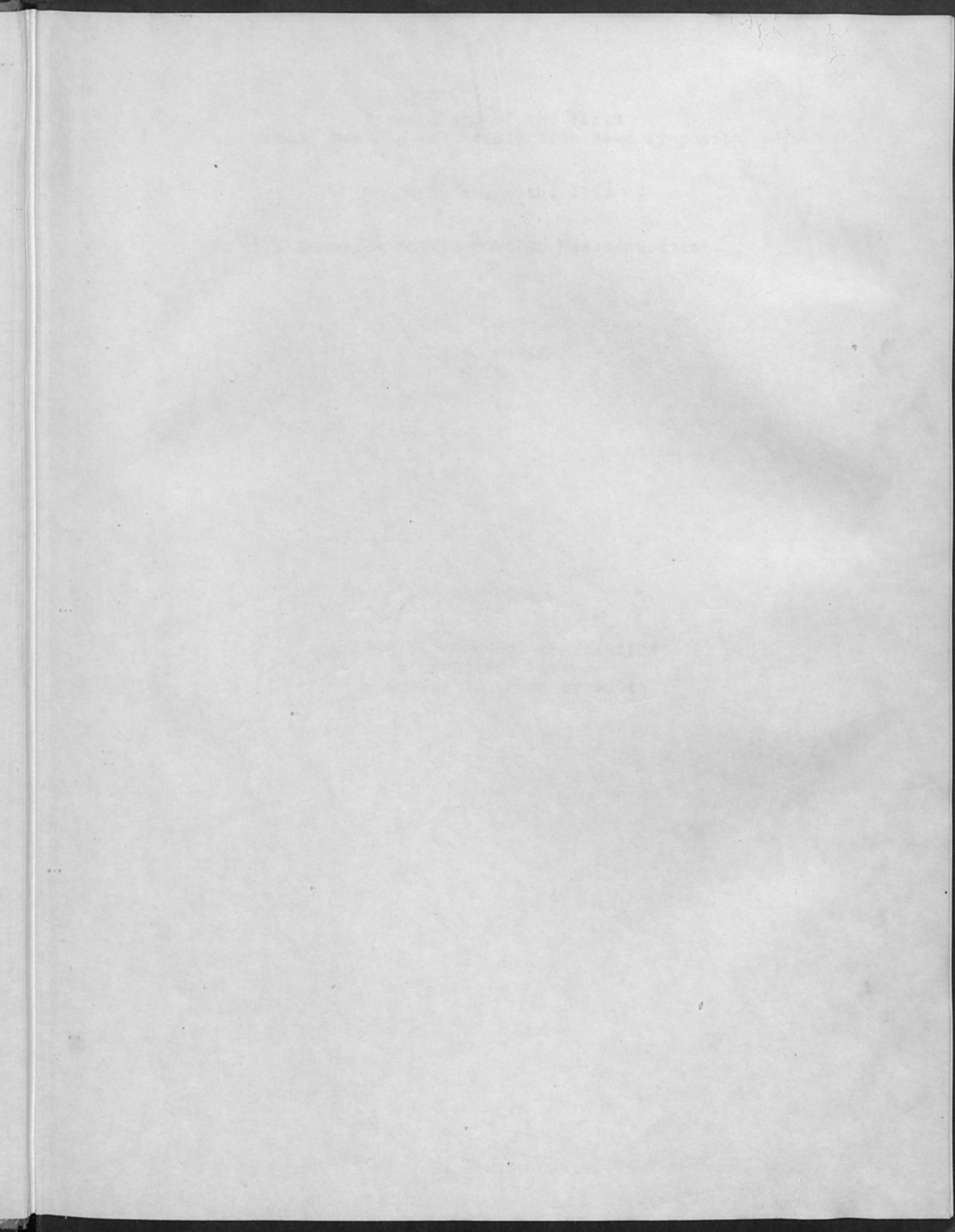

Proceedings of the Fifth Annual Meeting of the Electron Beam Symposium

March 28 and 29th, 1963

Somerset Hotel, Boston, Massachusetts

J.R. Morley
Editor

Sponsored
By

ALLOYD ELECTRONICS CORPORATION
35 Cambridge Parkway
Cambridge 42, Massachusetts

Copyright 1963 by The Alloyd Electronics Corporation
Published - April 1963

All rights of reproduction, including that of translation into another language are reserved by Alloyd Electronics Corporation. Abstracts of papers may be printed provided acknowledgement is made of the Electron Beam Symposium as the original source of the material. Prior written permission for reproduction of other parts of the text is required from Alloyd Electronics Corporation.

Copies of the Proceedings of the Electron Beam Symposium are available from Alloyd Electronics Corporation, 35 Cambridge Parkway, Cambridge 42, Massachusetts, USA. The year and price are as follows:

1959	-	$ 5.00
1960	-	$10.00
1961	-	$15.00
1962	-	$20.00
1963	-	$20.00

The complete set of five volumes is available for $65.00.

The Aims of the Electron Beam Symposia are:

1) To promote the establishment and renewal of personal contacts among engineers and scientists working in the field.
2) To promote the exchange of experiences and cooperation among scientific and engineering groups working independently both in this country and abroad.
3) To promote the application of electron beams to new and unique areas and thus affect technological progress.
4) To disseminate information pertinent to electron beam processes.

John R. Morley
Symposium Chairman

PROCEEDINGS OF THE FIFTH ANNUAL MEETING OF THE ELECTRON BEAM SYMPOSIUM

TABLE OF CONTENTS

Page

PREFACE... 1

ADDRESS TO SYMPOSIUM SPEAKERS
N. Wimmer. 3

DESIGN OF A HIGH VOLTAGE, HIGH POWER DENSITY ELECTRON BEAM
A.B. El-Kareh.. 7

THEORETICAL ASPECTS OF A HIGH RESOLUTION, LOW VOLTAGE, ELECTRON OPTICAL SYSTEM
J.W. Griffith, et al 62

ON THE SUPPRESSION OF GAS DISCHARGES BY AN ADDITIONAL ELECTRODE
M. Doctoroff... 73

THE TEMPERATURE DISTRIBUTIONS IN THIN FOIL AND SEMI-INFINITE TARGETS BOMBARDED BY AN ELECTRON BEAM
L.G. Pittaway.. 88

THEORETICAL TEMPERATURE RISE IN MATERIALS DUE TO ELECTRON BEAMS
G.E. Vibrans... 124

TEMPERATURE ANALYSIS OF ELECTRON BEAM MACHINING
N. Taniguchi & S. Maezawa 135

AN AUTOMATED MICROCIRCUIT ELECTRON BEAM PROCESSOR
A.H. Andrews... 149

THE "INTERCOL" ELECTRON BEAM SYSTEM USED FOR MICROCIRCUIT ETCHING
W.C. Nixon, R.V. Ely & C.R.E. Legg. 158

PRECISION ELECTRON BOMBARDMENT FURNACE FOR HIGH PURITY EVAPORATION OF SILICON
B.A. Unvala & C.W.B. Grigson.. 168

A COMPACT ELECTRON GUN FOR EVAPORATION
R.A. Denton & A.D. Greene 180

TABLE OF CONTENTS

Page

MASS FLOW DETERMINATION BY THE MULTIPLE CROSSED-BEAM TECHNIQUE
C.K. Crawford.. 198

FORMATION OF THIN POLYMER DIELECTRIC FILMS BY ULTRA-VIOLET IRRADIATION OF SURFACES IN CONTACT WITH MONOMER VAPOR
L.V. Gregor & H.L. McGee. 211

ELECTRON BEAM WELDING OF REFRACTORY MATERIALS FOR ION PROPULSION SYSTEMS
S. Robelotto... 218

MOLYBDENUM HONEYCOMB FOR AEROSPACE STRUCTURES
M.M. Schwartz.. 230

THE INFLUENCE OF GAS CONTENT ON CRACK PROPAGATION ENERGY
S.S. White 240

ELECTRON BEAM WELDING OF DISSIMILAR METALS
M.M. Schwartz.. 252

A CORRELATION OF WELDING VARIABLES
M.H. Hablanian. 262

A MAGNETICALLY FOCUSSED C.R.T. GUN FOR ADVANCED DEVICE FABRICATION
R.E. Peo.. 269

A PIERCE ELECTRON GUN OF HIGH POWER
Y.J. Langlet... 288

ULTRA HIGH VACUUM ELECTRON BOMBARDMENT FURNACE
A.W. Sweet 293

A BAKABLE U.H.V. ELECTRON MICROSCOPE FOR METALLURGICAL USE
J.W. Griffith, J.C. Mutton & W. Mason... 304

THE USE OF LASER BEAM FOR WELDING
R.H. Fairbanks. 315

GRID CONTROLLED PLASMA ELECTRON BEAM
M.A. Cocca & L.H. Stauffer 342

THE HOLLOW CATHODE DISCHARGE
J.R. Morley 368

ELECTRON BEAM WELDING AT ATMOSPHERIC PRESSURE
L.H. Leonard... 378

PREFACE

The technical content of papers given at the Fifth Annual Meeting of the Electron Beam Symposium follows the pattern established by previous meetings, by reporting on both theoretical aspects and experimental techniques associated with the development of electron beam technology. The generation of a particular type of focussed electron beam, and its use, are now taken for granted in the laboratory, and beams are also becoming more widely used as an industrial tool. It is therefore pertinent that at this meeting, attention is turned to the physics of the interaction of the beam with materials themselves, for this has long been in need of investigation and is little understood. Greater attention is also given to alternative methods of generating electron beams and to the potential utilization of other energy beams for fabrication purposes.

Any meeting concerned with the rapidly expanding technology of energy beams must be selective in its content. In a meeting of this nature, which has industrial sponsorship and which draws attendance from both laboratories and manufacturing organizations, it is our policy to provide a program concerned with three main topics. These are: the physics of electron beams; the application of electron beams to materials; and new energy beam equipment and processes.

The synopsis of a talk on "Professional Obsolescence" given by Dr. Neal Wimmer to Symposium Speakers is included in place of the usual Introductory Remarks, since sufficient interest was generated by his address to warrent its reproduction in these proceedings.

John R. Morley

John R. Morley
Symposium Chairman

Address to Symposium Speakers

PROFESSIONAL OBSOLESCENCE

BY: Dr. Neal Wimmer
Director, Science Education
Polaroid Corporation

It may seem a paradox that physical science, in its search for changeless truths, should create as its by-product constantly accelerating changes. But so it is. And since accelerating change means fast-acculating data, here we all are -- trying to keep pace with what is being accomplished all over the world in electron beam technology. So much is being done that we have to run a three-minute mile in order to stay in the same place - namely, in c ommand of our field. We are fighting a battle to keep up with all this fast-developing knowledge, a battle against our own professional obsolescence.

What is professional obsolescence? The problem was summarized in an article in "Chemical & Engineering News" of August 1962 in which engineering educators projected that unless the graduates of ten years ago spend ten percent of their time developing their knowledge beyond their graduation level, they cannot compete with new graduates. But this assumes that they have retained and use most of their previous training. If loss of unused knowledge is ten percent in addition, then they must grow academically at the rate of 20 percent a year, to remain of equivalent value to their employers, let alone to themselves.

In the past, industry could depend on scientific meetings of this kind to bring scientists up-to-date. But are such meetings effective? Because of the massive quantities of technical data available, some parts of them must be irrelevant to each individual's interest; other parts may demand considerable time to review the data in order to bring to light all possible applications. So that the success of scientific meetings depends on the quality of work submitted; on the selection of appropriate and well-presented materials; and on the energy with which members of the audience relate it to their own situation. Even so, such meetings are today insufficient to counteract professional obsolescence. Scientists and engineers must pursue additional more personal study, if they are to avoid becoming the victims of creeping obsolescence. And as a consequence, industry itself is gradually becoming aware that it must support within its means, flexible educational up-dating programs designed to meet the needs of professional personnel. This material must be immediate, relevant and practical. It can no longer be the classic theory of the classroom alone.

Furthermore,it must be integrated. For today we no longer teach physics in one classroom, math in another and chemistry in a third, with the doors locked firmly between, and the engineering in a totally separate establishment. The separation between the pure and applied disciplines is all but gone.

Just who in industry are we concerned about? There are three main groups involved:

- First the executives who must keep in touch with broad developments in order to direct their organizations successfully.

- Second, the scientists and engineers who must maintain a good knowledge of new theory and its applications in their own fields, both for their personal need, and in order to supervise todays young graduates,

- Third, scientists who have a limited knowledge of engineering, and engineers with a limited knowledge of science, who must work most closely together than ever before.

When scientific personnel are on the verge of obsolescence, they risk the loss of the drive and vision vital to a place at the forefront of technology, as well as the leadership and spark for which they were originally hired. Professional obsolescence can deliver a knock-out blow to the older worker who is unable to follow new theory. This is most costly in the case of long-service employees for whom an organization may feel some degree of employment responsibility. Industry cannot afford the waste involved when older scientists and engineers reach a stalemate in their careers long before retirement age. Industry must look to itself when this happens, and begin to undertake some of the responsibility for remedying the situation itself.

Accordingly, I would like to predict that the growth of tailored education programs within industry, designed specifically to combat professional obsolescence will be one of the great changes we will witness in the development of industrial education. And the first change will take place with the realization that scientists and engineers must get out of their cliques. Instead of hoarding knowledge for selfish reasons, they must share what knowledge they have and be constantly reviewing and enlarging it. One way of doing this is by ensuring that the right people attend meetings such as the one which begins tomorrow--not symposium "rats", who travel round from meeting to meeting for the benefit of their own reputation--but people who will both contribute the ideas and achievements of their whole work group, and will take back and present to that group the new ideas they collect, sharing new concepts with their colleaques and subordinates in a way that in turn prevents their professional obsolescence.

It is up to each individual to assist both himself and his employer by being aware of the continuing need for education; and by being willing to work with his own group and with professional educators, in order to develop programs and courses. Only by accepting the educator as a member of the industrial team, along with the scientist and engineer, and by bringing an open mind to the problem of communicating information and knowledge, can we effectively combat professional obsolescence.

DESIGN OF A HIGH VOLTAGE, HIGH POWER DENSITY ELECTRON BEAM

by

A. B. El-Kareh

Mem. Tech. Staff

RCA Laboratories

Princeton, N. J.

SUMMARY

The theoretical and experimental design of an electron-beam machine is discussed in detail. An analysis is given of all the limitations inherent in an electron optical system of an electron-beam machine, and it is shown that the spot size is largely limited by the spherical aberration of the last focusing lens and by the thermal limitation long before space charge plays any important role. It is shown theoretically that at 100 kv, a probe current of 5 milliampers can be focused to a .001 inch spot size. After reviewing all possible cathode and gun structures, a thermionic tungsten hairpin-filament emitter and a standard electron gun using a Wehnelt cylinder were chosen. An RCA EMU-3A electron microscope was converted according to the design specifications and a beam of 1 milliampere was focused to .001 inch diameter. A multivibrator circuit was used to pulse the beam from a few microseconds to several milliseconds.

INTRODUCTION

High density electron beams have been used for drilling, welding and milling various materials. The advantages of the electron-beam machine as compared to other heat sources are clearly shown in Table I.

The factors that determine the design of an electron-beam machine obviously depend to a large degree upon the nature of the job to be done. Among the factors to be considered are the ultimate spot size, the size of the workpiece, the volume of the vacuum chamber, the gas evolution expected, the level of energy concentration required, and the distance from the gun to the workpiece. After all these factors have been established, it is possible to select a suitable electron optical system, cathode, gun assembly, accelerating voltage and other elements and parameters.

GENERAL CONSIDERATIONS

It was decided to design a machine with a high power concentration. The quality and versatility of a machine are appreciably improved as the spot size is decreased and the power concentration increased. For the applications we had in mind, a spot size of 0.001 inch (25 microns) and a power concentration of 100 megawatts/cm^2 was desirable. For a 100-kv accelerating voltage, this represents a current of 5 milliamperes at the probe.

This objective presented a formidable task. As a first guess it might seem desirable to increase the energy by increasing the accelerating voltage; however, there is a practical limit to the voltage which may be used. Besides the increase in cost and the necessity of

x-ray shielding, insulation of the intricate parts becomes very complicated as the voltage is raised beyond a certain point. The task was therefore to design an electron optical assembly which could realize the indicated objective at a prescribed accelerating voltage.

It was necessary to investigate the limitations inherent to the electron optical system before a detailed theoretical and experimental study of the design and performance of the electron machine could be undertaken.

In general, there are four limitations that must be considered in this case. In the first place, there is no such thing as a perfect lens, i.e., a lens which will focus the electrons emitted from a point source into a point image. Second, the electrons forming the beam tend to repel one another, a phenomenon generally known as space-charge repulsion. Third, the electrons emerging from the emitter have a Maxwellian velocity distribution. Finally, diffraction effects will tend to set a lower limit to the beam diameter. An analysis is given here to see whether any of the above are instrumental in setting an upper limit to the current density and lower limit to the spot size for a given electron optical system, beyond the values that have already been selected.

DIFFRACTION LIMITATION

Let us consider a system where r_α is the focused spot radius and θ the half-angle of convergence of the beam. Then the radius of the first minimum of the diffraction image is given by

$$r_\alpha \cong \frac{0.6\,\lambda}{\theta} \qquad (1)$$

λ is the electron wavelength

$$\lambda = \frac{12.3}{V^{1/2}} \tag{2}$$

where λ is in Å and V in volts. From Equations (1) and (2),

$$r_\alpha \cong \frac{7.4\text{Å}}{\theta\, V^{1/2}} \tag{3}$$

For $V = 10^5$ volts, $\theta = 5 \times 10^{-3}$, $r_\alpha = 10^{-7}$ mm. It is obvious that in the system we have in mind the diffraction limitation is of no concern.

SPACE-CHARGE LIMITATION

The question of space-charge and thermal limitations has been investigated by many workers. However, each limitation has been investigated separately, and the physical assumptions on which they are separately based are very different. Attempts have been made by Cutler and Hines[1] and Danielson et al.[2] to analyze exactly the situation when both space-charge and thermal limitations are taken into account simultaneously. Their results are very intricate, being arrived at after a series of complex derivations. Fortunately, it is not imperative to study both limitations at the same time, because the transition region between the dominance of either effect is quite abrupt. Electron beams, over a rather wide range, are either almost totally space-charge limited or thermally limited. There is, indeed, a narrow region where both limitations are present, but this need not be taken into account in this analysis.

Schwartz[3] arrived at one of the most elegant solutions to the space-charge problem. By means of an ingenious normalization procedure he plotted a universal curve which can be used to obtain the space-charge-limited spot size quite readily as a function of other beam parameters and for a wide range of operating conditions. Following the excellent work of Thompson and Headrick[4], Schwartz started out by considering the charge per unit length of the beam, which is given by

$$\frac{I}{V_z} \qquad (4)$$

where I is the beam current and V_z the axial velocity. He used Gauss' Law to express the electric field just outside a long cylinder of charge as

$$F = \frac{I}{\pi \epsilon d (2\eta V_o)^{1/2}} \qquad (5)$$

where V_o is the accelerating potential,

η is the electronic charge to mass ratio: $e/m = 1.76 \times 10^{11}$ coulomb/kg,

ϵ is the permittivity of vacuum: 8.85×10^{-12} farad/meter,

d is the beam diameter.

After some manipulations Schwartz obtained

$$\left(\frac{\eta I}{\pi \epsilon (2\eta V)^{1/2}} \right)^{1/2} \frac{Z}{(2\eta V)^{1/2}} \quad \frac{2}{D_i} = \frac{f(\beta)}{\beta} \qquad (6)$$

where Z is the gun-to-screen axial distance and D_i is the initial beam diameter. $f(\beta)$ and β are defined by the transcendental equation

$$f(\beta) = 2\beta e^{-\beta^2} \left[u(\beta) + u\left(\beta^2 - \ln \frac{D_i}{d}\right)^{1/2} \right]$$

$$= 1 + \frac{d\beta}{D_i} \left[\left(\beta^2 - \ln \frac{D_i}{d}\right)^{1/2} \right]^{-1} \qquad (7)$$

where r is the instantaneous radius of an electron on the edge of the beam at its narrowest constriction, and β is so chosen as to make Equation (7) valid, and

$$u(x) = \int_0^x e^{t^2} dt \qquad (8)$$

Equation (6) simplifies to

$$I = 8.24 \times 10^{-6} \left(\frac{D_i}{z}\right)^2 \left(\frac{f(\beta)}{\beta}\right)^2 V^{3/2} \qquad (9)$$

Schwartz made the same assumptions as Thompson and Headrick, namely,

(1) the electron current density in the aperture is uniform,

(2) all the electrons have the same axial velocity,

(3) the radial velocity of the electrons, directed inwards, is proportional to their distance from the axis,

(4) the electrons move in a region which is field-free except for the field caused by the change density of the beam.

It is clear that the above assumptions do not always hold in every electron optical system, but the errors involved are not serious in our system.

Now let

$$\beta = \left(\ln \frac{Di}{d} + \delta^2\right)^{1/2} \tag{10}$$

Substituting this into Equation (7),

$$2\beta e^{-\beta^2} u(\beta) + 2\beta e^{-\beta^2} u(\delta) = 1 + \frac{d\beta}{D_i\delta} \tag{11}$$

$$u(\beta) = \int_0^1 e^{x^2}dx + \int_1^\beta e^{x^2}dx \tag{12}$$

or

$$u(\beta) = 1 + \frac{1}{3} + \frac{1}{5.2!} + --- + \frac{1}{2}\left(\frac{e^{\beta^2}}{\beta} - e\right) + \frac{1}{4}\left(\frac{e^{\beta^2}}{\beta^3} - e\right)$$

$$+ \frac{3}{4}\left(\frac{e^{\beta^2}}{\beta^5} - e\right) + \frac{15}{8}\left(\frac{e^{\beta^2}}{\beta^7} - e\right) + \frac{105}{8}\int_1^\beta \frac{e^{x^2}}{x^8}\,dx \tag{13}$$

This is found by repeated integration by parts. If we consider D_i/d as very large, $\delta = \left\{\beta^2 - \ln D_i/d\right\}^{1/2}$ is small and β is large. The value of the first series is 1.463, which is small compared to the second part of the expression as β is large. The residual integral in the second expression decreases with continued integration by parts, but begins to increase again when $\beta^2 \gtrsim n + 1/2$. Thus, the

error is least if the series is broken off near this point. For very large β, it is advisable to break off the series slightly sooner to make the neglected series

$$-e \left(\frac{1}{2} + --- + \frac{2n-1}{2n}\right)$$

small. Thus we obtain the semiconvergent expression

$$u(\beta) = \frac{1}{2}\frac{e^{\beta^2}}{\beta}\left(1 + \frac{1}{2\beta^2} + \frac{3}{4\beta^4} + \frac{15}{8\beta^6} + ---\right) \qquad (14)$$

Therefore, Equation (11) can be written

$$\frac{1}{2\beta^2} + \frac{1.3}{(2\beta^2)^2} + --- + \frac{2\beta}{e^{\beta^2}}(\delta)\left(1 + \frac{\delta^2}{3.1!} + ---\right)$$

$$= \frac{d}{\delta D_i}\left(\ln\frac{D_i}{d} + \delta^2\right)^{1/2} \qquad (15)$$

or

$$\frac{1}{2\ln\frac{D_i}{d}}\left[1 - \frac{\delta^2}{\ln\frac{D_i}{d}} + ---\right] + \frac{1.3}{4(\ln\frac{D_i}{d})^2}\left[1 - \frac{2\delta^2}{\ln\frac{D_i}{d}} + ---\right] + ---$$

$$+ \frac{\frac{2d}{D_i}\left(\ln\frac{D_i}{d}\right)^{1/2}}{1+\delta^2+\frac{\delta^4}{2!}}\left[\delta + \frac{\delta^3}{3.1!} + ---\right]$$

$$= \frac{d}{\delta D_i}\left(\ln\frac{D_i}{d}\right)^{1/2}\left[1 + \frac{1}{2}\frac{\delta^2}{\ln\frac{D_i}{d}} - \frac{1}{8}\frac{\delta^4}{(\ln\frac{D_i}{d})^2} + ---\right] \qquad (16)$$

We multiply throughout with δ and solve for δ,

$$\delta \left[\frac{1}{2 \ln \frac{Di}{d}} + \frac{1.3}{(2 \ln \frac{Di}{d})^2} + --- + \frac{2d}{D_i}(\ln \frac{Di}{d})^{1/2} \delta - \right.$$

$$\left. \frac{\delta^2}{2(\ln \frac{Di}{d})^2} - \frac{3}{2} \frac{\delta^2}{(\ln \frac{Di}{d})^3} + --- \right]$$

$$= \frac{d}{Di} (\ln \frac{Di}{d})^{1/2} \left[1 + \frac{1}{2} \frac{\delta^2}{\ln \frac{Di}{d}} + --- \right] \quad (17)$$

$$\delta = \frac{\frac{d}{D_i} (\ln \frac{D_i}{d})^{1/2}}{\frac{1}{2 \ln \frac{Di}{d}} + \frac{1.3}{(2 \ln \frac{Di}{d})^2} + ---} \quad (18)$$

with a relative error of the order

$$\delta^2 \cong 4 \left(\frac{d}{Di}\right)^2 \left(\ln \frac{Di}{d}\right)^3$$

Therefore

$$\frac{f(\beta)}{\beta} = \frac{1}{\beta} + \frac{d}{D_i \delta} = \frac{1}{(\ln \frac{D_i}{d})^{1/2}} \quad 1 - \frac{\delta^2}{2 \ln \frac{D_i}{d}} + \cdots$$

$$+ \frac{1}{2 \ln \frac{D_i}{d}} + \frac{1.3}{(2 \ln \frac{D_i}{d})^2} + \cdots$$

$$= \frac{1}{(\ln \frac{D_i}{d})^{1/2}} \left[1 + \frac{1}{2 \ln \frac{D_i}{d}} + \frac{1.3}{(2 \ln \frac{D_i}{d})^2} + \cdots \right] \qquad (19)$$

We thus obtain, for $V = 10^5$ volts,

$$I = \frac{260}{\ln \frac{D_i}{d}} \left(\frac{D_i}{z}\right)^2 \left[1 + \frac{1}{2 \ln \frac{D_i}{d}} + \frac{3}{(2 \ln \frac{D_i}{d})^2} \right.$$

$$\left. + \frac{15}{(2 \ln \frac{D_i}{d})^3} + \frac{105}{(2 \ln \frac{D_i}{d})^4} + \cdots \right] \qquad (20)$$

where I is in amperes.

The upper value of the space-charge-limited probe current has been computed with the use of this expression for d = 0.001 inch for two different working distances Z (1 inch and 4 inches) as a function of the initial beam diameter D_i. These values of Z correspond to the desirable working distances in the machine. The results are plotted in Figure 1.

Similar curves can be obtained for the gun we have chosen by reading directly from Schwartz's curve, reproduced and enlarged in

Figure 2. It can be seen that for values of $d/D_i > 0.04$ the curve is double valued. Here the space-charge effects are appreciable, and a plane of minimum sectional area exists between the screen and the lens where the minimum focused spot condition is achieved. However, our values fall well below 0.04.

Hollway[5] gives a somewhat equivalent treatment, and has since[6] published a design chart for calculating electron-beam parameters. Using the chart, it is possible to determine not only the space-charge-limited spot size for given gun data, but also thermal velocity spreading limitations. Reference to Hollway's charts will show that his results correspond very closely to those derived by Schwartz[7]. The chart shows that for the system being designed, there is no space charge limitation.

The whole derivation was made on the assumption that the beam travels in absolute vacuum. It has been shown[7] that under certain conditions, ions formed from the residual gas may be trapped in the beam, thus neutralizing some of the space-charge forces.

THERMAL LIMITATIONS

We use the well-known formula derived by Langmuir for the maximum current density achievable in an electron spot as limited by the thermal velocity distribution of the emitted electrons:

$$j_o = j_c \left(\frac{eV}{kT} + 1\right) \sin^2 \alpha \qquad (21)$$

Here the assumption is made that the electrons originate from a unipotential cathode having a Maxwellian velocity distribution corresponding to a uniform temperature T. j_c is the emission density, which is considered to be uniform. The converged electrons are in a field-free region and of uniform velocity V. α is the half angle of arrival at the plane where j_o is being defined. For small values of α, Equation (21) can be written

$$I = \frac{\pi d_o^2}{4} \alpha^2 \, 11600 \, \frac{V}{T} j_c \text{ amperes} \tag{22}$$

T is the temperature of the cathode in ^oK and j_c the emission per unit area (amperes/cm^2). Since the system is demountable and the filament or cathode can be replaced, we may assume for a tungsten cathode, $T = 3{,}000^oK$. With $V = 10^5$ volts we then have

$$I = 3.00 \, \alpha^2 \, d_o^2 \, 10^5 \, j_c \text{ amperes} \tag{23}$$

The permissible angle, α, is limited by the spherical aberration of the last lens. There is no point in computing Equation (23) for values of α for which the spherical aberration is already the limiting factor. It is therefore appropriate to consider together the limitations imposed by the temperature spread of the initial velocities and by spherical aberration.

The value of α is determined by

$$d = d_o + \frac{Cf\alpha^3}{2} \qquad (24)$$

where d_o is the beam diameter in the absence of spherical aberration, C is the spherical aberration constant and f is the focal length. This gives the beam diameter of a pencil with aperture angle α in the plane of narrowest constriction.

Combining Equation (24) with (23),

$$I = 3 \times 10^5 \; \alpha^2 \left(d - \frac{Cf\alpha^3}{2}\right) j_c \text{ amperes} \qquad (25)$$

We shall now choose α to maximize I; by setting $dI/d\alpha = 0$, we get

$$2\,\alpha \left(d - \frac{Cf\alpha^3}{2}\right) - 3\,\alpha^4\, Cf \left(d - \frac{Cf\alpha^3}{2}\right) = 0 \qquad (26)$$

or

$$\alpha^3 = \frac{d}{2Cf} \qquad (27)$$

We then have

$$\frac{1}{j_c} = 3 \times 10^5 \left(\frac{d}{2Cf}\right)^{2/3} \left(\frac{3d}{4}\right)^2 = 1.06 \times 10^5 \frac{d^{8/3}}{Cf^{2/3}} \qquad (28)$$

The smallest value of Cf which has been obtained for any symmetric electron lens is of the order of 0.1 cm. Therefore, for a beam diameter of 25μ, this represents a current I in ma, with j_c assumed to be 5 amps/cm^2

$$I = 5 \times 1.06 \times 10^{5} \times 10^{-8} \times 11.85 \times 10^{2/3} = 0.291 \text{ amperes} \quad (29)$$

This enormous current, attractive as it may seem, is of purely academic interest, since the value of Cf used represents a lens of almost no working distance.

In computing the Cf of a lens, it is necessary to know the lens configuration and the working distance. Some approximate values are selected initially for the purpose of the analysis; exact values are computed later, after the geometry of the system has been outlined.

Using the curves of Liebmann and Grad[8] and those given by Zworykin et. al.,[9] it is possible to derive the value of Cf for various lens configurations. Figure 3 shows the assumed lens cross section. Using the same notation as that of Liebmann and Grad, we have set the pole piece separation, α_p, equal to the bore diameter, D. For the range of working distances and lens diameters to be considered, the principal planes of this lens can be regarded as coinciding with its geometrical plane of symmetry, and thus the working distance is

$$z = f - D \quad (30)$$

Table II gives the results obtained with the chosen lens for various values of D and Z.

In making a comparison between the space-charge and thermal limitations, it should be noted that the beam does not fill the whole diameter of the lens. The diameter of the beam, D_i, and the lens diameter, D, are related by the following equation:

$$D_i = 2\ (z + D)_a = 2\ (z + D)\ \left(\frac{d}{2Cf}\right)^{1/3} \tag{31}$$

Table III gives a comparison for the values obtained with the two limitations taken one at a time. As stated previously, the spherical aberration of the focusing lens is already implied in the thermal limitation. It seems obvious that the minimum spot size will be limited by the spherical aberration of the last lens and the thermal limitation of the system long before space charge plays any important role.

CHOICE OF CATHODE

An ideal cathode is one which will require a minimum of attention for the maximum length of time. A cathode must be more or less self-supporting, it must not be poisoned by the gasses released from the metal or by the metal vapor itself and, above all, it must have enough electron emission to satisfy the electron optical requirement of the system. Generally, highest electron emissions are the most desirable.

If the criterion in the choice of a cathode for an electron beam machine is the emission of the largest possible number of electrons, a field emitter should theoretically surpass all other cathodes because of the almost inexhaustible reservoir of electrons inside a metal; current densities of millions of amperes per cm^2 should be obtainable.

It is therefore worthwhile to investigate this emitter to see whether it could be applied for our purpose.

Dolan and Dyke[10] recognize three kinds of field emission: (1) Temperature emission at high temperatures and low fields, as described by Richardson and Schotky; (2) the field emission at low temperatures and high fields investigated by Nordheim; and (3) the temperature-field or T-F emission at temperatures and fields intermediate between the two extremes, studied by Dolan and Dyke.

Schottky's[11] equation in its simple form is as follows:

$$j = j_o \exp \left[\frac{e}{k} \left(\frac{e}{4\pi\varepsilon_o}\right)^{1/2} \cdot \frac{F^{1/2}}{T} \right] \tag{32}$$

where j_o is the thermionic emission at zero field, e is the electron charge, k is Boltzmann's constant, ε_o is the permittivity of free space, and T is the temperature in ^oK. This can be written in its logarithmic form as

$$\log_{10} \left(\frac{j}{j_o}\right) = 0.1912 \frac{F^{1/2}}{T} \tag{33}$$

Taking tungsten as an example, the work function $\phi = 4.5$ ev, Table IV, gives values of j_o for various temperatures. Thus, at 2600^oK and a field of say 10^6 volts per cm, we have

$$\log_{10} \left(\frac{j}{0.70}\right) = 0.1912 \times \frac{10^3}{2600} \tag{34}$$

the emission is increased by a factor of less than 1.2. Schottky's relation holds as long as the field $F > 8.83 \times 10^3 \phi^{1/2} T$, where ϕ is the work function of the material. For tungsten, $F > 1.87 \times 10^4 T$. At higher fields the expression for the emission can be written[12]

$$\frac{j}{j_o} \approx 1 + \frac{\left(2.8 \times 10^4 \frac{\phi^{1/2} T}{F}\right)^2}{6} \tag{35}$$

Here j_o is now the field emission current at low temperatures. This should be accurate enough because low temperatures are considered here. Again, if tungsten is considered, we have

$$\frac{j}{j_o} = 1 + 6 \times 10^8 \frac{T^2}{F^2} \tag{36}$$

Table V gives the values of j_o as a function of F which are applicable in this relation.

When both the temperature and the field are high, the emission process is strongly dependent on both variables, and Dolan and Dyke[10] have shown that the enhancement of electron emission due to added thermal energy is much larger at low fields than at high fields, which is to be expected. An increase of current density by a factor of 5 over the value expected for the low-temperature emitter could be obtained. From the above analysis and examples, it can easily be seen that for large current densities, Schottky effect is not the answer. One has to depend on either true field emission or the T-F emission.

If we consider a pointed cathode of hyperbolical shape and of radius of curvature r_o, and an anode separated from it by a distance ,

the field can be expressed[13]

$$F = \frac{2V}{r_o \ln \frac{4R}{r_o}} \tag{37}$$

where V is in volts. Thus, if R = 1 cm and r_o = 4 microns, a field of about 5×10^7 volts per cm is obtained for V = 100 kv. The electrons are accelerated normally to the surface. Since, in order not to exceed the limit imposed by the spherical aberration of the focusing lens, the beam has to be restricted to 0.1 radian, the effective emission area is 1 micron. Strictly speaking, there is some convergence of the particles, but this is minor and will be neglected in this analysis. If now we wish a 5-ma total current, the emission density must be of the order of 5×10^5 amp/cm^2. Reference to Table IV will show that it is possible to obtain such a condition. Slightly better results can be obtained with a T-F emitter. It seems therefore as though field emitters would be very suitable for electron-beam machines. However, one major difficulty is lifetime. Experience with field emitters reveals erratic and unstable performance even in a clean and dust free tube, mainly due to cathode sputtering. Muller[14] measured the sputtering rate and found it to be approximately

$$t = \frac{10^{-8}}{ip} \tag{38}$$

where t is the time, in seconds, required to remove one layer; i is the emission current in amperes; and p the gas pressure in mm of Hg. On

the assumption that the life of an emitter extends to the point where 100 monolayers have been removed, the life can then be $10^{-6}/ip$. Thus, in a vacuum of about 10^{-5} mm Hg and with a current of 1 ma, the emitter life will be less than two minutes. Dolan and Dyke[15] have shown how favorable results could be obtained from a T-F field emitter under pulsed conditions. Here the buildup is limited during the time the field is on, and while the field is off, it permits surface forces to restore the original smooth, clean cathode surface. A tungsten cathode in the temperature range of 1700-2200 ^{o}K was used and fields up to 7×10^{7} volts per cm were applied in pulses as long as 0.01 second and duty cycles up to about 0.25. Stable current-voltage relationship was obtained even in vacuum as low as 10^{-4} mm Hg.

Even if the cathode life problem is solved, there seems to be very little advantage in cold-cathode field emission for spot radii of more than 1μ. The optimum magnification for imaging such small sources as are available with field emitters is close to unity. Also, there are unavoidable aberrations in the imaging lenses. From these facts, Cosslett and Haine[16] deduced that the current at the probe is limited and is much less than might be expected from the high brightness of the emitter.

One can therefore conclude that for our present application field emitters are not as attractive as hot cathode tungsten emitters. However, it seems quite likely that for small spot sizes, that is, of the order of less than 1μ, field emission might very well be the best choice.

Due to adverse conditions under which the cathodes would be called to operate, it is obvious that oxide cathodes, despite their

many advantages, are totally unsuitable for our purpose.

Lanthanum hexaboride (LaB_6) cathodes and uranium and zirconium carbide cathodes have been considered, but since insufficient data is available about them, they were discarded for the present.

The possibility of heating a refractory metal by electron bombardment using the scheme shown in Figure 4 was not very attractive because this is a somewhat complicated structure which requires an additional bombarding power supply floating at the cathode potential, in our case 100 kv.

It was therefore concluded that for our immediate application, the cathode that best satisfies the requirements is the pure hairpin tungsten filament. The emission is 5 amperes/cm^2 at a temperature of 2850 ^{o}K. The life under those conditions is about 10 hours for a 4-mil-diameter filament and 100 hours for a 40-mil filament. It is usually accepted that the useful life of a filament is determined by the time taken for its diameter to be reduced by approximately 12 per cent. The life figures are given for good vacuum; obviously the life will be considerably reduced if water vapor is liberated in the column. At poor vacuum levels, oxidation is a dominant factor in determining the life of the tungsten cathode.

CHOICE OF GUN

The electron gun is basically a triode. Sometimes the workpiece itself serves as the positive electrode and the system is then referred to as "work accelerated". Usually, as in our case, the accelerating anode is a separate electrode with a hole in the center to permit the passage of the electrons. Such an arrangement is called "self-accelerated".

many advantages, are totally unsuitable for our purpose.

Lanthanum hexaboride (LaB_6) cathodes and uranium and zirconium carbide cathodes have been considered, but since insufficient data is available about them, they were discarded for the present.

The possibility of heating a refractory metal by electron bombardment using the scheme shown in Figure 4 was not very attractive because this is a somewhat complicated structure which requires an additional bombarding power supply floating at the cathode potential, in our case 100 kv.

It was therefore concluded that for our immediate application, the cathode that best satisfies the requirements is the pure hairpin tungsten filament. The emission is 5 amperes/cm^2 at a temperature of 2850 ^oK. The life under those conditions is about 10 hours for a 4-mil-diameter filament and 100 hours for a 40-mil filament. It is usually accepted that the useful life of a filament is determined by the time taken for its diameter to be reduced by approximately 12 per cent. The life figures are given for good vacuum; obviously the life will be considerably reduced if water vapor is liberated in the column. At poor vacuum levels, oxidation is a dominant factor in determining the life of the tungsten cathode.

CHOICE OF GUN

The electron gun is basically a triode. Sometimes the workpiece itself serves as the positive electrode and the system is then referred to as "work accelerated". Usually, as in our case, the accelerating anode is a separate electrode with a hole in the center to permit the passage of the electrons. Such an arrangement is called "self-accelerated".

There are three kinds of guns which seem of interest and which use the hairpin tungsten emitter as a cathode.

(1) The classical gun which is normally used in the electron microscope.

(2) The Steigerwald gun.

(3) The Bricka and Bruck gun.

These three guns are shown in Figure 5. The Steigerwald gun[17] has been studied in detail by Braucks[18]. It is sometimes referred to as the distant focus or telefocus gun. The fundamental reason for the long focus effect is that the equipotential lines are concave towards the cathode due to the hollow shape and negative bias of the surrounding cup. Thus, electrons starting from the cathode are given radial outward velocity and the beam begins to diverge. Between the control electrode and the anode the equipotentials first become flat and then convex towards the cathode. The beam therefore is given radial inward acceleration but this only gradually overcomes the initial outward velocity. Consequently, the beam converges quite slowly and the beam forming field has a large focal length. The focal length can obviously be controlled by the bias voltage. A first look at the Steigerwald gun might indicate that a great advantage is to be gained by the elimination of the crossover and a consequent reduction of the aberrations. However, the sharply shaped grid field may be expected to be very sensitive to filament displacements, so that the image will be affected appreciably by any misalignment and improper placement of the filament.

In the Bricka and Bruck gun[19] a crossover is formed just beyond the cathode and this is reimaged at a considerable distance from the gun. It is said to be particularly satisfactory as far as align-

ment is concerned since the current drawn through the anode aperture is not affected by small filament displacements.

The classical gun was investigated by Borries[20] and by Dosse[21]. Further details are given by Haine and Einstein[22]. The crossover lies between the anode and cathode, nearer to the cathode. Despite the possible advantages presented by the other two types of guns, it was decided to use the standard gun since this presented the least modification in the equipment available for experimental verification.

DESIGN OF THE MACHINE

In order to speed up the construction of the electron beam machine, it was decided to convert an existing electron microscope - the RCA E.M.U.-3A. Figure 6 shows a functional diagram of the microscope column. The objective and the intermediate lens were removed. The projector lens was reversed. Figure 7 shows the simplified version of the column when adapted as an electron beam machine.

The accelerating voltage is 100 kv. The probe diameter of 0.001 inch is to be focused 2 inches below the lens center of the projector, leaving approximately 1 inch working distance for accommodating the deflection system and allowing vertical movement of the work. The standard electron gun is used. The data given by Borries on that gun refer to smaller currents than those required in our present system. However, since we are heating the filament to a temperature where space-charge limitation occurs, it is possible to scale voltages, distances and currents according to the rule

$$\begin{aligned} V' &= AV \\ d' &= A^{3/4}d \\ I' &= A^{3/2}I \end{aligned} , \qquad (39)$$

where A is a scaling factor. These are the well-known relations that prevail under space-charge-limited conditions. The crossover diameter, d_c, determined by the product of the time of flight d'/V' and the fixed initial lateral velocity component, transforms according to the relation $d_c' = A^{1/4} d_c$.

The dimensions given by Borries, which lead to very nearly optimal performance, and those obtained by scaling are shown in Table VI. The position of the crossover is not specified. The crossover lies near the cathode close to cutoff and moves forward towards the anode as the beam current is increased by reduction of the bias voltage. However, to a sufficiently close approximation, the crossover will be assumed to lie in the plane of the anode aperture.

These optimum dimensions, based on the results obtained by Borries, do not agree with those of Haine and Einstein[22]. According to the latter, the efficiency, defined as the ratio of probe current to total emission current, increases as the diameter of the hole in the Wehnelt cup and the distance from that hole to the tip of the filament is decreased. It is possible that as the filament is recessed further from the Wehnelt control cup, the field that penetrates imparts a radial velocity to the electrons and therefore decreases the over-all efficiency.

If we let u_1 and v_1 be the object and image distances of the condenser lens, and u_2 and v_2 those of the projector lens, reference to Figure 7 will give

$$u_1 = 4.625 \text{ inches},$$

$$v_1 + u_2 = 17.687 \text{ inches},$$

$$v_2 = 2 \text{ inches}.$$

Therefore,

$$\frac{2}{u_2} \times \frac{17.687 - u_2}{4.625} = \frac{0.001}{0.0046} \; . \tag{40}$$

Hence, $u_2 = 11.75$ inches and $v_1 = 5.94$ inches. The magnification and the focal lengths of the two lenses become

$$M_1 = 1.28,$$

$$\frac{1}{M_2} = 5.88,$$

$$f_1 = \frac{v_1}{M_1 + 1} = 2.60 \text{ inches},$$

$$f_2 = \frac{u_2}{\frac{1}{M_2} + 1} = 1.71 \text{ inches},$$

and the over-all magnification is $M = 4.6$. The spherical aberration of the condenser lens is negligible because of the small aperture angle of the beam. The spherical aberration of the projector lens is significant since, as we have seen previously, it might very well set a limit to the spot size. If we use the notations of Liebmann and Grad, as was done in the section dealing with limitations, the final lens in the present scheme has a ratio a_p/D (pole-piece separation to the internal pole-piece diameter) equal to 1.44. Interpolation of the results given by Liebmann and Grad gives $Cf = 5$ inches. This coefficient is computed for infinite magnification. It is therefore necessary to compute it for the actual magnification of the system.

Considering the lens as a thin lens, this can be done as follows. The usual lens equation is

$$\frac{1}{u} + \frac{1}{v} = \frac{1}{f} \; , \tag{41}$$

where v and u are the object and image distances, respectively.

$$\frac{1}{u} + \frac{1}{Mu} = \frac{1}{f}, \tag{42}$$

or

$$u = \frac{M + 1}{M} f. \tag{43}$$

If r_α is the height of incidence on the lens,

$$r_\alpha = \frac{M + 1}{M} f\alpha. \tag{44}$$

Now for a thin lens* we can write

$$\Delta r = MuKr_\alpha^{\ 3}. \tag{45}$$

K is independent of object position, hence the angular displacement due to spherical aberration,

$$\Delta\delta = \frac{\Delta r}{Mu} = Kr_\alpha^{\ 3}, \tag{46}$$

depends only on the height of incidence, r_α. For the object near the focal point,

$$\frac{\Delta r_\infty}{Mf} = \frac{MC_\infty r_\alpha^{\ 3}}{Mf^4} = Kr_\alpha^{\ 3}, \tag{47}$$

leads to

$$K = \frac{C_\infty}{f^4}. \tag{48}$$

Hence

$$\Delta r = v\Delta\delta = MuK_\infty r_\alpha^{\ 3}, \tag{49}$$

---

*See e.g. Eq. 17.4 of reference (9)

or

$$\Delta r = (M + 1)\ fK_\infty \left(\frac{M + 1}{M}\right)^3 f^3 \alpha^3, \tag{50}$$

$$\Delta r = C\left(\frac{M + 1}{M^3}\right)^4 \alpha^3 = MC_\infty \left(\frac{M + 1}{M}\right)^4 \alpha^2. \tag{51}$$

Now

$$\Delta r = C_s M\alpha^3. \tag{52}$$

We then have

$$C_s = \left(\frac{M + 1}{M}\right)^4 C_\infty = 9.4 \text{ inches.} \tag{53}$$

To compute the convergence of the beam at the crossover we shall use the Langmuir relation given in Equation (22).

$$I = c\ \frac{\pi d_o^2}{4} \alpha^2 \frac{V}{V_T} j_c. \tag{54}$$

$V_T = kT/e$: 0.25 volt which corresponds to the operating temperature of the filament. V is the beam voltage, d_o is the spot diameter, and j_c is the emission density at the cathode. The factor c would be unity if the current density at the spot were constant up to the edge and zero beyond, and if the same condition applied for the distribution of current in angle, i.e., constant current per unit solid angle up to the convergence angle α, and zero beyond.

In actual practice this is not the case. If the gun is not operated at a very low bias and low filament temperature, the intensity distribution across the crossover can be assumed to be Gaussian. If now

we define the edge of the spot at crossover as the point where the current density has dropped by the factor 1/e, and if we assume that the emission also falls off in Gaussian fashion by the factor 1/e at the point corresponding to the limiting convergence angle α, the value of c is about 1/3.

Strictly speaking, the angular distribution of current density across the beam is of Gaussian nature only at low beam currents. As the beam current is increased by decreasing the bias, the beam becomes "hollow". This was reported by some authors and shown by Haine and Einstein[22]. Borries assumed that the crossover diameter is that which encloses 93 per cent of the beam, based on a visual measurement. Borries crossover diameter must therefore be divided by

$$\sqrt{\frac{\ln 0.07}{\ln \frac{1}{e}}} = \sqrt{-\ln 0.07} = 1.63. \quad (55)$$

This was done in the tabulation of the results derived from the data of Borries. We therefore have at the crossover,

$$\alpha_c = \frac{1}{d_o} \sqrt{\frac{4}{\pi c} \frac{V_T}{V} \frac{I_b}{j_c}}. \quad (56)$$

For $V = 10^5$ volts, $c = 1/3$ and $V_T = 0.25$ volt, this gives

$$\alpha_c = \frac{0.00121}{d_o} \sqrt{\frac{I_b}{j_c}}, \quad (57)$$

where I_b is in amperes, j_o in amperes/cm^2, and d_o in inches. We can now use the scaled values of Borries;

$$\alpha_c = \frac{0.00121}{0.0046} \sqrt{\left(\frac{2.22 \times 10^{-3}}{j_c}\right)} \quad (58)$$

At $T = 2650^{o}K$, $j_c = 1.41$ amperes/cm^2. We then have $\alpha_c = 0.0116$ radian. Thus α_s at the spot will be

$$\alpha_s = M\alpha_c = 4.6 \times 0.0116 = 0.0533 \text{ radian.}$$

The minimum disc of confusion is then

$$\frac{1}{2} C_s \alpha_s^3 = \frac{1}{2} (9.4)(0.0533)^3 = 0.000715 \text{ inch.} \qquad (59)$$

This is less than 0.001 inch, so the dimensioning is adequate. The probe current is given as 2.2 ma. In order to increase the current to 5 ma, which was the initial objective, the filament temperature must be increased to approximately $2750^{o}K$. The spot size will not change under these conditions. The life of the filament as defined earlier should be of the order of 100 hours, assuming, of course, that the chamber is not opened too frequently. From the results obtained by Maloof[23], it seems possible that filaments formed from single-crystal tungsten wires have longer lives. However, no experimental data are available to prove this point.

DESCRIPTION OF THE MACHINE

Figure 8 shows a schematic diagram of the electron-beam machine. The filament and control cylinder are at -100 kv with respect to ground. All of the remaining parts are at ground potential. The bias and pulses are fed between the cathode and Wehnelt control cylinder at 100 kv level.

It was desirable to convert the EMU-3A electron microscope to an electron beam machine with a minimum of modifications. The chamber was considerably enlarged to allow more working space. The

new housing, shown in Figure 9, has a pyramidal shape and is made of aluminum. Several ports were installed for viewing, access to the housing, and for vacuum-tight electrical connections. Inside the housing a positioning table was incorporated to permit mechanical movement of the workpiece. The table is designed to have X and Y motion in the horizontal plane as well as rotation and elevation control. The X and Y motion have to be very accurate, preferably within one thousandth of an inch. There was no need to require the same kind of accuracy in the rotation and elevation control.

The drives for the X and Y motion were compounded and made concentric with each other. In this way, only one vacuum seal to the housing is necessary. There are two additional seals in the concentric shafts. Figure 10 shows a schematic of the arrangement. A lead screw mated with a nut and supported on its ends, free to rotate, forms the basic design. When the nut is locked by means of a long tubular connection, a motion in the Y direction is obtained by rotating the appropriate wheel at the control. If the screw and nut are locked together, the rotation at the control results in an X directed motion. The controls for the elevation and rotation are connected through flexible shafts. The connection to the vacuum chamber is made through O-rings. Figure 11 shows the positioning table and Figure 9 shows the mechanical controls. Whenever a workpiece calls for precision in the rotation control, a special jig, electrically motorized, is placed on the mechanical table. The motors are kept dry in a vacuum desiccator. Since the vacuum level at which the machine normally operates is poor (about 10^{-4} mm Hg), the introduction of motors does not increase the pumping time. Another jig, designed to provide rotation along an

axis perpendicular to that of the beam is also used when two tubular sections are to be welded together. Electrical motors with variable speeds provide the necessary rotation.

The mechanical table is electrically insulated from the housing. It is connected to ground through an ammeter. The probe current can thus be measured continuously. For accurate measurement, the table is moved until the beam strikes a Faraday cage so as to avoid any error due to secondary emission. For rough indications, secondary emission is generally neglected. The voltage across a resistor in series with the probe meter is fed to an oscilloscope which shows the waveform of the pulses at the probe.

The opening of the column that was formerly used for the intermediate lens was enlarged to provide room for the installation of a viewing system. A reflected view is provided by a mirror inclined at 45° with respect to the beam axis. A hole is drilled in its center large enough to let the beam pass freely. Observation is made with a microscope mounted at right angles to the column axis and facing the mirror. The mirror is located in the geometrical and optical center of the column. In order to maintain the field of view of the spot, it is necessary to move either the microscope or the mirror. The microscope is large and heavy, hence, it was found simpler to move the mirror. The mirror is mounted on a rectangular frame in such a way that the mirror center and that of the housing are coincident. A vacuum-sealed lead glass window in the wall of the housing permits observation of the mirror and workpiece. Separate drives through the vacuum provide the control of the position of the mirror. It can be pivoted about the beam axis or about an axis perpendicular to that of the beam.

Figure 12 shows the mirror housing. The microscope used for observation must have a focal length of nearly nine inches. Consequently, it measures 32 inches and weighs 35 pounds. It was therefore necessary to mount it on a boom pivoted from a right column so that it can be moved aside to permit access to the work chamber. A manually operated slide is used for positioning the microscope.

POWER SUPPLY

Many of the power supplies require a high degree of stability of the operating voltages and currents. The high-voltage supply is generated by a resonating LC series network. An inductor and its stray capacitor are connected in series, and a-c voltage at resonant frequency is applied. By careful design, the electrical losses are minimized and a high voltage is obtained across the inductor. The peak r-f voltage developed across the coil can be either 25 or 50 kv depending upon the plate and screen voltages supplied to the oscillators. The high resonant voltage is rectified and doubled by conventional means.

Stabilization is achieved by a feedback network. The high-voltage output is stabilized by changing the screen voltage of the oscillator tubes whenever the high-voltage output begins to deviate from its normal value.

The heating current for the filament is delivered at high-voltage level by means of r-f induction. A conventional oscillator circuit provides a 100 kc resonant frequency. The output is inductively coupled to the gun-filament circuit.

VACUUM INSTALLATION

The vacuum installation cinsists of a mechanical pump and a diffusion pump. An automatic system permits the admission of air to the

column only after the diffusion pump has been sealed off. Thus, during loading, the fore pump is connected to the diffusion pump while the column is filled to atmospheric pressure. Before operation, the diffusion pump is sealed off at both ends. The fore pump is connected directly to the column. When the pressure reaches a sufficiently low value, the fore pump is connected to the diffusion pump which, in turn, is opened to the column. The complete vacuum valving is carried out automatically. Electric motors actuate the valves and correct sequencing is obtained by the action of limit switches and relays. The danger of accidentally letting air to a hot diffusion pump is thus minimized.

Two vacuum gauges are used - a thermocouple gauge and a cold discharge gauge. The thermocouple gauge indicates the pressure reached by the fore pump. The cold discharge or ionization gauge is used to indicate the pressure in the column when the diffusion pump is connected to the column. The electrical signal from the cold discharge vacuum gauge is amplified and used to change the system from rough pumping to final pumping at the correct column pressure. The same gauge is also utilized to control the automatic valving sequence and prevent application of high voltage until the required degree of vacuum is obtained. This prevents the operator from touching the electron gun while the high voltage is on.

To avoid the resistance to pumping offered by the column, a by-pass connection is made from the housing to the gun area.

ALIGNMENT

The tungsten filament is 8 to 10 mils in diameter. It is positioned and spot welded to the holder with the help of a jig shown in Figure 13. The filament holder is installed in the cone with the

help of two screws. A second jig, shown in Figure 14, is used to provide the alignment of the filament with the Wehnelt cup. Should there still be any misalignment, there is enough play in the assembly to maneuver the filament holder until the correct position is found. The jig can then be removed and, with the help of a depth microscope, the distance from the tip of the filament to a fixed reference shoulder can be measured. By measuring the length of the Wehnelt cup, the correct spacing between the filament and cup can be determined. The gun can then be connected to the assembly.

The concentricity of the cathode and control electrode with the periphery of the column is effected with the help of a special jig. This screws to the cathode holder exactly as does the Wehnelt cup and is slightly smaller than the inside diameter of the column. With the help of feelers, concentricity is verified. The cone assembly can be shifted until alignment is obtained. The whole procedure has to be repeated only when the cone is removed for replacement or for trouble shooting.

The gun assembly can be mechanically displaced with respect to the condenser lens. This latter is fixed and its mechanical alignment with the rest of the column is obtained by carefully machined surfaces. Three screws spaced 120 degrees apart can be used to align the gun to the condenser.

The projector lens is held on the column by means of three screws. These allow the alignment of the lens with respect to the column and condenser. The mechanical alignment cannot be relied upon for perfect alignment due to the tolerances involved. Once the best mechanical alignment is obtained, final alignment is achieved with the help of electrical deflectors in the column.

There are two separate deflectors. One preceding the condenser lens which serves to align the gun assembly with the condenser, and another immediately after the condenser lens which serves to align the condenser with the projector. The deflectors are connected across a bridge circuit of resistors. If the bridge is in balance, there is no current flowing in either deflection coil. This is the neutral position. The knobs are then positioned in the center of the dial. Rotation of the knobs one way or another will allow current to flow in one direction or another with a corresponding deflection of the beam. The machine can be operated at either 50 or 100 kv depending on whether the input to the doubler is 25 or 50 kv. The field necessary to deflect the beam at 50 kv is less than that at 100 kv. A resistance is therefore introduced in series with the bridge circuit. This limits the current when operating at 50 kv but is disconnected by a relay when operation is at 100 kv. Smooth deflection control is obtained in this fashion. Alignment can be recognized by noting that a beam of electrons coincident with the axis of a magnetic electron lens does not shift as the strength of the lens is changed. If the beam is off the axis, it shifts as the strength of the lens is changed. The shift of an image point from a magnetic lens as the strength of the lens is changed becomes therefore a criterion for recognizing alignment. There can be a condition where the direction as well as the position are both off the axis in such a way as to obtain a stationary spot as the lens is energized. It is therefore necessary to reverse the magnetic field during the alignment procedure.

Sometimes, the aperture in the condenser lens becomes contaminated. By carefully defocusing the beam and increasing the emission, the aperture is heated and this generally eliminates the charging up.

ILLUMINATION

Correct observation of the workpiece during operation is very important for the successful operation of the machine. The illumination of the target presents some problems because of the close spacing between the final lens and the workpiece. The illumination was therefore provided by inserting six equidistant bulbs immediately above the working area. The bulbs have given some difficulties because of the insulated glass which charges up and distorts the beam and because of the loss of light when they get coated with the metal vapor after operation. The final solution was found by removing the glass and using bare filaments. By careful interlocking, the filaments are lit only when good vacuum is obtained. In order to be able to position the target properly, two bulbs are located at the extreme corners of the housing. These serve only during the time air is let inside the chamber and are not sufficient to illuminate the target during operation. The observation of the target while it is being bombarded by the beam is rather difficult due to the brightness of the spot. The microscope iris is used to cut down on the illumination, but this in turn results in loss of detail. Another method would be to use a television camera on the target; however, there are problems to be solved here too.

DEFLECTION

The deflection control is provided by means of four pole deflectors. The four coils are wound on a ferrite core and are arranged 90 degrees apart with their axis pointing inward at a common center. One method of deflection is achieved as follows: Two of the coils, 180 degrees apart, are connected in series and a sawtooth voltage is

applied to these coils. The other two coils are also connected in series and a square wave is applied to them. Now the beam will travel back and forth and is deflected left and right across the straight line of the sawtooth wave. If the two waves are not synchronized, the spot will hit all points of the periphery of the rectangle bounded by both wave-form amplitudes. As an example, if the two wave forms are periodically interchanged, a cross will be formed. The use of more poles will increase the number of geometrical configurations that can be machined. The maximum deflection is of the order of 1/8 inch from the center point due to the limit imposed by astigmatism.[24]

PULSE SYSTEM

As was indicated earlier, it is necessary to pulse the beam to reduce unwanted heating and melting at the target. The beam is biased off by applying a sufficiently negative voltage on the Wehnelt cylinder. If now a positive pulse is applied on the Wehnelt cylinder, the beam is automatically switched on for the length of time the pulse is applied. A first look at the problem might indicate that this is a simple matter, quite readily solvable. However, there are many difficulties involved which necessitate careful design of circuitry and insulation.

As indicated earlier, the anode and column are at ground potential, while the cathode and cup are at -100 kv with respect to the anode. Accordingly, the pulse has to be delivered at 100 kv level.

The requirement for the successful operation of the machine was to have a pulsing circuit that can deliver pulses from two to several hundred milliseconds in duration. For short pulses, the rise and decay time must be very short. This sets up an upper limit to the RC of the

network. The capacitance is already present in the gun system and it is estimated as 50 picofarads. In addition there is the stray capacitance of the circuit.

For long pulses, relatively long rise and decay times can be tolerated. However, it is preferable not to have any exponential decay of the pulse. This in turn presents some difficulties due to the RC of the network. A compromise must therefore be sought.

One method of obtaining the pulses is to feed the pulses through a pulse transformer insulated for 100 kv. The pulses are supplied to the primary winding from a pulser at ground potential. The pulse transformer is a 1:1 inverting transformer and can be designed to have a bandwidth which enables it to transmit rectangular pulses over a certain range. The scheme is shown in Figure 15. It has many advantages. However, it is well-known that a pulse transformer can only work over a narrow bandwidth. It is very difficult, if not impossible, to design a pulse transformer that will transmit undistorted pulses up to several hundred milliseconds. This scheme was therefore not chosen.

Another method considered was the use of a pulsed r-f carrier system by which the pulses can be brought to 100-kv potential and there rectified and stabilized in amplitude.

Figure 16 shows details of such a scheme. A 1/2-inch thick Pyrex insulator is used between the primary and secondary of the r-f coupling transformer. The circuit at the 100-kv level is a parallel tuned circuit with a half-wave series rectifier across it. The rectified pulses can be stabilized to the desired pulse amplitude by means of a Zener diode. In order to avoid the long tail at the trailing edge

of the pulse due to the charge stored in the Zener diode, a rectifier diode was connected in series with the Zener diode. This scheme has many merits but at the same time presents many difficulties due to the critical tuning involved.

A variation of this scheme is to use the r-f to supply not only the pulses, but also the bias. Thus, by simple amplitude modulation the potential difference between the Wehnelt cup and filament can be varied at will, thereby eliminating the bias supply with its own 100-kv insulated transformer. However, a simple computation will show that such a scheme is not feasible. The load capacitance is of the order of 50 picofarads.

If we require a minimum pulse width to be of the order of two microseconds, the minimum permissible rise and decay time would be of the order of 0.4 microsecond. The load resistance would have a maximum value

$$R = \frac{\tau}{C} = \frac{0.4 \times 10^{-6}}{50 \times 10^{-12}} = 8 \times 10^{3} \text{ ohms.} \qquad (60)$$

For a bias of about 1500 volts, this would present a power dissipation of

$$P = \frac{(1500)^{2}}{8 \times 10^{3}} = 280 \text{ watts.} \qquad (61)$$

It is clear that such a power dissipation at r-f frequency would not be very practical.

It was therefore decided to discard the r-f pulsing scheme. In view of the fact that the pulse circuit was to deliver pulses over

a wide range, the best solution was found by using a bistable multivibrator. The power supply which provides the variable bias voltage circuit provides the d-c plate voltages to the multivibrator at the same time. Figure 17 shows the circuitry used in such a scheme.

All of the electric components at 100-kv level are mounted inside a highly polished shielding bottle which plugs into sockets in the bottom of a ceramic insulator cone.

The high-voltage cable plugs into one side of the container or "bottle". A corona shield is provided around the cable to minimize the field strength. On the opposite side, a glass insulator with the differentiating transformer is mounted. The glass insulator is 1/2-inch thick in the center and is thicker at the rim. It is coated with a high resistance "TIC"(transparent iridized coating) coating of the order of 10^4 ohms/cm in the depressions of both sides. These coatings serve as field equalizers for the high voltage. The coupling transformer is made of a ferrite core split in two and mounted face to face on each side of the glass insulation. This provides the high-voltage insulation as well as the leakage for the differentiation of the pulses. All outside corners of the shield are well rounded to eliminate any high field regions, thus eliminating the chance of breakdown.

Tube T_2 is normally conducting while tube T_3 is kept close to cutoff by means of resistor R_4. A positive trigger pulse at the grid of bute T_1 turns this tube on and cuts off tube T_2. As a consequence, tube T_3 looses its bias voltage and becomes fully conductive. The bias voltage between the cathode and the control grid drop accordingly. The negative trigger pulse resets the system to the original conditions.

The advantage of this system as against others is the fact that very wide bandwidths can be covered by the same setup. In the very short pulse-width range, a fast rise and decay time is essential, but the exponential decay of the pulse due to the charging and discharging of the inherent capacitance in the system is negligible. For large pulse widths, the rise and decay time is negligible, but here the maintenance of a relatively horizontal pulse is important. It is therefore necessary to design two separate circuits which can be interchanged quite readily to suit the pulsing requirement at the target.

It was found advisable to set up the circuit in such a way as to maintain a fixed pulse amplitude. The level between the Wehnelt cylinder and cathode can be adjusted with the bias control. In this way only one 100-kv insulated control is necessary.

The "bottle" or shield is mounted inside a grounded container. The clearance between the two is maintained to a minimum of 1-1/4 inches throughout. Dow Corning silicone oil is used as an insulator. A viscosity of 1.0 centistoke at 25°C was chosen. The electric strength is 325 volts/mil.

The diodes used were good for 1000 volts peak inverse voltage and can carry from 300 to 400 ma d-c forward current depending on whether they are capacitively or inductively loaded. Figure 18 shows the circuit attached to the transformer and ready to be inserted in the bottle and oil. Figure 19 shows the complete electron-beam machine during operation.

While the objective of this paper is to describe the considerations which underlie the design of an electron-beam machine and its actual design, some examples of work performed with the completed machine are shown in Figures 20 to 23.

CONCLUSION

In conclusion, it has been shown that an electron-beam machine can be designed to obtain a high probe current of 5 milliamperes in a spot of .001 inch diameter. The spot can be deflected 1/4 inch without appreciable distortion. The beam can be pulsed from a few microseconds to several milliseconds very satisfactorily, using a multivibrator circuit. A mechanical table to provide flexibility in positioning and displacing the object is incorporated in the electron-beam machine. The viewing mechanism consists of a long-focus microscope and a 45° mirror with a hole through which the beam passes freely.

ACKNOWLEDGEMENTS

The work described in this report was performed under the leadership of H B. Law. L. Davne was largely responsible for the mechanical designs. The circuits in the pulse head were designed and improved by R. Lochinger and W. Moles. J. Reisner was consulted numerous times during experiments with the machine and supplied the pole pieces for the final lens. A considerable part of the theoretical work was contributed by E. G. Ramberg. Finally, the author wants to thank L. S. Nergaard and F. Norman for suggesting the use of a multivibrator to pulse the beam.

Table I

Heat Source	Min. Area (cm^2)	Max. Power Density $Watts/cm^2$
Oxyacetylene Flame	10^{-2}	10^4
Electric Arc	10^{-3}	10^5
Electron Beam	10^{-7}	10^9

Table II
(For d = 0.001 inch)

Z (inches)	D (inches)	Cf (centimeters)	$\frac{I}{j_o} \times 10^3$
1	1.6	27.00	1.39
1	0.4	62.50	0.794
1	0.1	490.00	0.203
4	1.6	250.00	0.323
4	0.4	1960.00	0.083
4	0.1	26000.00	0.014

Table III

Lens Bore Diameter, D (inches)	Beam Diameter at the Lens, D (inches)	Working Distance Z (inches)	$\frac{I}{jo} \times 10^3$	Space-Charge Limited Current (ma)
1.6	0.19	1	1.39	2500
1.6	0.19	4	0.323	160
0.4	0.076	1	0.794	500
0.4	0.076	4	0.083	30
0.1	0.030	1	0.203	115
0.1	0.030	4	0.014	7

Table IV

Free-field emission of tungsten as a function of temperature.

j_o amps/cm^2	T in ^{o}K
0.12	2400
0.30	2500
0.70	2600
1.6	2700
3.5	2800
7.3	2900
14.0	3000

Table V

jo amps/cm^2	F x 10^7 volts/cm
0.00047	2
37	3
1.1×10^4	4
3.9×10^5	5
4.2×10^6	6
2.3×10^7	7
8.7×10^7	8

Table VI

	(Borries)	(Scaled)
V	20 kv	100 kv
T	2650° K	2650° K
d_g	0.060 inch	0.200 inch
a_k	0.040 inch	0.133 inch
a	0.400 inch	1.333 inches
D_w	0.005 inch	0.017 inch
I_b	0.200 ma	2.220 ma
d_c	0.0031 inch	0.0046 inch

d_g is the aperture diameter of the Wehnelt cylinder,

a_k is the distance of filament point above grid aperture,

a is the distance between grid and anode,

d_w is the diameter of the filament wire,

I_b is the beam current,

d_c is the crossover diameter.

Fig. 1 - Upper limit to probe current established by space charge.

Fig. 2 - Space-charge limitations as derived by Schwartz.[3]

Fig. 3 - Assumed magnetic-lens configuration.

Fig. 4 - Bombarded cathode in the shape of a disc.

Fig. 5 - Beam-forming systems with thermionic cathodes.

Fig. 6 - Functional diagram of microscope column.

Fig. 7 - Electron optics of EMU-3A adapted for beam-drilling.

Fig. 8 - Electron-beam machine.

Fig. 9 - Controls for mechanical table and aluminum housing frame.

Fig. 10 - Schematic of the mechanical table.

Fig. 11 - Mechanical table.

Fig. 12 - Micropositioner for the viewing mirror.

Fig. 13 - Jig for spot-welding the filament.

Fig. 14 - Jig for positioning filament in the gun assembly.

Fig. 15 - Pulse control using insulated high-voltage pulse transformer.

Fig. 16 - Pulse-coupling lead using r-f scheme.

Fig. 17 - Multivibrator pulsing and bias supply.

Fig. 18 - Pulse circuit attached to transformer and ready to be inserted in the bottle and oil bath.

Fig. 19 - Electron-beam machine.

Fig. 20 - A butt weld of two pieces of molybdenum 5/1000 inch thick.

Fig. 21 - 2-1/2-mil holes drilled in molybdenum 5 mils thick.

Fig. 22 - Cross section of 1/4000 hole drilled in ferrite 10 mils thick.

Fig. 23 - Weld of two concentric nichrome tubes.

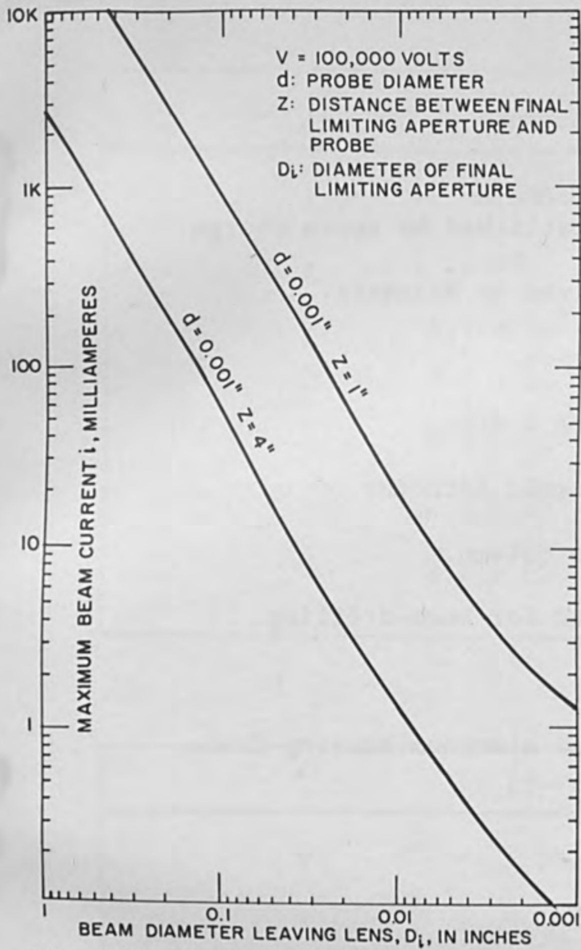

FIG. 1 UPPER LIMIT TO PROBE CURRENT ESTABLISHED BY SPACE CHARGE

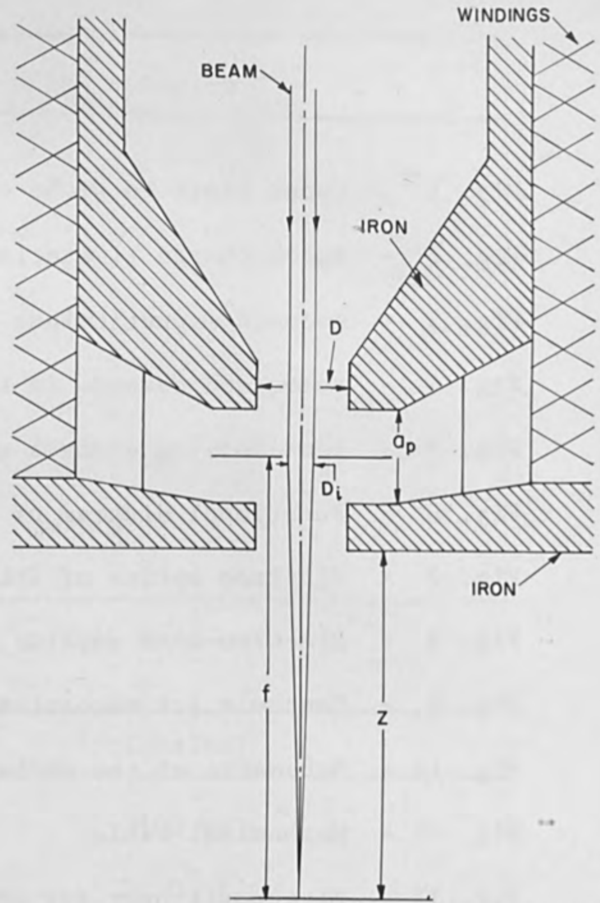

FIG. 3 ASSUMED MAGNETIC LENS CONFIGURATION

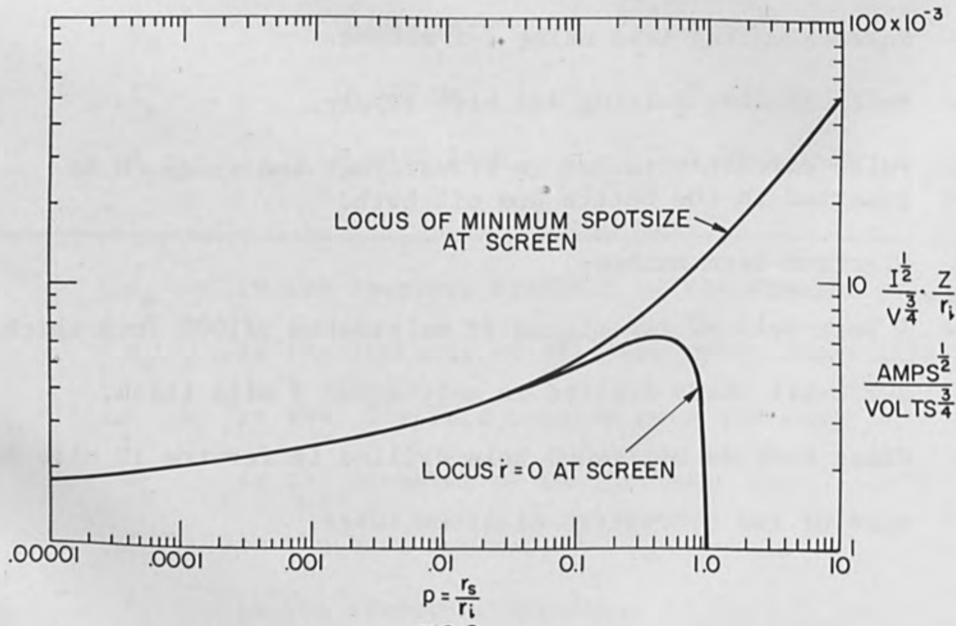

FIG. 2

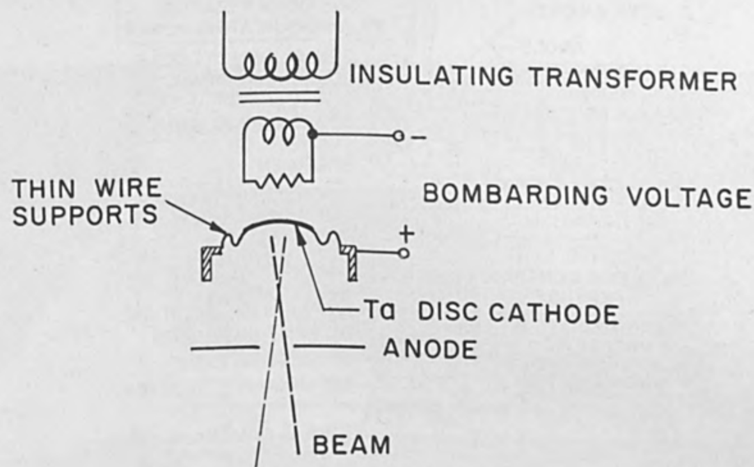

FIG. 4 BOMBARDED CATHODE IN THE SHAPE OF A DISC

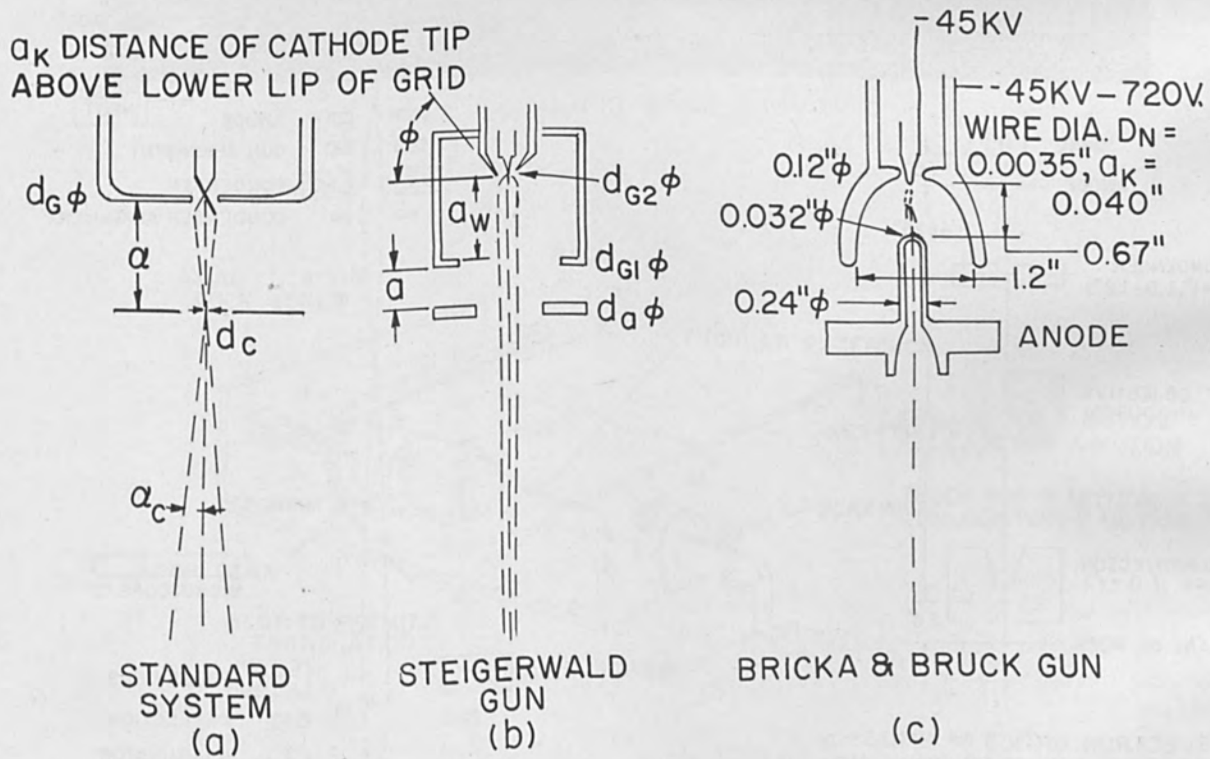

FIG. 5 BEAM - FORMING SYSTEMS WITH THERMIONIC CATHODES

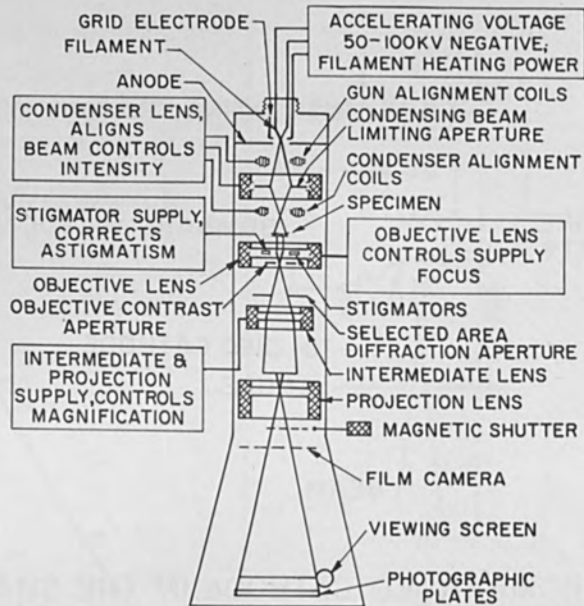

FIG.6 FUNCTIONAL DIAGRAM OF MICROSCOPE COLUMN

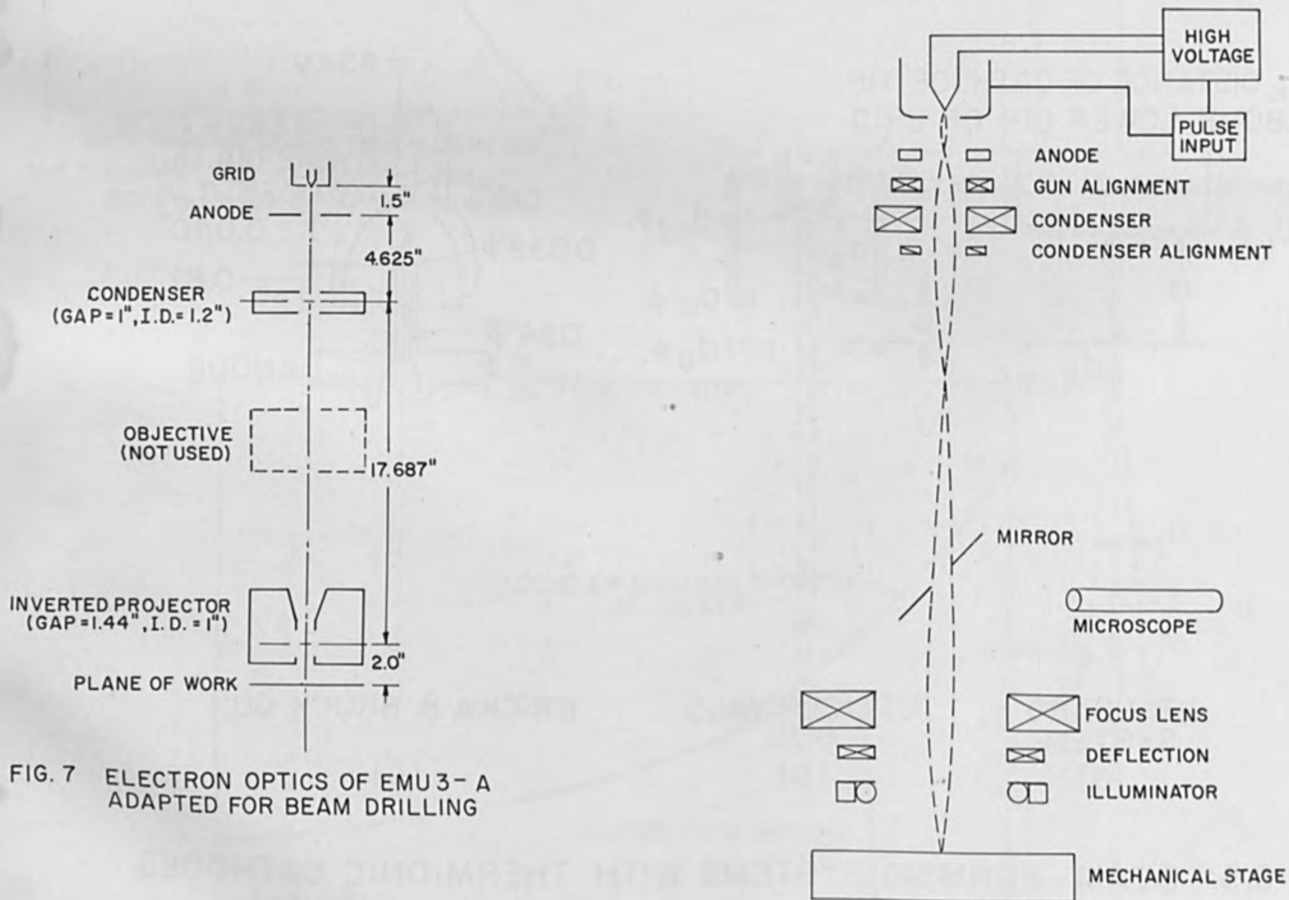

FIG. 7 ELECTRON OPTICS OF EMU 3-A ADAPTED FOR BEAM DRILLING

FIG. 8 ELECTRON-BEAM MACHINE

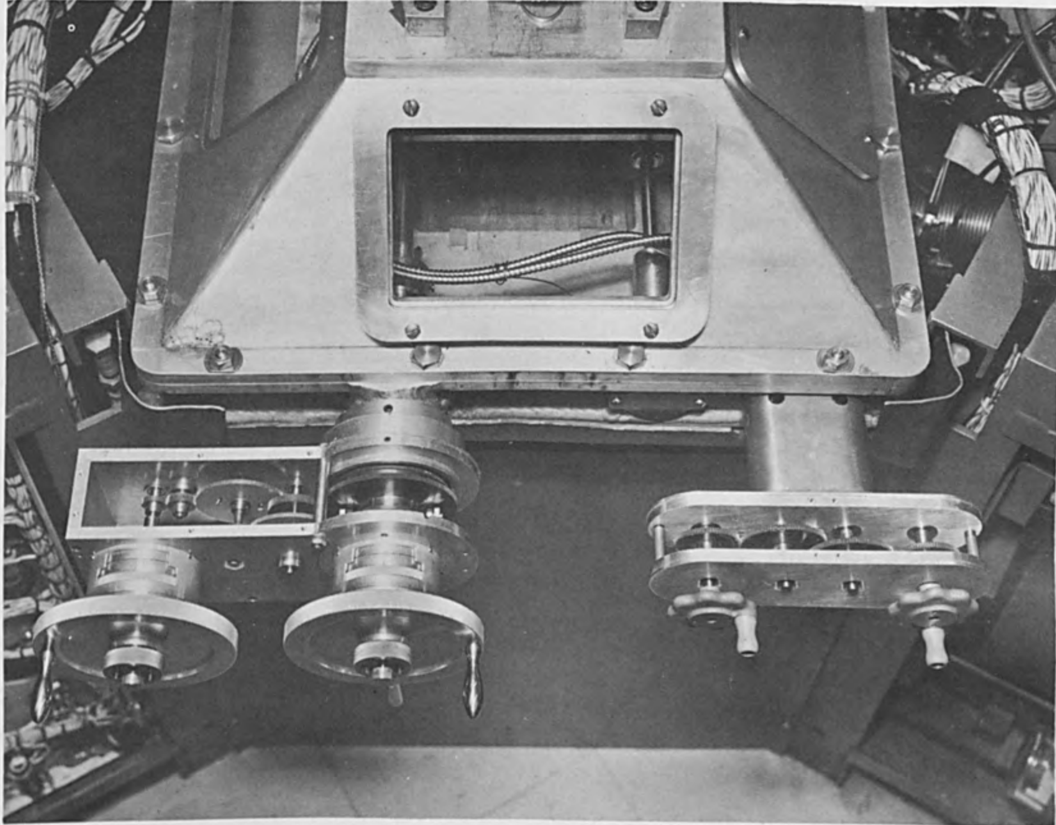

FIG. 9

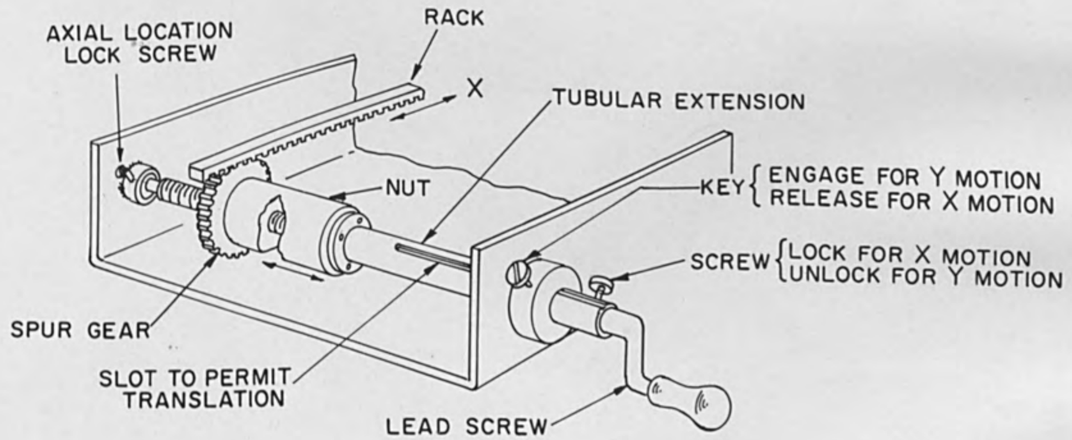

FIG. 10

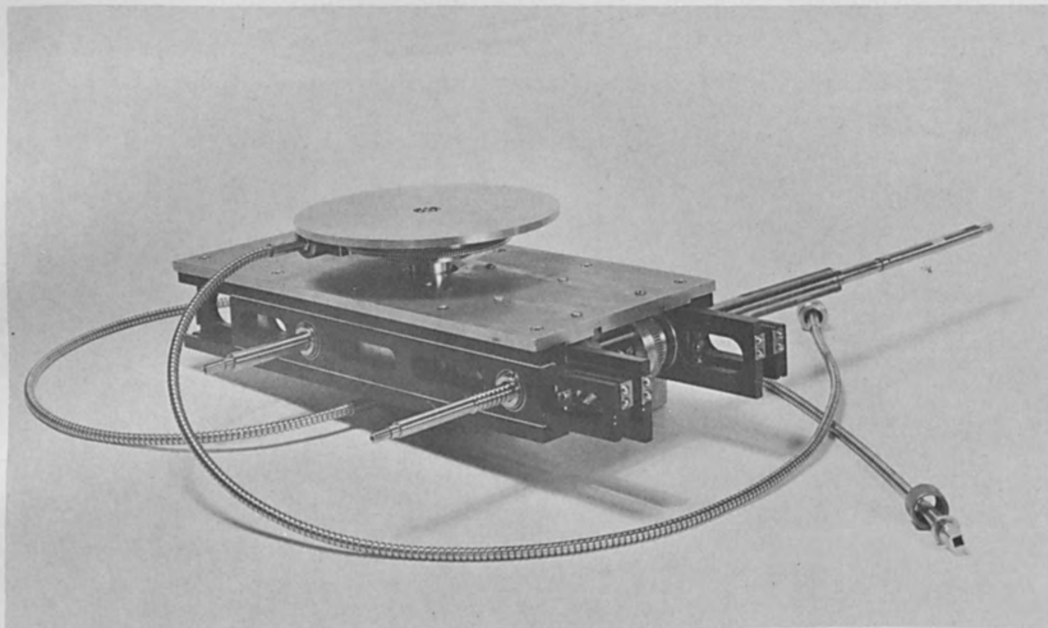

FIG. 11

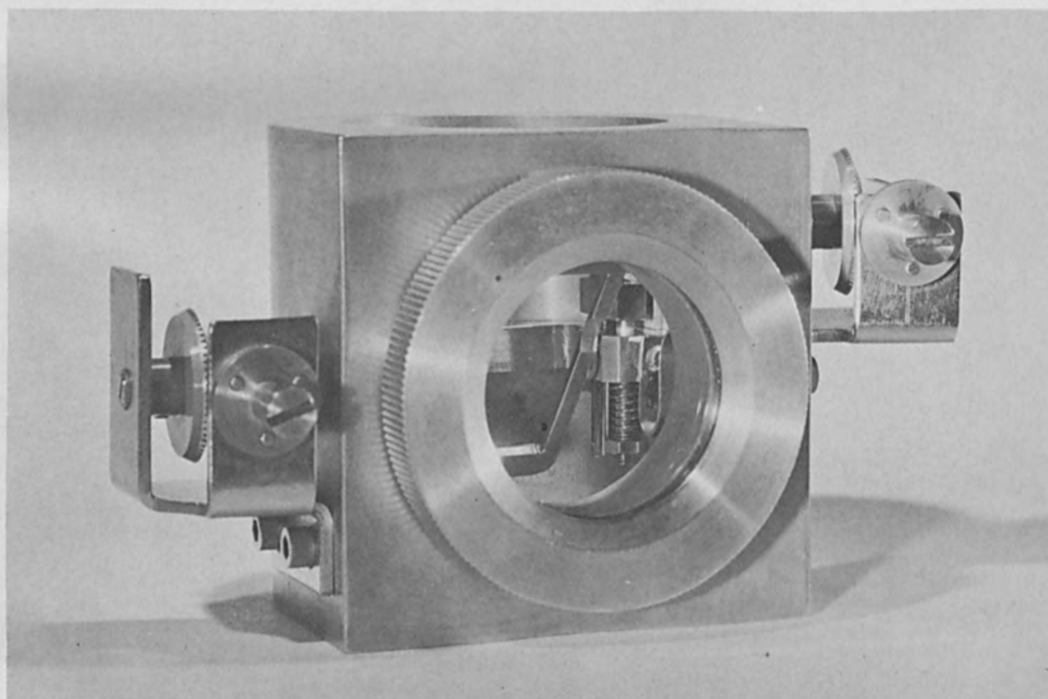

FIG. 12

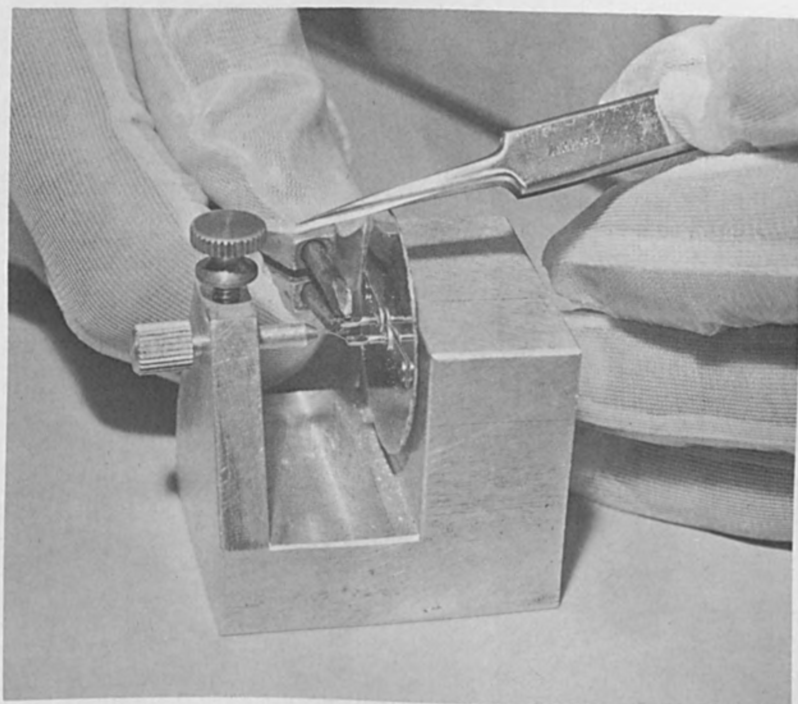

FIG. 13

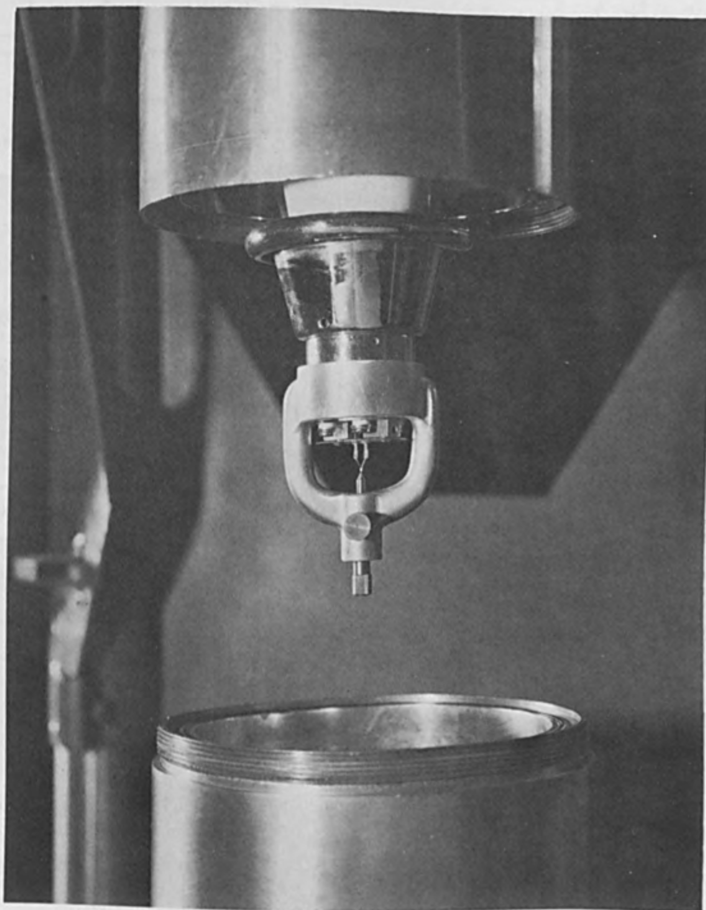

FIG. 14

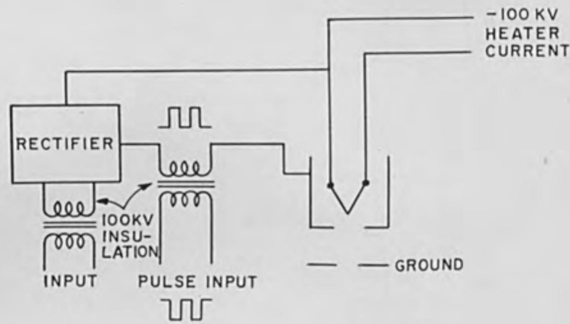

FIG. 15 PULSE CONTROL USING INSULATED H.V. PULSE TRANSFORMER

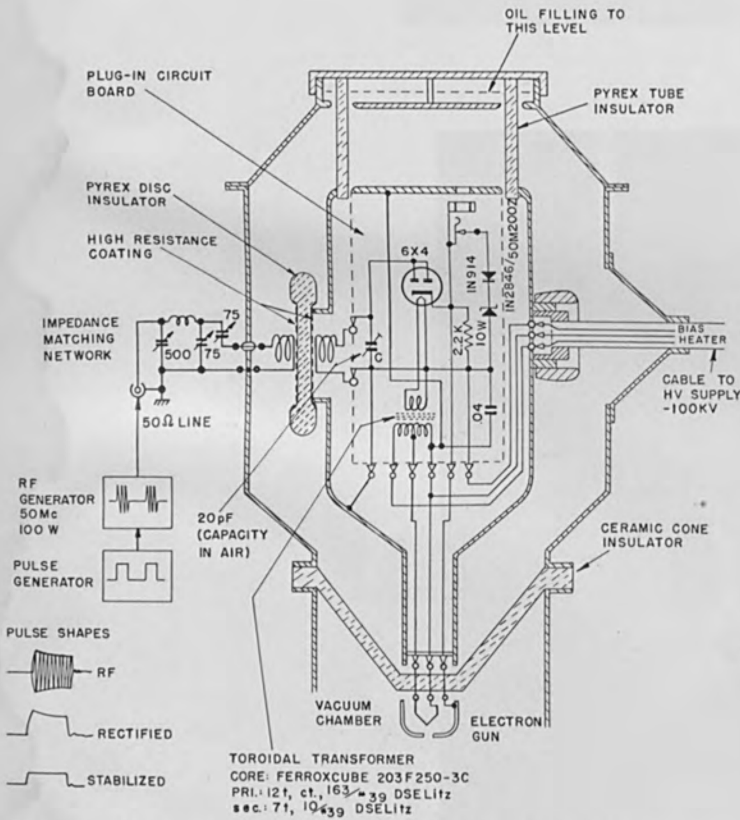

FIG. 16 PULSE COUPLING HEAD USING R.F. SCHEME

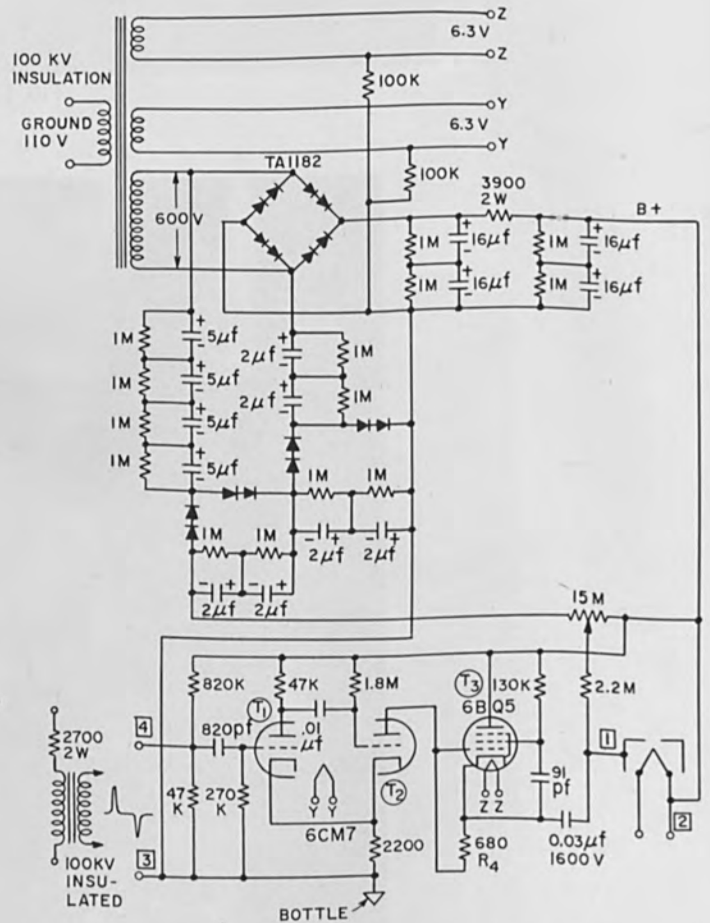

FIG. 17 MULTIVIBRATOR PULSING & BIAS SUPPLY

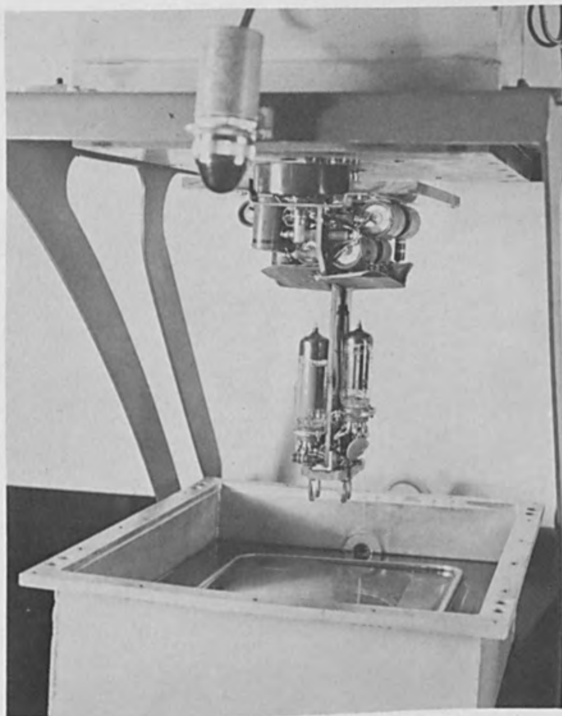
FIG. 18

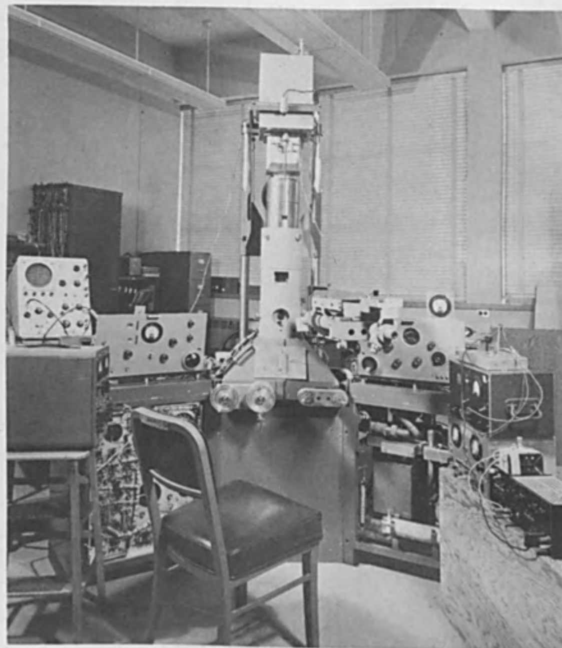
FIG. 19

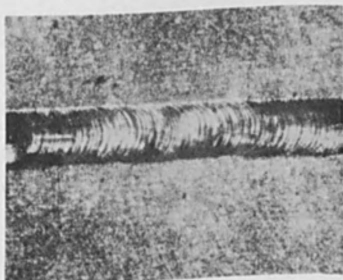
FIG. 20

FIG. 22

FIG. 21

FIG. 23

1. Cutler, C.C. and Hines, M.E., "Thermal Velocity Effects in Electron Guns", Proc. I.R.E., Vol. 43, p. 307, 1955.

2. Danielson, W.E., Rosenfeld, J.L., and Saloom, J.A., "A Detailed Analysis of Beam Formation with Electron Guns of the Pierce Type", Bell Syst. Tech. Jour., Vol. 35, No. 2, p. 375, March 1956.

3. Schwartz, J.W., "Space-Charge Limitation on the Focus of Electron Beams", RCA Review, Vol. 18, No. 1, p. 3, March 1957.

4. Thompson, B.J. and Headrick, L.B., "Space-Charge Limitations on the Focus of Electron Beams", Proc. I.R.E., Vol. 28, No. 7, p. 318, July 1940.

5. Hollway, D.L., "The Optimum Space-Charge Controlled Focus of an Electron Beam", Australian Jour. Sci. Research, Vol. 5, Series A, p. 430, 1952.

6. Hollway, D.L., "Design Chart for Calculating Electron-Beam Parameters", Electronics, Vol. 35, No. 7, p. 50, Feb. 16, 1962.

7. Hernqvist, K.G. and Linder, E.G., "Space-Charge Effects in Electron Beams and Their Reduction by Positive Ion Trapping", Jour. Appl. Phys., Vol. 21, No. 11, p. 1088, Nov. 1950.

8. Liebmann, G. and Grad, E.M., "Imaging Properties of a Series of Magnetic Electron Lenses", Proc. Phys. Soc. (London), Vol. 64, Sec. B, Part 11, p. 956, Nov. 1951.

9. Zworykin, V.K., Morton, G.A., Ramberg, E.G., Hillier, J., and Vance, A.W., Electron Optics and the Electron Microscope, p. 614, John Wiley and Sons, Inc., New York, N.Y. 1945.

10. Dolan, W.W. and Dyke, W.P., "Temperature-and-Field Emission of Electrons from Metals", Phys. Rev., Vol. 95, No. 2, p. 327, July 15, 1954.

11. Nottingham, W.B., "Thermionic Emission", Handbuch der Physik, Vol. 21, p. 1, Springer-Verlag, Berlin, 1956.

12. Good, R.H. and Muller, E.W., "Field Emission", Handbuch der Physik, Vol. 21, p. 190, Springer-Verlag, Berlin, 1956.

13. Eyring, C.F., Mackeown, S.C., and Millikan, R.A., "Field Currents from Points", Phys. Rev., Vol. 31, No. 5, p. 900, May 1928.

14. Muller, E.W., "Field Emission and Cathodic Dispersion of Thoriated Tungsten", Z. Physik, Vol. 106, p. 132, 1937.

15. Dyke, W.P. and Dolan, W.W., "Field Emission", Advances in Electronics and Electron Physics, Vol. 8, p. 167, Adademic Press, Inc., New York, N.Y., 1956.

16. Cosslett, V.E. and Haine, M.E., Proc. International Conf. on Electron Microscopy, London, P. 639, 1954.

17. Steigerwald, K.H., "Ein Neuartiges Strahlerzeugungs-System fur Elektronenmikroskope", Optik, Vol. 5, p. 469, Nov.-Dec. 1949.

18. Braucks, F.W., "Untersuchungen an der Fernfokuskathode Nach Steigerwald", Optik, Vol. 15, p. 242, April 1958.

19. Bricka, M. and Bruck, H., "Sur Un Nouveau Canon Electronique Pour Tubes A Haute Tension", Annales Radioelectricite, Vol. 3, p. 339, Oct. 1948.

20. Borries, B. V., "Die Energetischen Daten Und Grenzen Der Ubermikroskopie", Optik, Vol. 3, p. 389, July-Aug. 1948.

21. Dosse, J., "Theoretical and Experimental Investigations of Electron Emitters", Z. Physik, Vol. 115, p. 530, 1940.

22. Haine, M.E. and Einstein, P.A., "Characteristics of the Hot Cathode Electron Microscope Gun", Brit. Jour. Appl. Phys., Vol. 3, p. 40, Feb. 1952.

23. Maloof, S.R., "Growth of Tungsten Single Crystals by the Strain-Anneal Method Using Electron-Beam Heating", Proc. 4th Symp. Electron Beam Technology, Boston, P. 190, March 1962.

24. Glaser, W., Grundlagen der Elektronenoptik, Springer-Verlag, Wien, 1952. See Equation (143.6), page 285.

THEORETICAL ASPECTS OF A HIGH RESOLUTION, LOW VOLTAGE, ELECTRON OPTICAL SYSTEM

BY

J. W. Griffith
Research Director

J. C. Mutton
Electronic Supervisor

W. Mason
Physicist

L. J. Abney
Electronic Engineer

ELECTRO-GLASS LABORATORIES, INC.

BEAVERTON, OREGON

THEORETICAL ASPECTS OF A HIGH RESOLUTION, LOW VOLTAGE, ELECTRON OPTICAL SYSTEM

A requirement arose calling for the design and construction of a facility for evaluating the resolution and other characteristics of phosphor-fiber optics systems. The facility consisted of a demountable cathode ray tube with a gun projecting a 5 micron diameter spot upon a phosphor carried on a fiber optical panel. It was necessary to deflect the spot over the entire area of the phosphor in a raster pattern capable of being reduced to 100 line pairs per mm. The demountable cathode ray tube consisted of a bell jar and an ultrahigh vacuum ionization pumping system bakeable to 400° C.

Electronic considerations for providing the proper presentation include a stable step generator, a precise sweep circuit and a beam wobulator. The combination enables the investigator to select a raster of any number of lines up to 128 with uniform light to dark spaces with uniform illumination over the entire line width. The system is sufficiently stable to be able to see the jitter in a Tektronix oscilloscope.

The step generator (Fig. 1) consists of multivibrator adding circuits with proper digital feedback to provide stopping the count at any point up to 127. Extra care was used in selection of components so that uniform steps resulted. Fairly large voltage steps were used so that stability of voltage comparitors was ensured. Precision attenuators, fully compensated for the frequency band pass, provide the operator with the opportunity of squeezing the raster to 127 lines per mm with equal light and dark spaces.

The step generator is triggered and synchronized with the sweep circuit. A multivibrator is used as a stable rate generator. The output is fed into shaping circuits which provide exceedingly linear voltage versus time changes. The linear sweep signal is fed into a precision differential amplifier and into an amplifier-attenuator circuit before driving the deflection plates of the demountable CRT.

To maintain uniform light and dark spaces in the presentation with the 5 micron spot, it is necessary to wobulate the beam an amount which is inversely proportional to the number of lines. This is done by a precision high frequency wobulator feeding the deflection

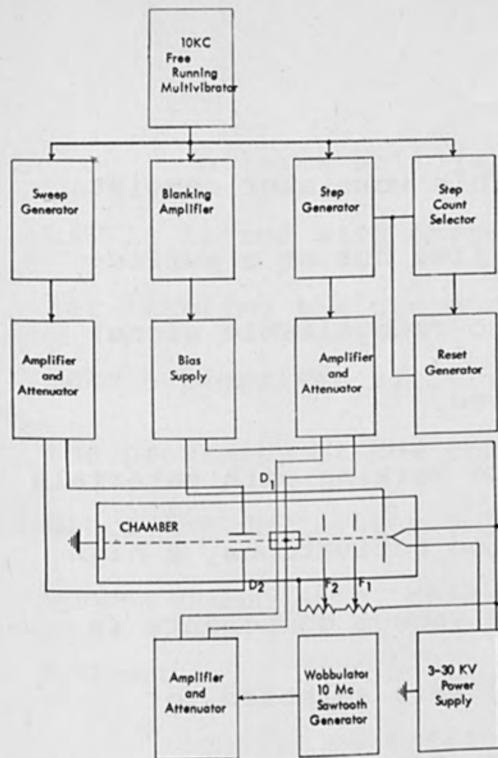

Figure 1 Circuit Block Diagram

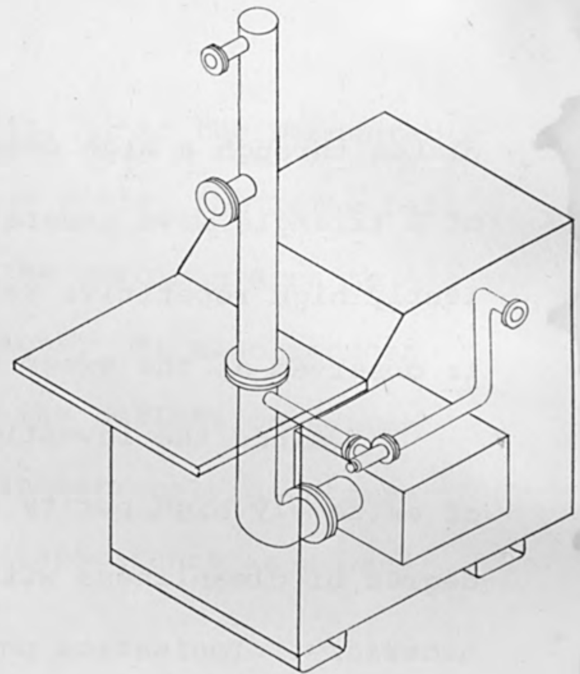

Figure 2 Vacuum Pumping System

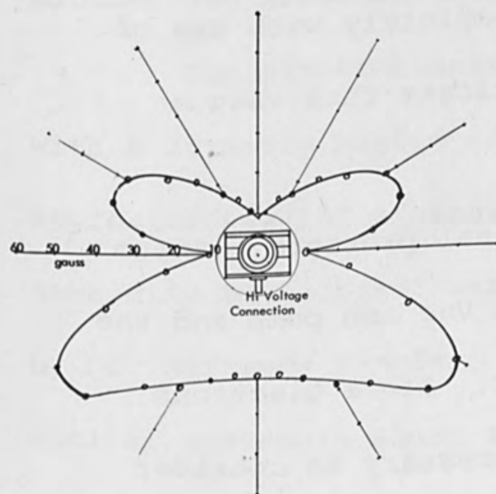

125 l/s Vaclon Pump
On horizontal plane through the center of pump. Field strength on 10 3/8" radius from center.

Figure 3 Stray Magnetic Field Plot

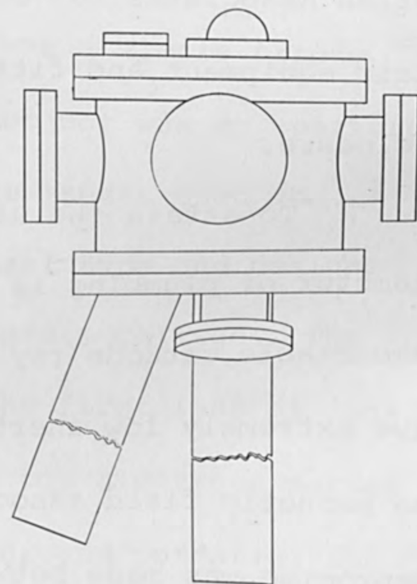

Figure 4 Bell Jar

plates through a high pass filter. This wobulator consists of a triangle wave generator running free but at a sufficiently high repetitive rate so that no recognizable signal is observed at the sweep rates involved.

Since the investigator will be working with materials of extremely high purity and controlled activations, a high degree of cleanliness with vapor-free vacuum components is necessary. Ionization pumps (Fig. 2) were selected for this purpose with roughing pumps of a cryostatic type. Since the entire system is to be baked, stainless steel vacuum plumbing with copper compression gaskets are used. Varian Associates has co-operated completely with use of their equipment and fittings to fabricate this vacuum enclosure.

To attain the ultimate in final pressure, maxium diameter of plumbing is used between Vac ion pump and the demountable cathode ray tube chamber. Since electrons have extremely low inertia, it is necessary to consider the magnetic field associated with the vacuum pump. A compromise was made between the distance between the pump and the chamber and the magnetic field. Fortunately, the vacuum pump has a node in its field[1] (Fig. 3). The pump is placed in an optimum position for use in this system.

A large bell jar portion (Fig. 4) to the demountable CRT is fitted with copper compression seals, the large bell jar enabling the operator to reach the specimen area to make appropriate electrical connections. It also reduces the proximity of the enclosure from the deflection system. Since the deflection voltages contain extremely high frequency components, this decrease in capacitance is advantageous.

Quartz to metal seals for optically flat quartz windows enable the investigator to make spectral measurements over a large portion of the light spectrum. These windows are arranged so that light pumping can be attempted.

The electron source, or gun, was a simple triode with a directly heated cathode. The object was an aperture approximately 100 microns square. The lenses used to demagnify this object were of the Einzel type and designed by Dr. Gertrude Rempfer, of Portland State College. The optical system is shown in Fig. 5. The first lens or condenser is just below the grid and its top electrode serves as the anode. This electrode was at ground potential and the entire gun, power supplies and all, were elevated to 30,000 volts. The condenser converges the beam through the aperture and onto the second or objective lens. This

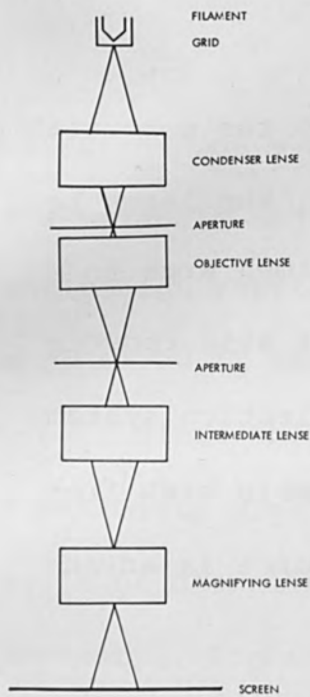

Figure 5 Optical System

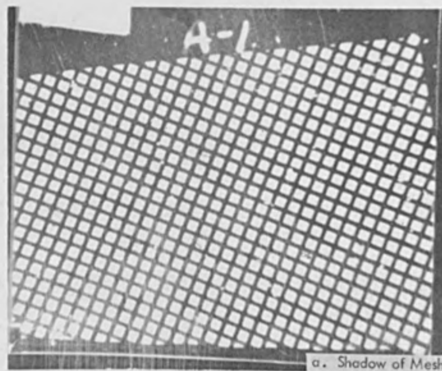

a. Shadow of Mesh

b. Enlarged Spot

Figure 6 Spot Size Determination

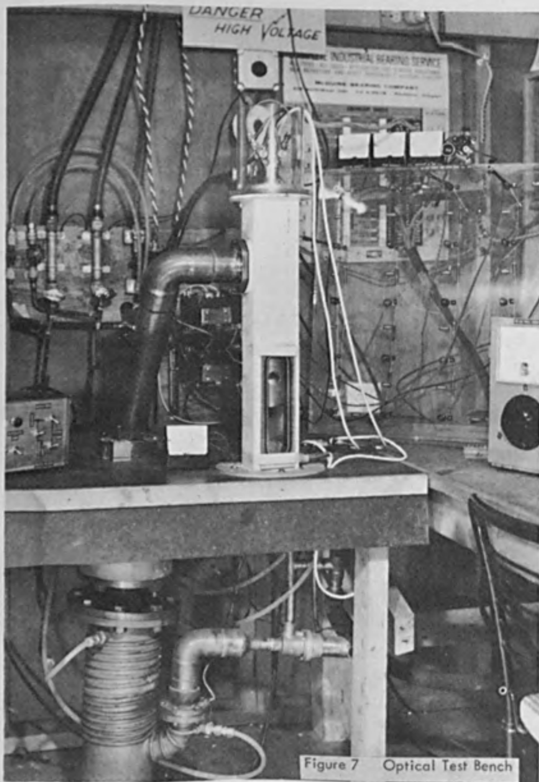

Figure 7 Optical Test Bench

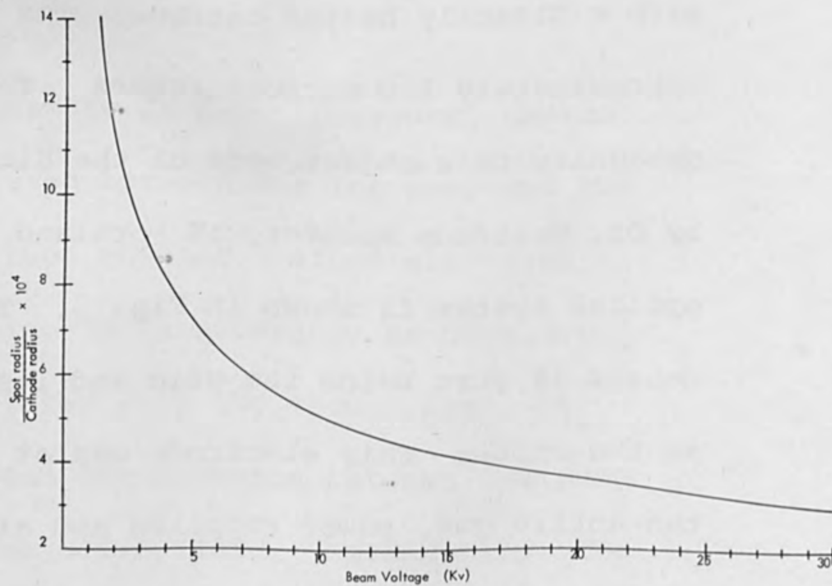

Figure 8 Image Radius Curve

aperture is outside the focal length of the objective lens and thus is demagnified. The focal point of this lens is approximately one-half centimeter from the top electrode. The third, or projector, lens projects the image formed by the objective onto the specimen.

In order to evaluate the image formed by the first three lenses, a fourth, or magnifying, lens was added. On the top electrode of this lens, a 1,000 mesh screen was placed and the spot projected in the plane of this screen. Two photographs (Fig. 6) were then made; one with the projector lens defocused to illuminate the whole mesh and the other with the spot focused. The magnifying lens power was not changed, and it magnified the mesh and spot by the same amount. The photographs could then be compared and the size of the spot determined. The second aperture in the figure was used to reduce the effective aperture of the objective lens, thus reducing to a minimum the spherical aberration with this configuration. The spot size was limited to 7.5 microns in the test facility (Fig. 7) because it was not possible to increase the distance between the first aperture and objective lens. Spot sizes from two to three orders of magnitude smaller are attainable with systems of this type and are employed in the final device.

With the requirement for such a small spot to be generated with an electrostatic optical system, space charge and aberration conditions had to be investigated. Spherical aberrations are of little consequence because they are proportional to the third power of the half angle of convergence.

Using the well known formule[2] for the circle of least confusion

$$r_{ic} = \frac{C \alpha^3 f}{4} \quad \text{where}$$

r_{ic} = circle of least confusion

C = spherical aberration constant

α = half angle of convergence, of the order of 10^{-3} radians

f = focal length of lens, of the order of 20 centimeters,

it is found that even allowing C to go as high as 20, the circle of least confusion will be on the order of 10^{-9} centimeters. This shows that lens aberration of a spherical nature is no problem.

The spot size is also limited by the distribution of velocities of electrons emitted by the cathode. With the ratio of cathode image radius to cathode emission radium small, the familiar Langmuir relation holds.

$$\frac{J_m}{J_o} = \left(1 + \frac{eV}{kT}\right) \sin^2 \alpha, \text{ where}$$

J_m = maximum current density

J_o = cathode emission current density

e = electronic charge

k = Boltzmann's constant

T = temperature

α = half angle of convergence

V = accelerating voltage.

Assuming uniform current density and 100 percent efficiency of the optical system, it is possible to solve for the ratio of image radius to cathode emission radius. A plot of this ratio vs accelerating potential is shown in Fig. 8. It may be seen from this curve that over the voltage range used, the worst condition is at 3 KV and even there, a cathode diameter of one-half contimeter would produce a 5 micron spot.

It is intuitive and has been calculated that with the small current densities involved, space charge limitation of spot size is not a great factor.

To produce a demountable ultrahigh vacuum cathode ray tube, an electrostatic optical system was used to withstand baking temperatures. Ion pumping system and metal compression gaskets aided in obtaining the low

ultimate pressures. A raster generator of great stability was coupled to an electrostatic deflection system to present 100 line pairs per mm with the 5 micron spot projected from the electron gun.

Appreciation is expressed for the work of Y. S. Lee, C. Haase and Charlot Benedict. The patient consideration and aid of E. G. Burroughs and W. Liebson of Ft. Belvoir is also appreciated.

REFERENCES

(1) Varian Associates, private communication.

(2) Zworykin, Morton, et al, "Electron Optics and the Electron Microscope," J. Wiley & Sons, N.Y., 1948, p. 205 & following.

General

(3) Spangenberg, K., "Vacuum Tubes," McGraw Hill Book Co., 1948.

ON THE SUPPRESSION OF GAS DISCHARGES BY AN ADDITIONAL ELECTRODE

Michael Doctoroff
Sylvania Electronic Systems
A division of
Sylvania Electric Products Inc.
100 First Avenue
Waltham 54, Massachusetts

Abstract

In electron beam welding and evaporation processes, gas is frequently liberated from bombarded materials, giving rise to disruptive electric discharges. In the past, differential pumping of the electron gun has been used to overcome the discharge problem by providing a high vacuum ambient around the electron gun. In this paper, a second, low-cost, more compact and versatile method for suppressing high voltage gas discharges is discussed. In order to suppress the discharges simply and economically, a ground shield has been placed concentrically around the high voltages of the electron optical system. Townsend theory predicts that as the product of pressure and distance between the high voltage electrodes and ground decreases, the voltage necessary to cause a discharge goes through a minimum and then increases for smaller pressure-distance products. Hence, for a given operating pressure, the ground shield electrode increases the upper limit of operating voltage. Data is presented which describes the operation of the electron guns at pressures between 10^{-5} and 10^{-3}mm Hg. Special emphasis is given to the characteristics of guns employing the ground shield electrode which shows that this inexpensive additional electrode enables trouble free electron gun evaporation in the 10^{-3} mm Hg. range.

ON THE SUPPRESSION OF GAS DISCHARGES BY AN ADDITIONAL ELECTRODE

INTRODUCTION

Operation of an electron gun becomes difficult at pressures above 5×10^{-4} mm Hg due to gas discharges produced by high voltages. We have found that these gas discharges can be suppressed during electron gun operation by placing a ground shield around the high voltage members of the electron-optical system. In our laboratory such a ground shield, positioned close to electron beam guns has permitted controlled operation at pressures above 8×10^{-3} mm Hg. Basically, this ground shield consists of an open ended cylinder which has been placed concentrically around the high voltage electrodes of the electron gun to form a critical annular separation. Employing this ground shield, power densities high enough to evaporate carbon can be attained at 10^{-3} mm Hg.

The ground shield concept has been discussed by Holland[1] in his work on suppressing extraneous discharges during sputtering. The basic phenomenon was observed experimentally by Paschen[2], and treated theoretically by Townsend[3]. Holland has shown that discharges around the high voltage wire of a sputtering system are suppressed by surrounding the wire with a ground shield. In sputtering this is a useful tool in directing and controlling the gas discharge. The ground shield suitable for use with electron guns is a direct extrapolation of the shielding used in sputtering.

---

1. Holland, L. Vacuum Deposition of Thin Films, John Wiley and Sons, N.Y. 1956, p. 90

2. Loeb, L.B. Fundamental Processes of Electrical Discharges in Gases, J. Wiley, 1938.

3. Townsend, J.S. Electronics in Gases, Hutchinson, 1948

In electron gun operation it is the gaseous discharges due to gas bursts from the source that are troublesome. Gas bursts emanating from an electron beam heated target limit the rate at which evaporation, heating, and welding may be performed, and in addition, they cause uncontrollable variations of some of the operational parameters. At the Sylvania Microelectronics Laboratory, gaseous discharges present an acute problem since much of our work is done in the 10^{-4} and 10^{-3} mm Hg. range. Although this pressure range is beyond the range of usefullness recommended by most gun manufacturers, the electron gun evaporation technique is preferred for its versatility. Therefore methods have been sought to operate electron guns at the higher pressures.

A brief description of the Sylvania approach to microelectronics will explain our need to evaporate at elevated pressures. In the Sylvania microelectronics approach, resistor, semiconductor and dielectric thin films are prepared by vacuum evaporation in high (7×10^{-4} mm Hg.) oxygen partial pressures. In this system, the evaporant is a metal such as titanium, and the composition of the deposit is varied from titanium metal to titanium dioxide by changing the partial pressure of oxygen during deposition. In the development of a machine for the production of microcircuits, Sylvania foresees a system whereby complete circuits are fabricated by changing the mask configuration and oxygen partial pressures. As a result, it has been necessary to demonstrate the feasibility of continuously operating electron guns at 10^{-3} mm Hg. without electrical breakdown.

In the following text, the structure of the ground shield will be described, pertinent theory will be reviewed, and results will be shown to illustrate the usefullness of the ground shield in electron gun operations at 10^{-3} mm Hg.

DESCRIPTION OF THE GROUND SHIELD:

It has been stated that the ground shield consists of an open ended hollow cylinder positioned around the high voltage electrodes to form a critical annular separation. Figure 1 shows a schematic diagram of this device. The shield is shown surrounding both the high voltage lead-in wires and the high voltage electrodes. It is necessary that every high voltage member be surrounded with a ground shield.

This shield has been arranged so that it can be removed in order to change the gun filaments. In this design, the shield around the bias cup can be lifted over the upper ground shield surrounding the high voltage wires, and in this way access to the filament is gained. Maximum spacing between the high voltage and ground is shown to be about 4 cm. This dimension is not critical when operating at 10^{-3} mm Hg., and as a result it has been made comfortably large. Theoretical considerations will show that best results for effective discharge resistance at the elevated pressures are obtained when the ground to high voltage distance is minimized.

Figure 2 is a picture of one commercially available electron gun mounted in a 30" diameter tank evaporator. Figure 3 is a close-up picture

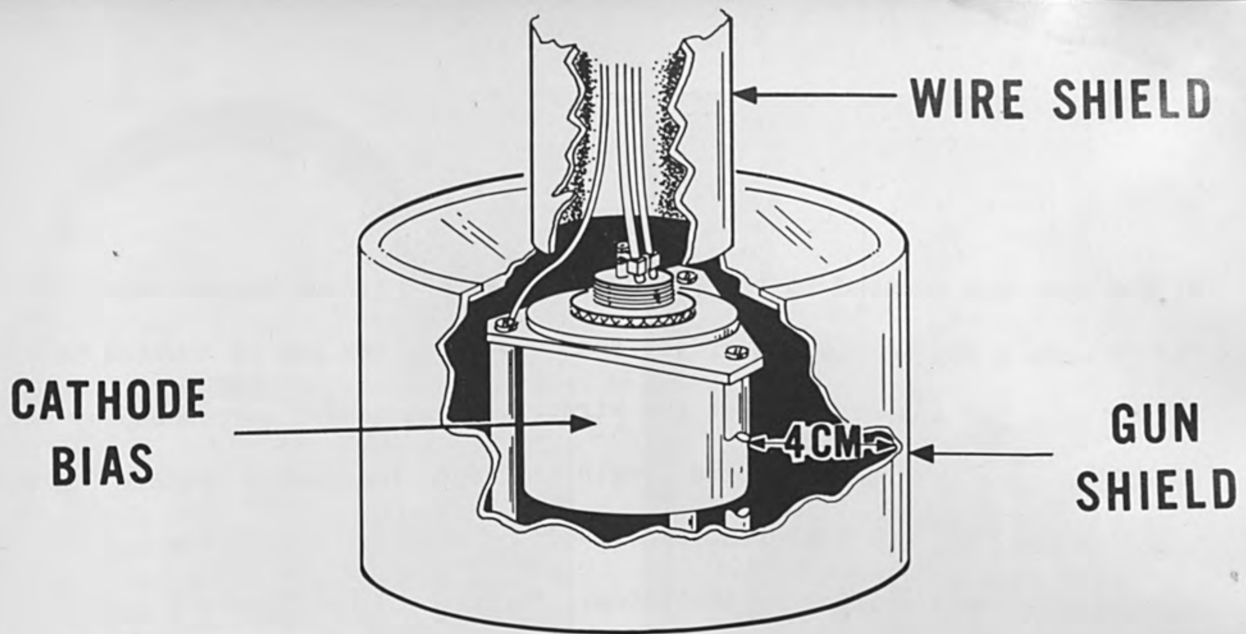

Figure 1 - Schematic diagram of the ground shield surrounding an electron gun.

Figure 2 - A commercial electron gun suspended vertically in a vacuum evaporator.

of the same gun mounted in the evaporator with the ground shield added. Figure 4 is a second picture of the same gun where the gun is mounted in an 18" bell jar and, to protect the wires, they have been surrounded by waveguide tube over their entire length inside of the vacuum system. Note that the only way the evaporant can reach the high voltage electrodes is through the small orifice in the anode. Figure 5 illustrates a second commercially available electron gun. Because of the design of this gun, the only shielding required is that around the high voltage lead-in wires; in this case, the shielding is a copper mesh. Where structural support is not required, this type arrangement is recommended for mechanical simplicity and high pumping conductance. How this ground shield works will be clarified in the following section.

THEORY:

In the discharge process, it is within the cathode dark space that electrons are accelerated enough to produce positive ions on collision with gas molecules. If the anode is moved to within the cathode dark space, the discharge can not exist. The interrelationship between the pressure (p), the distance between electrodes (d), and the voltage (V_s), at which breakdown occurs was summarized by Paschen who observed experimentally that when the length of a discharge gap and the gas pressure are altered so their product remains unchanged, the magnitude of the breakdown voltage remains constant.

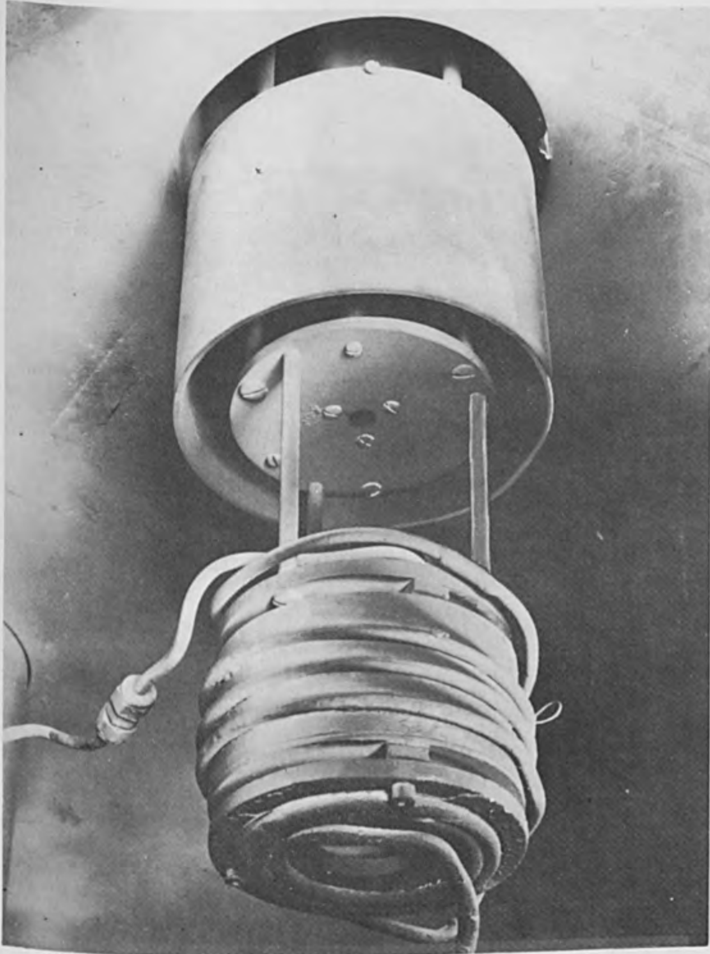

Figure 3 - Detail picture showing electron gun with ground shield.

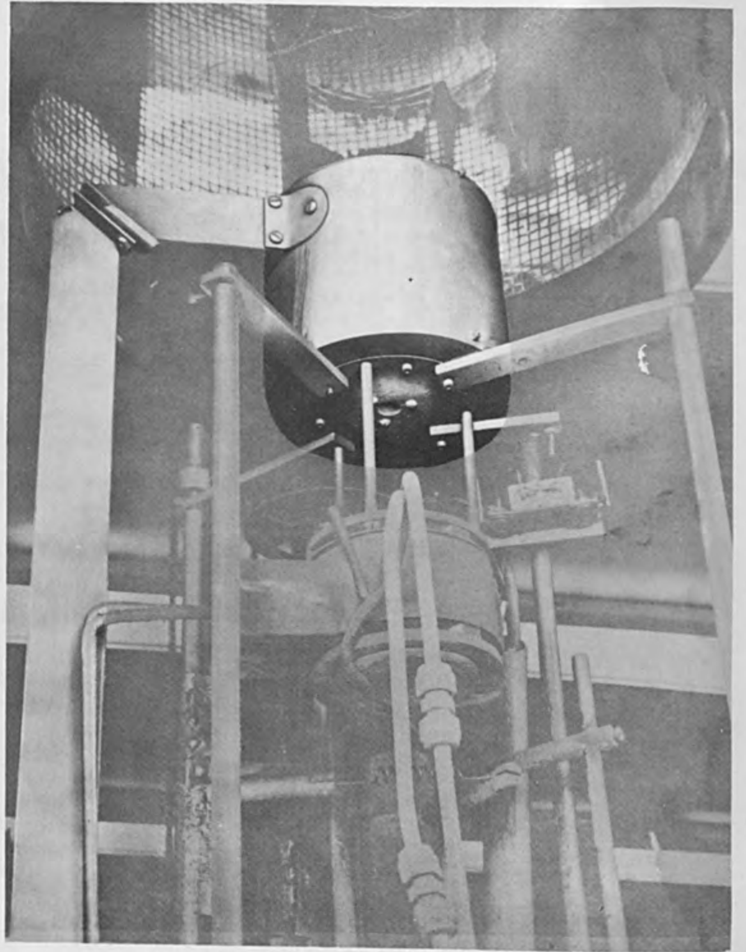

Figure 4 - Use of ground shield with an electron gun which has been mounted from the evaporator base plate.

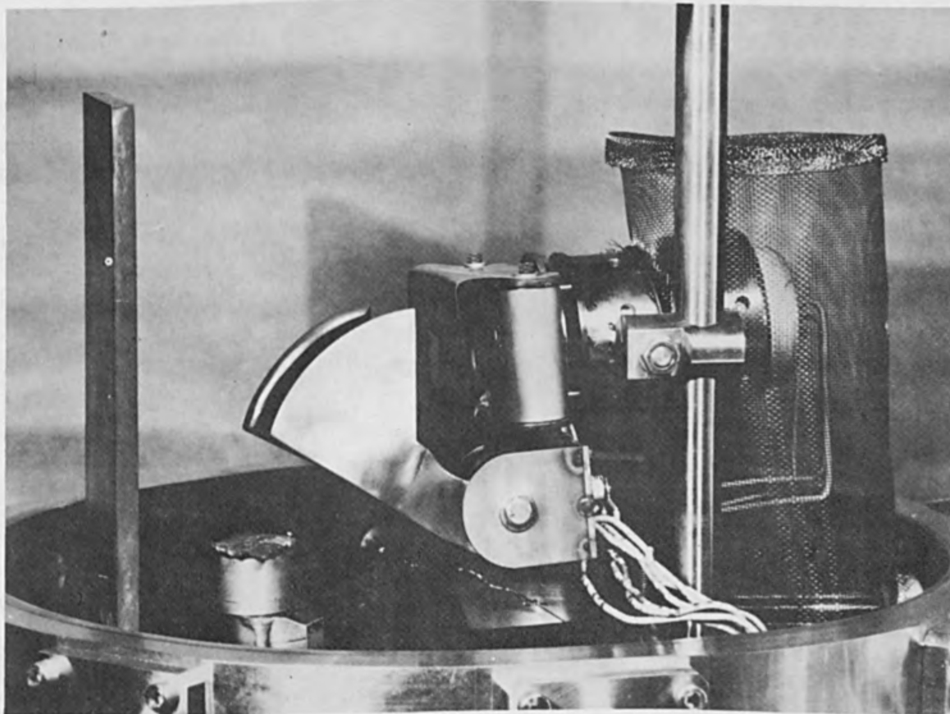

Figure 5 - A second type of commercial electron gun with ground shield.

Paschen's Law can be explained from the fact that the number of molecules in the discharge gap is proportional to the pd product. According to the classical picture of ionization by electron bombardment, an electron must have an energy within specific limits to have the highest probability of ionizing a gas molecule. Because an electron is accelerated in moving from the cathode to the anode, there is a finite distance in which ionization can occur. If at a given voltage, the distance between electrodes is increased, the space in which effective ionization can occur is also increased. Similarly, an increase in the system pressure will decrease the mean free path of an electron in the gas, and as a result the probability of ionization can be raised. As long as the pd product remains unchanged, the number of molecules in the discharge gap remains fixed, and as a result the voltage at which ionization and breakdown occur does not change.

Figure 6 shows a family of curves for different gases relating the breakdown voltage with the pd product. This data has been prepared from that presented by Von Engel.[4] In this data, it was assumed that breakdown occurs when the current multiplication becomes infinite, and no foreign agency is necessary to produce an initial electron.

The existence of minima in these pd vs. V_s curves can be explained. Consider the case in which d is constant. At low pressures the mean

---

4. Von Engel, A. Ionized Gases, Oxford at the Clarendon Press, 1955

free path is large and few electrons cause ionization before striking the anode. In order to have a discharge at low pressures, the voltage must be increased so that more ionization will occur before the electrons strike the anode. At high pressures, the mean free path is small, and few electrons acquire sufficient energy to ionize. In order to produce enough ionization in the gap, the voltage must be increased as the pressure is increased. Therefore, a minimum sparking potential will occur at intermediary pd spacings.

In Figure 1, it was shown that a gap distance of 4 cm had been selected for working at pressures of 10^{-3} mm Hg. cm. In this case, the pd product is approximately 10^{-2} mm Hg. cm. Therefore, the device is effective because it is based on the left hand side of the curve before the minima, where decreasing distances give higher breakdown resistance. Some results obtained by Quinn[5] for the breakdown of a 1.7 cm gap in several gases are shown in Figure 7. Data in this region is difficult to obtain since if a longer alternative discharge path is available, the discharge will follow the longer path. Quinn overcame the problem of longer alternative discharge paths by selecting electrodes which consisted of two coaxial nickel cylinders with hemispherical ends. Cerwin[6] (Figure 8) investigated the breakdown voltage curves in air as a function of gas pressure for different gap lengths. The dotted vertical line at 10^{-1} mm Hg.

---

5. Quinn, R. B. Phys. Rev. 55, 1939, p. 482.
6. Cerwin, S. S. Phys. Rev. 46, 1934, p. 1054.

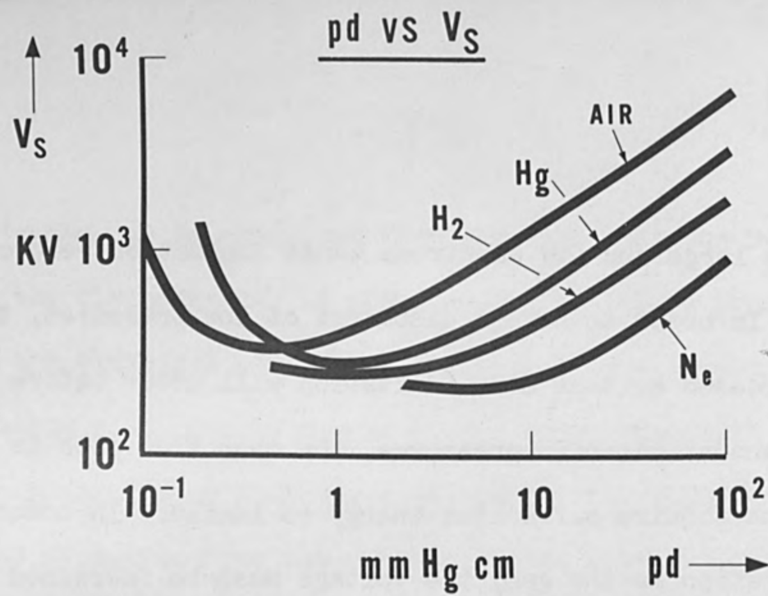

Figure 6 - Curves showing the breakdown voltage as a function of the pressure distance product for various gases.

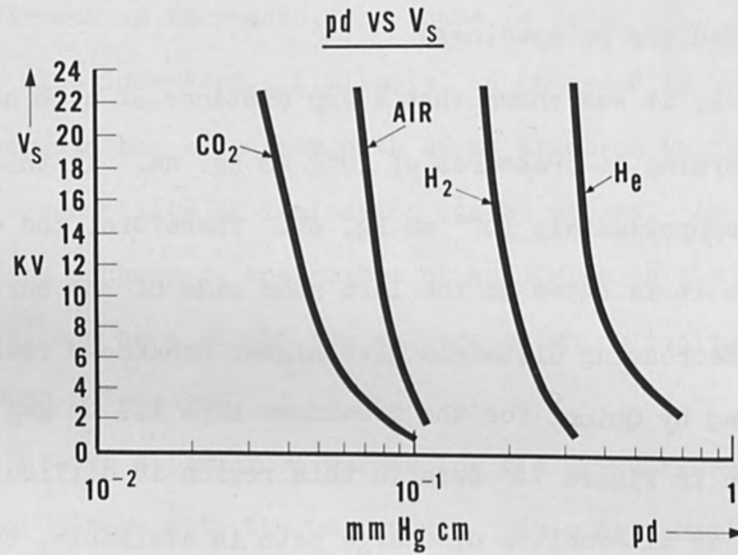

Figure 7 - Curves showing the breakdown voltage as a function of the pressure distance for various gases at low pressure-distance values.

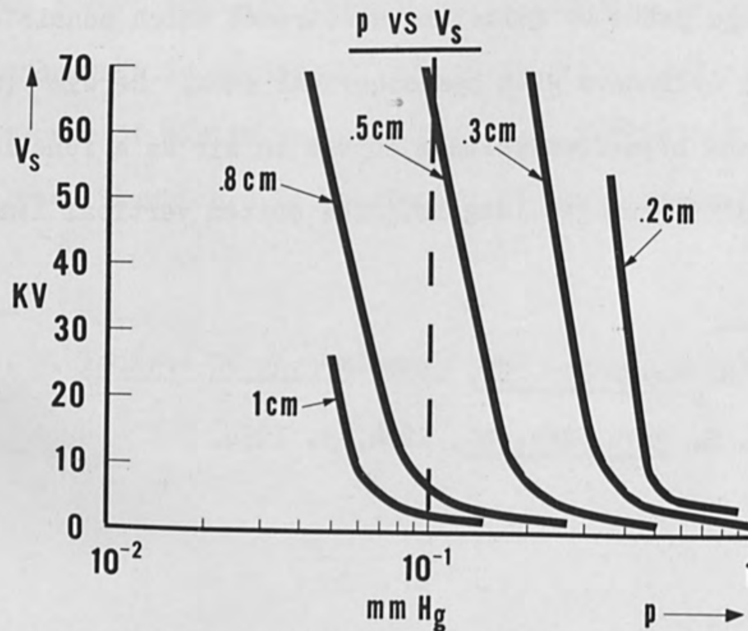

Figure 8 - Breakdown voltage curves in air as a function of gas pressure for different gap lengths.

indicates that the voltage can be increased by decreasing the gap length. A gap of .5 cm at a pressure 10^{-1} mm Hg. sparks at over 60 KV. Doubling the gap length allows discharges at voltages less than 10 KV.

Gaseous discharge theory has been treated by Townsend.[7] According to Townsend, the current i flowing between parallel plates on an applied voltage is given by:

$$i = i_o e^{\alpha d} \tag{1}$$

where i_o is the initial current which corresponds to photocurrents at the cathode, α is the number of electrons produced by one electron in a path of 1 cm., and d is the gap length in cm.

In this expression, the term α is referred to as Townsend's First Ionization Coefficient. Townsend's Second Ionization Coefficient is obtained by considering that secondary electrons are produced at the cathode by positive ion bombardment. Townsend defines γ as the number of electrons formed per incident positive ion. It follows that:

$$i = (i_o + i_+)e^{\alpha d} \tag{2}$$

$$i_+ = \gamma[i - (i_o + i_+)] \tag{3}$$

where i_+ is the number of electrons produced at the cathode by positive ion bombardment. Eliminating i_+ by substituting (2) into (3), one obtains:

$$i = i_o \frac{e^{\alpha d}}{1 - \gamma(e^{\alpha d} - 1)} \tag{4}$$

---

7. Meek, J. M. and Craggs, J. D. Electrical Breakdown of Gases, Oxford Clarendon Press, 1953.

Breakdown will occur when $\gamma e^{\alpha d} = 1$ since at breakdown $e^{\alpha d} \gg 1$.

It can be shown that $\alpha/p = F_1(E/p)$ and $\gamma = F_2(E/p)$. From this it follows that $V_s = f(pd)$.

In the expression $\gamma e^{\alpha d} = 1$, note that the breakdown characteristics are effected by the type of discharge gas and by the type of cathode material. This follows from the fact that α, the number of electrons formed by collision, is a function of the ionization cross section of the gases involved, and γ, the number of secondary electrons formed at the cathode, depends on the work function of the cathode surface. Experimental verification of the effect of the cathode material has been done by Llewellyn Jones and Davies.[8]

RESULTS:

In the system shown in Figure 3, the addition of a ground shield has resulted in increasing the useful range of gun operation by over one order of magnitude. More specifically, an electron gun, operating in a 30" diameter vacuum system could not be operated without erratic breakdown problems at power settings above 10KV and 150 ma when the system pressure was greater than 5×10^{-4} mm Hg. The addition of a ground shield around this gun has made possible electron gun operation at pressures as high as 3×10^{-3} mm Hg. with the gun being operated at 10KV and 150 ma. In these

---

8. Llewellyn Jones, F. and Davies, D. E. Proc, Phys. Soc. B, 64, 397, 1951

experiments, the limit was set by our inability to monitor higher pressures with a Bayard-Alpert ionization gauge. In the system shown in Figure 5, the gun was not recommended by its manufacturers for use at pressures above 5×10^{-4} mm Hg. due to gaseous discharge problems. With the addition of a ground shield around the high voltage wires, the range of operation of this electron gun was increased as follows. In oxygen, the range could be extended to 5×10^{-3} mm Hg., and with air, the range could be extended to 8×10^{-3} mm Hg. while operating at 13KV and 150 Ma. In this work the evaporations were performed on titanium bar stock in a standard 18" x 30" bell jar, and the pressure was monitored with a Hastings thermocouple gauge.

Filament lifetimes for electron guns operating in such a system have been measured. The filament lifetime at pressures as high as 1×10^{-3} is several hours with some standard electron gun filaments. This time is sufficient for many evaporation cycles. In our experimentation, in order to prolong the lifetime of the filaments, the filament heater current was gradually reduced as the filament aged, but at all times the filament was operated space charge limited.

The relatively short filament lifetime is not a problem for two reasons. First, a filament can be chosen which will not burn out rapidly at the increased pressures, and secondly, due to the simplicity of the system, the filament can be changed in less than two minutes.

To change the filament in this time demands that the filament be changed during that part of the evaporation cycle when the vacuum chamber is open to the atmosphere. It is not difficult to predict when to change the filament since the remaining filament life can be estimated with some accuracy by intermittently noting the filament current necessary for space charge limitation.

It has been noted that space charge effects of the ionized ambient gases at the elevated pressures result in an ability to draw greater electron currents from the cathode. This increased current can be controlled by increasing the negative potential on the cathode bias. By utilizing this space charge neutralization, it has been possible to heat more efficiently at the elevated pressures than at the low pressures.

Finally it has been observed that cathode sputtering is undetectable by X-ray analysis of deposited films and by visual observation of the cathode bias after over 100 hours of operation. It was suspected initially that cathodic sputtering might be a problem due to the high pressures and voltages associated with the process.

CONCLUSIONS

In conclusion, it has been shown that the addition of a ground shield to the electron gun system has enabled operation at pressures as high as 8×10^{-3} mm Hg. It has been shown that the distance between shielding and high voltage should be held to a minimum for the effective elimination of gas discharges. The maximum pressures attained without discharges are a

function of the type of gas, the nature of the cathode material, and the operating voltage of the electron gun.

Also, it has been shown that filament lifetimes during gun operation at these pressures are sufficiently long so that many evaporations may be performed with each filament. In essence, employing this technique provides a simple and economical method for extending the range of operation of electron guns by the elimination of gas discharges.

For these reasons, the ground shield can be a useful tool for replacing differential pumping in many situations where moderate to high gas pressures are involved.

ACKNOWLEDGEMENTS

The author wishes to acknowledge Dr. Gene Mannella and Mr. William MacDonald for their numerous discussions regarding this presentation. Thanks are also due to Mr. Guy Indelicato for his assistance in much of the experimental work.

The work reported in this paper was funded by Sylvania Electric Products, a subsidiary of General Telephone and Electronics Corporation.

THE TEMPERATURE DISTRIBUTIONS IN THIN FOIL AND SEMI-INFINITE TARGETS BOMBARDED BY AN ELECTRON BEAM

by

L. G. Pittaway
Physicist
Mullard Research Laboratories
Redhill, Surrey,
England.

ABSTRACT

The equations describing the temperature distributions, produced by surface heating, in the target of an electron beam machine are developed from the general heat flow equation. Thin foil and semi-infinite targets are considered for both stationary and scanning beams, the radial intensity variation of which obeys the Gaussian distribution law. The energy of the beam is assumed to be absorbed in the surface of the target and no account is taken of electron penetration or scattering, or of any change of state of the target material.

The equations thus derived are solved in a general manner and graphs are given of the results. These are applicable to any combination of target material and beam parameters. The general form of the presentation makes the graphs suitable for use in problems other than that for which they were originally prepared.

THE TEMPERATURE DISTRIBUTIONS IN THIN FOIL AND SEMI-INFINITE TARGETS BOMBARDED BY AN ELECTRON BEAM

1. INTRODUCTION

In the process known as Electron Beam Machining the source of heat is best applied to the work-piece, or target, in one of two ways; firstly, by means of a succession of very short high energy pulses at one point on the target, or secondly, by a continuous beam which scans the surface of the target at a constant velocity. Whichever of these methods is used, it is essential in most cases that the heating time at any one point be short so that the temperature rise of the target is confined to the area which is being machined, otherwise the precision and usefulness of the process cannot be employed to its full advantage.

During the application ofshort pulses of energy, having a duration of only a few microseconds or less, the temperature of the target at the point of incidence of the beam, which we shall call the spot, may well rise to several thousand degrees. Such pulses of heat are too short for an equilibrium state to be reached and it is necessary, therefore, to consider a source of heat which is instantaneously applied at time $t = 0$ and then remains constant in magnitude until the beam is switched off. If the beam is switched off at time $t = t_1$ the temperature may be calculated at time $t = t'$, where t' may be greater or less than t_1.

In this paper it will be assumed that the absorption of heat takes place only in the surface of the target, which means that no account will be taken of electron penetration or scattering. This renders the results approximate for an electron beam although they will be correct for a laser beam in which case the energy is absorbed in the

surface. It is assumed that the thermal properties of the target material such as its thermal conductivity, specific heat, etc., are independent of temperature and, furthermore, that no physical change other than a change in temperature occurs in the target. The electron beam will be assumed to have constant total energy and to have a radial distribution of intensity which obeys the Gaussian distribution law. That is to say, the energy density at distance s from the centre is given by Ce^{-s^2/d^2}, where C is a constant and is the maximum value of the energy density, at s = 0, and d is the standard deviation of the distribution.

Equations describing the temperature distribution in a foil, thin enough for the temperature to be uniform throughout its thickness, and also the distribution in the surface plane and in a direction normal to the surface at the spot centre, of a semi-infinite target, are derived, using the solution of the general heat flow equation for an instantaneous point source. In addition, a simple extension to the theory gives these temperature distributions as functions of the time after the beam has been switched off. These equations are developed as special cases of a more general theory, in which the distance of the point at which the temperature is to be determined, from the centre of the spot, is considered as a linear function of time. This general form gives the temperature at a point in the surface plane of the target as the beam moves towards it from an infinite distance, at a constant velocity, and then passes by it at a given distance of closest approach.

The assumption has been made that the only flow of heat from the spot is that conducted through the target material. There will of course

be a certain amount lost by radiation and by conduction and convection to the surrounding medium if the target is not in vacuo but these will normally be negligible. For thin foils, however, this heat loss will be doubled due to the two surfaces involved. In the case of very thin foils the loss may become comparable with the incident energy since the heat required to give a certain temperature rise in the foil is proportional to its thickness. The equations are presented in terms of standardized parameters which allow their application to any target material, provided that the above conditions are satisfied. Results have been computed for a range of values of the parameters, and displayed in graphical form.

Most of the intermediate mathematics relevant to the derivation of the equations has been omitted from this paper and may be found together with a more comprehensive treatment and rather fuller curves in reference (1).

2. THE INSTANTANEOUS POINT SOURCE

The basis of the heat flow equations which are given in the following sections is the solution of the differential equation of heat conduction which describes the temperature distribution produced in an infinite, isotropic solid by an instantaneous point source. The term 'instantaneous pointsource' is used to describe a finite quantity of heat liberated instantaneously at a given point and time in the solid. By integrating the solution for an instantaneous point source with regard to appropriate space and time variables, one can obtain solutions for instantaneous and for continuous sources of any spatial configuration[2]. For instance, integration of the instantaneous point source solution with

respect to time gives the solution for a continuous point source, corresponding to the liberation of heat at a fixed point and at a prescribed rate. If this rate is constant and has continued for a long time, the solution becomes, in the limit, that for a steady point source.

The equation for the temperature distribution due to an instantaneous point source in an infinite solid is

$$T = \frac{Q}{8(\pi kt)^{3/2}} e^{-r^2/4kt} \qquad (1)$$

where,

T = temperature at distance r from the point source

t = time

$k = \frac{K}{pc}$ = thermal diffusivity

K = thermal conductivity

p = density of material

c = specific heat

Q = the strength of the source

Qpc = the amount of energy liberated

In the two dimensional case of a thin foil extending to infinity in the x and y directions and of finite thickness D in the z direction, such that D is small enough for the temperature to be constant throughout the thickness of the foil, the equation for the temperature distribution becomes

$$T = \frac{Q}{4\pi ktD} e^{-r^2/4kt} \qquad (2)$$

3. THE GENERAL EQUATION FOR A MOVING BEAM

In the general equation for a moving beam we require an expression for the temperature at a point in the surface plane of the target while the beam traverses the surface, at constant velocity from infinity in one direction to infinity in the other, passing either through or adjacent to the point of interest. The distribution due to a stationary beam is then a special case of this expression in which the distance of the beam centre from the point remains constant.

3.0 The Moving Beam on a Thin Foil

Consider the temperature at the origin 0 (Figure 1) due to a beam of electrons with a Gaussian intensity distribution, as defined in section 1, incident on the foil with the centre of the spot at C(x,y). The spot moves towards the y-axis along a straight path parallel to the x-axis with a constant velocity v. The co-ordinates of C(x,y) are functions of time t.

Now first of all, we wish to know the temperature at 0 at a time t' due to point sources reaching the foil at time t, where t is less than t'. The t in equation (2) must now be replaced by (t' - t), this being the time interval between the arrival of the point sources and the time at which the temperature is required to be known. The temperature rise at 0 at time t' due to the amount of energy incident at time t over an elemental area δa is first found using equation (2) and this is then integrated with respect to θ and s to cover the whole area of the source.

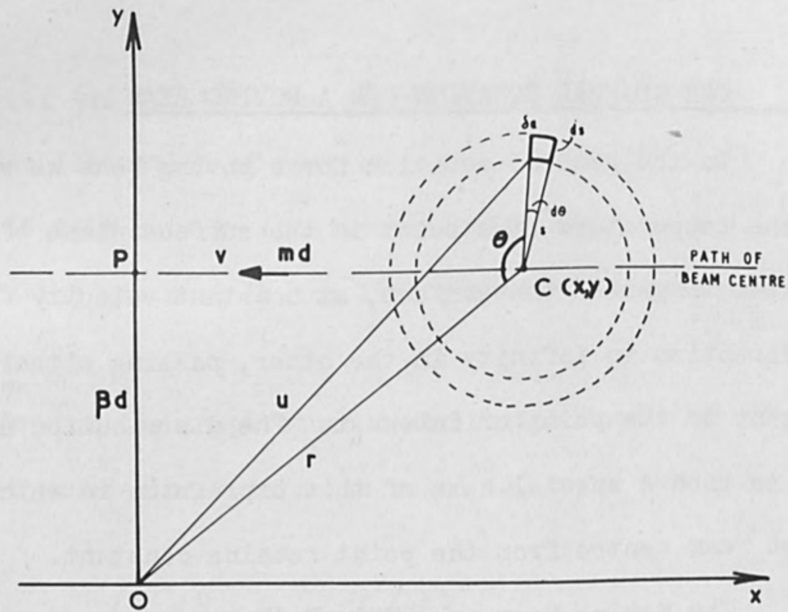

Figure 1 The Moving Beam on the Surface of the Target.

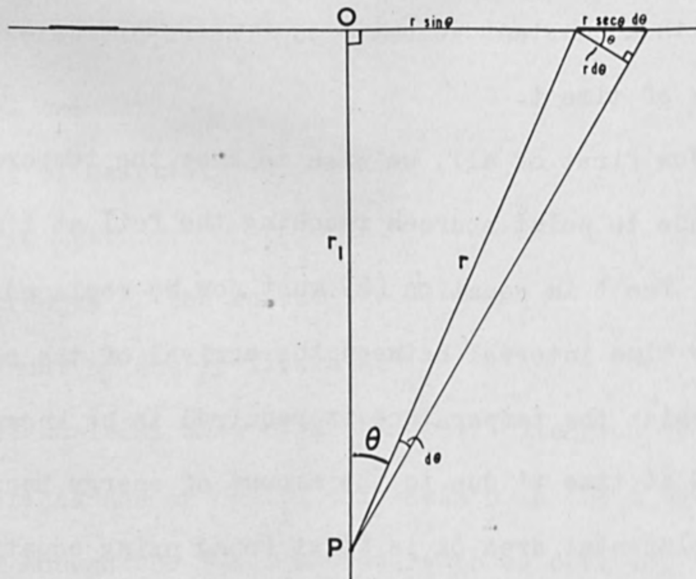

Figure 2 The Temperature Along the Normal to the Surface.

The energy density E(s) at any point distance s from the spot centre is of course a function of s, and is given by

$$E(s) = \frac{E_o \Upsilon}{\pi} e^{-\Upsilon s^2}$$

where d is the standard deviation of the distribution, $\Upsilon = 1/d^2$ and E_o is the total energy liberated by the source per second.

Having found an expression for the temperature rise at 0 at time t' due to the whole source at time t, we now integrate this over the time for which the source is applied, that is from t = 0 to t = t'.

Thus we obtain an expression for the temperature at 0 at time t', which is

$$T = \frac{E_o \Upsilon}{\pi \rho c D} \int_0^{t'} \frac{1}{1 + 4k\Upsilon(t' - t)} \exp\left[\frac{- \Upsilon r^2(t)}{1 + 4k\Upsilon(t' - t)}\right] dt \qquad (3)$$

In order that the final results may be in a more convenient form, we choose the standard deviation d as the unit of length in which to measure the distance of the point from the spot centre.

Let $r^2(t) = x^2(t) + y^2(t)$

then $x(t) = x_o - vt$

and $y(t) = \beta d = \text{constant}$

where β is the distance of the spot centre from the x-axis in units of d and x_o is the value of x when t = 0. For the case of a stationary beam r is independent of t.

3.1 The Moving Beam on a Semi-Infinite Block

In an infinite solid there is no net heat flow across any plane containing the point source, that is to say the heat flows radially outwards from the point source. As the semi-infinite block which we are considering loses no appreciable quantity of heat from its surface, the temperature distribution produced in it by a point source at the surface, of strength Q, will be the same as that produced by a source of strength 2Q in an infinite solid. Hence, if we use a source of strength 2Q in equation (1), where Q is the strength of the source actually applied to the semi-infinite target, and proceed in the same way as in section 3.0 using equation (1) instead of equation (2), then we arrive at the following equation for T, namely

$$T = \frac{E_o \Upsilon}{\pi^{3/2} \rho c} \int_0^{t'} \frac{1}{k^{\frac{1}{2}}(t' - t)^{\frac{1}{2}} \left[1 + 4k\Upsilon(t' - t)\right]} \exp\left[\frac{-\Upsilon r^2(t)}{1 + 4k\Upsilon(t' - t)}\right] dt \quad (4)$$

This equation, which is very similar to equation (3), the corresponding equation for a thin foil, gives the temperature T at the origin O in the surface of a semi-infinite target at time t', due to a continuous Gaussian source moving at a constant velocity v.

4. THE TEMPERATURE DISTRIBUTIONS DUE TO A STATIONARY BEAM

4.0 The Stationary Beam on a Thin Foil

In this instance, we require an expression for the temperature distribution at time t', produced in a foil by a stationary and continuous beam switched on at time t = 0.

We now make r independent of t in equation (3) and use md as the distance r of the spot centre from the point at which the temperature is to be determined. It is convenient to use TKD/E_o which is a dimensionless quantity as a standardized temperature, in order to make the results applicable to any combination of target material and beam parameters.

The parameter $\lambda = k\Upsilon t'$, which is also a dimensionless quantity, will be used for the same reason.

Therefore, if we use these parameters and make the substitution

$$n = \frac{\Upsilon r^2}{1 + 4k\Upsilon(t' - t)}$$

in equation (3) we have

$$\frac{TKD}{E_o} = \frac{1}{4\pi} \int_{\frac{m^2}{1+4\lambda}}^{m^2} \frac{e^{-n}}{n} \, dn \qquad (5)$$

This equation is an expression for the temperature distribution in a thin foil, which is heated by a continuous Gaussian source instantaneously applied at time t = 0, in terms of the parameters $\lambda = k\Upsilon t$ and $m = r/d$. TKD/E_o as a function of m has been computed from this expression for various values of λ and the results are shown in Figure 3.

When r = 0, equation (3) reduces to

$$\frac{TKD}{E_o} = \frac{1}{4\pi} \log_e (1 + 4\lambda) \qquad (6)$$

This equation gives the temperature at the centre of the spot as a function of λ.

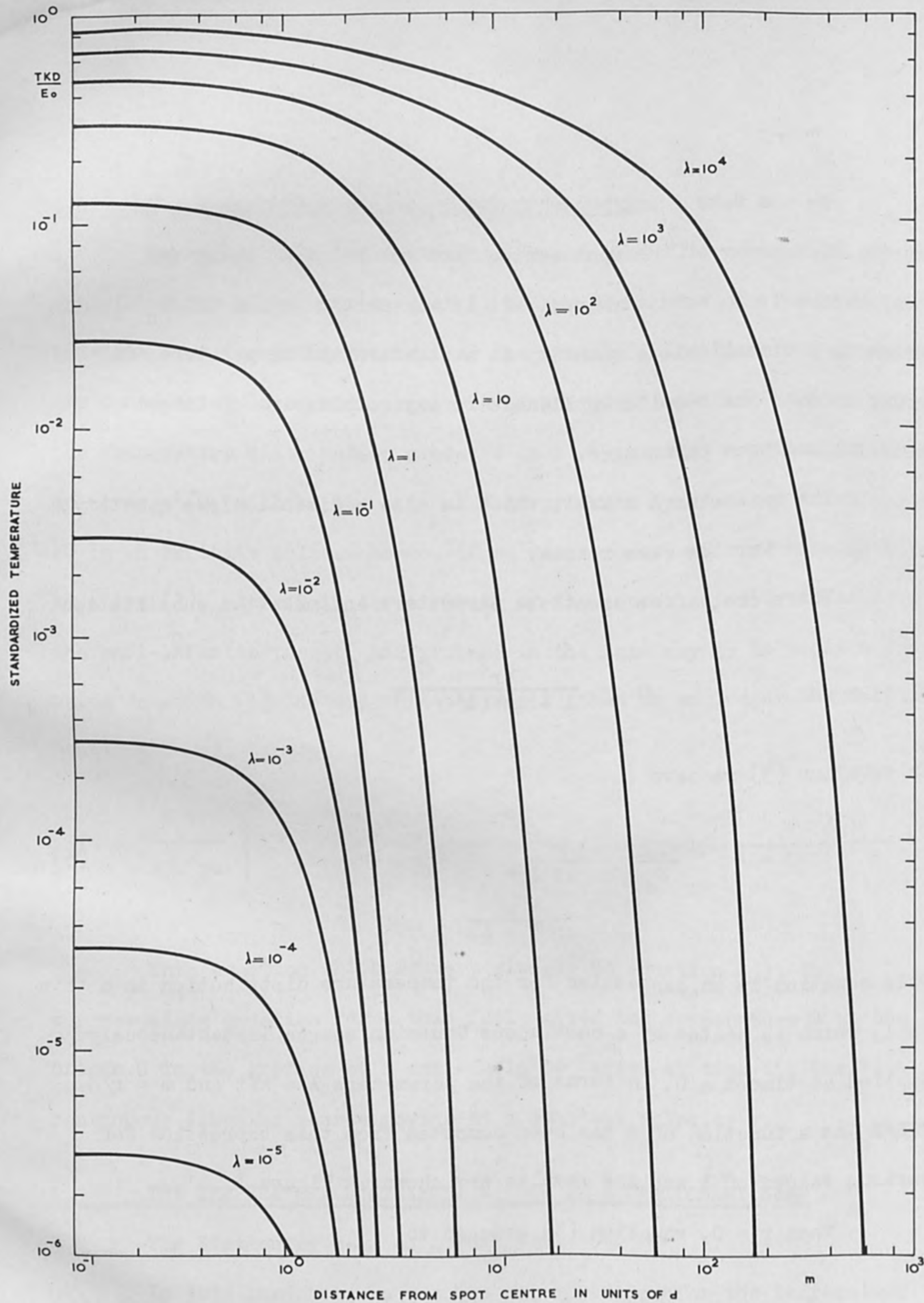

Figure 3 The Temperature Distribution in a Thin Foil due to a Stationary Beam.

4.1 The Cooling of the Thin Foil

The temperature distribution in the foil at time t', when the beam has been switched off at time t_1 ($t_1 < t'$) is found simply by integrating in equation (3), with r constant, between the limits 0 and t_1, instead of 0 and t'.

Equation (5) then becomes

$$\frac{TKD}{E_o} = \frac{1}{4\pi} \int_{\frac{m^2}{1+4\lambda}}^{\frac{m^2}{1+4(\lambda-\lambda_1)}} \frac{e^{-n}}{n} \, dn \qquad (7)$$

where $\lambda_1 = k\Upsilon t_1$

TKD/E_o as a function of m has been computed for several values of λ and curves for four values of λ_1 are shown in Figure 4. The top curve in each case is for $\lambda = \lambda_1$ and gives the temperature distribution at the time when the beam is switched off. When $r = 0$, we have

$$\frac{TKD}{E_o} = \frac{1}{4\pi} \log_e \left[\frac{1 + 4\lambda}{1 + 4(\lambda - \lambda_1)} \right]$$

which gives the temperature at the centre of the spot as the foil cools down. For $\lambda = \lambda_1$ this equation reduces to equation (6).

4.2 The Stationary Beam on a Semi-Infinite Block

For the semi-infinite target we can derive an expression for the temperature distribution in the surface plane at time t', produced by a stationary and continuous Gaussian beam switched on at time $t = 0$.

The procedure is similar to that used in section 4.0 using equation (4) and making the substitution

$$1 + 4k\Upsilon(t' - t) = \operatorname{cosec}^2\eta$$

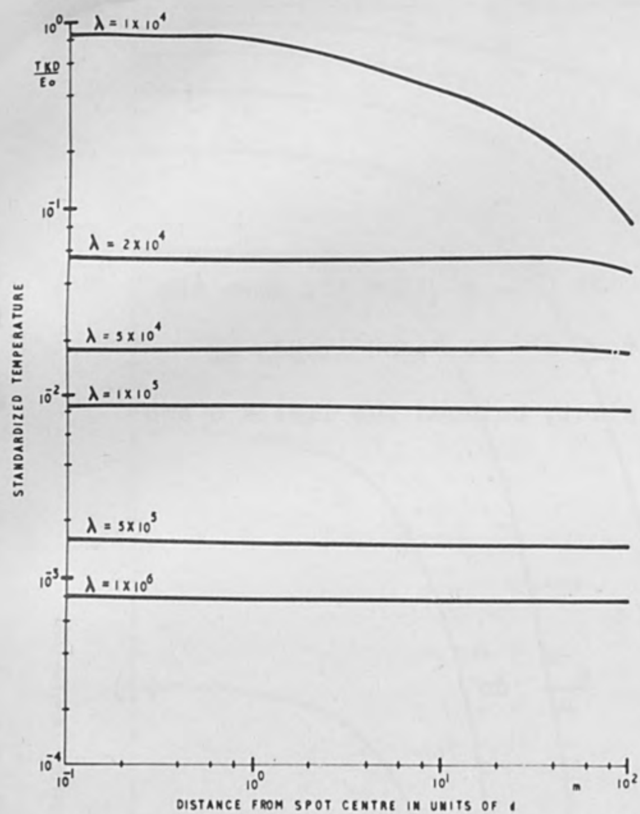

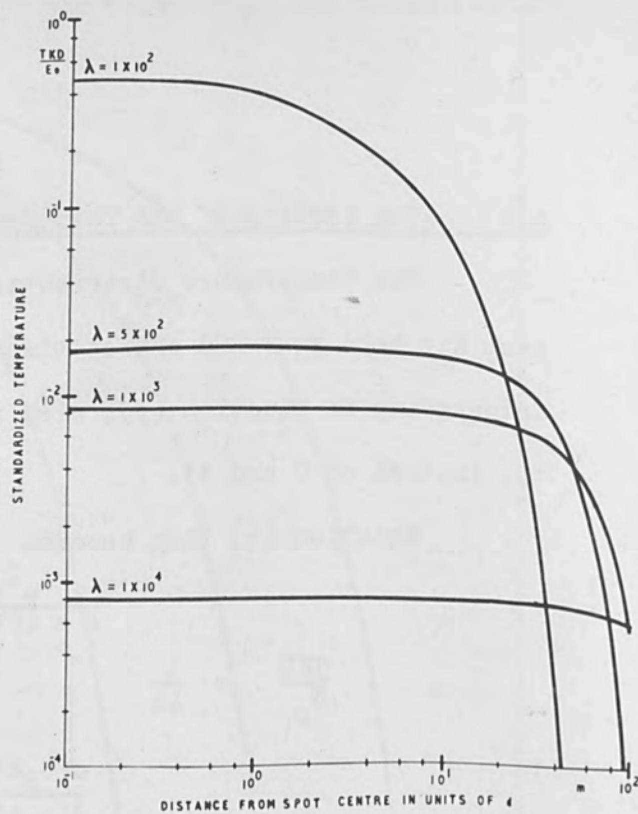

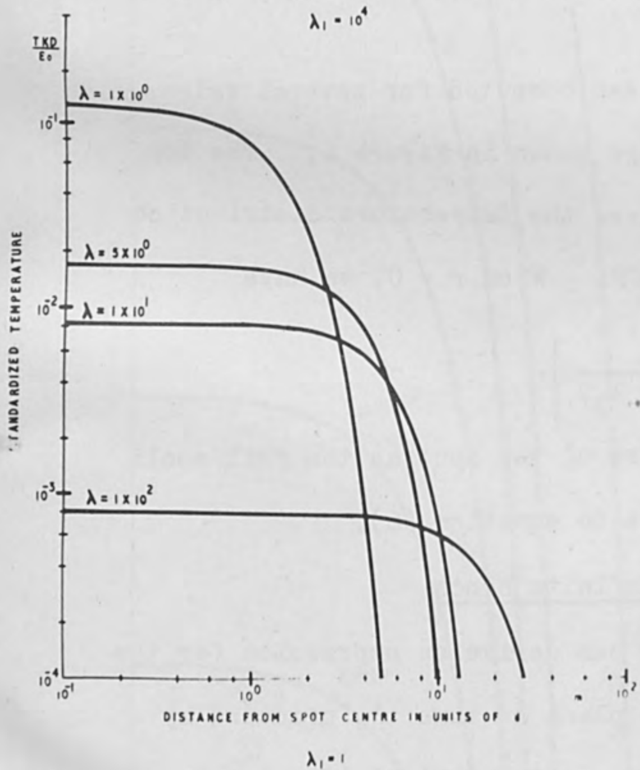

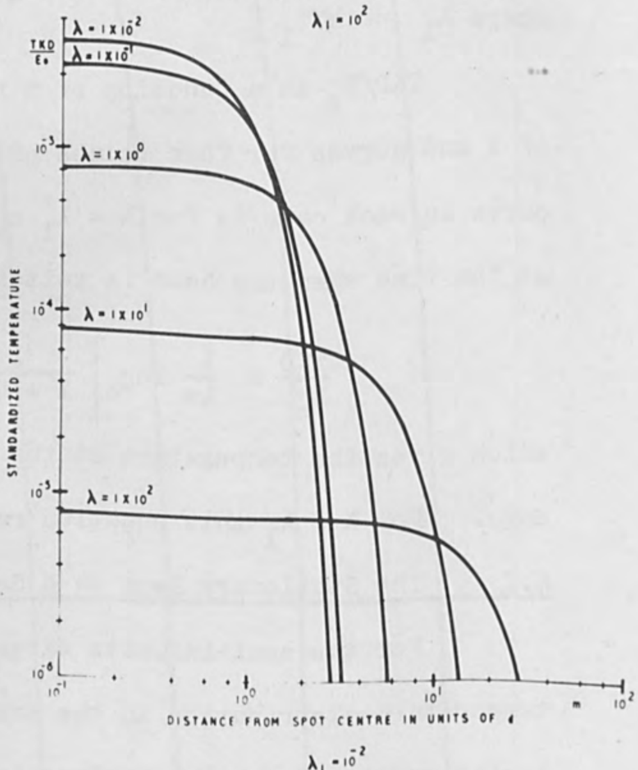

Figure 4 The Temperature Distribution in a Thin Foil During Cooling, after the Stationary Beam has been Switched Off.

Then, choosing TKd/E_o as the standardized temperature, we have

$$\frac{TKd}{E_o} = \frac{1}{\pi^{3/2}} \int_{\tan^{-1} \frac{1}{2\lambda^{\frac{1}{2}}}}^{\pi/2} e^{-m^2 \sin^2 \eta} \, d\eta \qquad (8)$$

Thus, equation (8) gives the standardized temperature at time t' at a point in the surface plane of a semi-infinite target, distance md from the centre of a continuous and stationary Gaussian source of heat generated in the surface plane and switched on at time $t = 0$. Graphs of TKd/E_o as a function of m for various values of λ are shown in Figure 5.

When $m = 0$, equation (8) reduces to

$$\frac{TKd}{E_o} = \frac{1}{\pi^{3/2}} \tan^{-1} 2\lambda^{\frac{1}{2}} \qquad (9)$$

This equation gives the temperature at the centre of the spot as a function of λ.

4.3 The Cooling of the Semi-Infinite Block

The cooling equation is obtained by integrating equation (4), with r constant, between the limits 0 and t_1; the limit t_1 being the time at which the beam is switched off. Thus we have

$$\frac{TKd}{E_o} = \frac{1}{\pi^{3/2}} \int_{\tan^{-1} \frac{1}{2\lambda^{\frac{1}{2}}}}^{\tan^{-1} \frac{1}{2(\lambda-\lambda_1)^{\frac{1}{2}}}} e^{-m^2 \sin^2 \eta} \, d\eta \qquad (10)$$

where $\lambda = k\Upsilon t'$ and $\lambda_1 = k\Upsilon t_1$

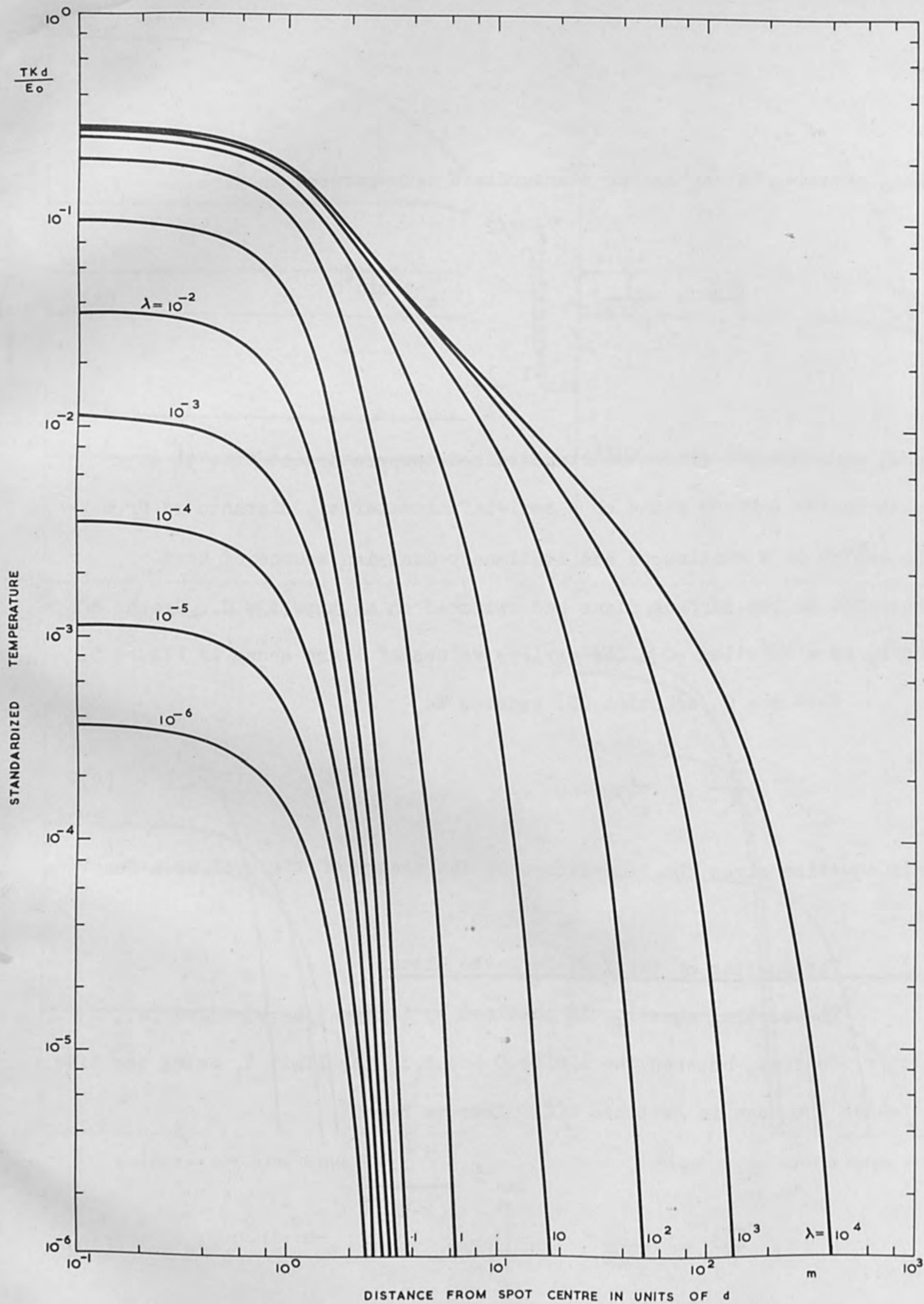

Figure 5 The Temperature Distribution on the Surface of a Semi-Infinite Block due to a Stationary Beam.

Curves of $TK\partial/E_o$ against m for several values of λ and four values of λ_1 are shown in Figure 6. As in Figure 4 the top curve in each case corresponds to $\lambda = \lambda_1$.

For m = 0, equation (10) reduces to

$$\frac{TK\partial}{E_o} = \frac{1}{\pi^{3/2}} \tan^{-1} \left[\frac{\lambda^{\frac{1}{2}} - (\lambda - \lambda_1)^{\frac{1}{2}}}{2\lambda^{\frac{1}{2}}(\lambda - \lambda_1)^{\frac{1}{2}} + \frac{1}{2}} \right]$$

This equation gives the temperature at the centre of the spot after the beam has been switched off. For $\lambda = \lambda_1$ it reduces to equation (9).

4.4 The Temperature Distribution in the Block along the Normal to the Surface at the Centre of the Stationary Source

Another useful equation is that describing the temperature inside the block, along the axis of the electron beam. This may be derived quite easily by considering the temperature rise at time t' at a point P on the axis (Figure 2), produced by the point sources arriving over an elemental ring of radius $r \sin \theta$ and width $r\sec\theta \, d\theta$, at time t. θ is half the angle subtended by the ring at point P and r is the distance of P from any point on the ring. The value of the temperature rise so obtained is then integrated over the total area of the source to give the temperature rise at P at time t' due to the source at time t. Finally this in turn is integrated with respect to time from 0 to t' to give the total temperature rise at P at time t' due to the continuous source from 0 to t. Using md as the distance of the point P from the surface and the parameter $\lambda = k\Upsilon t'$ the equation is

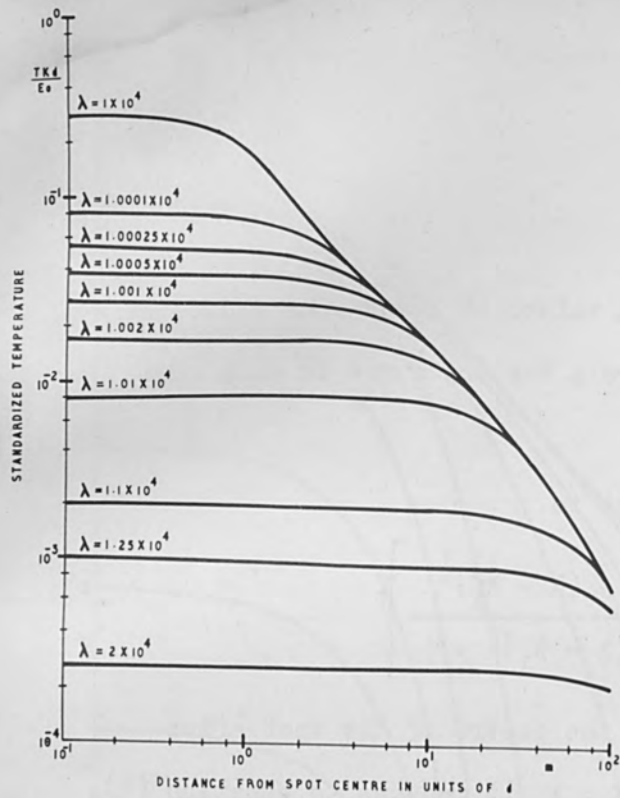

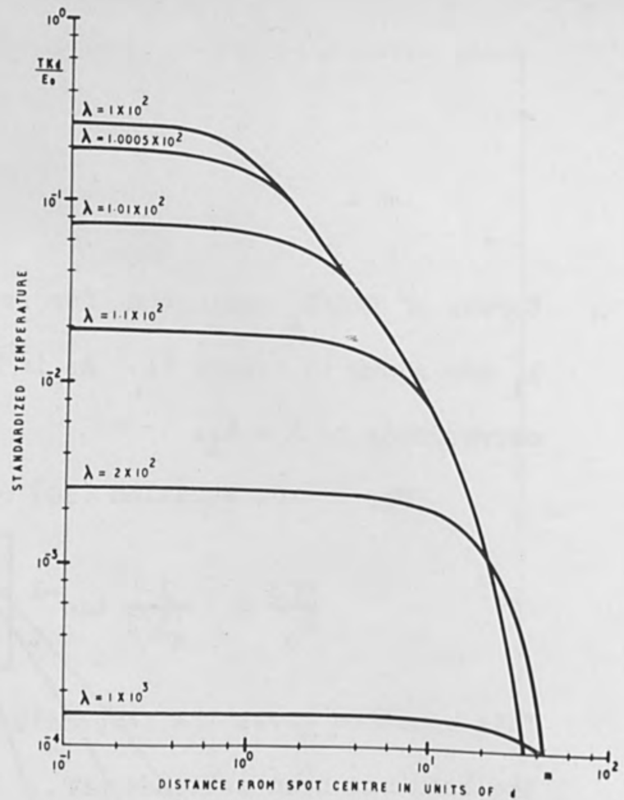

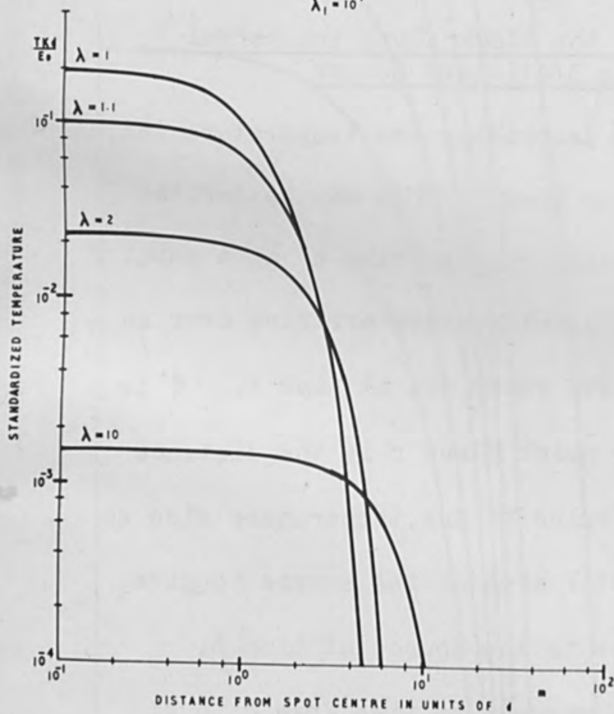

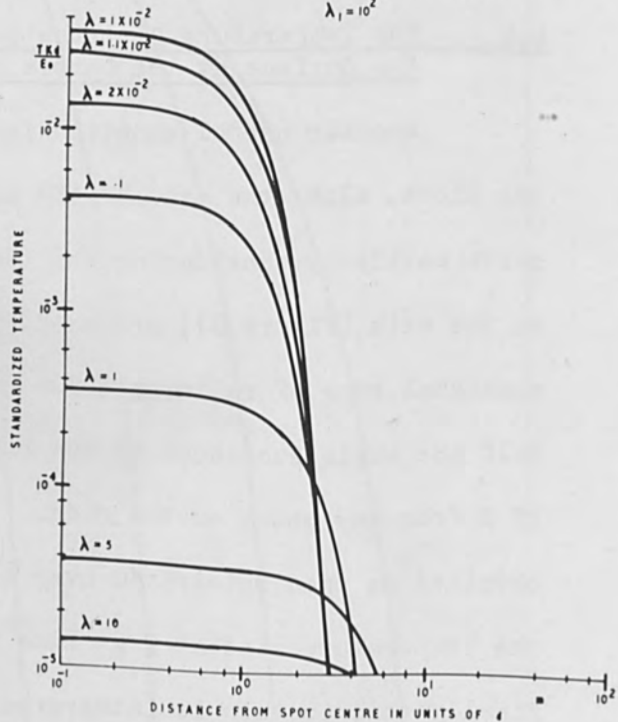

Figure 6 The Temperature Distribution on the Surface of a Semi-Infinite Block During Cooling, after the Stationary Beam has been Switched Off.

$$\frac{TKd}{E_o} = \frac{1}{\pi^{3/2}} \int_{\tan^{-1}\frac{1}{2\lambda^{\frac{1}{2}}}}^{\pi/2} e^{-m^2\tan^2\omega} \, d\omega \qquad (11)$$

where $\cot^2\omega = 4k\gamma(t' - t)$.

It will be seen that when $m = 0$, this equation reduces to equation (9).

Curves showing TKd/E_o against m for a range of values of λ are given in Figure 7.

5. THE TEMPERATURE DISTRIBUTIONS DUE TO A MOVING BEAM

5.0 The Temperature Distribution in a Thin Foil

Now that the distributions due to stationary beams have been discussed we shall go back to equation (3) and continue the derivation for the general case of a moving beam. There are several possible units of length which may be used, for example d, $(kd/v)^{\frac{1}{2}}$, vd^2/k or k/v all of which have the dimension of length. However, the unit d has already been chosen and the others will not be discussed further in this paper.

Now we have

$$r^2(t) = (x_o - vt)^2 + \beta^2 d^2$$

where βd is the distance of closest approach of the spot centre to the point O and x_o is the x co-ordinate of C the spot centre when $t = 0$.

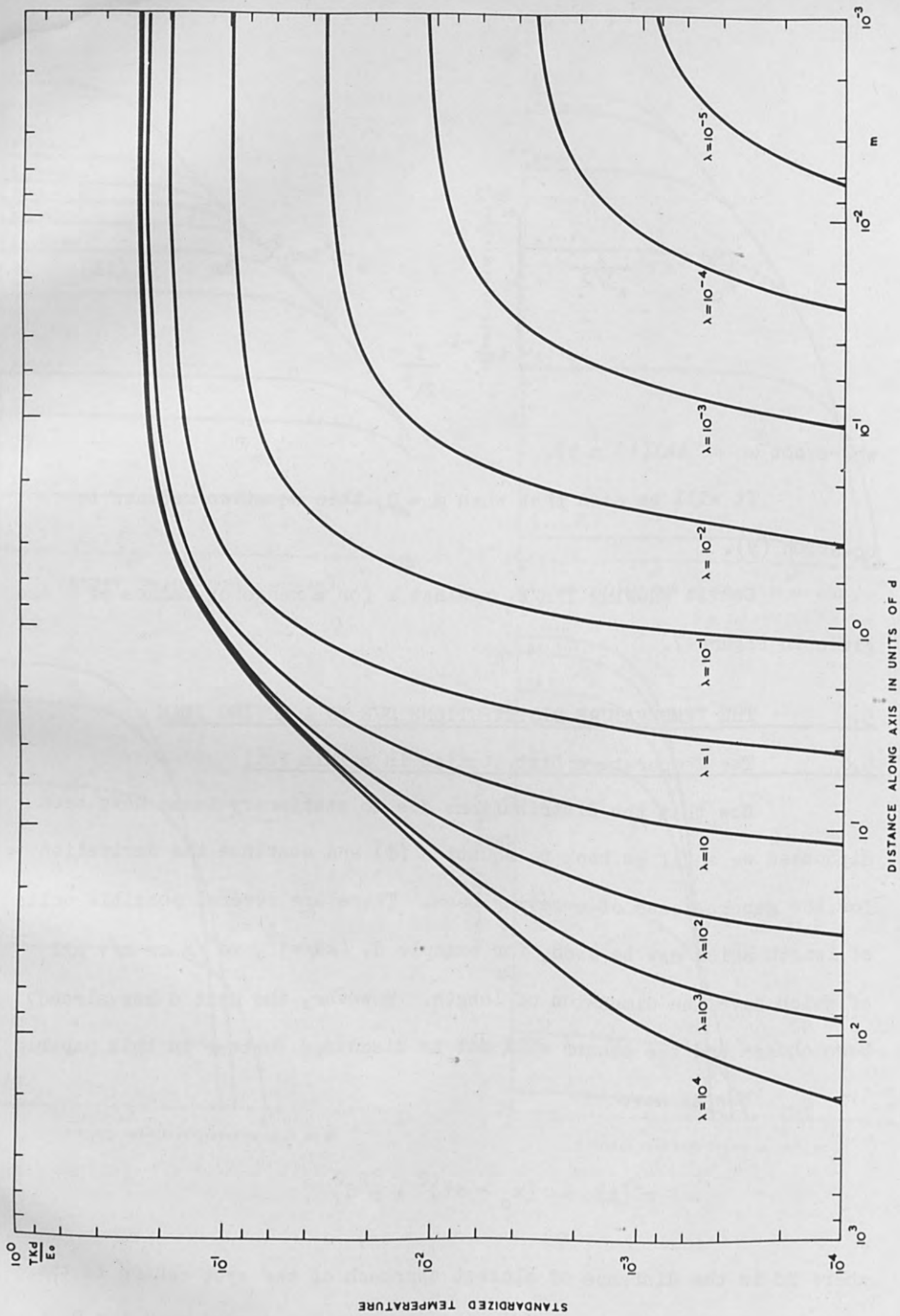

Figure 7 The Temperature Distribution along the Normal to the Surface of a Semi-Infinite Block, at the Spot Centre, due to a Stationary Beam.

Let $x_o - vt = m_t d$

and $x_o - vt' = md$

$m_t d$ and md are the distances between spot centre C and point O for times t and t' respectively.

If we now substitute for r in equation (3), we have

$$T = \frac{E_o \Upsilon d}{\pi\rho c D v} \int_{m}^{x_o/d} \frac{1}{1 + \frac{4k\Upsilon d}{v}(m_t - m)} \cdot \exp - \left[\frac{m_t^2 + \beta^2}{1 + \frac{4k\Upsilon d}{v}(m_t - m)} \right] dm_t$$

There is now no reason why x_o should not be made infinite, instead of some large finite value, as we shall now be considering the temperature when the spot is situated at various finite distances from the origin rather than after certain times.

We now choose a dimensionless parameter $a = \frac{4k}{vd} = \frac{4k\Upsilon d}{v}$ in order that the resulting equation may be in a general form applicable to any target material etc.

After making these substitutions, the above equation can be written in the form

$$\frac{TKD}{E_o} = \frac{a^2}{4\pi} \int_0^{\infty} e^{-z} \cdot f(z)dz \qquad (12)$$

where $$f(z) = \frac{1}{1 + a^2 z} \exp - \left[\frac{(2ma - 1)z + \beta^2 + m^2}{1 + a^2 z} \right]$$

and $$z = \frac{m_t - m}{a}$$

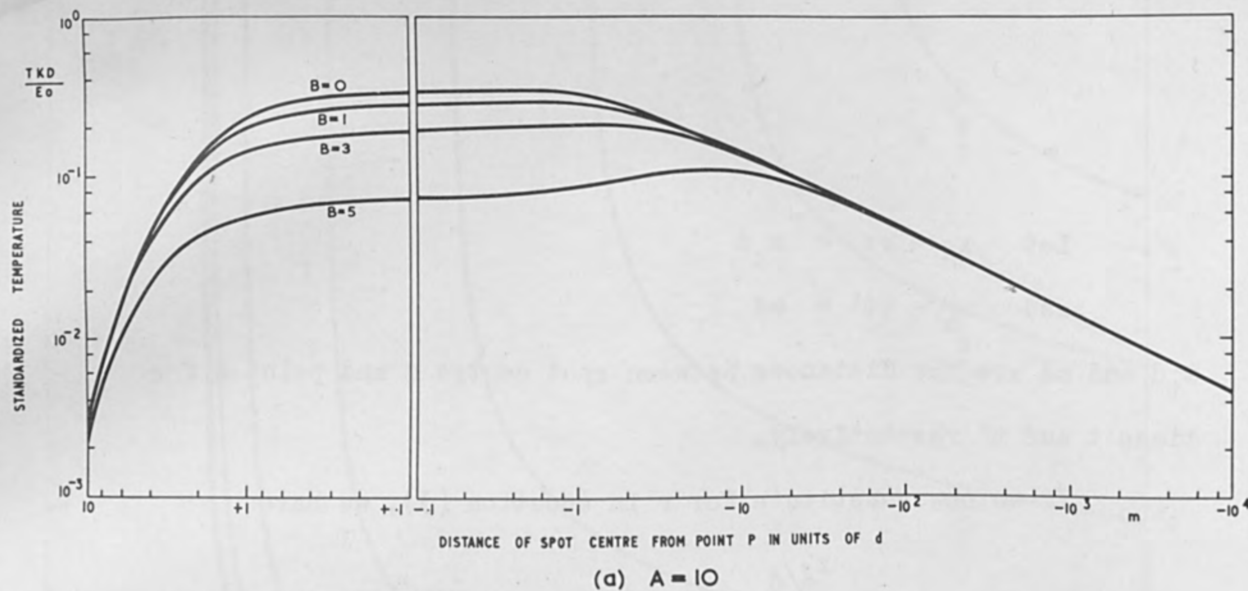

(a) A = 10

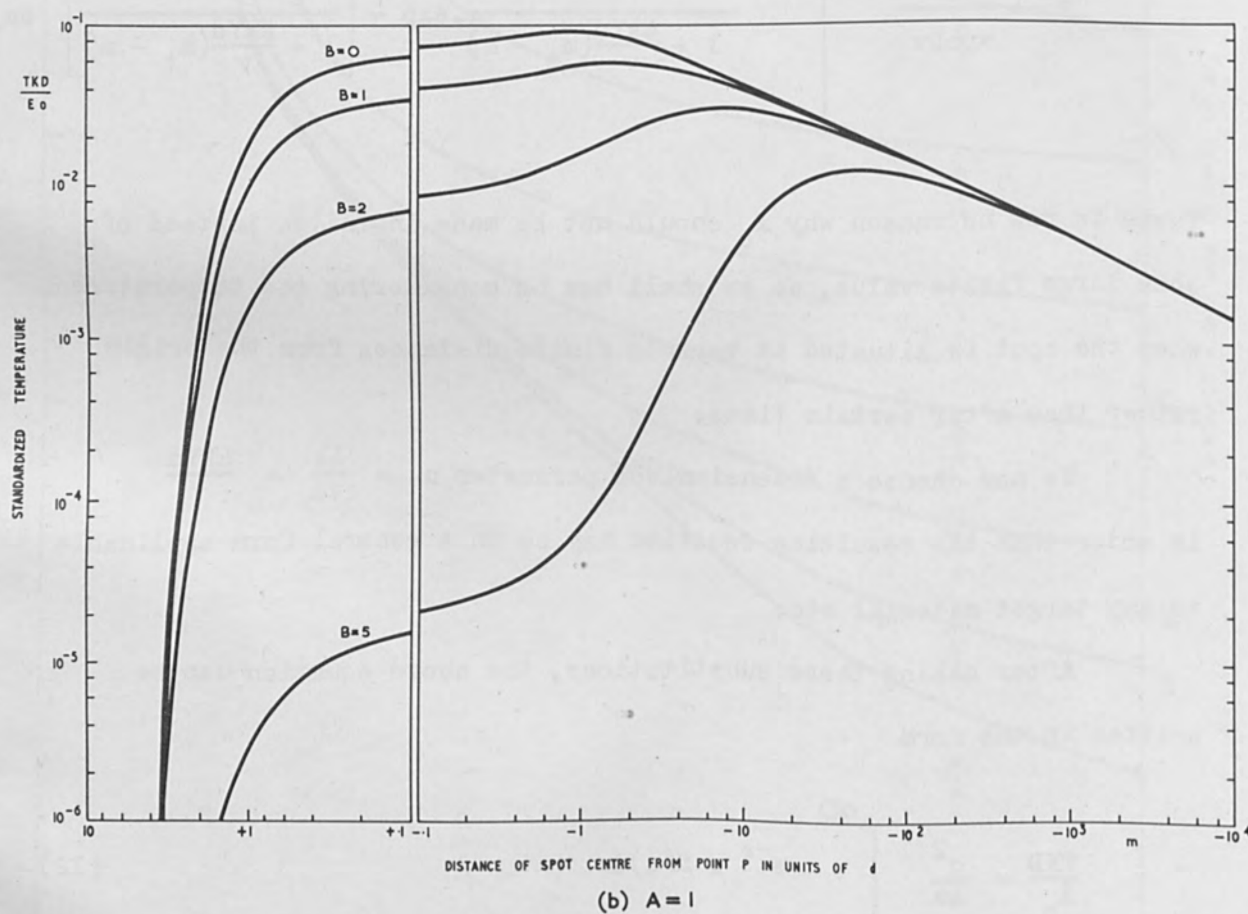

(b) A = 1

Figure 8 (a) and (b) The Temperature Variation at a Point in a Thin Foil due to a Beam Moving at Constant Velocity (Logarithmic Scale).

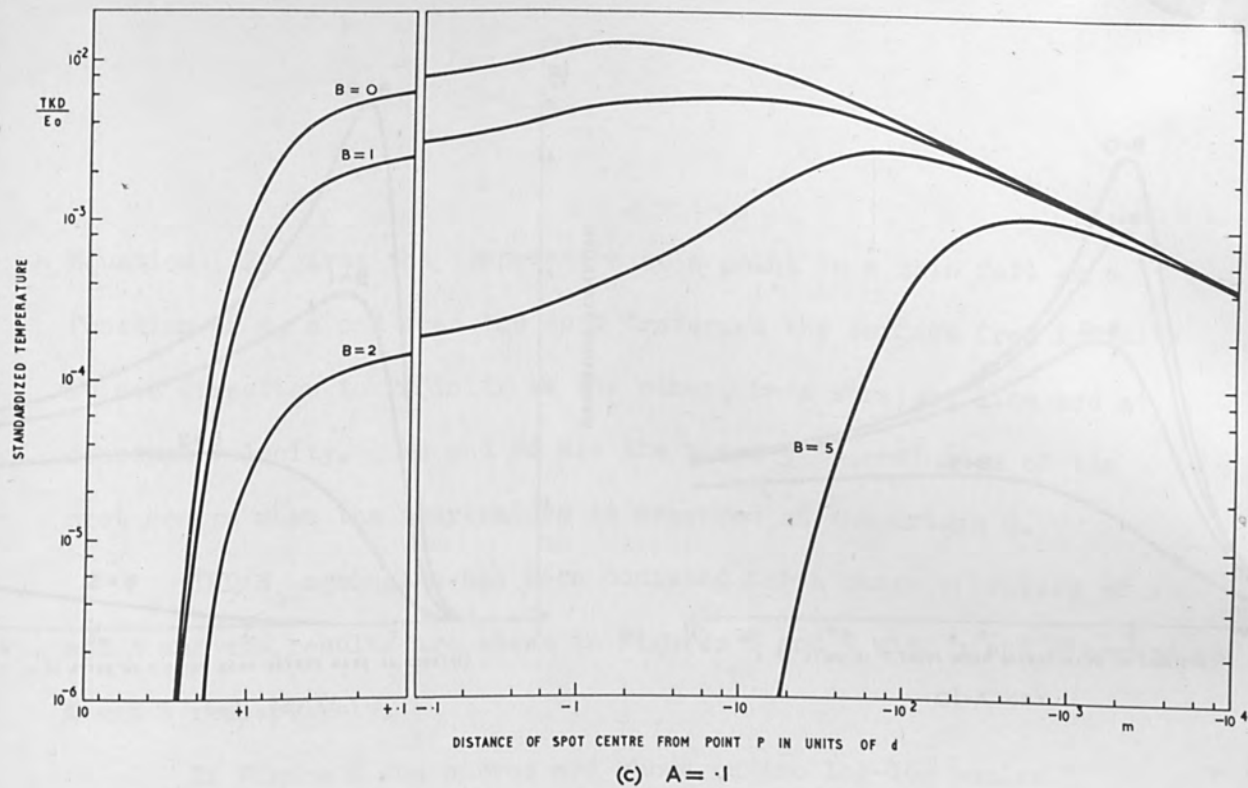

(c) A = ·1

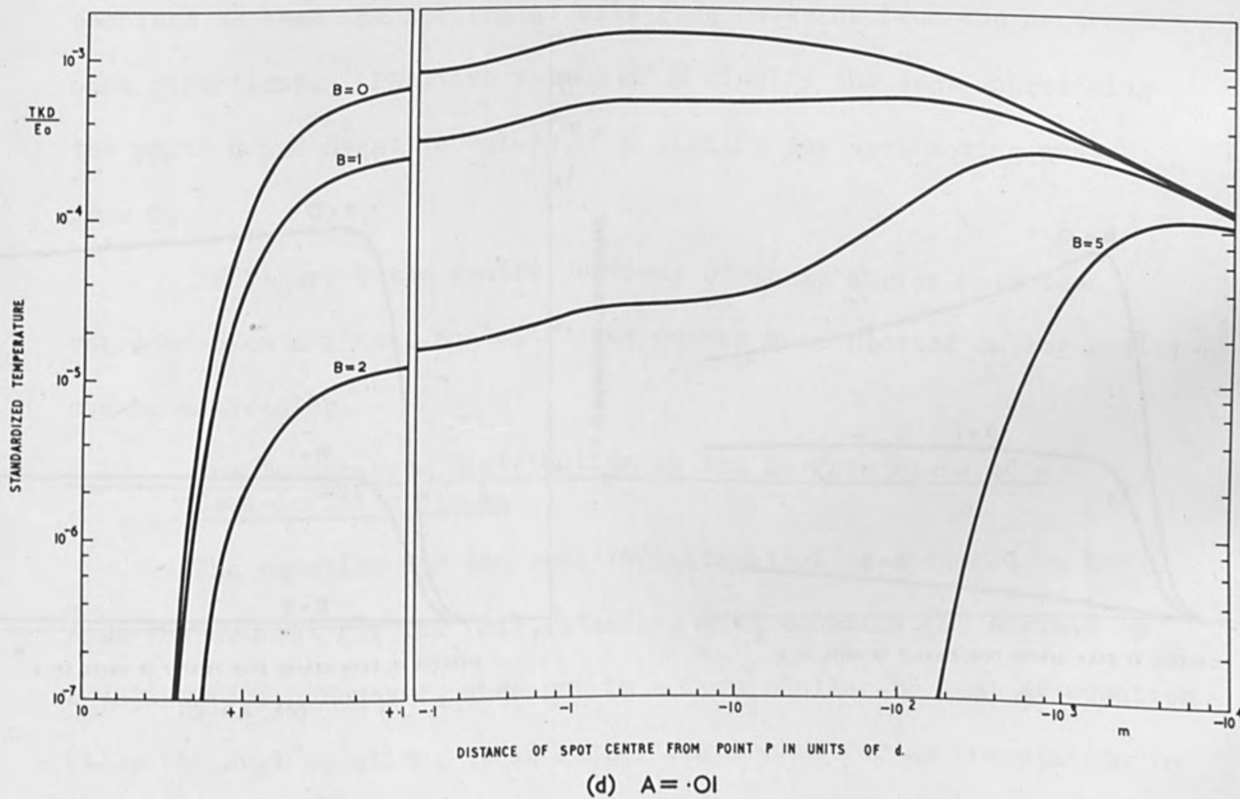

(d) A = ·01

Figure 8 (c) and (d) The Temperature Variation at a Point in a Thin Foil due to a Beam Moving at Constant Velocity (Logarithmic Scale).

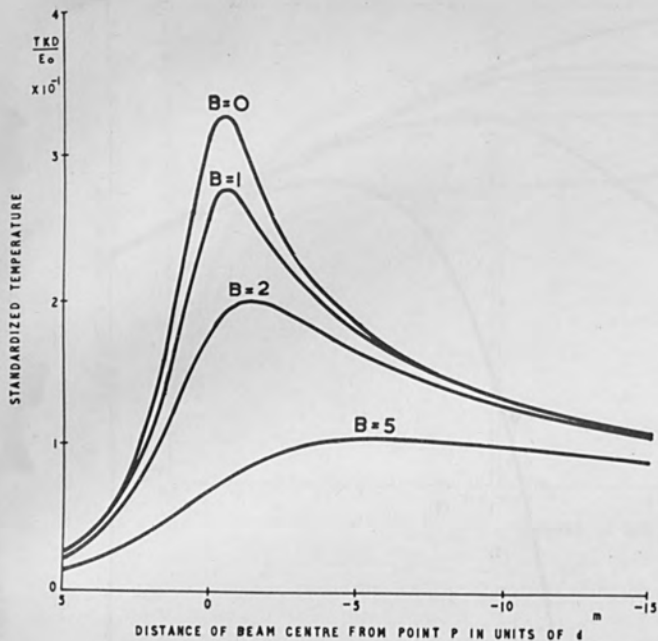

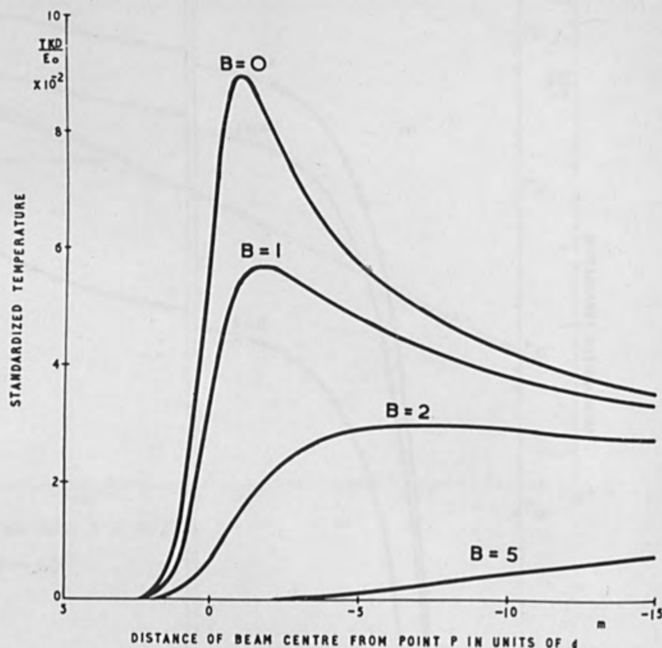

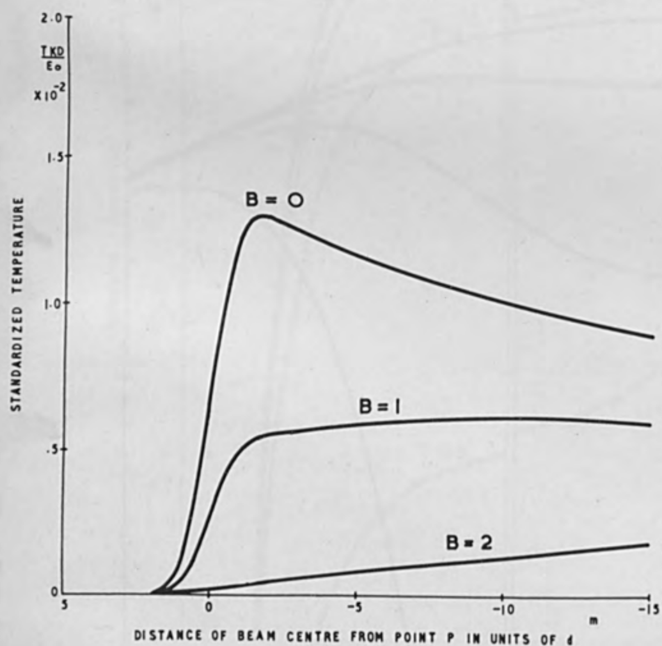

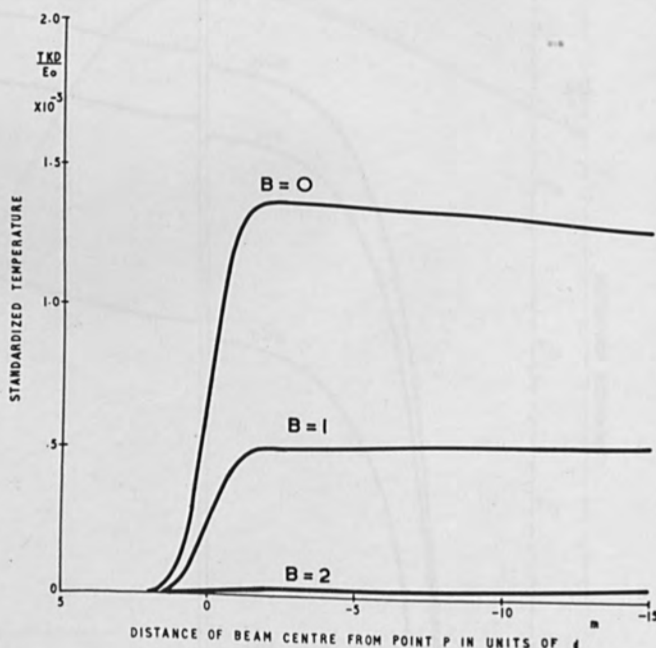

Figure 9 The Temperature Variation at a Point in a Thin Foil due to a Beam Moving at Constant Velocity (Linear Scale).

Equation (12) gives the temperature at a point in a thin foil as a function of m, β and α as the spot traverses the surface from infinity in one direction to infinity in the other, in a straight line and at constant velocity. md and βd are the x and y co-ordinates of the spot centre when the temperature is measured at the origin O.

TKD/E_o against m has been computed for a range of values of α and β and the results are shown in Figures 8 and 9 with α and β marked as A and B respectively.

In Figure 8 the curves are shown on two log-log scales combined so that the horizontal axis runs outwards from the centre in both directions. Positive values of m signify the spot approaching the point O and negative values of m signify the spot moving away from O.

In Figure 9 the centre portions of these curves have been reproduced on a linear scale, as the curves when plotted on log scales can be misleading.

5.1 The Temperature Distribution in the Surface Plane of a Semi-Infinite Block.

The equation for the semi-infinite block is obtained in the same way as that for the foil, starting with equation (4) instead of equation (3). However, when put in a form similar to that of equation (12), the foil equation, it is rather complex as far as computation is concerned and so a trigonometrical substitution $\alpha(m_t - m) = \tan^2\mu$ was used.

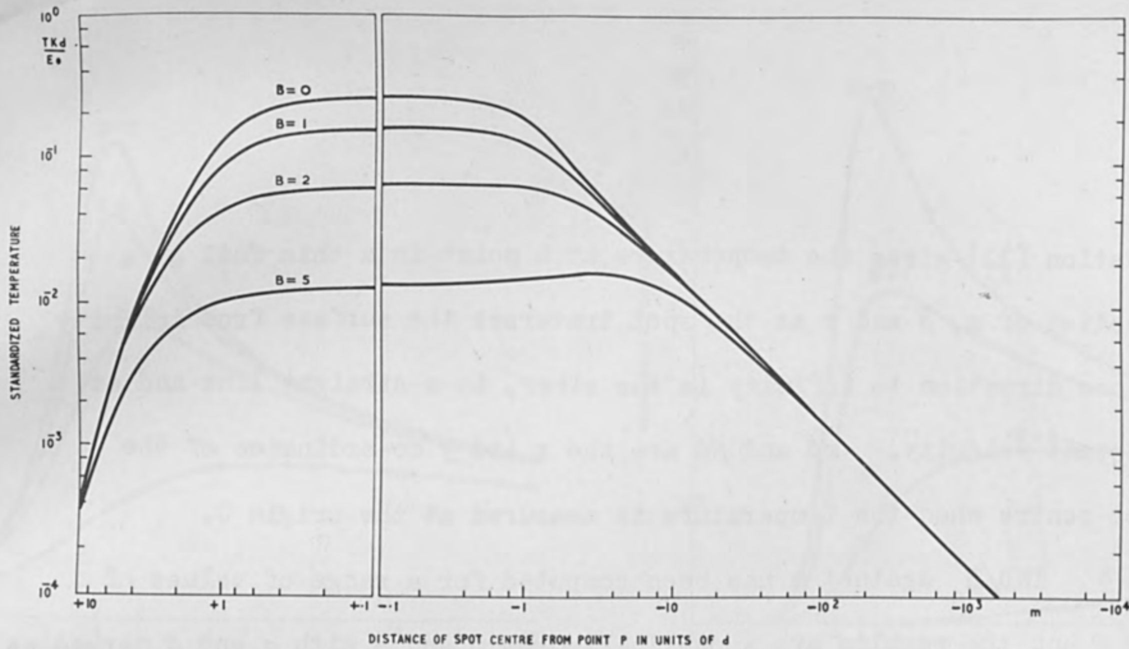

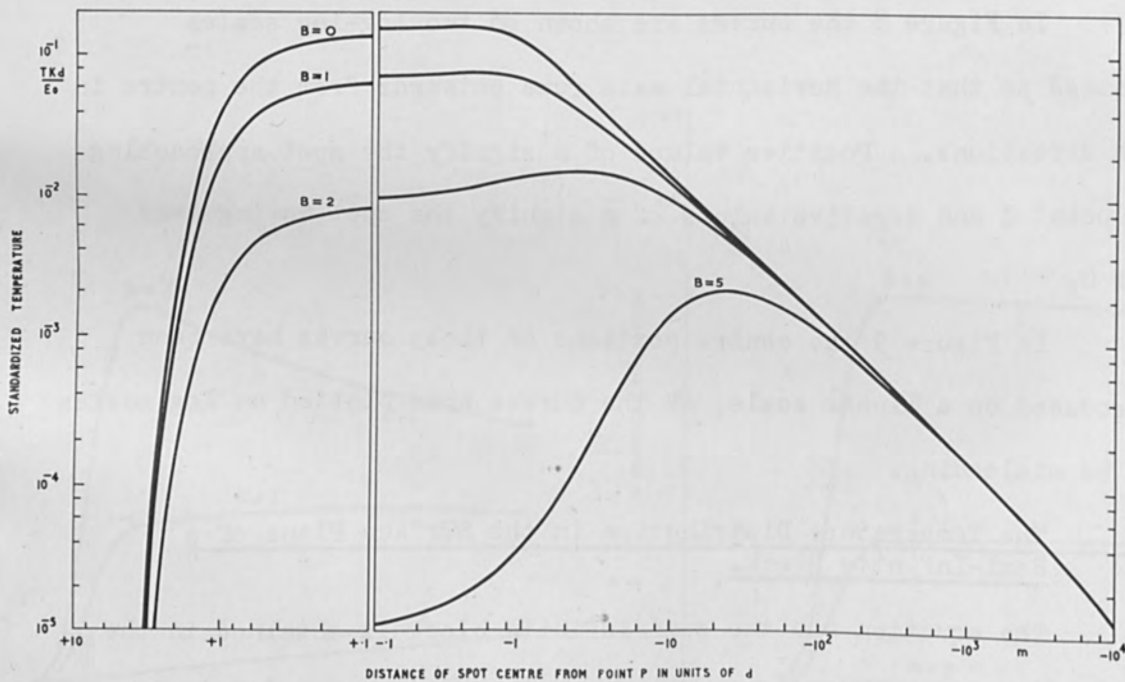

Figure 10 (a) and (b) The Temperature Variation at a Point on the Surface of a Semi-Infinite Block due to a Beam Moving at Constant Velocity (Logarithmic Scale).

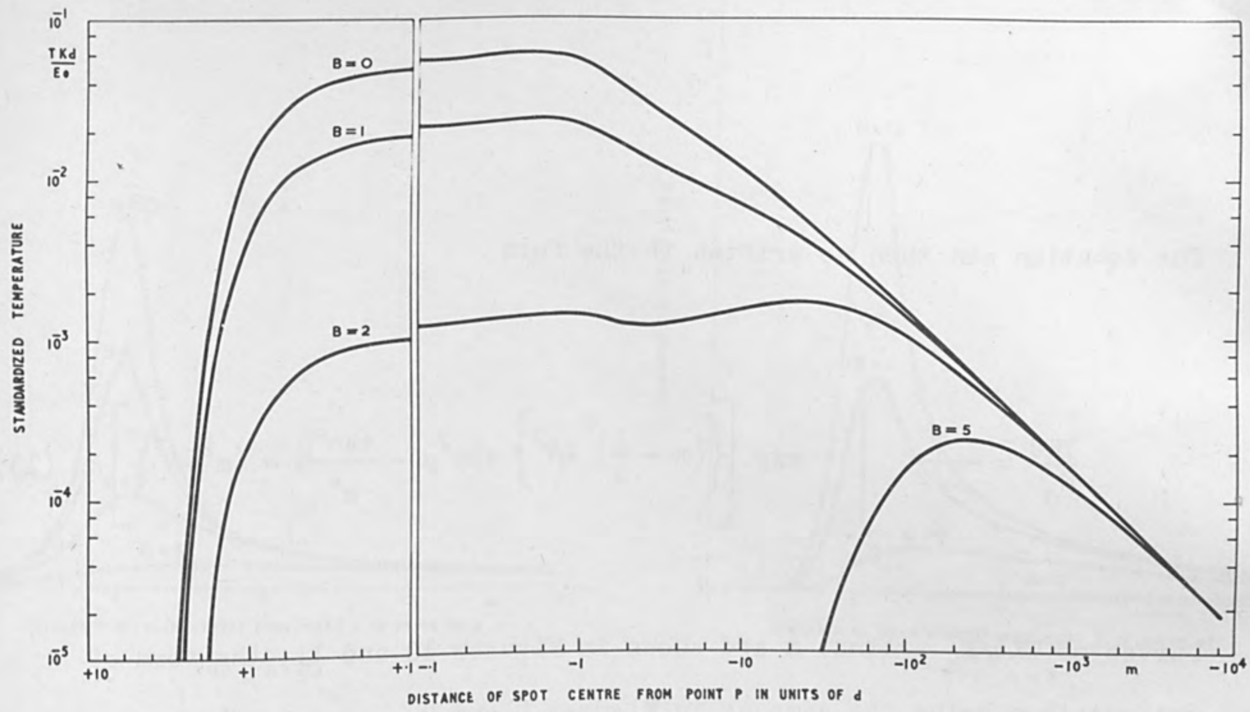

(c) A = ·1

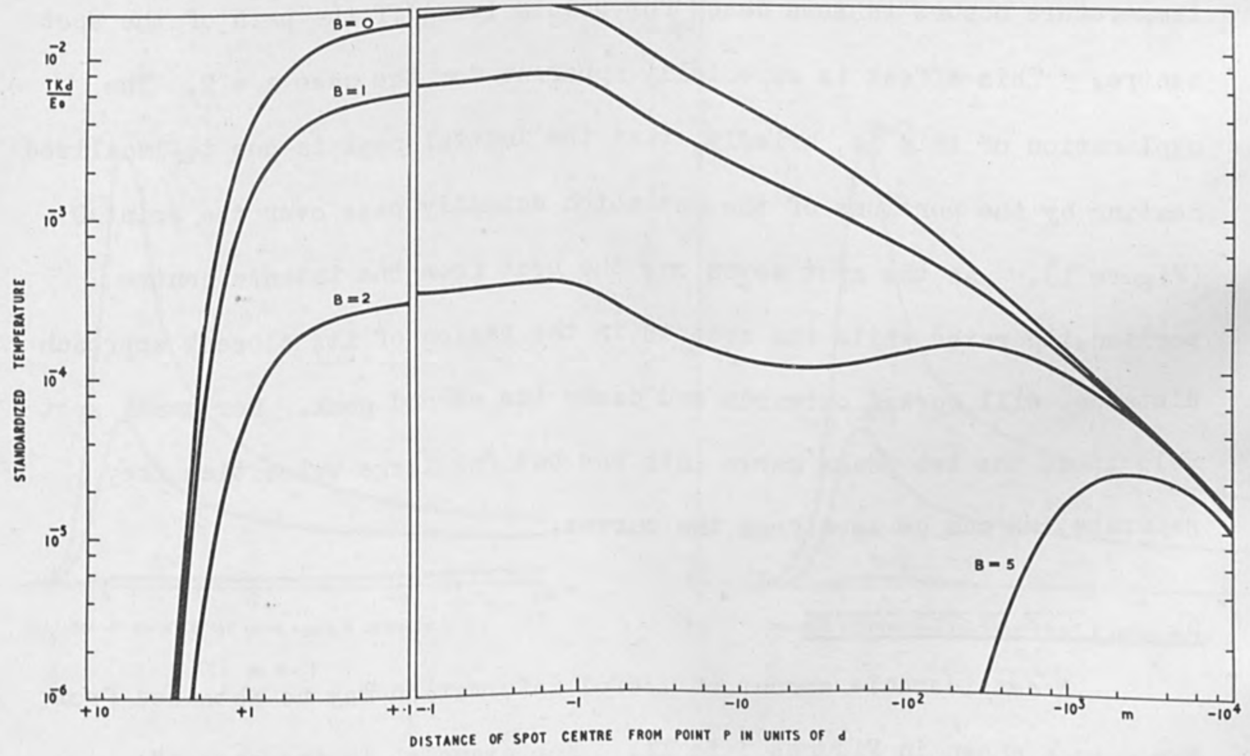

(d) A = ·OI

Figure 10 (c) and (d) The Temperature Variation at a Point on the Surface of a Semi-Infinite Block due to a Beam Moving at Constant Velocity (Logarithmic Scale).

The equation can then be written in the form

$$\frac{TKd}{E_o} = \frac{1}{\pi^{3/2}} \int_0^{\pi/2} \exp\left[\left\{(m - \frac{1}{a})^2 + \beta^2\right\} \sin^2\mu - \frac{\tan^2\mu}{a^2} - (m^2+\beta^2)\right] d\mu \quad (13)$$

Curves of TKd/E_o against m are shown in Figures 10 and 11, the form of presentation being the same as in Figures 8 and 9.

It will be seen from Figure 10 that a double rise and fall of temperature occurs in some cases for points lying off the path of the spot centre. This effect is especially apparent for the case $a = 2$. The explanation of this is, briefly, that the initial peak is due to localized heating by the portions of the spot which actually pass over the point 0 (Figure 1). As the spot moves on, the heat from the intense centre portion, liberated while the spot is in the region of its closest approach distance, will spread outwards and cause the second peak. For small spot velocities the two peaks merge into one but for large velocities they separate, as can be seen from the curves.

6. USE OF THE CURVES

A considerable amount of useful information may be obtained from the curves shown in Figures 3 to 11. For example, in the case of stationary beams one can obtain an estimate of beam energy and deviation necessary to melt a portion of the target to a given radius. The pulse length is also important, since this affects the range of the

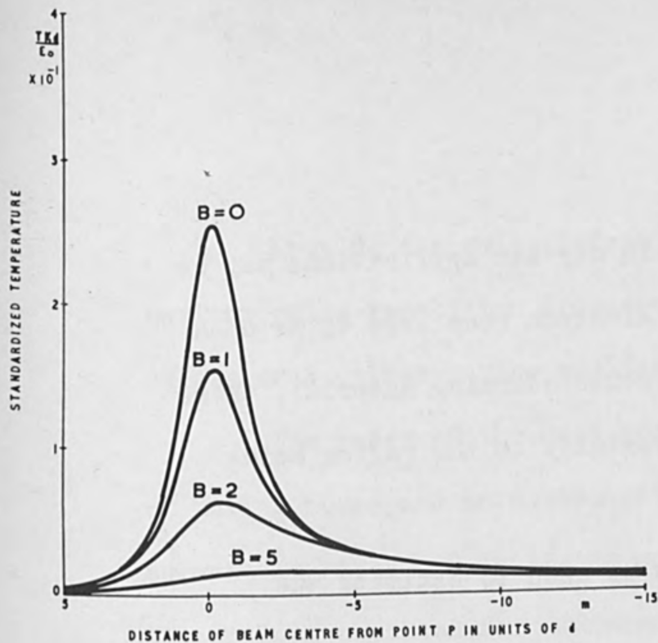

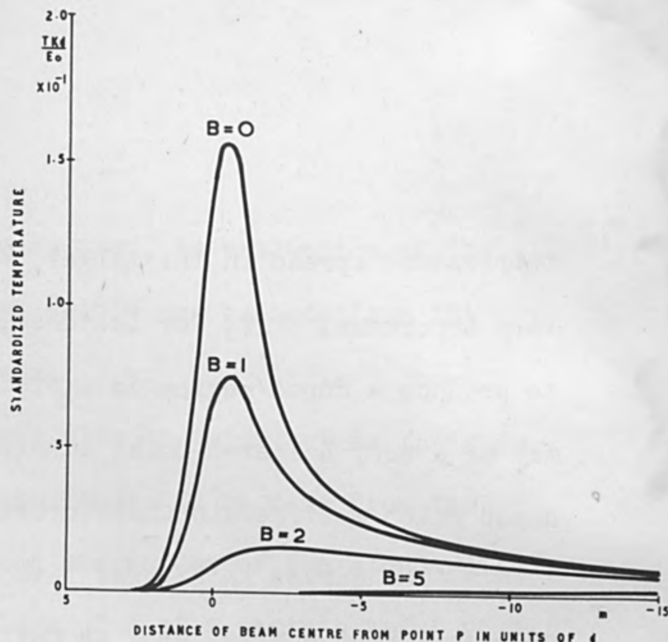

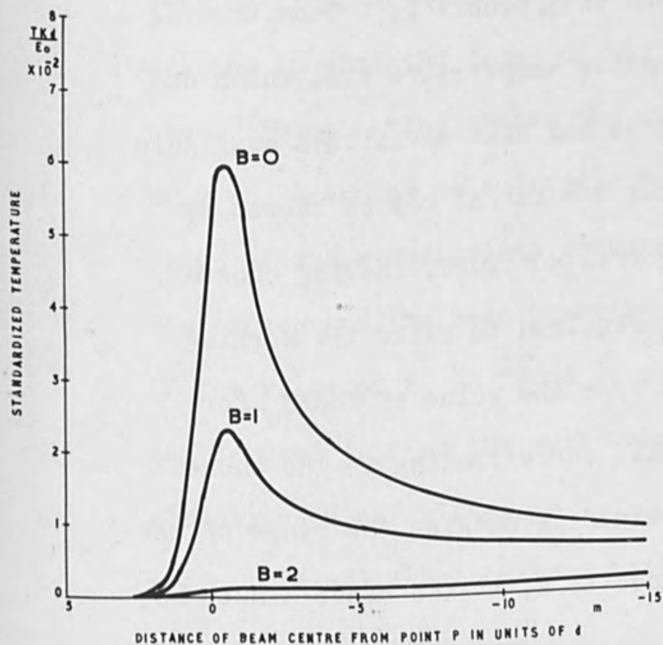

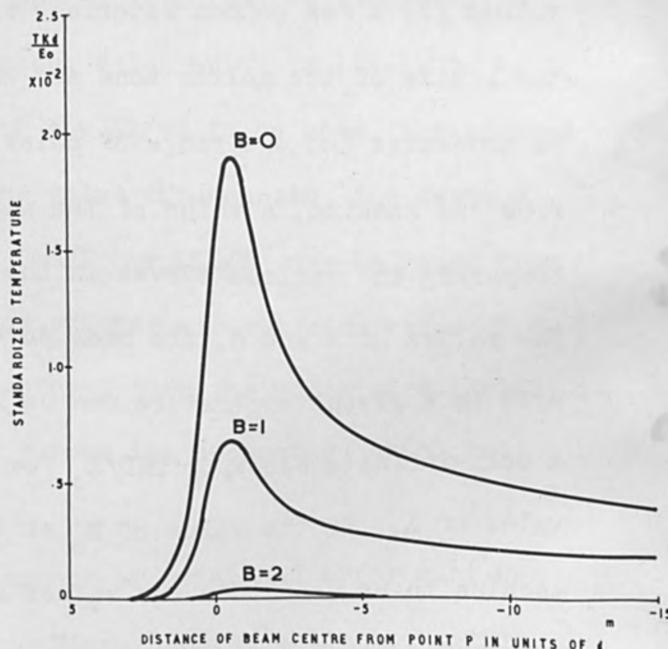

Figure 11 The Temperature Variation at a Point on the Surface of a Semi-Infinite Block due to a Beam Moving at Constant Velocity (Linear Scale).

temperature spread in the target, which in certain applications may be very important. If, for instance, the electron beam were to be used to produce a doped region in a piece of semiconducting material, there may be a soft soldered joint in close proximity to the region being doped which must remain undisturbed.

The curves in Figures 3 to 7 may be used to estimate the necessary beam energy, etc. as follows:

For a given target material the values of the thermal diffusivity k and conductivity K are known. A table of approximate values for a few common materials is given in appendix 1. Then, knowing the limits of the molten zone and surrounding temperature rise which can be tolerated and the range of pulse lengths and beam deviations available from the machine, a value of the parameter $\lambda = kt'/d^2$ may be chosen by comparing the various curves in the appropriate Figure. Having chosen the values of λ and d, the beam power E_o required to raise the working area to a given temperature can be found from the value of TKd/E_o for a semi-infinite block, or TKD/E_o for a foil, corresponding to the chosen value of λ. If the value of E_o so determined is outside the range of the machine to be used then the values assigned to d, t' and hence λ must be arranged so that E_o is within the power range available.

Alternatively, if the available beam power and spot size is strictly limited then the order must be reversed so that TKd/E_o, or TKD/E_o, is first calculated and then the required value of λ and hence t' can be found from the curves.

Knowing the pulse length t' to be used, an estimation of the maximum pulse repetition frequency permissible can be made from the values of λ, given in the cooling curves.

The range of the heat spread may also be important in the case of moving beams and an assessment of the range may be made from the curves, in Figures 8 to 11, by comparing the values of the standardized temperature obtained for different values of β at a certain value of α.

In order to assess the beam velocity and spot deviation required it is best to decide first of all which value of α from the curves would best satisfy the range of temperature spread which can be tolerated, bearing in mind the order of the deviation value which is likely to be used. Then, having chosen the value of $\alpha = 4k/vd$ to be used, the product of v and d can be calculated. With the value of α chosen, the maximum value of the standardized temperature TKd/E_0 or TKD/E_0 may be found from the curves and the beam power E_0 worked out for a particular value of d. If the value of E_0 so found is satisfactory, then the value of d chosen can be used to find the spot velocity v from the product vd which has already been calculated.

In all these cases a certain amount of trial and error must be adopted in choosing values in order to obtain figures which are within the scope of the machine to be used. Appendix 2 contains a list of the symbols used in this paper to enable reference to be made more easily.

7. LIMITATIONS AND CONCLUSIONS

The equations derived and the results shown in this paper give the temperature distributions produced in thin foils and in semi-infinite

blocks by an incident electron beam which has a Gaussian energy distribution cross-section. Stationary and moving beams have been considered and also cooling effects in the former case. The following limitations and assumptions have been used in the calculations:

(i) The beam has a Gaussian energy distribution cross-section.

(ii) The energy of the beam is totally absorbed in the surface of the target in the case of a semi-infinite block. That is to say, no allowance has been made for electron penetration or scattering.

(iii) The thermal and other physical properties of the target material have been assumed to be independent of temperature.

(iv) Any small losses of heat from the target to its surroundings, which may occur, have been neglected.

(v) No account has been taken of the change of state of the target material, such as melting and vaporization.

The assumption that the electron beam has a Gaussian cross-section would appear to be a reasonable one[4].

The third assumption may cause errors of up to 10% to occur in the results and in the case of a semi-infinite target, the second assumption may well cause even larger errors. Significant variations in the value of the temperature should be expected when either the range of appreciable heat flow during the pulse, or the size of the spot,become small enough to be comparable with the range of the electrons in the material. Backscattering of electrons from the surface of the target may cause the absorbed energy to be less than the incident energy by

as much as 30%[5]. Electron scattering in the material should not appreciably affect the results for a thin foil, since the foil is supposed to be thin enough for the temperature to be uniform across its thickness. However, it must be remembered that the energy E_0 absorbed per second in the foil will not necessarily be the total energy of the incident beam, since, for certain conditions of beam energy and foil properties, a large number of electrons will pass right through the foil without losing an appreciable quantity of their initial energy.

Once the material of the target begins to melt these results will cease to be applicable, since, during the absorption of latent heat of fusion and of vaporization, the source would need to be one of constant temperature rather than constant energy in-so-far as the remainder of the target is concerned.

Within the limitations listed above these results provide a valuable insight into the heat flow problems which may be expected to arise in the process of electron beam machining. In addition, the fact that electron penetration and scattering are ignored does make the results applicable to problems involving heating by sources other than an electron beam.

Experimental work is in progress to check the results and it is hoped that further theoretical work may permit the removal of many of the present limitations.

8. ACKNOWLEDGMENTS

The author would like to thank Mr. H. N. G. King, Mr. J. Kelly and Mr. K. Tweedale of Mullard Research Laboratories for many helpful suggestions and criticisms.

9. REFERENCES

1. Pittaway, L. G. — The Temperature Distributions in Electron Beam Targets. M.R.L. Report No. 463, 1963.

2. Oosterkamp, W. J. — The Heat Dissipation in the Anode of an X-ray Tube. Philips Research Reports, Vol, 3, 1948, p.161.

3. Carslaw, M. S. and Jaeger, J. C. — Conduction of Heat in Solids, 2nd ed., 1959, p. 255.

4. Gale, B and Hale K. F. — Heating of Metallic Foils in an Electron Microscope. Brit. J.A.P., Vol.12, No.3, March, 1961, p.115-117.

5. Heil, O and Vogel, S. — Pulse Heating of Materials by Highly Concentrated Electron Beams. AD 275 265, Eitel-McCullough Inc., 1962.

10. APPENDICES

Appendix 1.

The Conductivity and Diffusivity of some Common Materials.

The values given below are approximate, since the physical properties of the materials vary with temperature.

The units are c.g.s.; joules and °C and conductivities are given at 100°C unless otherwise stated.

Substance	Conductivity K	Diffusivity k
Aluminium	2.30	0.97
Copper	3.82	1.08
Glass (Crown)	0.0105 at 20°C	0.0058
Gold	3.10	1.27
Iron	0.69	0.18
Lead	0.33	0.21
Mild Steel (0.1%C)	0.46 at 20°C	0.12
Molybdenum	1.43 at 0°C	0.47
Nickel	0.83	0.19
Platinum	0.72	0.25
Silver	4.17	1.61
Tin	0.60	0.36
Tungsten	1.70 at 0°C	0.62
Zinc	1.09	0.35

Appendix 2

List of Symbols used in the Text

$\alpha = 4k/vd =$ a dimensionless parameter used in the moving beam equations. (A in the Figures).

$\beta =$ distance of closest approach of spot centre to the point O at which the temperature is calculated (in units of d cm). (B in the Figures).

$\Upsilon = 1/d^2$.

$c =$ specific heat of target material. (joules. gm^{-1}.deg.$^{-1}$).

$d =$ standard deviation of the radial energy distribution of the beam (cm).

$D =$ foil thickness (cm).

$E_o =$ the total energy liberated in the target per second (watts).

$k = K/pc =$ thermal diffusivity of target material (cm^2.sec^{-1}.).

$K =$ thermal conductivity of target material (joule cm.cm^{-2}.sec.$^{-1}$deg.$^{-1}$C).

$\lambda = k\Upsilon t'$, $\lambda_1 = k\Upsilon t_1$ — dimensionless parameters used in the stationary beam equations.

$m =$ distance of spot centre from a line through the point O, perpendicular to the path of the spot (units of d cm).

$p =$ density of target material (gm. cm^{-3}).

$Q =$ strength of point source (deg C. cm^3).

$Qpc =$ actual energy liberated by point source (joules).

$r =$ distance of spot centre from point O at which the temperature is calculated (cm).

$t =$ time (sec).

$t' =$ time at which temperature is calculated (sec).

t_1 = pulse length for cooling equations (sec).

T = temperature above ambient (deg. C).

v = velocity of moving beam across the surface of the target ($cm.sec^{-1}$).

$\frac{TKd}{E_o}$, $\frac{TKD}{E_o}$ — dimensionless quantities used as standardized temperatures for the semi-infinite and thin foil targets respectively.

THEORETICAL TEMPERATURE RISE IN MATERIALS DUE TO ELECTRON BEAMS

Gerwig E. Vibrans
Lincoln Laboratory,* Massachusetts Institute of Technology

*Operated with support from the U.S. Advanced Research Projects Agency

THEORETICAL TEMPERATURE RISE IN MATERIALS DUE TO ELECTRON BEAMS

INTRODUCTION

In high-power electron tubes, for example klystrons, the anode is bombarded with high current density during short pulses. The local heating of the target during the pulse, imposes a limit on the beam power density at the anode.

At Lincoln Laboratory we have investigated the temperature of a target versus time of bombardment, especially for short times and large power density. The geometry is shown in Fig. I. The beam hits the solid, the electrons penetrate to a certain depth while converting their energy into heat.

Usually, three important assumptions are made in order to calculate the temperature on the bombarded surface:

(a) The temperature distribution in the solid is one dimensional. This assumption usually holds true for short pulses since the electron penetration depth is small compared to the dimension(s) of the bombarded areas.

(b) Radiative heat flow into the vacuum is negligible. This assumption is valid for all temperatures in the ranges encountered in electron tubes.

(c) The electron energy is converted into heat at the surface and a suitable temperature gradient builds up instantaneously so that heat flows into the solid. This assumption applies asymptotically if the penetration depth of the heat is large compared to the penetration depth of the electrons (for relatively long times and moderate beam voltages). The surface temperature rises as $(\text{time})^{1/2}$.

or (d) The electron energy is converted adiabatically into heat more or less uniformly within a volume defined by the area of the beam and the penetration depth of the electrons. The surface temperature rises linearly with time.

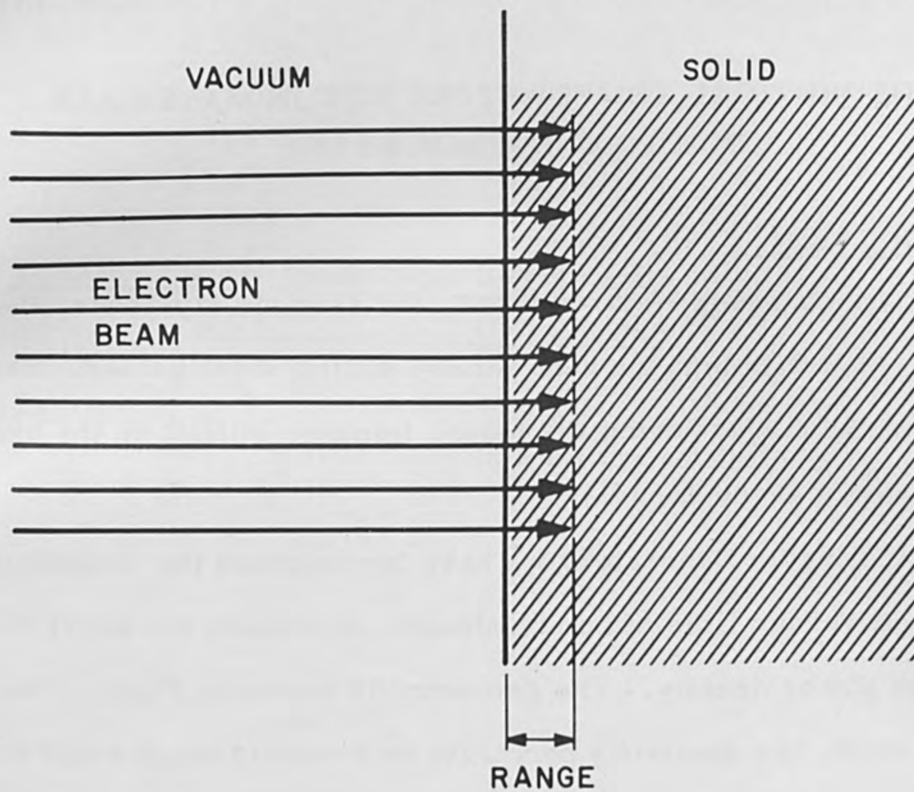

FIGURE 1

Temperature Rise of a Bombarded Target
According to Different Assumptions.

Beam Voltage: 25 kv Power Density: 0.5 Mw/cm^2
Time: 0.25 μsec

	Copper ΔT	Tungsten ΔT	Stainless Steel ΔT
Surface heating [assumption (c)]	75°	120°	350°
Volume heating [assumption (d)]	290°	780°	230°
Energy dissipation derived from range	70°	120°	155°
Spencer's energy dissipation	60°	95°	155°

No thermodynamic phase changes are taken into account

FIGURE 2

In the following we have accepted a one dimensional temperature distribution and have neglected any radiation.

We look for a better approximation than surface or volume heating, since these are asymtotic solutions of the problem, which fail for the conditinns we are interested in. Both tend to give too high a value for the surface temperature.

In Fig. II we compare temperatures obtained with the different assumptions. For comparison, the temperatures as computed in the following are also included.

DERIVATION OF SURFACE TEMPERATURE DUE TO SIMULTANEOUS PRODUCTION AND DIFFUSION OF HEAT UNDER ELECTRON BOMBARDMENT.

It is possible to compute the exact surface temperature by using the classical theory of heat conduction. Fig. III gives the appropriate equation. T is the temperature at a location x, and at a time t, as it is induced by the heat source distribution f. The heat sources, which we introduce into this equation are the energy losses of electrons per increment of depth. The surface of the target is impermeable to heat. Therefore we suppress the heat flow through the surface $x = o$ by extending the heat sources symmetrically.

We need now the energy dissipation of the electrons. One way to obtain it is to derive it from the well known range-voltage relationship[1]. We attribute a range to the electron, not only before it hits the target, but also after it has penetrated to a certain depth and lost some energy. Looking again at Fig. I we let the electron penetrate to a depth dX, its energy will decrease by a differential dE.

$$T(x_1, t_1) = \frac{1}{\rho c} \int_0^{t_1} \int_{-\infty}^{+\infty} f(x, t_1 - t) G(x_1 - x, t_1 - t) dx dt$$

$$G = \frac{1}{\sqrt{4\pi(t_1 - t)\lambda / c\rho}} \exp\left[-\frac{(x_1 - x)^2}{4(t_1 - t)\lambda / c\rho}\right]$$

Temperature Induced by Distributed Heat Sources

FIGURE 3

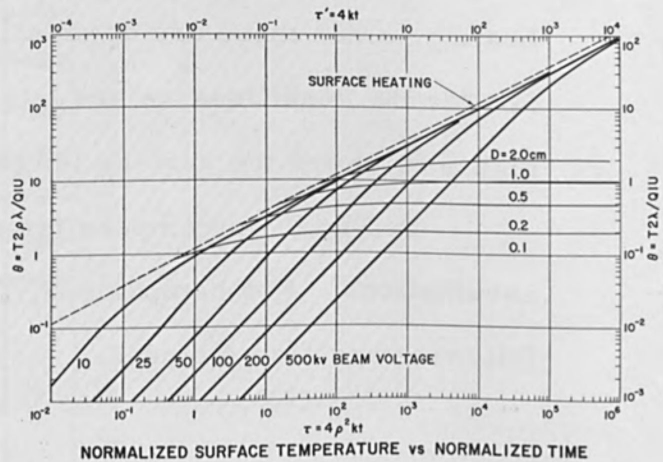

NORMALIZED SURFACE TEMPERATURE vs NORMALIZED TIME

FIGURE 4

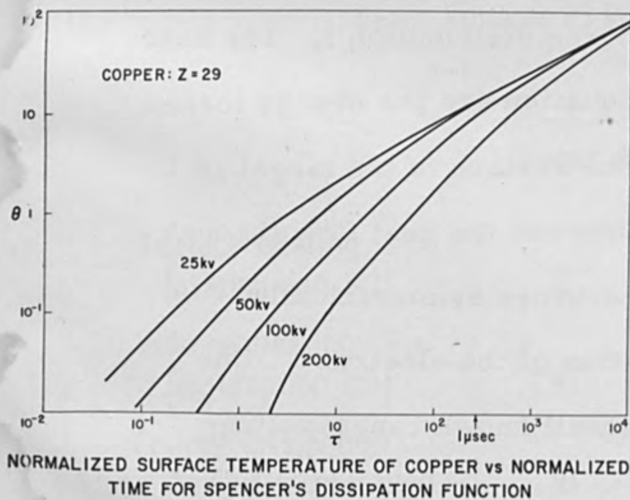

NORMALIZED SURFACE TEMPERATURE OF COPPER vs NORMALIZED TIME FOR SPENCER'S DISSIPATION FUNCTION

FIGURE 5

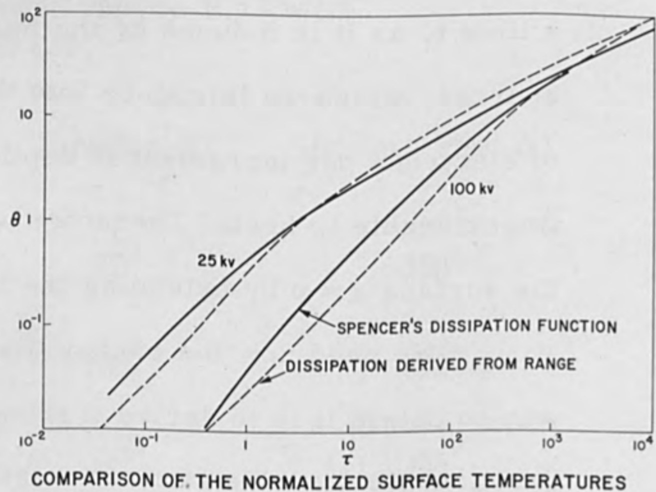

COMPARISON OF THE NORMALIZED SURFACE TEMPERATURES

FIGURE 6

Its range has also decreased by dX. We see that the energy dissipation is obtained by simply differentiating the range-voltage relationship. But we must keep in mind that this is only an approximation. Actually, the loss of energy is statistical.

Nevertheless it is useful to take this simple form of energy dissipation as heat source distribution. It turns out, that after some mathematical transformations, the integral becomes independent of the properties of the target. We evaluate the integral numerically and plot a universal diagram of normalized temperature versus normalized time, Fig. IV. This applies to 1 Mw/cm^2. Any other power density just changes the temperature proportionally. We see that all curves reach the $\sqrt{t}$ – law. But for longer times, the temperature will not follow indefinitely this straight line, even if the power density is low enough, that the melting point is still far away. Sooner or later the final diameter of the beam will limit the temperature, and this is shown by the second set of curves with different diameters indicated. These curves are plotted for one kw/cm^2 and the scales are on top and right.

Going back to the short time part of the diagram we must keep in mind, that it is based on the very simplified energy dissipation, neglecting all scattering.

If we want to take into account the scattering of electrons, the calculation becomes rather difficult. Tables of the computed dissipation for the elements carbon, aluminum, tin and lead are given by L. V. Spencer(2). With Spencer's energy dissipation we have again computed the temperature versus time and plotted the corresponding diagram, Fig. V. This diagram is not a priori universal. It applies

only to copper. But if we plot it in normalized form, and compare it with the diagrams obtained for tin and lead, we see that except at low temperature, this new diagram is the same for all three elements; it can again be taken for universal, at least for the elements from copper on (considering the atomic number).

A comparison of the two diagrams is shown in Fig. VI.

DISCUSSION

The diagrams show that at the beginning the temperature rises with the first power of time, the rate being given by the energy dissipation at the surface (volume heating). For an intermediate time the exponent becomes slightly greater than one. For longer times the temperature approaches the half power of time (surface heating). The anomaly of the temperature rise at the transition from volume heating is due to the inhomogeneous distribution of heat sources. It is the heat produced at a certain depth which appears now at the surface.

For long times Spencer's dissipation gives lower temperatures, because Spencer made allowance for the energy loss by reflected electrons. At the other end of the diagram it gives higher temperatures for short times while at still shorter times, below the range of the diagram, the solid curves tend to go again below the dotted curves, because the energy dissipation at the surface is smaller in Spencer's computation, whereas his maximum dissipation is much closer to the surface. So the heat produced at some depth already appears on the surface at the beginning of the time scale. In the dotted curve this effect appears in the middle of the diagram because

the maximum of heat production is at maximum depth. One should assume that the solid curve gives the better representation of the surface temperature.

We can draw this conclusion from looking at the diagram: for a pulse length of 10 μsec or less and voltages of 200 kv or more, targets of copper or tungsten have not yet reached the $\sqrt{t}$ law. This applies for even longer pulse lengths for the poorer heat conductors. If we want to use the diagram to compare the behavior of many different solids under various conditions, we can simplify the task by taking a transparent grid with a time-temperature scale as shown in Fig. VII and put it on top of the diagram. This delivers us from computing the normalized times and temperatures for every reading.

An experimental check of the temperature rise within very short times has been undertaken by Mr. Silverman at Lincoln Laboratory. His results were published last year(4). The apparatus is shown in Fig. VIII. The light intensity from the target is measured with a multiplier and displayed with an oscilloscope. A red filter is put in front of the multiplier (not shown in the figure). We cannot look into the many difficulties, calibrations, secondary measurements etc. Only the final results are shown in Figs. IX, X, XI. The voltage is varied, and the corresponding power density is determined (independently). The "predicted" temperature after 10 μsec is taken from the computed diagram, and shown as solid points connected by the line. The conditions are such that both diagrams give practically the same temperature. The open circles represent the optically measured temperature. The agreement seems to be fairly good.

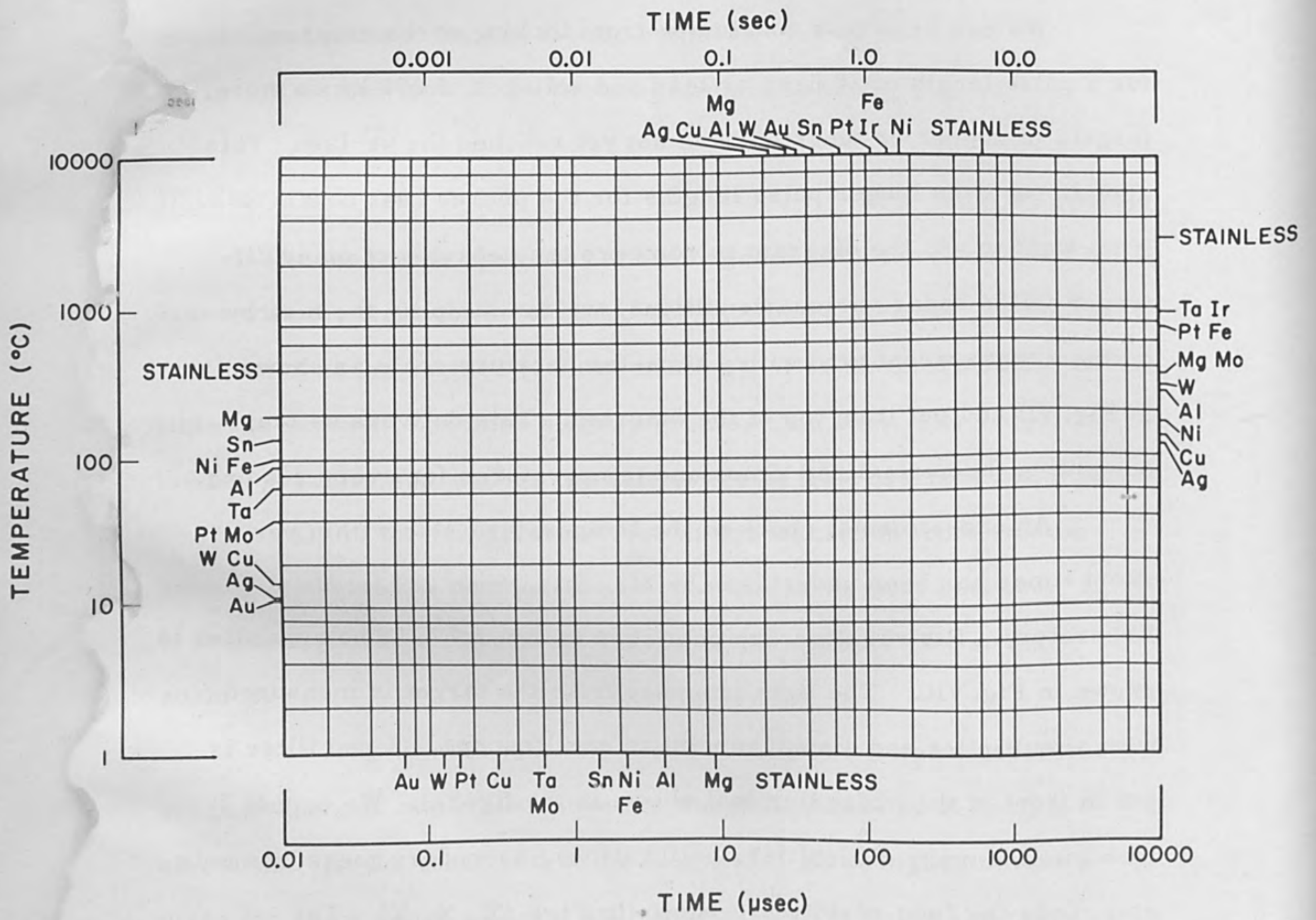

FIGURE 7

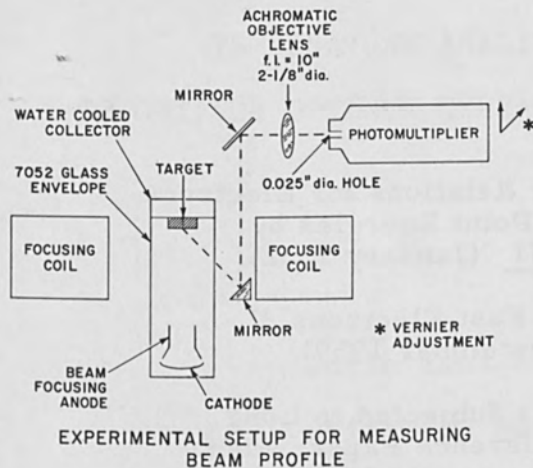

EXPERIMENTAL SETUP FOR MEASURING BEAM PROFILE

FIGURE 8

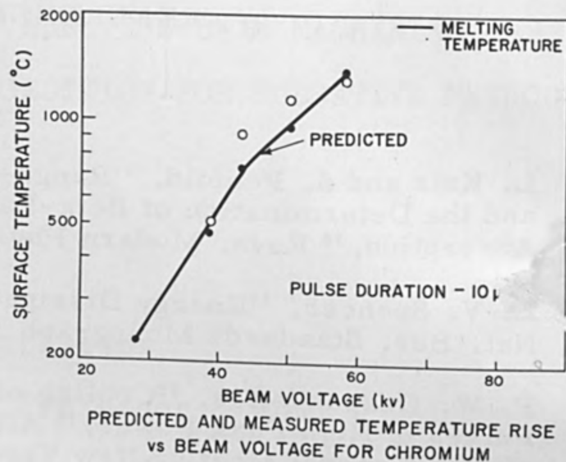

PREDICTED AND MEASURED TEMPERATURE RISE vs BEAM VOLTAGE FOR CHROMIUM

FIGURE 9

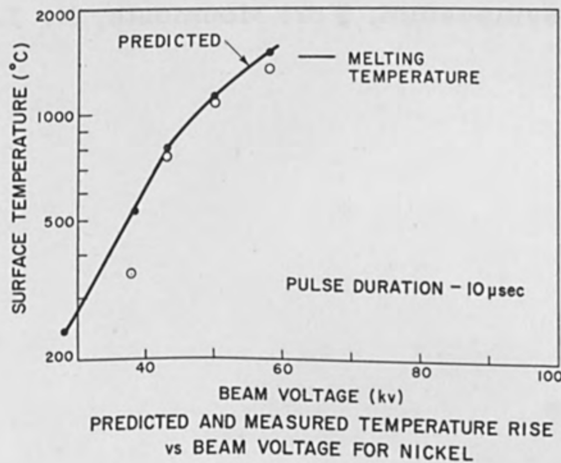

PREDICTED AND MEASURED TEMPERATURE RISE vs BEAM VOLTAGE FOR NICKEL

FIGURE 10

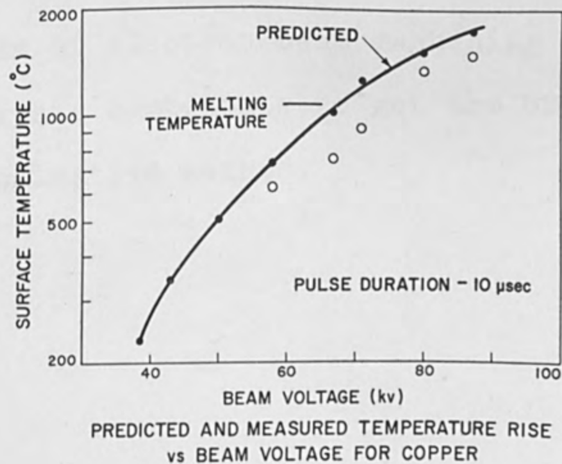

PREDICTED AND MEASURED TEMPERATURE RISE vs BEAM VOLTAGE FOR COPPER

FIGURE 11

REFERENCES

1. L. Katz and S. Penfold, "Range-Energy Relations for Electrons and the Determination of Beta-Ray End-Point Energies by Absorption," Revs. Modern Phys. 24-N1 (January 1952).

2. L. V. Spencer, "Energy Dissipation by Fast Electrons," Nat. Bur. Standards Monograph 1 (10 September 1959).

3. P. W. Crapuchettes, "Cooling of Anodes Subjected to Long Pulses of High Peak Power," AIEE Conference Paper, AIEE Winter General Meeting New York (29 January to 3 February 1961).

4. E. Silverman, "Measurement of the Surface Temperature of a Solid Under Electron Bombardment," Conference Paper High Power Microwave Symposium, Fort Monmouth, N. J. (24 September 1962).

TEMPERATURE ANALYSIS OF ELECTRON BEAM MACHINING
--TO GET THE OPTIMUM OPERATING CONDITION FOR PULSATIVE METHOD--

BY

Norio Taniguchi, Professor

Seiichiro Maezawa, Professor

Department of Mechanical Engineering, Yamanashi University

Kofu, Japan

ABSTRACT

A temperature analysis starting from plausible assumptions on the mecnanism of electron beam machining is given. The results of analysis contribute to get the optimum operating condition for pulsative method.

Temperature Analysis of Electron Beam Machining

-- To get the Optimum Operatig Condition for Pulsative Method --

I. Introduction.

It is the usual practice, that when performing the electron beam machining the beam of electrons is applied in the form of periodic series of pulses. It is said that the pulsative application, with the sharp focussing, of the beam secures the concentration of the temperature rise to the sufficient small region and contributes to the accuracy of machining.

Starting from the plausible assumptions about the mechanism of machining, we take up and analyse the temperature distribution of a semi-infinite body subject to a periodic series of heat pulses on the small circular area in its surface, the other part of which is impermeable to heat.

The results of analysis confirm the above features of the praxis. Moreover, they give some directory informations for determining the length of period, the duration of pulse, the diameter and the total wattage of the electron beam for the particular material to be machined.

II. Theoretical Formulas.

A semi-infinite body ($z \geqq 0$) of thermal conductivity K cal/°C cm sec and of diffusivity κ cm^2/sec is subject to a periodic series of heat pulses on the circular area of radius a cm ($x^2 + y^2 \leqq a^2$, $z = 0$) in its surface, the other part of

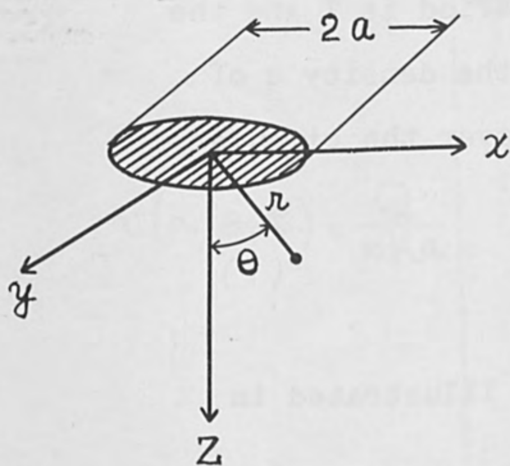

Fig. 1

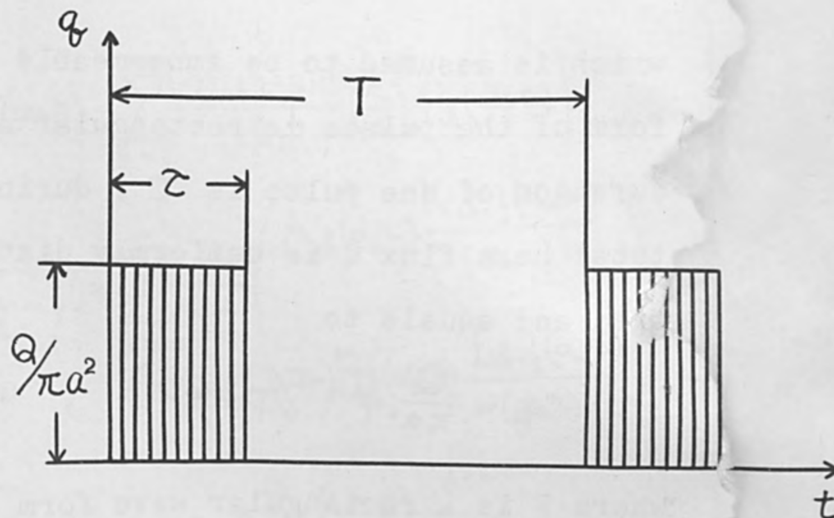

Fig. 2 Rectangular wave form function

$q = \frac{Q}{\pi a^2} F(\tau/_T, \omega t)$

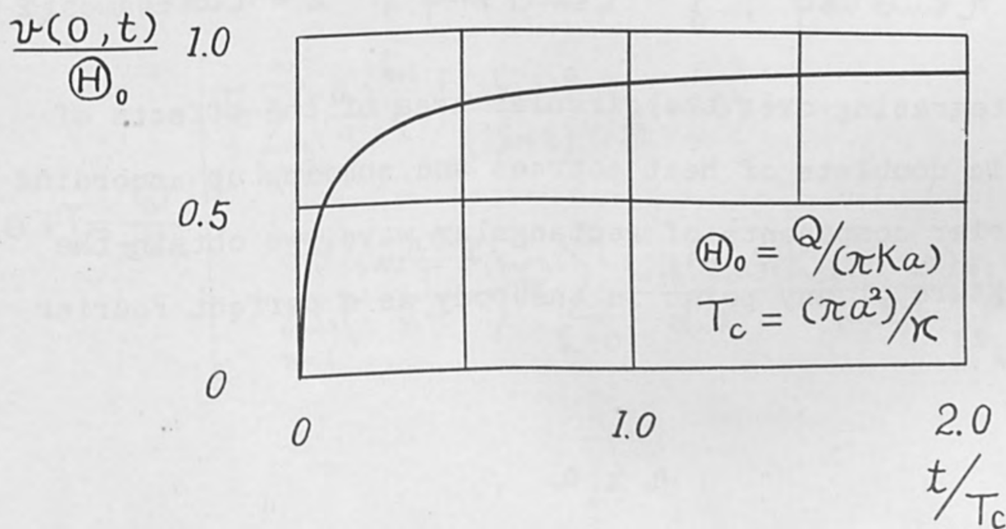

Fig. 3 Temperature of the centre due to step heat flux $Q(t \geqq 0)$

which is assumed to be impermeable to heat. (Fig.1) The wave form of the pulses is rectangular and the period is T and the duration of one pulse is τ , during which the density q of total heat flux Q is uniformly distributed over the circular area and equals to

$$q = \frac{Q}{\pi a^2} F(\tau/T, \omega t) \quad , \quad \omega = \frac{2\pi}{T} \qquad (1)$$

where F is a rectangular wave form function illustrated in Fig.2.

We consider the steady periodic temperature distribution after the transient phenomena having already died out. Adopting the spherical polar coordinates (r, θ , ϕ), which gives

$$x = r\sin\theta\cos\phi \;,\; y = r\sin\theta\sin\phi \;,\; z = r\cos\theta \qquad (2)$$

and integrating over the circular area of the effects of periodic doublets of heat sources and summing up according to Fourier components of rectangular wave, we obtain the temperature of any point in the body as a perfect Fourier series.[2)]

For

$$r \leqq a \;,$$

it is given as

$$v(r,\theta,t)=\frac{Q}{\pi K a}\left[\begin{array}{l}\frac{\tau}{T}\left\{1-\frac{r}{a}P_1(\cos\theta)-\sum_{k=1}^{\infty}\frac{(-1)^k(2k-3)!!}{(2k)!!}\left(\frac{r}{a}\right)^{2k}P_{2k}(\cos\theta)\right\} \\ +\sum_{n=1}^{\infty}\left(\frac{\sin\frac{n\tau}{T}\pi}{n\pi}\right)\mathcal{R}\sum_{k=0}^{\infty}\frac{1}{\alpha_n a}\left(\begin{array}{l}A_{2k}(\alpha_n r)\frac{K_{2k+\frac{1}{2}}(\alpha_n r)}{(\alpha_n r)^{\frac{1}{2}}} \\ +B_{2k}(\alpha_n r)\frac{I_{2k+\frac{1}{2}}(\alpha_n r)}{(\alpha_n r)^{\frac{1}{2}}}\end{array}\right)\times \\ \times P_{2k}(\cos\theta)e^{jn\omega t}\end{array}\right]$$

.... (3)

And for

$$r \geqq a$$

it becomes

$$v(r,\theta,t)=\frac{Q}{\pi K a}\left[\begin{array}{l}\frac{\tau}{T}\sum_{k=0}^{\infty}\left(\frac{a}{r}\right)^{2k+1}(-1)^k\frac{(2k-1)!!}{(2k+2)!!}P_{2k}(\cos\theta) \\ +\sum_{n=1}^{\infty}\left(\frac{\sin\frac{n\tau}{T}\pi}{n\pi}\right)\mathcal{R}\sum_{k=0}^{\infty}\frac{C_{2k}(\alpha_n a)}{\alpha_n a}\frac{K_{2k+\frac{1}{2}}(\alpha_n r)}{(\alpha_n r)^{\frac{1}{2}}}P_{2k}(\cos\theta)e^{jn\omega t}\end{array}\right]$$

...........(4)

where $\mathcal{R}$ represents the real part of the succeeding expression and

$$\alpha_n=\frac{1+j}{2}\sqrt{\frac{n\omega}{\kappa}}\quad,\quad j=\sqrt{-1} \qquad (5)$$

$$A_{2k}(\alpha_n r) = 2(4k+1)P_{2k}(0)\int_0^{\alpha_n r} I_{2k+\frac{1}{2}}(z)\, z^{\frac{1}{2}}\, dz \qquad (6)$$

$$B_{2k}(\alpha_n r) = 2(4k+1)P_{2k}(0)\int_{\alpha_n r}^{\alpha_n a} K_{2k+\frac{1}{2}}(z)\, z^{\frac{1}{2}}\, dz \qquad (7)$$

$$C_{2k}(\alpha_n a) = 2(4k+1)P_{2k}(0)\int_0^{\alpha_n a} I_{2k+\frac{1}{2}}(z)\, z^{\frac{1}{2}}\, dz \qquad (8)$$

$$\left.\begin{array}{l} (2k-1)!! = 1.3.5\ldots\ldots(2k-1)\ ,\ (2k)!! = 2.4\ldots\ldots(2k) \\ (-1)!! = 0!! = 1 \end{array}\right\} \qquad (9)$$

III. Mean Temperature on the hemisphere of radius r

To obtain the general outlook, we leave the variation of temperature due to the polar angle Θ out of consideration, namely we study the mean temperature $\bar{v}(r,t)$ on the hemisphere of arbitrary radius r.

For

$$r \leqq a \quad ,$$

this mean temperature is calculated from (3) as

$$\bar{v}(r,t) = \frac{Q}{\pi K a}\left[\frac{\tau}{T}\left(1-\frac{1}{2}\frac{r}{a}\right) + 2\sum_{n=1}^{\infty}\left(\frac{\sin\frac{n\tau}{T}\pi}{n\pi}\right)\mathcal{R}\left\{\frac{\left(\begin{array}{l}1-e^{-\alpha_n r}\\ -e^{-\alpha_n a}\sinh\alpha_n r\end{array}\right)}{(\alpha_n a)(\alpha_n r)}\, e^{jn\omega t}\right\}\right] \qquad \ldots\ldots\ldots\ldots(10)$$

and for

$$r \geqq a \quad ,$$

we obtain from (4)

$$\bar{v}(r,t) = \frac{Q}{\pi K a}\left[\frac{\tau}{T}\frac{1}{2}\frac{a}{r} + 2\sum_{n=1}^{\infty}\left(\frac{\sin\frac{n\tau}{T}\pi}{n\pi}\right)\Re\left\{\frac{\cosh \alpha_n a - 1}{(\alpha_n a)(\alpha_n r)}e^{-\alpha_n r}e^{jn\omega t}\right\}\right]$$

$$\ldots\ldots\ldots\ldots(11)$$

Especially for the centre of the area

$$r = 0 \quad ,$$

it becomes

$$\bar{v}(0,t) = \frac{Q}{\pi K a}\left[\frac{\tau}{T} + 2\sum_{n=1}^{\infty}\left(\frac{\sin\frac{n\tau}{T}\pi}{n\pi}\right)\Re\left\{\frac{1 - e^{-\alpha_n a}}{\alpha_n a}e^{jn\omega t}\right\}\right]$$

$$\ldots\ldots\ldots\ldots(12)$$

IV. Time constant T_c and saturation temperature Θ_0

We introduce the following time interval as the time constant for our problem, that is

$$T_c = \pi a^2 / \kappa \tag{13}$$

The physical meaning of this constant is made clear by the following considerations. If our semi-infinite body were subject to a step input of heat flux Q for $t \geqq 0$, instead of the periodic series of heat pulses, on the circular area,

the temperature of the centre would become [3)]

$$\vartheta(0,t) = \frac{Q}{\pi K a}\left\{\frac{1}{\sqrt{\pi}}\frac{1-e^{-\xi^2}}{\xi} + \operatorname{erfc}\xi\right\} \qquad (14)$$

where

$$\xi = \frac{1}{2\sqrt{\pi}}\left(T_c/t\right)^{\frac{1}{2}} \qquad (15)$$

By plotting this relation (14), we obtain Fig.3, on which we see at $t = T_c$ the temperature of the centre reaches nearly 80% of its saturation temperature

$$\Theta_0 = Q/(\pi K a) \qquad (16)$$

We can write generally

$$\vartheta(r,\theta,t) = \Theta_0 \Phi_1\left(\frac{\tau}{T}, \frac{T}{T_c}, \frac{r}{a}, \theta, \omega t\right) \qquad (17)$$

and

$$\bar{\vartheta}(r,t) = \Theta_0 \Phi_2\left(\frac{\tau}{T}, \frac{T}{T_c}, \frac{r}{a}, \omega t\right) \qquad (18)$$

while as $T/T_c \to \infty$ we obtain the quasi-static temperature variation as follows, where F is the foregoing rectangular wave form function,

$$\left.\begin{aligned} \lim_{T/T_c\to\infty} \bar{\vartheta}(r,t) &= \Theta_0\left(1-\frac{1}{2}\frac{r}{a}\right)F\left(\frac{\tau}{T}, \omega t\right), \quad r \leqq a \\ \lim_{T/T_c\to\infty} \bar{\vartheta}(r,t) &= \Theta_0 \frac{1}{2}\frac{a}{r} F\left(\frac{\tau}{T}, \omega t\right), \quad r \geqq a \end{aligned}\right\} \qquad \ldots\ldots\ldots(19)$$

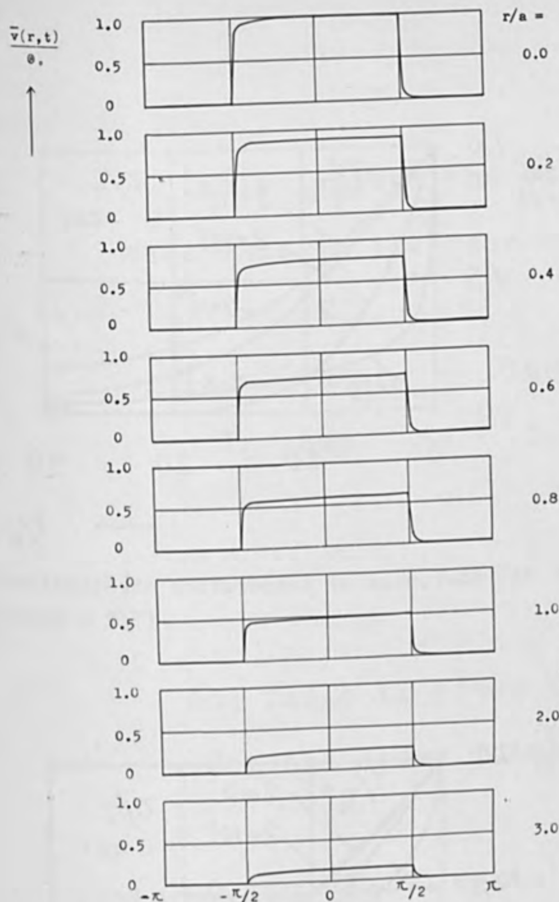

Fig. 4 $\frac{\bar{v}(r,t)}{\Theta_0}$ (τ/T = 0.5 , T/T_c = 2.0)

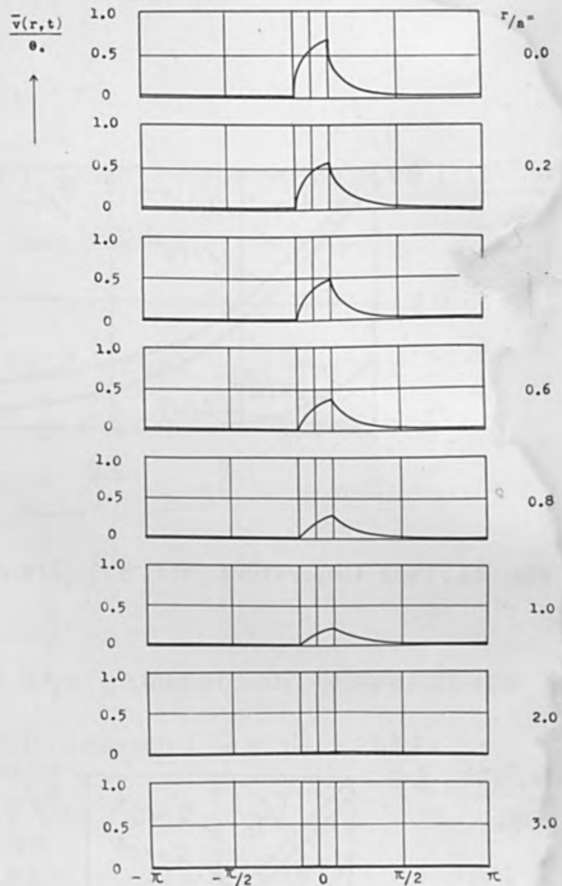

Fig. 5 $\frac{\bar{v}(r,t)}{\Theta_0}$ (τ/T = 0.1 , T/T_c = 2.0)

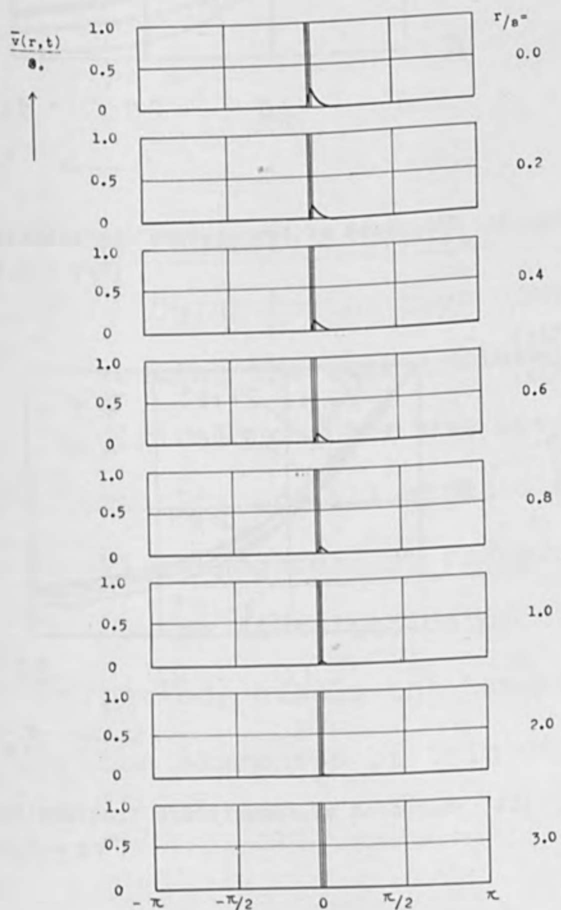

Fig. 6 $\frac{\bar{v}(r,t)}{\Theta_0}$ (τ/T = 0.01 , T/T_c = 2.0)

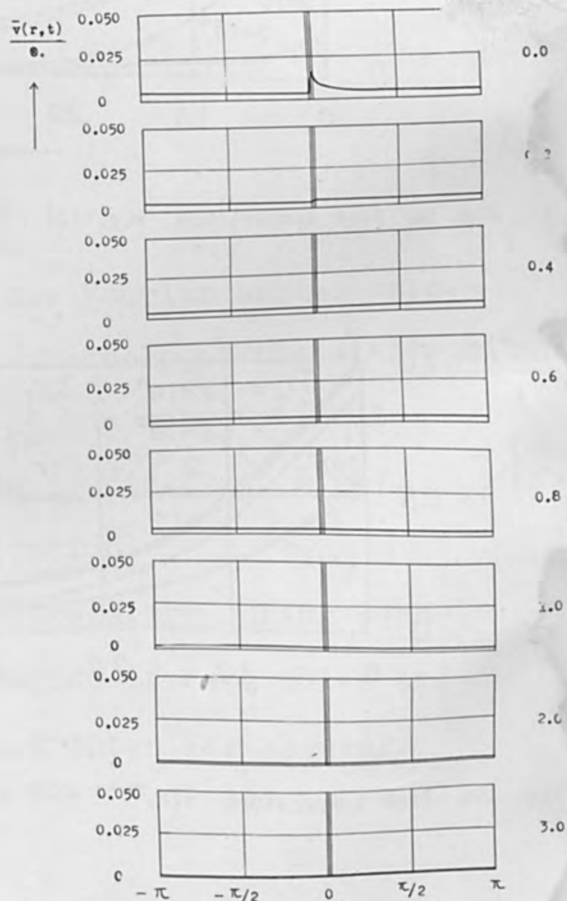

Fig. 7 $\frac{\bar{v}(r,t)}{\Theta_0}$ (τ/T = 0.01 , T/T_c = 0.02)

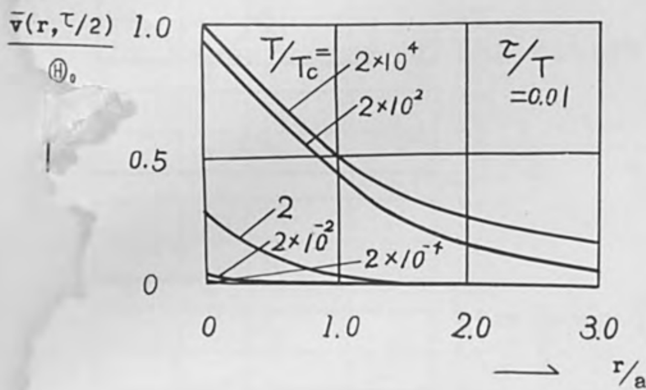

Fig. 8a Peak temperature $\bar{v}(r,\tau/2)$ (τ/T = 0.01)

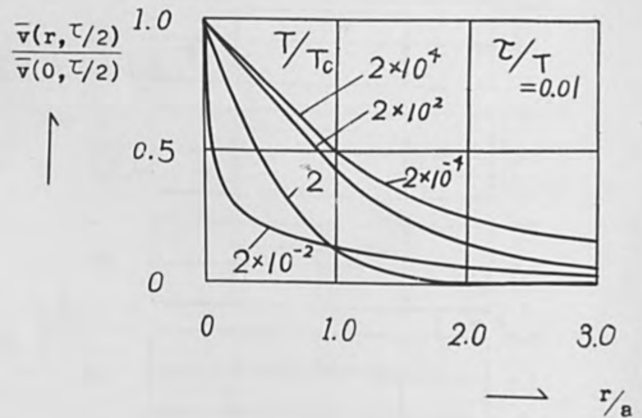

Fig. 8b Sharpness of temperature distribution (τ/T = 0.01)

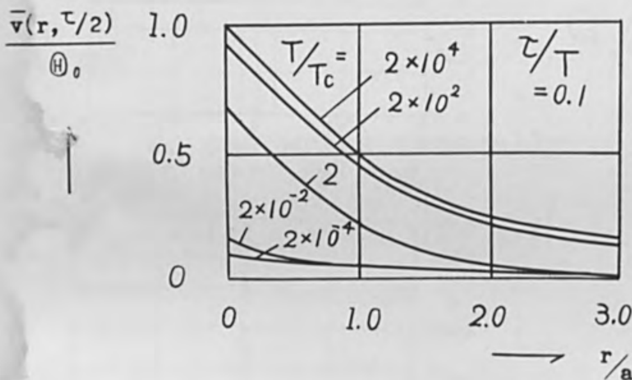

Fig. 9a Peak temperature $\bar{v}(r,\tau/2)$ (τ/T = 0.1)

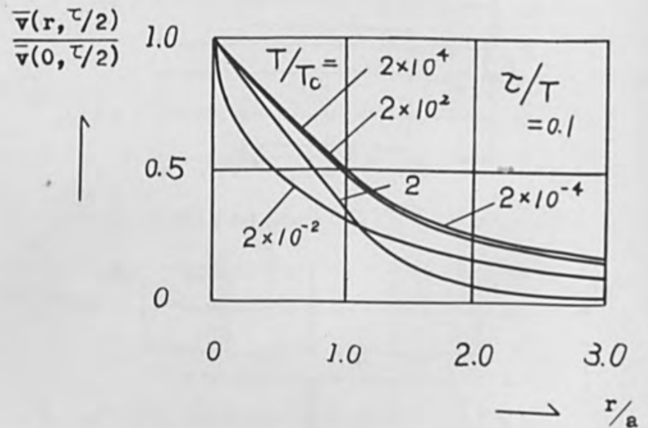

Fig. 9b Sharpness of temperature distribution (τ/T = 0.1)

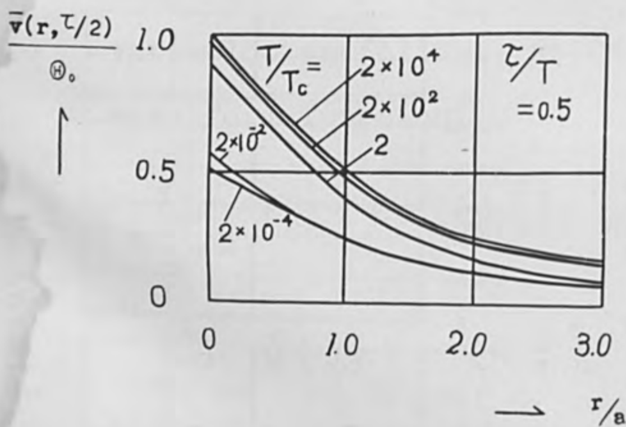

Fig. 10a Peak temperature $\bar{v}(r,\tau/2)$ (τ/T = 0.5)

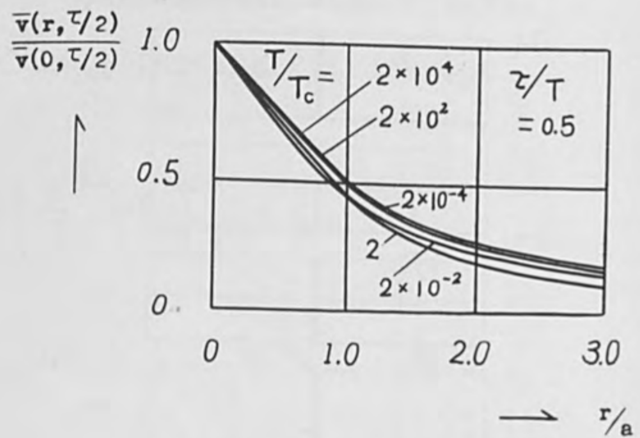

Fig. 10b Sharpness of temperature distribution (τ/T = 0.5)

Table I gives the values of T_c for some representative materials in the case of the radius of beam a = 0.1mm.

(a = 0.1mm)	Clown glass	mild steel	copper
T_c sec	5.5×10^{-2}	2.6×10^{-3}	2.75×10^{-4}

Table I

And Table II gives the values of the saturation temperature for the above materials for a = 0.1mm and Q = 50 watts.

(a = 0.1mm, Q = 50 watts)	Clown glass	mild steel	copper
$\Theta_0 = Q/\pi K a$ °C	140000	3450	408

Table II

V. Numerical Results.

Owing to the poor convergency of the Fourier series representing the mean temperature $\overline{v}(r,t)$, the help of the electronic digital computer was needed.[4)] Some of the computational results are illustrated in Fig.4, Fig.5, Fig.6 and Fig.7.

VI. Sharpness of temperature distribution.

The distribution of the maximum temperature during each period, namely the temperature at the end of each pulse and the sharpness of this distribution are shown for several

working conditions in Fig.8a, Fig.8b, Fig.9a, Fig.9b, Fig.10a and Fig.10b. From these figures we may conclude that in order to get the sharp concentration of temperature rise, we must take the pulse-period ratio τ/T small with the corresponding appropriate value of T/T_c. For example, in the case of τ/T 0.01, the optimum value of T/T_c lies somewhere between 0.01 and 0.1. The small value of τ/T is seen to be effective for securing the good accuracy, as much as for obtaining the great working energy per one pulse for the given mean wattage of the apparatus.

VII. Discussions.

The maximum temperature of any point may be considered as composed of two distinct parts. The first is the base temperature and is due to the continuous application of the mean flux $(\tau/T)Q$. The second is the peak of the fluctuating temperature due to the periodic pulsating flux.

The distribution of the base temperature is the same to that of the quasi-static temperature variation (19). On the other hand, the distribution of the peak of the fluctuating temperature changes according as the pulse-period ratio τ/T and the specific period T/T_c.

For the given τ/T, at the large values of T/T_c this distribution is again the same as that of the quasi-static one, but as T/T_c becomes smaller, this tends to be more sharp. However, at the same time, the absolute value of the peak itself becomes

also smaller.

Thus, as a whole, the distribution of the total maximum temperature, as T/T_c becomes smaller, at first is equal to the quasi-static one and then becomes more or less sharper by the degree according to the value of τ/T and lastly comes back again to the quasi-static one of the base temperature alone. Therefore, somewhere inbetween there must be the optimum operating condition.

In the above considerations, the transient phenomena directly after the commencement of beam bombardment is neglected. But, as seen from Table I, T_c is a very short interval and T is still more short, therfore in the scarecely appreciable time this transient must have died out and our steady state of temperature is established.

At the ideal condition of machining, probably the work may be evaporated bit by bit by means of the energy of each one pulse. Therefore, after determining the optimum values of τ/T and T/T_c, we must give the sufficient wattage to the electron beam to rise the temperature above the evaporating point by each one pulse.

For example, in the case of the glass as the material to be machined, we choose $\tau/T = 0.01$ and $T/T_c = 2\text{x}10^{-2}$. (Fig.7). From Table I, $T_c = 5.5\text{x}10^{-2}$, so $T = 1.1\text{x}10^{-3}$ and the frequency is 1.1 kc. From Table II, $\Theta_0 = 1.4\text{x}10^{5}$ and $\bar{v}(0, \tau/2) = 0.036\,\Theta_0 = 4900\ ^\circ C$ for $Q = 50$ watts. Assuming the evaporating tempe-

rature 1000°C, we need 50x(1000/4900) = 10watts for a = 0.1mm.

The finiteness of the actual work to be machined and the existence of radiation and conduction through its surface both contrary to our assumptions may change the absolute value and the distribution of the fluctuating and especially base temperature. But, this change may not be so great that it obliterates the general conclusions of our analysis.

References.

(1) Panzer, S. and Steigerwald, K.H., E.T.Z. A81(1960), p. 925.

(2) Maezawa, S., 12th Japan Nat. Congr. appl. Mech. 1962, Preprint.

(3) Carslaw, H.S. and Jaeger, J.C., Conduction of Heat in Solids, Oxford, 1959, p. 264.

(4) The authors owe very much to Dr. Nagami of the Central Institute of Tokyo Shibaura Electric Co.

AN AUTOMATED MICROCIRCUIT E. B. PROCESSOR

By

A. H. Andrews
Manager
Electron Beam Section

CBS Laboratories
227 High Ridge Road
Stamford, Connecticut

AN AUTOMATED MICROCIRCUIT E.B. PROCESSOR

The original request from the Naval Avionics Facility was for an experimental processor for the deposition of thin films using various conductive, resistive or dielectric materials. The request arose from the fact that no appropriate commercial equipment existed.

The entire equipment was to be experimentally oriented and to incorporate the latest vacuum practices, mask alignment devices and monitoring techniques. To the greatest extent possible, the equipment was to utilize commercially available components and materials. Reliability, performance, ease of maintenance, safety and flexibility were to be emphasized. Although the concepts of experimental orientation and inherent flexibility were to be the overriding ones, provisions should be made for easy conversion to automatic operation at some later date.

In a late issue of the magazine "Electronic Design"[1] is an article on the four chamber in-line vacuum system developed under this contract by IBM of Kingston, New York. This equipment has a top speed of 750 circuits per hour, that is about 3,000 components. All these components are passive ones, of course.

The equipment I am going to describe can most readily be used to extend the scope of what will then be a five chamber in-line processor, into the field of active microcircuit components, by the spot alloying of deposited thin films with an electron-beam.

(1) Electronic Design, Vol. 11, #4, Page 47

The electron beam processing chamber can also be used for etching and machining, or for the welding of leads to finished micro-circuit modules. Also, the beam when unmodulated, but still in the scanned mode of operation, must be capable of use for surface conditioning for the polymerization or nucleation of substrates over an area of one inch square. Initially, the fifth chamber is to be employed as a single experimental unit, so that techniques and correct operating parameters, for any particular function, may be determined.

The E.B. Processor consists of four basic units: the electron-gun and its power supplies; the electron-beam deflection programmer; a 14" TV type monitor to display what the gun should be doing; and of course, the vacuum chamber and its pumps. To ensure absolute compatibility with the other four chambers, a fifth vacuum system was ordered from C.V.C. and the lower port modified to accept the electron-gun tube and current feed-throughs.

The vacuum chamber is approximately 2 ft. wide x 18 inches high x 2 ft. deep. It is pumped by a 4,000 litre/sec diffusion pump with a cooled chevron baffle. The diffusion pump is backed by an 80 cu.ft./min. mechanical pump and 3 cFm. holding pump. The holding pump is also used to rough out the electron-gun chamber, if a cathode has been replaced. All the valves are electro-pneumatic. Pump down cycle-time is to the low 10^{-6} Torr, in less than one hour from cold.

When designing the electron gun and its programmer for this processor, several criteria were of the utmost importance:

1. Power capability of the electron-beam

2. The impinging spot-size

3. X-ray hazards

4. General Safety

5. Type of programming

6. Deflection power requirements

7. Cables and insulation

Under the first heading of beam power capability little data was generally available when this project was undertaken, with the exception of some figures on tungsten foil machining from Steigerwald of Zeiss. His figures of $10^4 A/cm^2$ for 10 nanoseconds gives a requirement for 10^{-4} coulombs/cm^2.

A reasonably high voltage, at which to operate, would be 20-30KV from the points of view of negligible X-ray hazard, low deflection power requirements and readily available cabling, in the form of small X sectional coax-cable, also ideal from the video aspect of the programmer.

Steigerwald's figures show that to punch a hole through thin tungsten foil, we would require 600 μA at 30 KV, into a 1 mil diameter spot for a pulsewidth of 1 μ second. These are reasonable figures from all aspects: KV, current, power density (10 MW/cm^2), impinging spot size and timing. Now, if we consider that our substrate is most likely to be a rectangle 1/2" x 3/8", then maintaining our maximum spot size requirements, we require that there be 500 elements in the major dimension with a 1 μ second dwell time for each element.

Naturally enough, at CBS we have a bias towards TV programming, so let's see how these requirements resolve themselves into circuit parameters.

Surface conditioning a one inch square with a 1 mil spot means that we require 1,000 elements per line. To maintain the same resolution, in the vertical, we have to have 1,000 written lines, i.e. 2,000 TV.

There is no need to raise the scan time above 500 μ secs, in this application the surface is to be conditioned, not machined.

Fig. 1 is a schematic of the circuitry. Top left inside the dotted lines, denoting a light tight enclosure, is a 5" high resolution cathode ray tube, a 100 mm f2 lens, a slide carrier and a 3" ten stage photomultiplier. The flying spot on the C.R.T. face traces a 2,000 TV line raster. After imaging by the lens, the flying spot scans a slide about 35 mm size, the P.M. develops a signal, only where the slide is transparent.

On the substrate, the impinging position of the electron-beam is synchronized with the flying spot on the slide. In order to dictate what parts of the substrate will be alloyed or etched, or where welds are to be made, a negative photoreduction is made of a black and white drawing, those parts to be machined are "filled in" black. This slide is then used in the F.S.S. optical bench.

The upper limit to writing speed is set by bandwidth limitations of the video amplifier, 20 megacycles is a reasonable figure, so this means the fastest scan time will be 50 μ seconds. To maintain versatility, and cover most requirements for later automation, a timer circuit is incorporated, to expose any number of frames from 1 to 100.

Since the slides will be in a light tight enclosure during operation a 14" TV monitor is provided, driven as a slave of the F.S.S. C.R.T. and it displays, constantly and greatly magnified, the circuit to be "machined".

Over to the right of the schematic is the work chamber and gun assembly that will be described later.

The first example of some packaged equipment can be seen in the first photograph (Fig. 2) and this shows the desk console with F.S.S. bench and controls. The high resolution C.R.T. with its focus and deflection coils is to the left on the 120 cm optical bench, center is the lens and the slide carrier. The lens is mounted on an adjustable cross slide, needed to center the raster on the programmer slide. Normally the panels are closed, the center one only can be hinged up whenever a slide is to be changed. Either side of the knee hole are power supplies for the F.S.S., the P.M. and the timer circuit control.

The next photograph (Fig. 3) shows the remainder of the system. The D.E.L. high-voltage power supply, including video input circuits for the electron-gun, is to the right. To the left is the 14" monitor with its associated circuits and the timer circuits controlling the electron-gun. Center is the vacuum chamber with the gun tube hanging down from the bottom flange. The electron-gun itself is in the large diameter enclosure at the lower end, and the high-voltage feed-throughs are inside the Lucite enclosure carrying the cable clamps. Just above the gun enclosure is the condenser-focus coil,required to prefocus the beam to paraxial. This prefocusing is necessary to enable the originally divergent beam to travel the full length of the tube. The length of the electron gun side arm arises from having to provide a roughing port and isolation valve, for the easy replacement of cathodes.

The entire electron-gun is angled slightly, so that even when programming over the largest area contemplated of one inch square, none of the work area can be "seen" by the cathode. In this way, there is

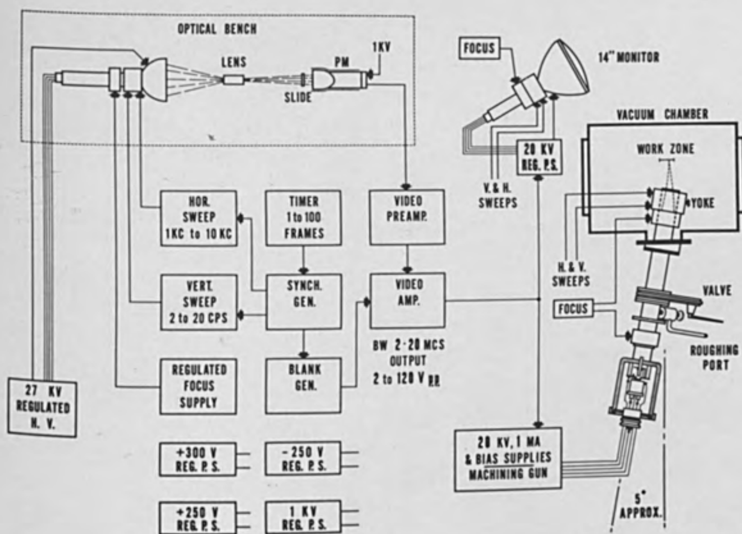

FIGURE 1

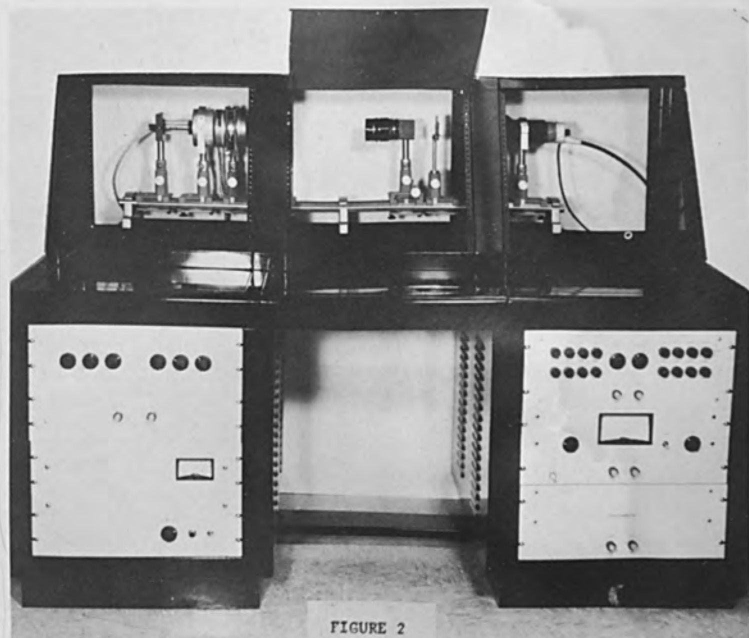

FIGURE 2

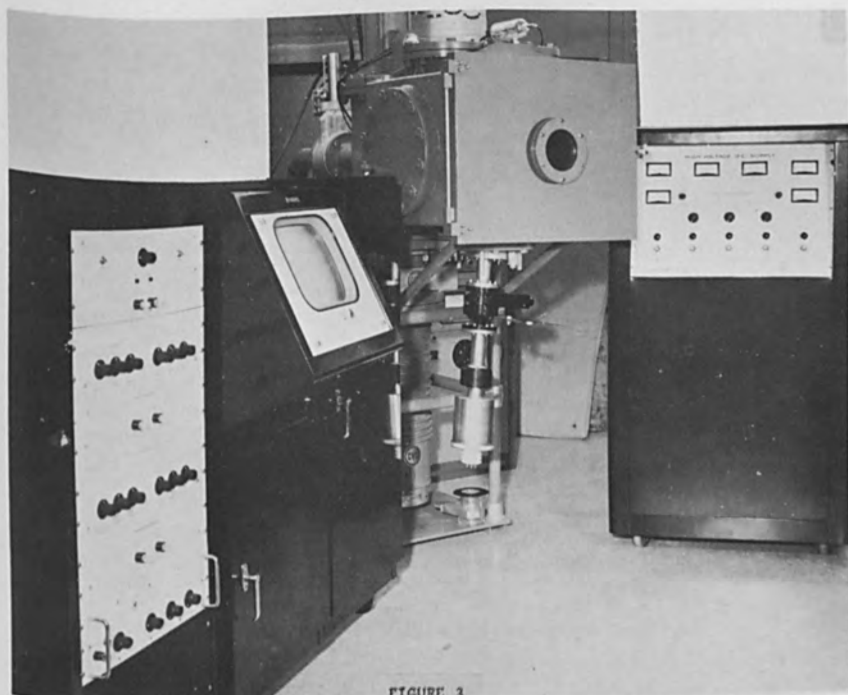

FIGURE 3

FIGURE 4

less cathode contamination, ion trapping is provided and electron exposure of photoresist will be possible, without light-exposure from the cathode.

The final focus-coil and the deflection coils driven by the programming system are sealed units, located inside the vacuum chamber. Using vacuum sealed coils, inside the work chamber, was the best solution to the problem of having to be close to the work zone with the final focus coil, to optimize spot-size requirements. The current feed-throughs are in the bottom 10" flange of the chamber. There are two octal headers and three higher current singles for the monitoring of the test modules, or they may be required to operate motors or solenoids in the vacuum chamber.

The electron-gun is shown in Figure 4. It is of the C.R.T. type and, in cross section, is similar to the one I described in my paper presented here last year. The method of construction is obviously rugged. Grid #1 is of aluminum, the other grids are of 303 stainless. All grids have tantalum or graphite aperture-inserts. The insulators are of boron nitride, the 60° thread machined over their lengths is there to double the surface leakage path. The modulator grid is machined to accept either a 1/8" diameter oxide cathode button, as used in C.R.T., or an 8 mil tungsten wire hairpin as used in electron microscopes, and this latter type is the one shown in the exploded view below.

This gun snaps into place within its enclosure and the four contacts required, or five when an oxide cathode is used, are made by spring loaded plungers mounted on the feed-throughs. The maximum electron beam current available is 1 mA, and this is capable of being modulated with a grid drive of up to 120 V.

Perhaps some of you are wondering how an experimental facility like this, which has a total of 48 variable control knobs, with 8 indicating meters, 17 switches and a requirement for 10 mechanical adjustments, can perform automatically. To explain how this can be done, it is necessary to describe briefly the "set up" when integrated into a five chamber system. Through the five chambers an interrupted feed mechanism will run the entire length, dwelling the necessary time for deposition in each chamber. It is only necessary to have the substrate index in the last chamber and, when at rest, automatically fire the timer with a simple contactor and use a delay circuit to allow the substrate to come completely to rest.

The optimized characteristics of this equipment are yet to be determined under a continuing study program. It is hoped, later, to publish some results of this study phase.

THE "INTERCOL" ELECTRON BEAM SYSTEM USED FOR MICROCIRCUIT ETCHING.

by

W.C. Nixon,
Engineering Laboratory, Cambridge University, England,

R.V. Ely and C.R.E. Legg,
Electron-Physical Instruments Ltd., 99 Malden Road,
New Malden, Surrey, England.

ABSTRACT

The "Intercol" interchangeable electron beam system is a vertical electron optical bench that may be assembled in many different ways. One use is for microcircuit etching with a scanning electron probe. By operating at 5kV it is possible to remove very thin layers of material of a few hundred Angstroms thickness in a single scan.

THE "INTERCOL" ELECTRON BEAM SYSTEM USED FOR MICROCIRCUIT ETCHING.

The "Intercol" interchangeable electron beam system consists of an electron optical column with the electron gun at the bottom and any combination of electron lenses, working chambers, intermediate stages, etc., mounted vertically above the gun. A two lens system is shown in Fig. 1 and a photograph of such a unit in Fig. 2. The construction is completely interchangeable in that each lens or other unit may be fitted anywhere in the column and in any order or orientation. The weight of the column is taken by the supporting pillars and not by the electron optical elements themselves. In this way each lens may be translated for alignment purposes without moving any other part of the column either above or below that lens. A sliding vacuum seal maintains the low pressure within the system during translation. A column may be built up very quickly from a series of parts with the exact number of lenses, position of intermediate viewing screens, etc., decided upon when the exact purpose of the experiment is known.

The uses of such a column fall into two broad categories:

(1) Point source devices where the electron source in the electron gun is reduced in size.

(2) Image magnifying instruments where a primary image is enlarged and recorded.

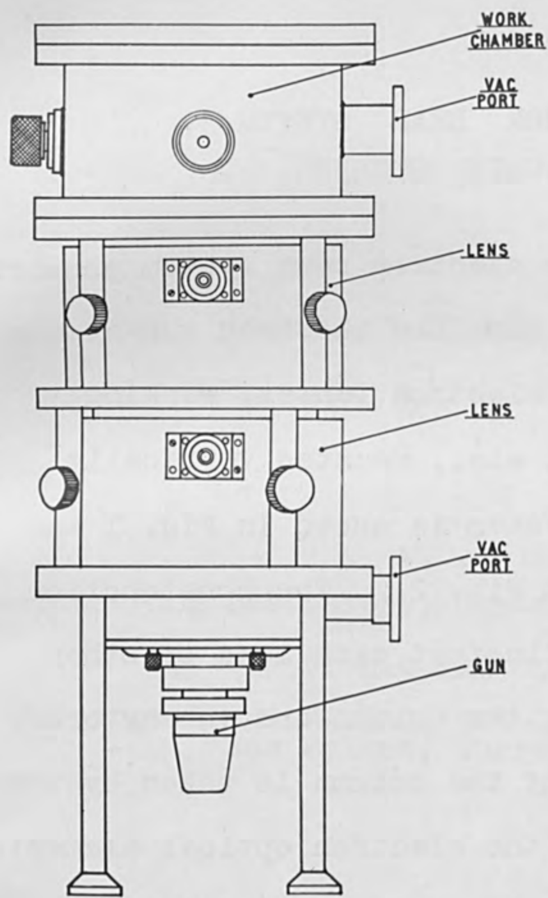

FIGURE 1

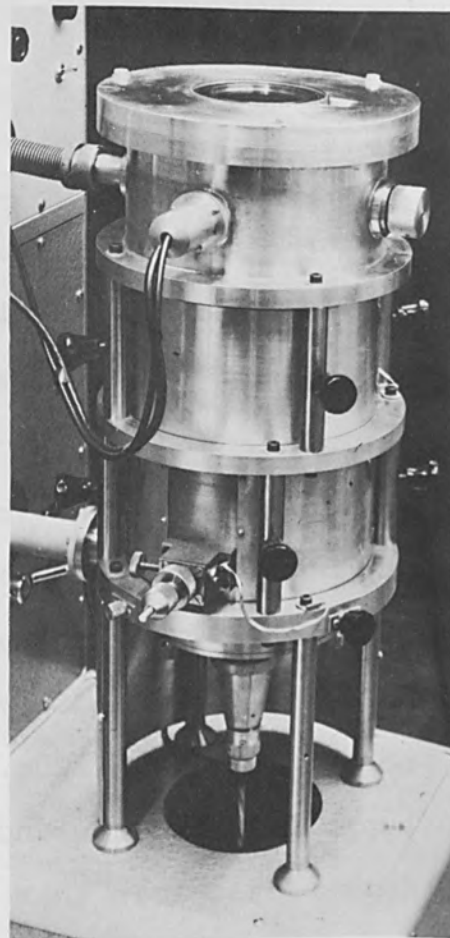

FIGURE 2

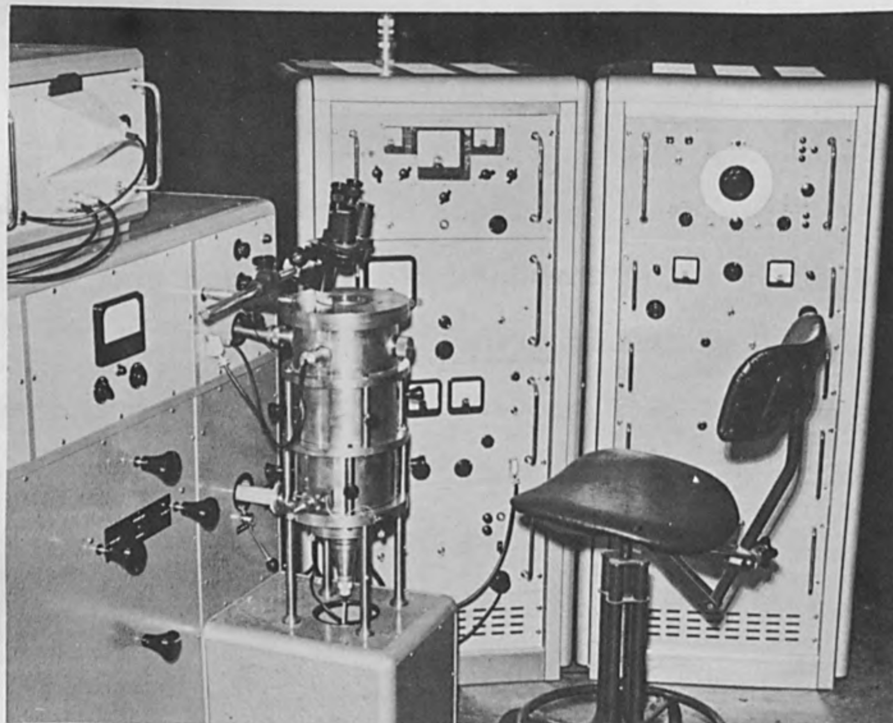

FIGURE 3

In the first category all forms of electron probe instruments may be assembled for applications such as X-ray microanalysis (absorption, fluorescence, emission), X-ray microdiffraction, divergent beam or Kossel line diffraction, cathodoluminescence, static or scanning electron diffraction and many others. This type of scanning electron probe may be used for microcircuit etching as in this paper or for microforming with electrons by thermal or chemical means. In all of these instruments the electron optical components are the necessary parts for production of an electron beam focused and controlled to fine limits irrespective of the final use to which the electron beam is applied.

The other category includes the transmission electron microscope, particularly for low voltage and high contrast, thermionic emission, secondary emission and mirror electron microscopy. All of these applications also require an electron optical column of flexible design but rigid construction and rapid interchange from one mode to another.

The one application under consideration here is the use of a fine focus electron beam for microcircuit etching in microelectronics. A complete unit is shown in Fig. 3. The vacuum pumps and gauges are behind the column within the cubicle. The high voltage supply, lens, filament and bias supplies are in the first rack on the right of the column. The second rack contains the scanning electronics coupled to the beam modulation and control system part of

which is seen on the left of the photograph. This unit operates at 5kV to 30kV and up to 2.5mA. This current is more suitable for drilling small holes or for fine welding of leads and much less current is needed for microetching. The scanned area may be up to 2cm by 2cm with the focal plane 4cm above the top of the lens. The spot size used depends on the speed of scan needed and the material being etched but may be from 5 to 10 microns.

One feature of this instrument is the design of the electron optics for use at relatively low voltages such as 5kV or lower. Other instruments are more suitable for 50kV to 150kV and were not designed with low voltages as a major mode of operation. By operating at this voltage level the power available is dissipated in a much smaller volume so the watts per cubic cm may be higher although the power density per unit area may be less. The total power varies with the high voltage and the gun brightness also varies. The electron penetration varies with some power of the voltage such as V^2 or more recently the correct value may be $V^{1.7}$. If we compare two electron beams with the same current density at 50kV and 5kV we see that the total power will fall by 10 but the power per unit volume will rise by a factor of 10 if V^2 is used or by 5 if $V^{1.7}$ is substituted. The same current density is not impossible in actual cases since neither gun will be operating at 100%

efficiency and so the true ratio of currents will depend on the relative efficiencies of the two guns at the respective kilovoltages.

In any case, whatever the exact increase in power/unit volume is in practice, this power is dissipated more nearly in the surface layer when a low kilovoltage is used. In this way the layer that must be evaporated first at the very surface is the first to be heated and not some layer underneath where the peak value of power loss is found at higher voltages. Similarly, with a reduced electron range there is less chance of thermal damage to sensitive layers in a multilayer device below the area that is being removed. With such a low voltage it is possible to remove from the surface extremely thin layers of a few hundred Angstroms in one scan. An opaque evaporated layer of silicon on a clear substrate has been etched selectively so that fine lines appeared at first dark brown and then light orange and then clear when viewed in transmitted light, after successively deeper scans. Selective etching in depth of multilayer devices is thus possible in principle. The depth could be monitored by interference microscopy, detection of characteristic X-rays, or changes in the electrical properties of the remaining material. Finally, if the voltage is low enough the number of secondary electrons produced will balance the number of incoming primaries and so insulated

surfaces should not charge up [1]. As a result it should be possible to etch insulators as well as conductors or semiconductors indiscriminately and without any further treatment to avoid charging. Although the number of electrons is balanced the secondaries are of very low energy and so there is still a net power input to the surface.

Results.

Some results using this method of electron beam micro-etching are shown in Fig. 4, at a magnification of 100x. The parallel lines in Fig. 4(a) are about 20 microns in width and have been etched through a thin evaporated layer of aluminium and photographed in transmitted light. A similar etched layer is shown in Fig. 4(b) where the thick line at the bottom is about 50 microns in width. The dotted lines show a spot size down to 5 microns and demonstrate beam modulation. The small size of this group of lines and dots makes it difficult to locate again unless a surrounding rectangle cut with an enlarged probe is scribed to enclose the area of interest. The broad line at the bottom is part of this rectangle and lines of this size, 50 microns, are easily seen with the naked eye.

The same area of a partially etched aluminium-gold double layer film is shown in Figs. 4(c), (d), (e) and (f). In (c) transmitted light is used and the three bright white spots show where the beam has been allowed to etch completely

(a) 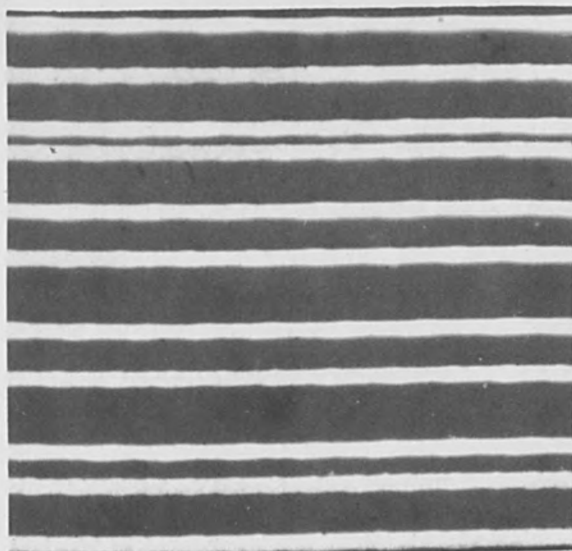

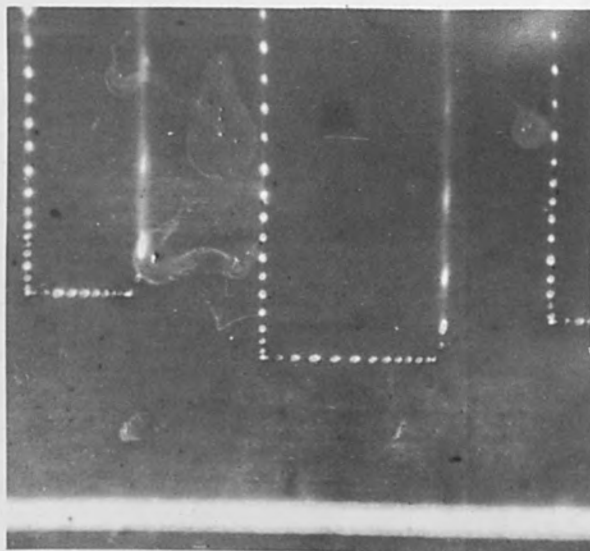 (b)

(c) 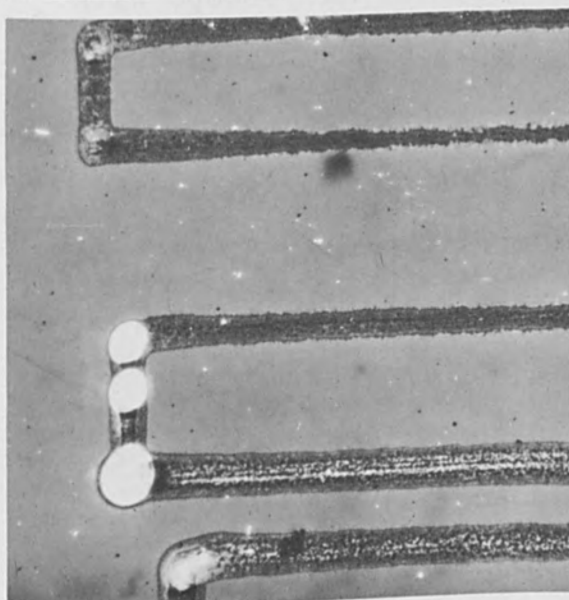

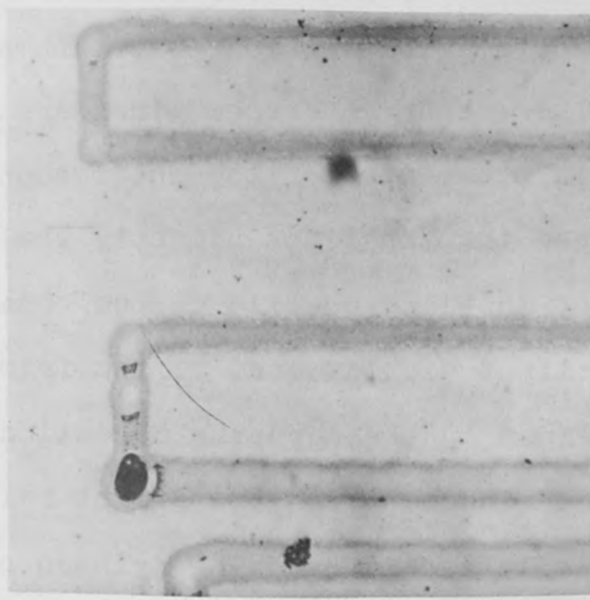 (d)

(e) 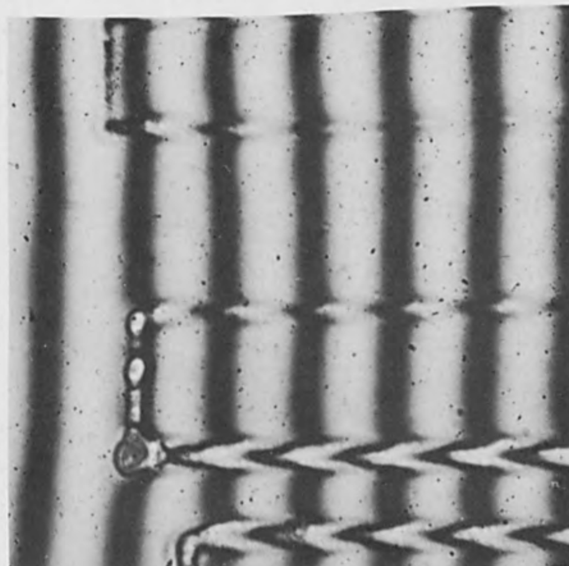

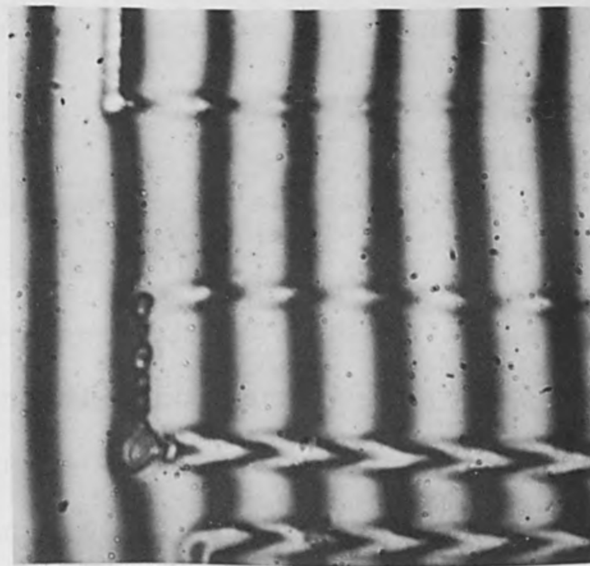 (f)

MAGNIFICATION = 100X

FIGURE 4

through the double layer and all of the light is recorded. The lines are of sufficient depth to remove the aluminium but leave the gold. The same area is seen in (d) in reflected light and now the bright dots have changed contrast and the largest is dark where the incident light has not been reflected at all. A slight ridge along the two edges of each line can be seen. This same area is shown in (e) and (f) using an interference microscope with sodium illumination to obtain a measure of the line depth. The deeper reference lines are about 1200A, the next line in the centre of the photograph is 400A to 600A in depth and the top lines slightly shallower than this. Some idea of the line profile can be obtained and, in particular, a slight displacement of the fringes at the edges of the lines in the opposite direction to the groove depth corresponds with the slight raised edge seen in (d) in reflected light. The fringes of (e) have been reversed in direction in (f) to obtain both interference patterns of the same area.

Conclusions.

These results show the line and spot widths readily obtained with a 5kV electron beam microetching instrument. In addition the low voltage permits removal of very thin surface layers from multi-layer films. Electrical scanning of this beam over a large area allows these conditions of etching to be reproduced following a

predetermined pattern for thin film circuit fabrication in microelectronics and microminiaturization.

Reference.

(1) THORNLEY, R.F.M. Proc. European Conf. Electron Microscopy, Delft, 1960, page 173.

PRECISION ELECTRON BOMBARDMENT FURNACE FOR HIGH PURITY EVAPORATION OF SILICON

By: B.A. Unvala

&

C.W.B. Grigson

Engineering Laboratory
University of Cambridge, England

ABSTRACT

The paper descirbes an electron bombardment furnace and control equipment used for high purity evaporation of silicon and stabilized either for a constant power input or for operation at a constant temperature. The silicon is evaporated at about 1800°C by focussing the electron beam into the center of a silicon rod held in a water-cooled copper pedestal, both the evaporating silicon and the substrate are shielded from the direct line of sight of the tungsten cathode of the electron gun and for evaporation at constant temperature a photoelectric feedback loop is used: the light from the heated spot is reflected by a mirror of vacuum deposited silicon into a photo-multiplier, the output of which controls the bombardment power. The temperature is thus stabilized to better than ± 0.1%.

PRECISION ELECTRON BOMBARDMENT FURNACE FOR HIGH PURITY EVAPORATION OF SILICON

1. INTRODUCTION

Electron bombardment heating has been successfully used for zone refining of silicon[1] and for pulling single crystal silicon from the melt.[2] Until recently attempts[3,4,5] at evaporating silicon by electron bombardment heating have yielded rates of evaporation too low to produce films without significant contamination from the residual gases in the vacuum. For example Namba[5] has found as much as 10% oxygen in his silicon films evaporated at the rate of 0.5 Å/sec in a vacuum of 1-2 x 10^{-5} torr.

This paper descirbes an electron gun and its control system which evaporates silicon with minimum contamination and at high and accurately controlled rates. This gun has recently[6] been used for producing epitaxial layers of silicon by vacuum evaporation.

In the past,electron bombardment furnaces have been controlled by stabilizing the electron current and thereby the input power, but direct control of the furnace by a signal derived from the temperature of the hot zone of the specimen has not been attempted. In the furnace described,direct control has been achieved by using a photomultiplier to indicate the temperature and hence to govern the power. Photoelectric control is used as it provides the only method of stabilizing the temperature

directly without the risk of contamination which can be serious when thermocouples or resistance pyrometers are used. The optical path is so arranged that the deposited material does not affect the transmission of light from the hot zone to the photomultiplier.

2. DESCRIPTION OF THE FURNACE

The furnace is contained by a 12" bell jar evacuated through a liquid nitrogen trap by a 3 stage oil diffusion pump. All the large seals are viton A. The vacuum throughout evaporation of silicon is 10^{-6} to 10^{-5} torr. and limited by outgassing when silicon is heated. With these vacuum conditions the rate of deposition of the evaporated silicon must be several hundred Å/sec if the rate of arrival of the residual gas molecules especially oxygen is to be negligible in comparison with the rate of arrival of silicon. The faster rate is also required to limit the diffusion of impurities across the junction produced by epitaxially deposited layers. To evaporate silicon at this rate its temperature has to be about 1800°C, well above its melting point of 1420°C. This rules out the hanging drop method[3,5] of evaporation as this does not allow the silicon to be heated appreciably above its melting point. The furnace is therefore designed for upward evaporation.

The gun geometry (Figure I) is derived from that of Cole et al[7]. The tungsten ring filament and the outer

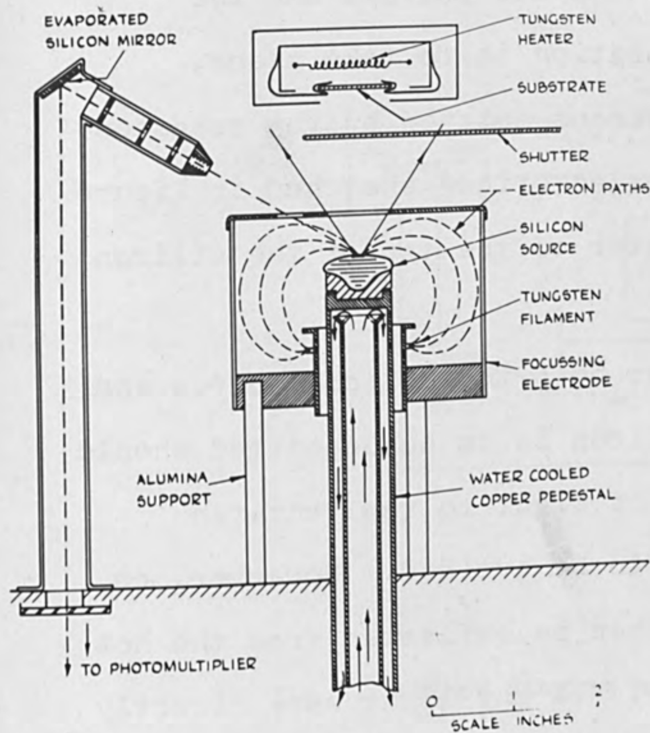

Fig I. Schematic diagram of the furnace.

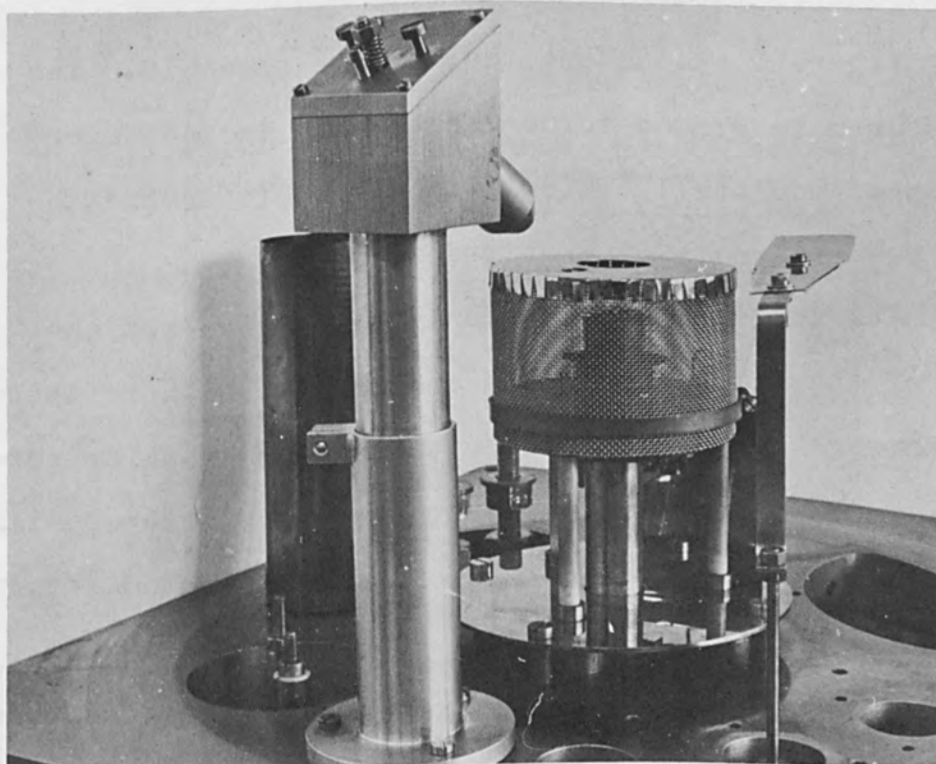

Fig 2. The furnace assembly.

electrode are held at a high negative voltage and the silicon rod, from which evaporation is to take place, at earth potential. The electrons emitted by the tungsten filament follow the curved trajectories* sketched in Figure I and are focussed to the center of the top of the silicon rod.

It is essential that both the silicon source and the substrate on to which silicon is to be deposited should be shielded from direct line of sight to the tungsten filament if contamination is to be avoided. Moreover, no light from the filament can then be reflected from the hot zone into the photomultiplier. If any light were directly reflected it would not only cause an error in the temperature indication but could also cause instability in the feedback loop.

Figure I also shows the furnace assembly. The silicon source is ground to be a close fit in the water-cooled copper pedestal. This is important to ensure the greatest possible rate of heat transfer.

The collimator allows only the light from the hot zone of the silicon to reach the mirror which reflects it down through the base plate to the photomultiplier outside the vacuum. This mirror is itself an evaporated silicon layer so that temperature indication via the photomultiplier

---

* The trajectories have been computed, on the assumption of the neutralization of space charge by trapped ions, by B.A. Hardisty on EDSAC II. Private communication.

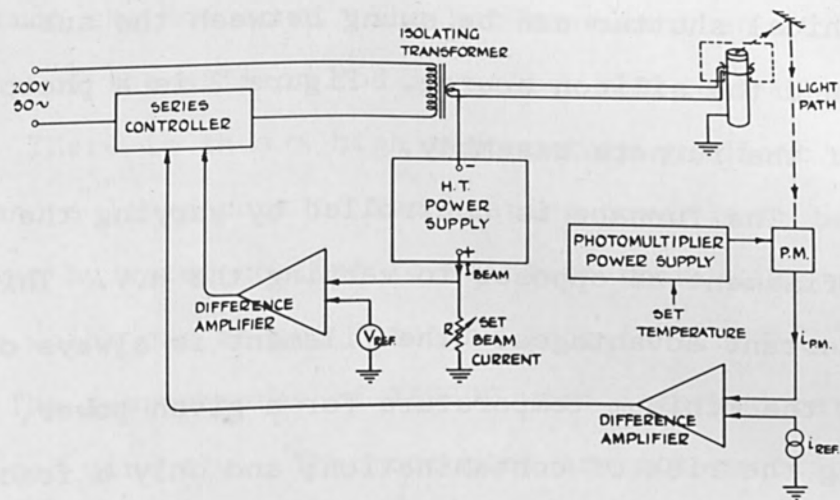

Fig 3. Block diagram of the control circuit.

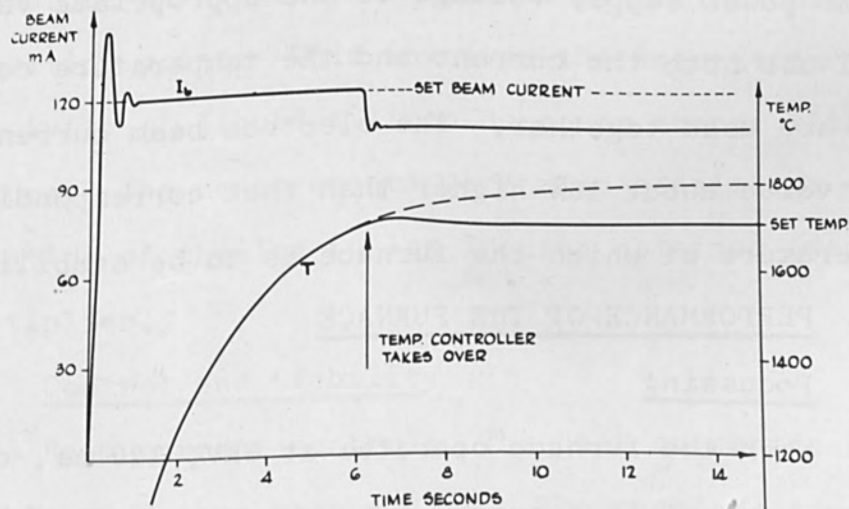

Fig 4. Time response of the control circuit.

system is unaffected by the deposition of more silicon. A mechanical shutter can be swung between the substrate and the silicon source. Figure 2 is a photograph of the furnace assembly.

The furnace is controlled by varying the power to the filament as opposed to varying the H.V. This has two important advantages: the filament is always operated at the minimum temperature for a given power, thus reducing the risk of contamination; and only a fraction of the total furnace power needs to be handled by the control circuit. The block diagram of the control system is shown in Figure 3. The furnace can either be set for a constant power input depending on the value of R (Assuming the H.V. to remain constant) or it can be stabilized for a constant temperature operation by setting the photomultiplier power supply voltage to the appropriate value. In actual use both the current and the temperature control circuits are used together. The electron beam current is set at a value about 10% higher than that corresponding to the temperature at which the furnace is to be stabilized.

3. PERFORMANCE OF THE FURNACE

Focussing

When the furnace operates at 9KV, 120 ma, over 90% of the current is focussed into a spot of diameter less than 3 mm. on the silicon surface. Under these conditions, the silicon evaporates fast enough to give a

deposition rate of 500 Å/sec. on a substrate at a distance of 5 cm. from the hot zone. The hot zone is then at 1800°C, and the top of the silicon rod is molten out to a diameter of 20 mm. There is thus a high temperature gradient across the melt and a large part of the heating power must be carried away by water cooling to maintain this. The maximum power which can be put into the spot is 1.5KW at 9KV.

The temperatures of 1800°C were inferred rather than measured directly. Thermocouples are not practicable owing to attack by molten silicon; optical pyrometry is difficult but not impossible because of the rate at which glass windows get covered by evaporated silicon; and lastly the emissivity of molten silicon at 1800°C is not known.

Temperatures above the melting point of silicon were therefore inferred by an optical pyrometer calibrated at the melting point. This involves the assumption that the emissivity of liquid silicon does not change with temperature. The measurements were also consistent with extrapolation of the log iv log T curve obtained from the photomultiplier.

<u>Control and Stability</u>

Beam current control: The beam current can be held stable to better than ± 0.2%. The response time to a disturbing step function is 200 m. sec. This is sufficient

to deal satisfactorily with gas discharges.

Temperature control: The temperature of the hot zone can be held stable to better than 1 part in 1000. (In fact the photomultiplier current is stable to this order and since $\delta i \propto 4 \delta T$, this figure is conservative.) The stability is limited mainly by the drift of the d.c. amplifier which compares the photomultiplier current with the reference current; and by the drift in the voltage of the stabilized power supply to the photomultiplier.

Response time of the temperature control circuit corresponds to the thermal time constant of the heated material, which is the dominant time constant in the loop. The response to gas discharges is very much faster, as the photomultiplier responds to the light from the flashes.

The temperature control system is stable for a 1:5 range in heating power, typical limits might correspond to a range from 900°C to 2000°C of the hot zone temperature. Instability occurs at the upper temperature limit owing to the rapid increase in loop gain; since the loop gain depends on a high power of the hot zone temperature. The instability is prevented by ensuring that control is taken over by the current control system at a suitable level.

For a desired temperature within the limits of the temperature control, the furnace could be switched on from cold; it would then be controlled initially on beam current, and then the temperature control system would take over as the material heated up above its lower temperature limit.

The behaviour of the system can be most easily understood by reference to the curves of Figure 4 and the following example. The full lines show the response of the system with the I_{beam} set at 120 ma and the temperature set at 1700°C. The dotted line shows the response with only I_{beam} set at 120ma. For a typical silicon slug 2 cm. dia. x 5 mm. high the time to stabilize at 1700°C is about 7 seconds.

<u>Reproducibility and Purity of the Deposit</u>

Thickness of evaporated layers deposited at the same temperature setting and for the same duration of time were measured on a 'Talysurf' profile measuring machine, and were found to be equal to within the experimental accuracy 1% in measurement.

Neutron activation analysis has been used to detect impurities in both the source and the deposited silicon. The silicon source which has been analysed had been used for several evaporations, totalling in all about 5 hours. As the molten silicon freezes on cooling it rises to a tip on the top center of the silicon slug. Material around this tip where the impurities could segregate and the material which had remained solid in close contact with copper pedestal were separately analysed. The results are as follows.

Impurity Element	Impurity content in Atoms/cc in			
	Source silicon		Evaporated layer	Silicon Substrate
	'molten'	'solid'		
Tungsten	1×10^{13}	3×10^{11}	3×10^{17}	3×10^{19}
Tantalum	not detected	not detected	3×10^{12}	3×10^{12}
Copper	3×10^{12}	1×10^{15}	not detected	not detected
Molybdenum, Gallium, Sodium, Indium and Gold not detected.				

The comparatively large amounts of tungsten in the evaporated layer and even larger amounts in the substrate are almost certainly due to the tungsten heater (Figure 1) which heats the substrate held in tantalum clips to temperatures up to 1200°C.

CONCLUSION

The furnace described in this paper evaporates silicon at temperatures of upto 1800°C without using a crucible. It has been used successfully to grow epitaxial layers of silicon of the purity and perfection required for semi-conductor work. The furnace gives a high degree of reproducibility of temperature and evaporation conditions.

The major impurity in the evaporated layer was the tungsten, and as the concentration of tungsten(compared to that in the layer) was higher in the substrate and much less in the source material it would be reasonable to suppose that if the substrate had also been heated by electron bombardment that the impurity level in the epitaxial

layer would be at least as low as that in the source material, i.e. less than 10^{13} atoms/cc.

ACKNOWLEDGMENTS

The authors wish to thank Porfessor C.W. Oatley for providing the experimental facilities for this work, Texas Instruments Ltd., Bedford, for supporting B.A. Unvala at Cambridge University and J.Weaver of Texas Instruments Ltd., for neutron activation analysis of the silicon samples.

REFERENCES

1. Calverley, A., Davis, M., and Lever, R.F. Jour. Sci. Instr. 34, 142 (1957)
2. Gasson, D.B. Proc. I.E.E., 106 BS 15-18 854 (1959)
3. Voitenko, R.M., Dunaeva, T.N., and Kolenko, E.A. Soviet Phys. Solid State 1. 2 (1959)
4. Thun, R. and Ramsey, J.B. 6th National Symp. on vac. tech. trans., Pergamon Press. 192 (1959)
5. Namba, S. Proc. 4th Symp. Electron Beam Tech. Bost, Mass. 304 (1962)
6. Unvala, B.A., Nature. 194, 4832, 966 (1962)
7. Cole, M., Fisher, C., and Bucklow, I.A. Brit. J.App. Phys. 12 577 (1961).

A COMPACT ELECTRON GUN FOR EVAPORATION

Richard A. Denton, Vice President and Albert D. Greene, Laboratory Supervisor

ELION INSTRUMENTS, INC.

A COMPACT ELECTRON GUN FOR EVAPORATION

The development of practical, high energy electron guns together with the rapid development and expansion of high vacuum techniques has made it possible to accomplish many formerly impossible tasks. Among these are the welding, melting and vaporization of refractory materials and production of products of extreme purity. Various schemes providing electron bombardment in high vacuum have been employed including the ring filament cathode with the evaporant as the anode, a similar set-up with a small filament and an electrode to focus the beam on the evaporant-anode, and finally the self-accelerated gun which contains its own anode. This paper deals with a compact self-accelerated gun developed specifically for vaporization of substances to produce vacuum coatings on suitable substrates. The gun provides localized heating by conversion of most of the kinetic energy when accelerated electrons strike the target material.

There are many references in the literature to the use of electron beam evaporation and it is not within the scope of this paper to summarize the entire history of the art. It is interesting to note that a U.S. patent was issued in 1947 to R. Ruhle[1], a German, in which many of the techniques perfected during recent years were anticipated, including use of what is not directly described as, but is apparently, a self-accelerated electron gun, two stages of magnetic focusing, differential pumping, cold and hot cathodes, electrostatic and magnetic deflection, etc. The application was made early in 1940. There is no indication as to whether this was actually reduced to practice. Figure 1 shows the drawings on the first page of this patent.

(1) Ruhle, R., U. S. Patent #2,423,729, July 8, 1947.

The first serious use of a self-accelerated electron beam for evaporation in the U.S.A. was probably in Dr. Hass's laboratory at ERDL, Ft. Belvoir, Virginia. Figure II shows a drawing from the paper by Thun & Ramsey[1].

Based on many years of experience with vacuum evaporators and vacuum filming techniques, there seemed to be a need for a compact electron gun that could be used in both existing and new evaporators. The original tentative requirements were:

1. Fit and operate completely in a standard 18" x 30" bell jar, and (hopefully) into a 12" or 14" diameter bell jar; i.e., the gun should be compact and focus a few inches away.
2. Have a closed housing to keep evaporated material out of the gun.
3. Be fabricated from materials suitable for high vacuum and not add substantially to the gas load of the pumping system.
4. Use a non-poisoning filament with long operating life.
5. Operate at voltages below the X-ray penetration limit for Pyrex bell jars.
6. Supply enough energy at sufficient concentration to vaporize any material.
7. Be easily demounted, cleaned and reassembled without expensive tools or super-skilled personnel.
8. (Hopefully) incorporate a bending attachment to bend the beam sufficiently to substantially avoid back evaporation into the gun.
9. (Hopefully) operate in baked ultra-high vacuum systems.

(1) Thun, R. and Ramsey, J. D., "A New Electron Gun for the Vacuum Evaporation of Metals and Dielectrics", Transaction Sixth National Vacuum Symposium, American Vacuum Society, 1959, Pergamon Press.

First it was necessary to choose a general type of gun design. The two most generally used gun types are the Pierce[1] and the Steigerwald[2] or telefocus guns.

Both guns attain focus by means of the electrostatic field due to the geometry of the cathode and surrounding elements. The Pierce gun uses the known field between two concentric spheres; the Pierce gun is shown in Fig. III, taken from his book. The equipotential surfaces are sections of concentric spheres between the concentric cathode and anode. The Steigerwald gun employs a different, triode geometry based on the use of a bias or higher negative potential on the elements surrounding the emitter. Figure IV taken from Brauck's[3] paper shows 3 operational modes of the Steigerwald gun. The equipotential lines are shown.

The Steigerwald design seemed capable of producing a smaller, less critical and more efficient gun, so this general type was chosen and plain tungsten filaments were used exclusively. With this design it was not found possible to produce sufficient power by the direct electrostatic focussing of the cathode structure, so a magnetic lens was added. Nor did the use of large area flat-wound emitters either helical or bifilar wound suit the Steigerwald configuration. No attempt was made to use an indirectly heated electron bombarded cathode since this introduced complications which would have defeated the concept of the simple, rugged type of gun that was the desired result.

(1) Pierce, J. R., "Theory and Design of Electron Beams", Van Nostrand, 1949.
(2) Steigerwald, K. H.,"Untersuchungen an der Fernfokuskathode nach Steigerwald", Optik 5, Heft 8, 9, 1949.
(3) Braucks, F. W., "Physikalisches Institut der Technischen Hochschule Braunschweig", Optik 15, Heft 4, 1958.

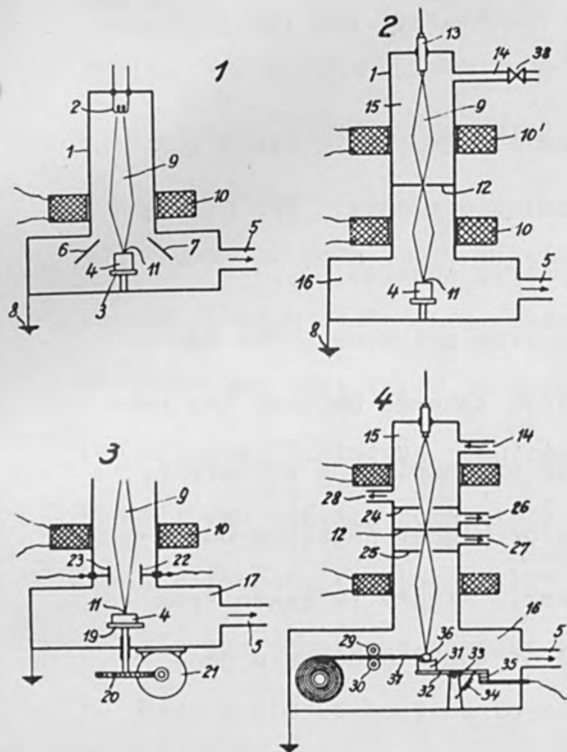

FIG. I. EARLY ELECTRON GUNS FOR VAPORIZATION BY RUHLE

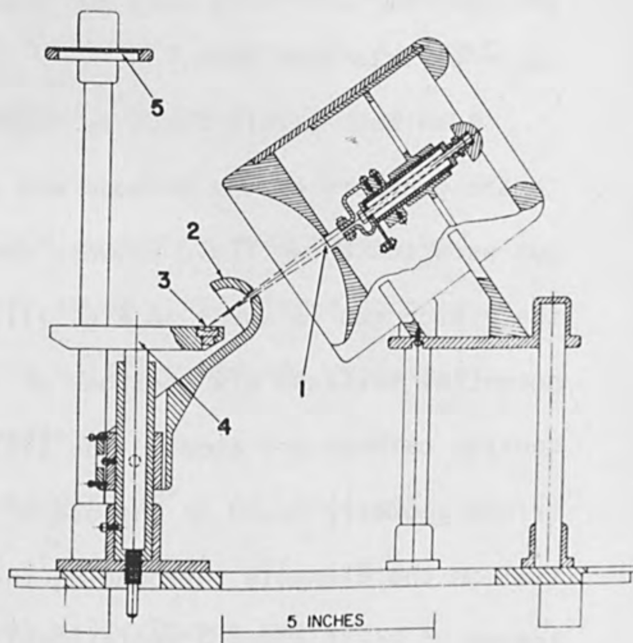

FIG. II. LARGE ELECTRON GUN BY THUN AND RAMSEY

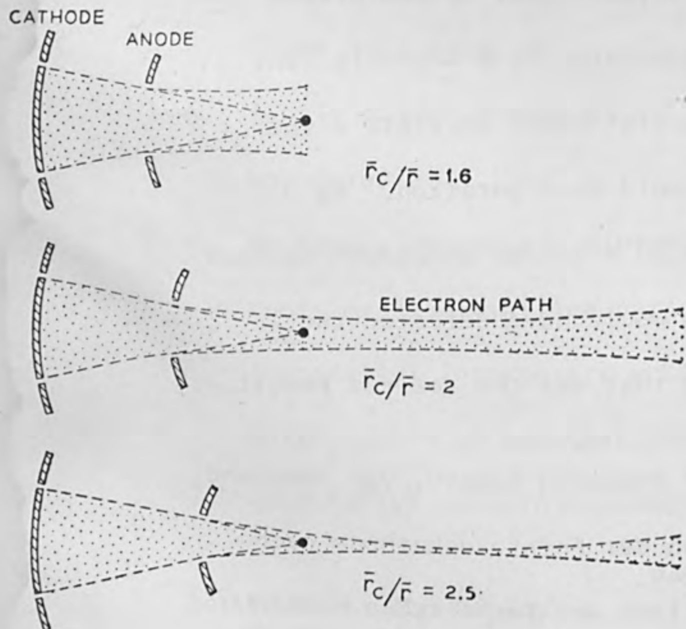

FIG. III. PIERCE TYPE ELECTRON GUNS

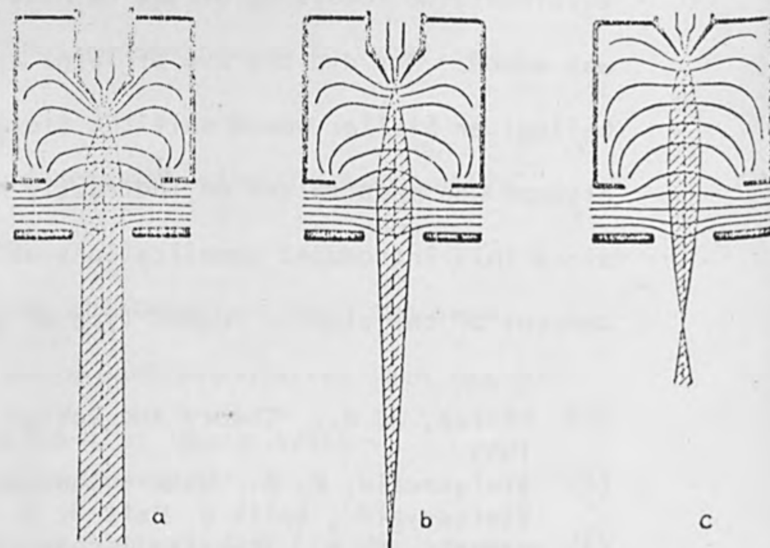

FIG. IV. STEIGERWALD TYPE ELECTRON GUNS

After considerable experimentation, a hairpin filament was developed that gives adequate beam current. It is made from 0.040" diameter tungsten wire. This filament draws from 60-70 amps. current at a few volts and does produce a very small emitting area. Over 225 ma have been drawn from it. It is fed with 60 cycle A.C.; D.C. has been tried without any appreciable benefits.

This filament, which is a somewhat unusual type for the currents involved, has influenced the gun design in several ways. First, it requires several hundred watts of heat. In a vacuum, this means that the gun heats up rapidly. Larger diameter wires and feed-throughs are required to supply the filament power; fortunately these are not expensive. However, there are some benefits as well. The heat dictates that refractory materials, which do not produce vapors or gas when heated in vacuum, be used exclusively in the gun structure. The least temperature resistant material employed is stainless steel. The filament holders are molybdenum with stainless steel set screws; the structure surrounding the cathode is mostly tantalum and molybdenum and the anode is tantalum. The insulators are alumina and quartz with one exception, and no high voltage gradient exists over the exception.

The result is that the gun structure heats up rapidly--any outgassing occurs immediately and yet five to ten minutes cooling is sufficient before breaking vacuum. Perhaps most important is the remarkable filament life. Unless the filament is subjected to excessive power or the gun is exposed to atmosphere with current through the filament, very long life results. Breakage usually occurs only if it is necessary to remove the filament during cleaning, maintenance

or for other purposes. Hot, operating filaments have been exposed to bleed-in of air or oxygen for periods of a quarter of an hour or more and still functioned properly. Of course, life at higher pressures is not expected to be as long as if low pressures are always maintained when the filament is hot.

The gun structure as evolved is a reentrant type utilitizing a controllable bias and a curved anode. The general geometry is shown schematically in Figure V. The geometry is such as to cause the beam to work at optimum efficiency in conjunction with the focussing lens. The tungsten filament has the point of the hairpin approximately in the plane of the filament housing aperture cone. The geometry and bias are such as to make the apparent source approximately two inches behind the actual source; in this way the apparent solid angle of emission is kept small although the actual electron flux is maintained high.

The high density electron beam, being slightly divergent, acts as if having come from a point on the axis well behind the operating focal length of the magnetic lens. The lens therefore acts as a projector, delivering a somewhat magnified image of the apparent source, but an image which is only about twice the size of the actual source. The working image, i.e., focused "spot" for evaporation is accordingly only about 3/32" diameter at a throw of 8" from the anode plane. With the lens in place, the working distance is over 6 inches.

The focussing lens itself is a thin lens with an iron-clad coil using about 550 ampere turns. At 13KV the focussing current is approximately $2\frac{1}{2}$ amperes. Since the lens is designed to be optically thin, there is no polepiece and the bore is approximately one inch in diameter. This lens, as are the cylindrical bending lenses described below, is wound with a fairly high temperature insulated wire and must be pumped

by the vacuum system. All lenses are so mounted and heat-shielded that no gassing difficulties are experienced in operation. A sealed high temperature bakeable lens has been designed for ultra high vacuum work.

The optical influence of the lens effectively immerses the outermost part of cathode structure and assists in the shaping of the beam. By maintaining a minimum current of about 1 amp. in the lens whenever high voltage is on, bombardment of the anode and the lens by the beam is minimized and no undesirable heating effects are produced. The overall dimension of the gun is 3¼" maximum diameter x 4-1/8" long. The lens adds approximately 1½" more length. The gun and lens are shown assembled and in exploded form in Figure VI. The assembled gun is at the top.

In the exploded illustration, the elements that make up the gun are shown consecutively as they fit together. At the left is the cylindrical stainless steel gun housing with the lens attached. Next is the insulator which centers and retains the structure above the elements that fit into it the anode and the insulators between the anode and cathode structure and the assembled cathode structure with molybdenum electrodes. Next toward the right are the two insulators which hold the cathode structure in place, and finally is seen the stainless steel ring which screws over the large insulator onto the housing. One part simply slides into another, and all are held in place by the final ring. Below is shown the cathode structure as two sub-assemblies, with the filament holder removed from the rest of the structure to its left. This has been accomplished by removing the 4 stainless steel nuts. The filament is now easily removed and replaced and a simple adjustment permits proper location of the filament with relation to the rest of the

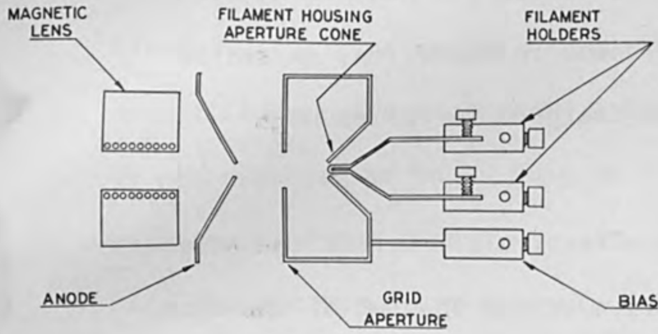

FIG. V. SCHEMATIC STRUCTURE OF GUN

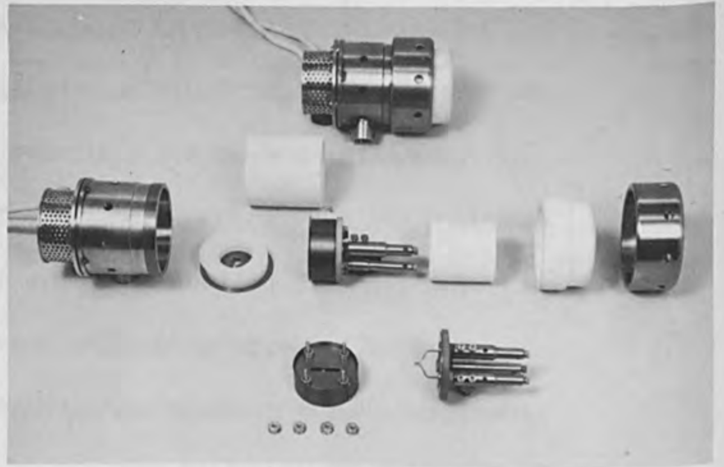
FIG. VI. ASSEMBLED AND DISASSEMBLED VIEWS OF ELECTRON GUN

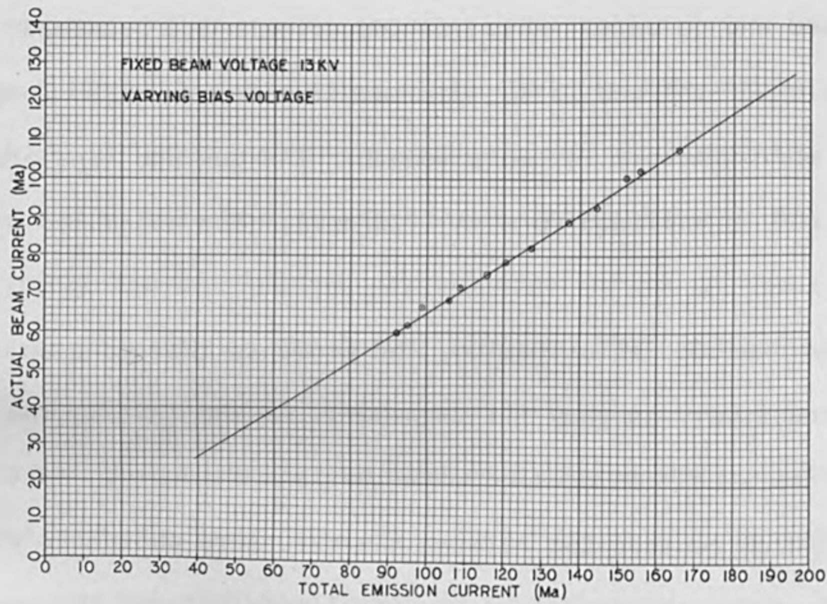

FIG. VII. TOTAL EMISSION VS. ACTUAL BEAM CURRENT

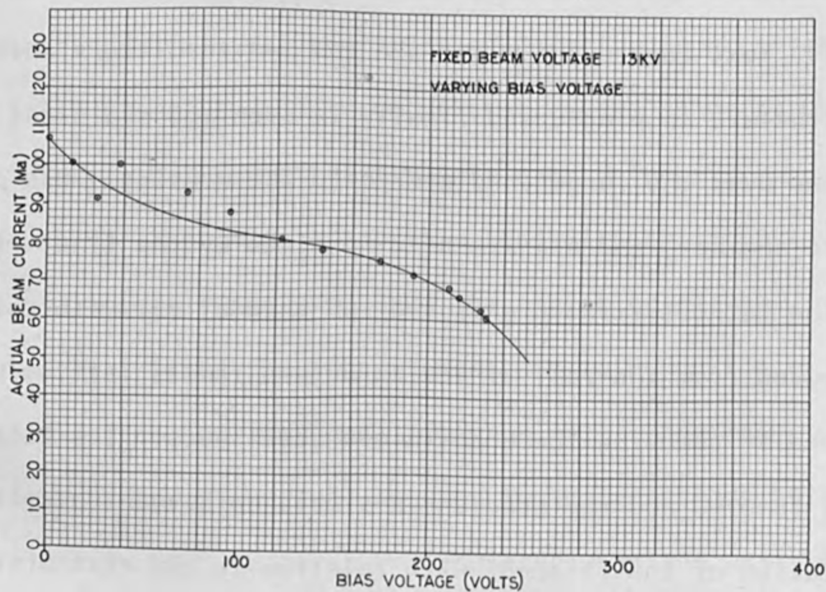

FIG. VIII. BIAS VOLTAGE VS. ACTUAL BEAM CURRENT

structure. The entire gun may be disassembled and the filament replaced in the proper position within 15 minutes.

The gun will produce at least 150 ma. of emission of total current drain through the high voltage power supply. This can be produced at 13KV and at somewhat lower voltages. At 20KV, 220 ma. total drain and 165 ma. actual beam current can be employed with the same spot size.

No X-rays through several different Pyrex bell jars or Pyrex windows in metal tanks can be measured at 13KV. With a 20KV supply, copious X-ray penetration through Pyrex bell jars and windows occurs at 15KV and higher. This is stopped by 1/16" of lead shielding, or the standard 1/8" thickness of a stainless steel bell jar, or 1/4" thick X-ray lead glass. The 13KV use of the gun is the most common, since any material can be evaporated at this accelerating voltage, and most of our work has been done within this voltage limit. The only reason for going to higher accelerating potentials is to produce faster evaporation rates or to overcome conditions of very rapid heat drain.

Figure VII shows a graph of total emission vs. measured beam current at 13KV, with movable bias. Efficiency is consistently about 65%. At 20KV we have measured 220 ma. total and 165 ma. beam current, which indicates about 70% efficiency.

Figure VIII shows actual beam current plotted against bias voltage at 13KV. The beam current varies inversely with bias, as might be expected from a space charge limited gun.

Bending and positioning of the beam is desirable not only to center the beam on target or to change from one source to another, but to place the source in such a position that the aperture of the

gun can be shielded from back evaporation. Such shielding is accomplished with a 90° bend. This amount of bending also permits the gun to be mounted horizontally and to evaporate in the most conventional upward direction.

Figure IX shows the gun mounted vertically above a 20" baseplate. It can be oriented in any direction and effectively operated at 45°, focussing onto a horizontal sample, and has been used successfully in a 12" diameter x 18" Pyrex bell jar on one of our smallest evaporators.

Figure X shows the mounting with the bending and deflection system in place. The high voltage feed-through and a water cooled copper crucible assembly are mounted in a collar. The bell jar (not shown) seals to the top surface of the collar.

The large bending coil with continuously variable current control is connected to iron polepieces. This field bends the beam to over 90°. The vertical member to the right is a safety heat sink. If one forgets to apply current to the bending coil, or if this current should fail, this heat sink saves wear and tear on the bell jar. Actual current requirements will vary with voltage, distance between and configuration of polepieces. About 2-3 amps. with 1500 turns are most commonly used. The configuration of the polepieces is very important not only to bend the beam without excessive smearing, but also to permit evaporation from a position where the source can "see" a reasonably large substrate without shadowing by the polepieces or the gun. This has been achieved and a complete 60° included angle can be handled. At 90° of bending, substantially full performance of the beam is achieved with the same spot size undistorted. Beam current

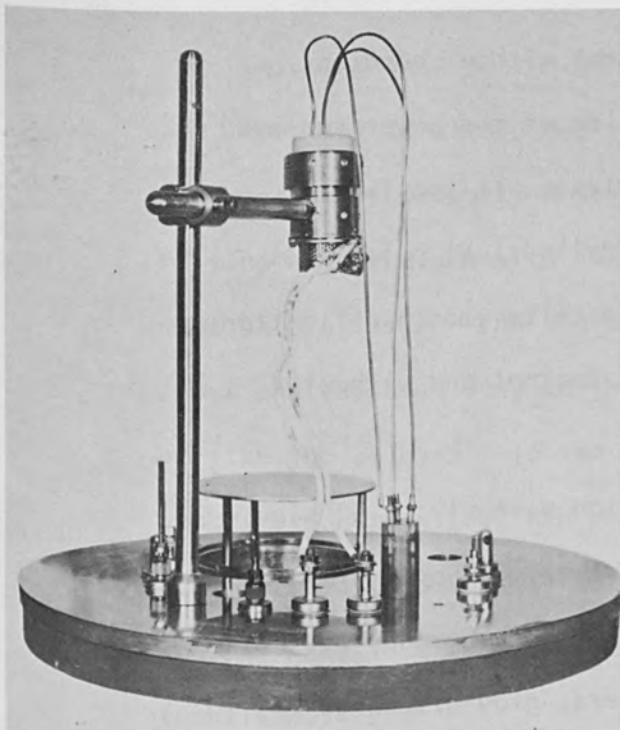

FIG. IX. ELECTRON GUN MOUNTED OVER 20" DIA. BASEPLATE

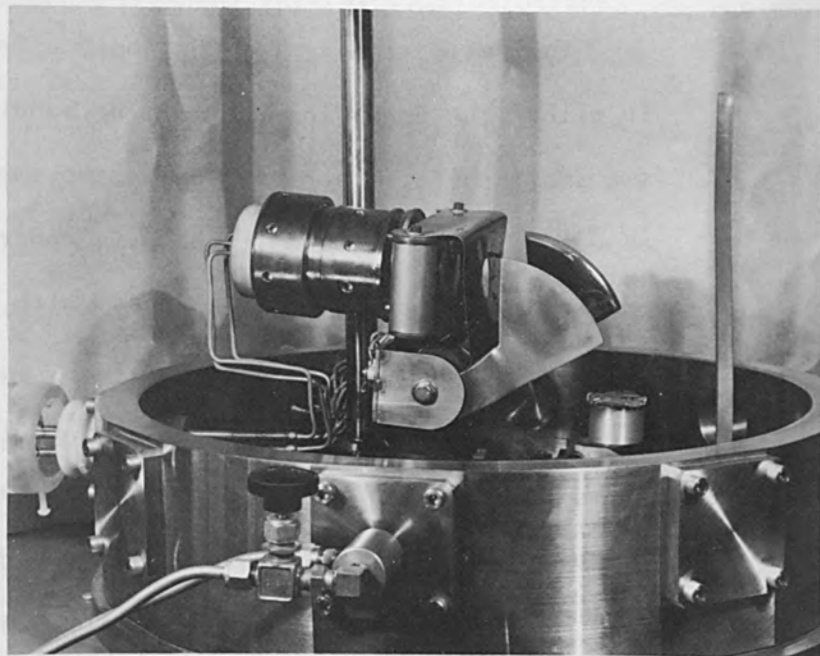

FIG. X. ELECTRON GUN WITH BEAM BENDING AND DEFLECTION SYSTEM

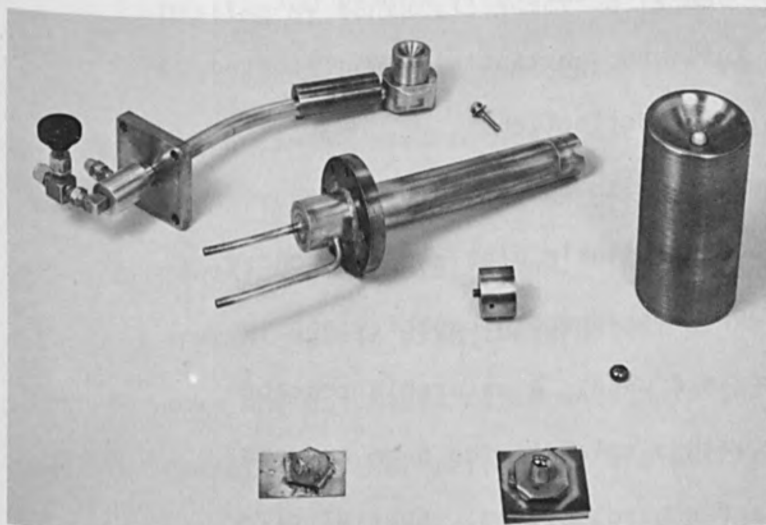

FIG. XI. SOURCE HOLDERS FOR ELECTRON BEAM EVAPORATION

MATERIAL	TIME TO PRODUCE OPAQUE FILM OR QUARTER WAVE FILM (500-1000 A°) AT 9-12" FROM SOURCE	CRUCIBLE TYPE "COPPER = WATER COOLED OR MASSIVE UNCOOLED COPPER CRUCIBLE
Aluminum	1/2 - 2 Min.	Carbon-Copper
Copper	Less than 1/2 Min.	Tantalum Crucible
Gold	1 Min.	Tungsten
Iron	1 Min.	Copper
Chromium	1/2 Min.	Copper or Tungsten
Nickel	1 Min.	Copper
Stainless Steel	1 Min.	Copper
Titanium	1 Min.	Copper
Zirconium	1 Min.	Copper
Silicon	3 - 5 Min.	Copper
Molybdenum	4 Min.	Copper
Platinum	5 Min.	Copper
Rhodium	5 Min.	Copper
Niobium	5 Min.	Small rod on Tungsten
Tantalum	5 Min.	Small rod on Tungsten
Tungsten	5 Min.	Small rod on Tungsten
Magnesium Fluoride	Less than 1/2 Min.	Copper
Silicon Monoxide	Less than 1/2 Min. to 3 Min.	Copper or Tungsten
Silicon Dioxide	1/2 Min.	Copper
Aluminum Oxide	1 Min.	Copper
Cerium Dioxide	1 Min.	Copper
Titanium Dioxide	1 Min.	Copper
Zirconium Dioxide	1 Min.	Copper

FIGURE XII - Deposition Rate and Crucible Data for Various Materials

at 90° bending is within 2% of the beam current without bending.

The deflection system uses only a fraction of the power employed in either the focussing lens or the bending lens. It consists of two small coils in series feeding two small cylindrical polepieces above and below the beam. The D.C. control permits smooth deflection to either side of the bending plane with one control and without switching to reverse current.

The entire gun with bending and deflection assembly is 5" high. It is possible to employ the entire upper part of the bell jar in a normal, useful manner with substrate holding fixtures occupying the full diameter of the jar near the top. Heaters, glow discharge electrodes, shutters and other such equipment may also be employed.

It is not a simple matter to design, mount and shield three magnetic focussing attachments, simultaneously avoiding interaction and complications. Time and space do not permit a discussion of all the design problems, but the positioning and configuration of each element with relation to the others had to be carefully worked out to obtain the achieved results of a full and substantially undistorted beam bendable to 90° plus a 3" total side deflection.

The power supplies normally employed with the gun are full-wave rectified low ripple supplies with a controllable bias and, of course, a high voltage insulated filament supply of adequate capacity and variable voltage. Silicon rectifiers are used. A saturable reactor in the primary is employed together with a relay in the beam current return line to limit total current and control arcing. Special circuitry is employed to make the current limit adjustable, and to set the "pull-in" and "drop-out" points of the relay.

In using an electron gun for vaporization, several considerations are important to attain desired results. The material to be evaporated must be thoroughly degassed. This is frequently done by premelting with the gun with shutter in place. Adequate watt density must be available. The thermodynamic balance between the beam heat input and the heat loss to the evaporant holder must be correct for the job at hand. If the right conditions are established, any vaporization task that can be done by resistance heating can be accomplished (and usually better) by electron beam heating and, of course, many jobs impossible by resistance heating are easily accomplished.

The great advantage of electron beam heating for vaporization is that the evaporating material is the hottest point in the system, i.e., the heat goes directly into the evaporant. It has always been difficult to evaporate quartz by resistance heating for example, because (1) the quartz absorbs very little radiant energy and (2) heating by contact conduction is not successful because of the low heat conductance of the quartz; in addition, tungsten and other metals which can be used to heat quartz chemically reduce it, so that the actual material evaporated by such techniques is mostly silicon monoxide plus metal oxide. The electron beam will evaporate fused or crystal quartz with the greatest of ease. It is not necessary to have any hot metal close enough to the quartz for any chemical reaction. Other refractory dielectric materials such as aluminum oxide, cerium dioxide, zirconium oxide, zircon, etc. are also very easily vaporized. It is, of course, desirable to have a conducting surface at ground potential near such dielectric materials since, if

the distance to ground is too long, these materials will charge up and deflect the beam.

The evaporant must be supported of course. In some cases, a rod of the material may be held in a water cooled clamp or rest on a suitable base, but a water cooled copper crucible (or an uncooled but massive copper crucible) is ideal for most materials. Some metals are very active in alloying with other materials, e.g., nickel, aluminum, platinum. When beam melted in a water cooled copper crucible, the top of the puddle or ball may be kept extremely hot, molten and vaporizing, but the bottom where it is in contact with the water cooled copper apparently has a thin frozen skin, and no alloying or contamination results.

Figure XI shows several source supports for electron beam heating. At the top is a water cooled copper crucible holder which fits in the collar previously shown in Figure X. A stainless steel bolt is fed through the hole in the center of the copper block and a solid copper crucible is drawn down tight against the water cooled surface. With both surfaces machined smooth, excellent heat transfer is attained. Next, below and to the right is a water cooled copper post for mounting through a baseplate. Here a stainless steel stud threaded into post and crucible is used to permit tightening to obtain good thermal contact. An extra crucible with stud is also shown. To the lower right is a massive heat sink may by machining a dish in the top of a 3" diameter x 6" high copper bar. As long as evaporations not much longer than 5 minutes or perhaps 10 minutes are carried out, this massive heat sink works very well. Nickel and molybdenum buttons used in this crucible are shown. For protracted evaporations, the water

cooled copper is better. At the lower left is a small tantalum dish setting on a tantalum plate. This has been used resting on stainless steel. With this setup, several grams of copper have been vaporized within periods of about 10 minutes. The heat necessary to vaporize copper does not affect tantalum and copper does not form alloys with tantalum so that very rapid evaporation may be obtained.

Finally, to the lower right is a setup used for evaporating tantalum. Rolled up tantalum strip has been set on a sheet of tantalum resting on several sheets of tungsten. With very refractory metals, evaporation rates from water cooled crucibles become slower and more working power is needed. This may be obtained by using more power or by taking less away. Tantalum, niobium and molybdenum all have good surface tension properties. A small bar or lump of these materials set up as shown can be vaporized at reasonably good evaporation rates off the top while the bottom, although incandescent, is still solid and not alloying with the underlying tungsten.

Using suitable conditions as shown in the slide, the gun operating at13KV will vaporize any material that does not decompose at the necessary temperature. Once a pure element is thoroughly outgassed, heat can be poured to it very rapidly without many problems. Compounds are more temperamental and the watt density must be more carefully controlled to avoid decomposition.

Next is presented data on materials which have been vaporized with this gun to form films on substrates. No attempt has been made to vaporize every possible element or every compound. The times given are approximate. Some are based on one test, and others on many runs.

The purpose of presenting this data is to show an order of magnitude of what can be done with this gun with emphasis on the 13KV or below operation. In general, the data are conservative as far as rates are concerned and it is likely that those who concentrate on certain materials and the best methods for handling these materials will be able to produce faster rates and better results.

None of the materials was obtained in the preferred form of arc melted, vacuum melted, special high purity, deoxidized, etc. This means that a dry run or sintering or melting down with the substrate shuttered has been done in every case. The pre-treatment has given reasonable assurance that any volatile impurities have been distilled off.

It is generally known that proper cleaning and preparation of the substrate combined with suitable treatment in the vacuum chamber (including sometimes the deposition of a thin undercoat of a bonding material) is required to produce satisfactory films. All depositions were made on cleaned glass microscope slides. Most of these substrates were baked in the vacuum so that the coatings were applied to a hot surface. In some cases glow discharge was used. In general, all of the coatings adhered well to the substrates. No electrical properties were measured, but the optical properties of the films were generally in accordance with what was to be expected.

In the table, the materials are listed plus the time required to produce on optically opaque film or a 1/4 wave length film at a distance of 9-12". Opacity is defined by some as exhibiting less than 1% light transmission. With various metals this may vary from about 500 angstroms up to over 1000 angstroms. A 1/4 wave length of a transparent material is 5500/4 divided by the refractive index

of the film. This also gives thicknesses in the 500-1000 angstrom region.

The crucible type is listed either as copper or alternate. Where copper is listed, either the water cooled crucible or the massive heat sink crucible were used and either would be satisfactory.

Figure XII gives data on materials which have been vaporized with the gun. The data has been taken at 13KV or below. Using 20KV these rates are nearly double.

In closing, it is emphasized that the rate data is approximate and no attempt has been made to determine and list the fastest possible rate obtainable. We have shown that this gun will evaporate any material and most materials rapidly enough for most purposes and will produce satisfactory films.

Acknowledgement is gratefully made to all those who have assisted in this project including A. G. Bennett, L. Shapiro and J. Wojcik.

Mass Flow Determination

by the Multiple-Crossed-Beam Technique

by

C.K. Crawford

Laboratory for Insulation Research
Massachusetts Institute of Technology
Cambridge, Massachusetts

MASS FLOW DETERMINATION BY THE MULTIPLE-CROSSED-BEAM TECHNIQUE

Introduction

Last year at this meeting a new method of determining absolute mass-flow rates in ultrahigh vacuum was discussed.[1] At that time this "multiple-crossed-beam" method (MCB) had not been demonstrated. Since then, however, the necessary equipment has been completed and successful operation has been achieved.

The Multiple-Crossed-Beam Technique

Determination of mass flow, or gas density by electron ionization by high vacuum, depends upon the equation

$$I = in\ell q, \tag{1}$$

where I is the ion current formed by the passage of an electron current i through a distance ℓ of a vapor of density n. Unfortunately, however, the ionization cross section q is not known for most materials. Thus the evaporation-rate gauges currently used in thin-film evaporation, analytical mass spectrometers, and similar equipment must be calibrated separately for each material. Often such calibration is very difficult or even impossible because of the lack of an independent method for determining n. The measurement of the weight loss of a known sample cannot be used when the material evaporates as a mixture of elements and compounds, or where chemical reactions take place.

The multiple-crossed-beam technique avoids these problems by incorporating additional electron beams. Consider the arrangement shown in Fig. 1. An atomic beam is caused to pass through two ionization chambers in sequence. Two ion beams are formed by atomic collisions with the electron beam passing through each chamber. The strength of

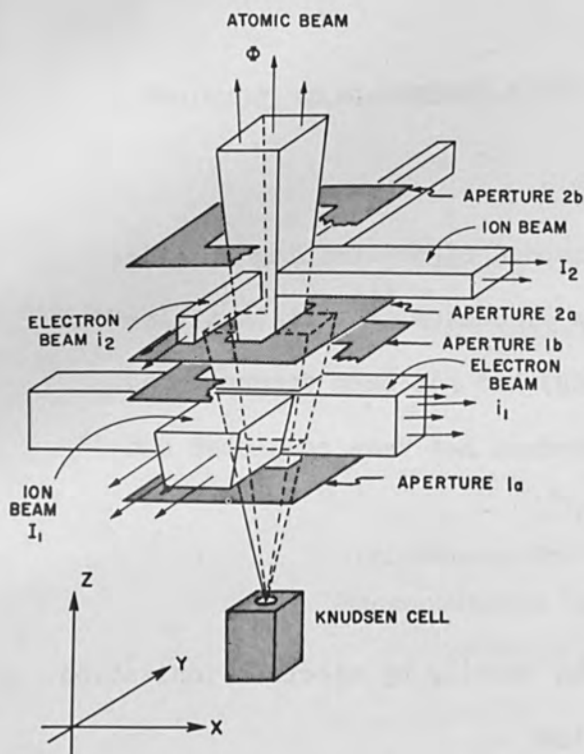

Fig. 1. Beam-intersection geometry for the multiple-crossed-beam technique.

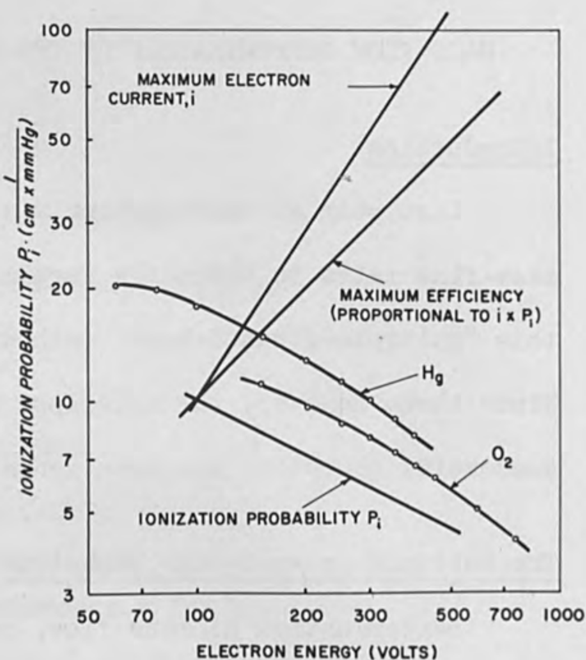

Fig. 2. Relationship between ionization efficiency, and the electron energy.

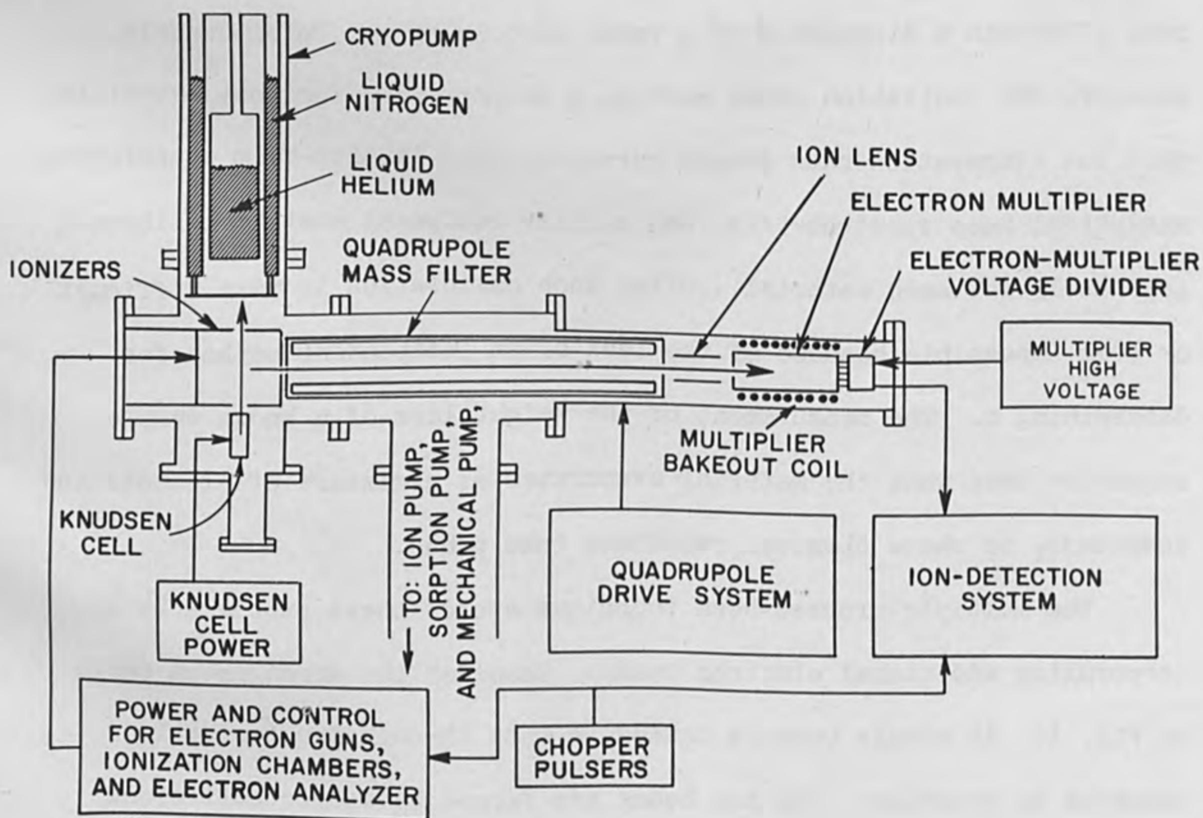

Fig. 3. The qudrupole mass spectrometer and associated equipment.

the atomic beam passing through the second chamber will be reduced due to the presence of the first electron beam; some of the atoms passing through the first chamber are removed as ions. If the electron beam in the first chamber is pulsed, a modulation will result on the atomic beam which can be detected in the second chamber. If the geometry and ion optics are carefully controlled, and an annoying number of second-order effects are suppressed, the following equation applies:

$$\frac{I_1}{\Phi_1} = \frac{I_2'}{I_2} . \tag{2}$$

In other words, the ratio of the ion current I_1 removed in the first chamber, to the atomic beam strength entering the first chamber Φ_1, equals that of the modulation amplitude impressed on the second ion current I_2', to the maximum amplitude of the second ion current I_2. Here Φ_1 must be expressed as an equivalent current, i.e., the current which would flow if each atom would carry one electronic charge. To minimize errors due to electron density variations, the present apparatus has been designed with the electron beams at right angles to each other, and the apertures as shown. This is not the only possible geometry, but the one that appears most convenient at present.

Only one mass spectrometer is required to analyze the ion currents arising in the second chamber, because the second chamber sees the same spectrum as that occurring in the first, when the first electron beam is pulsed off. Thus the fraction of I_1 due to each component of a mixture is the same as the fraction of I_2 due to the same component. Of course, the ionization cross sections must be made equal in both chambers; thus, the two electron beams must run

at the same electron energy. This latter is not required if the atomic beam has only one component.

To make the ionization efficiency (the percentage of the atomic beam removed as an ion current) as large as possible, high-energy electrons should be used. The efficiency is proportional to the product of the ionization cross section and the available ionizing electron current. Although the cross sections in general decrease as $V^{1/2}$ after their maximum is passed at 50 to 100 volts, the electron current available in a space-charge-limited gun increases as $V^{3/2}$. The efficiency is therefore approximately proportional to V. The power dissipated is proportional to $V^{5/2}$, however; this sets a limit because of a maximum allowable operating temperature. It should be possible to decelerate the electrons prior to collection as in a klystron and decrease the power, but this has not yet been done. The relation between efficiency and energy is shown on log-log plot in Fig. 2.

By using two electron beams it is possible to measure flow rates for each component of a mixture directly, independent of the electron-ionization cross sections, the magnitudes of the electron currents, the source temperature, or the shape of the atomic velocity distribution curve. Unfortunately, however, the sensitivity is proportional to the ionization efficiency which is difficult to increase much over 0.1 percent. Therefore the MCB technique has a sensitivity about three orders of magnitude smaller than an ordinary electron ionizer. In many cases it will thus be desirable to measure ionization cross sections by using this technique, for future use in conventional ionizers.

To measure cross sections, however, additional conditions must be met. The vapor density n_1 in the first chamber must be thermodynamically determined from the flow rate Φ_1. Because the ions formed must be mass-analyzed, the measurements should be made in the second chamber, and n_2, the density in the second chamber must be related to n_1 using geometry considerations. Also, the conditions described last year for the ionizing electron beam must be met. But it is not possible, due to space-charge and intrinsic brightness problems, to obtain a beam sufficiently monoenergic to measure cross sections and yet intense enough to detect the modulation signal. Hence, a third electron beam is required. This beam passes through a 127° electron analyzer before entering the second chamber, where it travels along the axis of the second electron beam, but in the opposite direction. The two gun structures alternately function as electron emitter and collector. They are never run simultaneously. The husky second gun is used to calibrate cross sections at one point, at a fairly high electron energy, where they vary slowly. The low-current monoenergetic gun is then used to sweep out cross-section curves and look for fine structure.

The necessity for using thermodynamics to relate the density to the flow rate is unfortunate. It forces use of a Knudsen cell-type atomic beam source with its thermodynamic equilibrium, rather than a Langmuir type source which is always simpler. A Langmuir source, though it does not operate in thermodynamic equilibrium, could also provide a much higher atomic beam strength and is free from the contamination problems common with Knudsen cells. In addition, virtually all thin-film evaporators are Langmuir sources.

There is a way to avoid the use of thermodynamics: to observe the atomic transit times between the two ionization chambers, or between a mechanical chopper introduced for the purpose and one of the chambers. These transit times could be determined as a phase shift, a change in modulation wave form, or a change in modulation amplitude as the modulation frequency is increased. Knowledge of the transit-time-distribution curve and the flow rate Φ_1 is then sufficient to determine n_1. Measurement of a phase shift alone requires that a Maxwellian velocity distribution be assumed. The other two methods could determine the shape of the distribution independently.

A study of transit times would also be very useful in determining pre-ionization masses. Such data would allow distinguishing between ionization reactions of the types

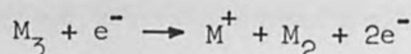

$$M_3 + e^- \rightarrow M^+ + M_2 + 2e^-$$

and

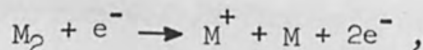

$$M_2 + e^- \rightarrow M^+ + M + 2e^- ,$$

both of which would result in a peak at the same e/m.

A mathematical analysis of the problems associated with cross-section measurement was published in a recent technical report.[2]

Construction and Operation

All experiments were performed in an ultrahigh-vacuum system evacuated by an ion pump and a cryopump. Ions were analyzed in a quadrupole mass spectrometer after the type invented by Paul.[3] This particular instrument is 56 cm long, has an inscribed radius of 0.839 cm and a maximum resolution of about 700 at half height. By

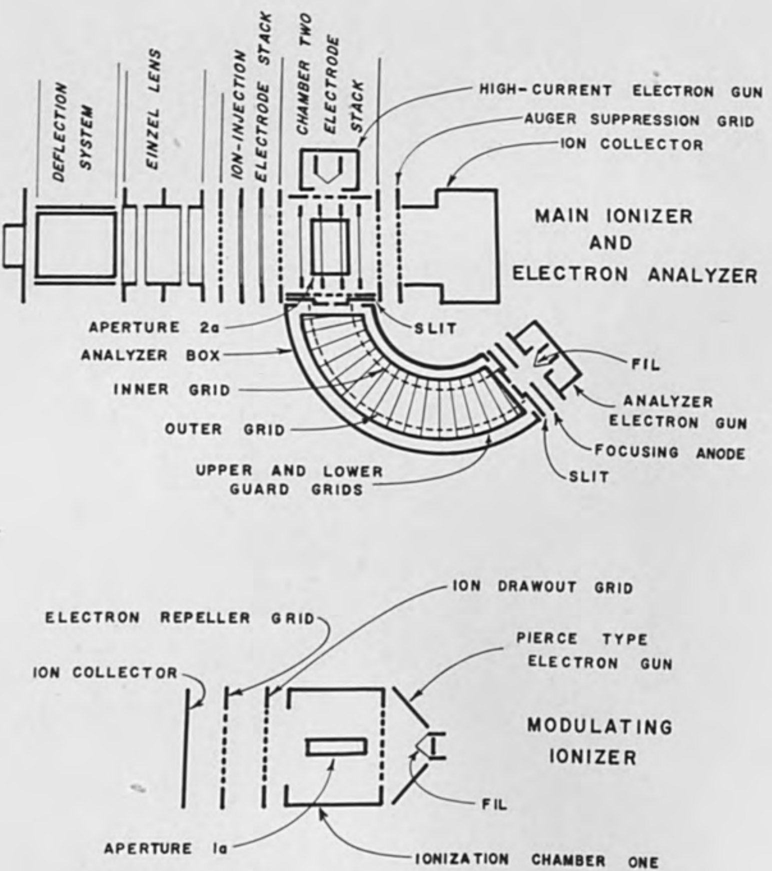

Fig. 4. Electrode placement in MCB source number IV.

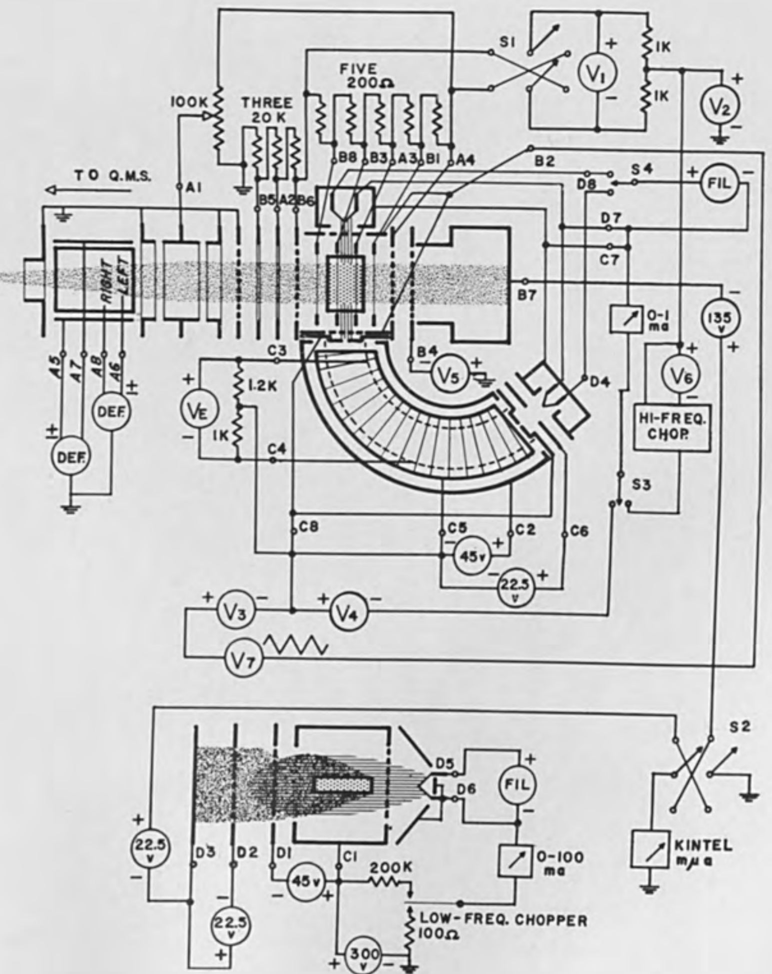

Fig. 5. Electrode potential generation for source IV.

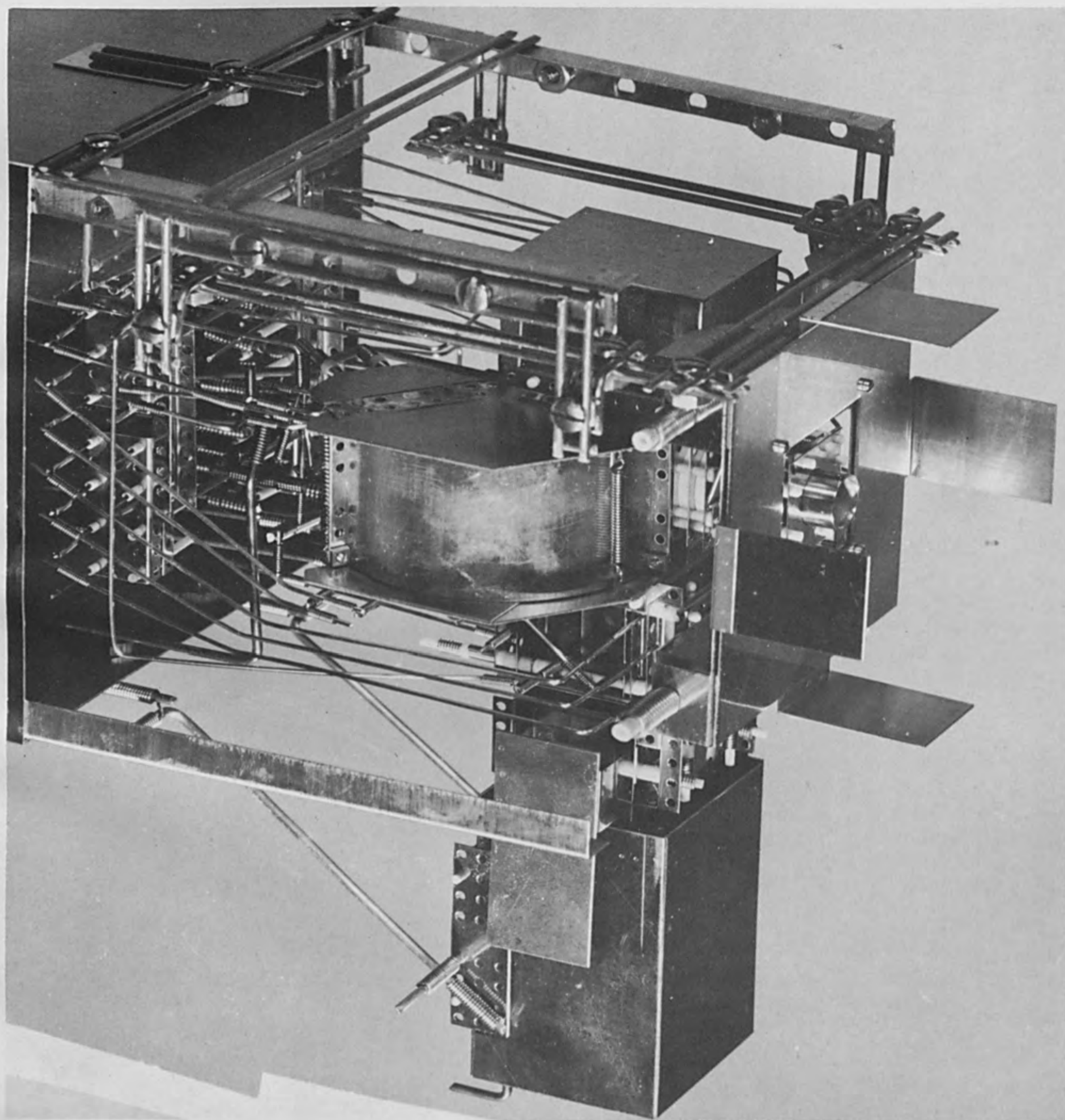

Fig. 6. Source IV viewed from the electron-analyzer side.

switching the drive frequency four mass ranges are available: 1 to 50 amu, 2 to 100 amu, 4 to 200 amu, and 8 to 400 amu. In addition, by use of zero-offset and sweep-amplitude controls, any portion of any range can be swept, or, the spectrometer can continuously monitor a single mass. An electron multiplier is used to monitor the ion currents leaving the spectrometer; since gains of about 10^6 were achieved, it is possible to detect single ions. The spectrometer and its associated equipment are extensively described in another recent technical report;[4] a diagram of the system is shown in Fig. 3.

Due to the low level of the modulation signal, the number of electron and ion beams, and the large number of extraneous effects which must be suppressed, the experimental apparatus tends to be complicated. Over forty electrodes are needed for the two ionization chambers alone. The electrode arrangements and typical wiring are shown in Figs. 4 and 5. A photograph of the same source is shown in Fig. 6. Unless eliminated, the following effects may mask the modulation signal:

1) Stray ions from the first ionization chamber may enter the mass spectrometer.

2) Stray electrons from the first may pass through the second chamber, generating an ion current.

3) Either stray ions or stray electrons may change the potential in the ion-generating region through the space-charge wells they create. This potential change affects the electron energy of the second electron beam, thus changing the cross section.

4) Stray signals may arise through leakage across insulators, common power supplies, or by stray pickup.

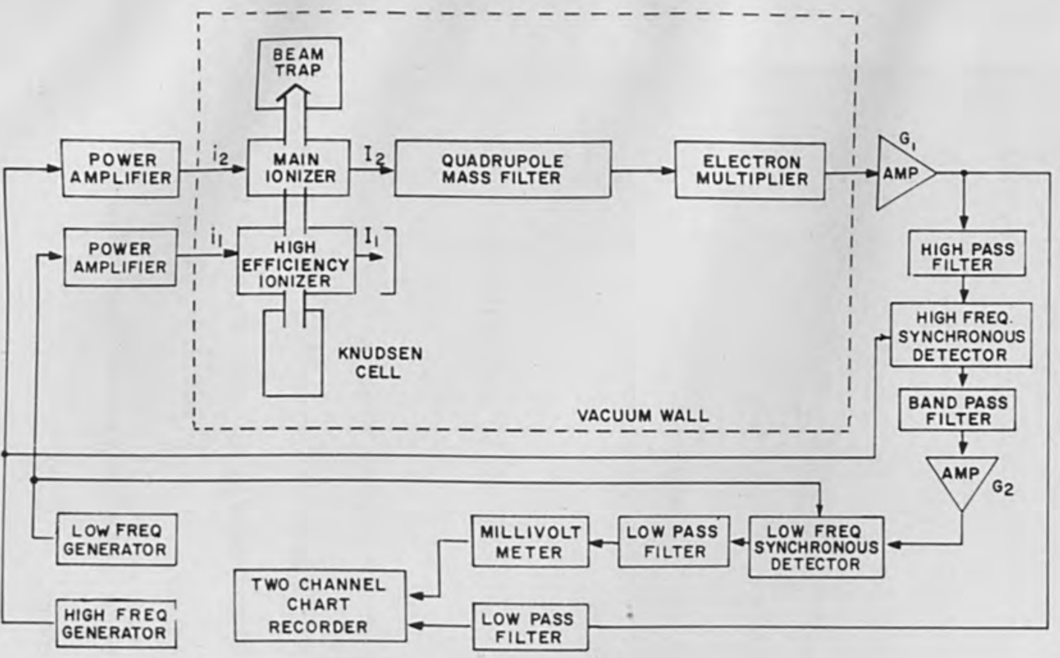

Fig. 7. Detection system for measuring I_2' and I_2.

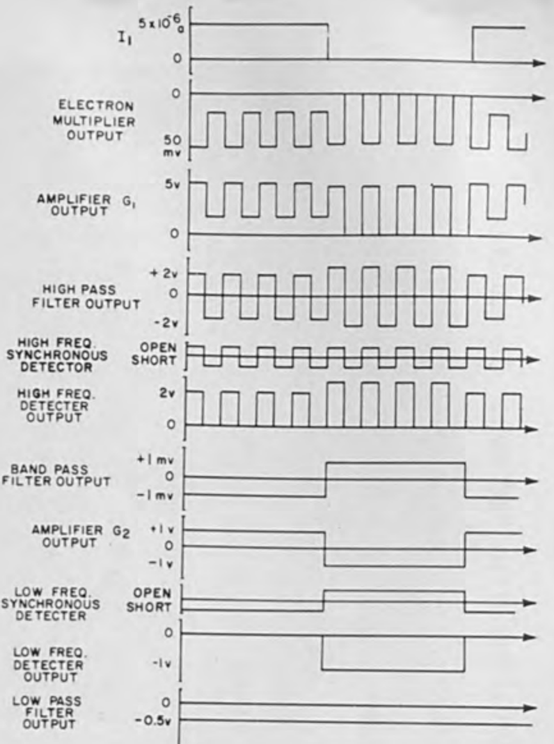

Fig. 8. Idealized wave forms occurring in the detection system.

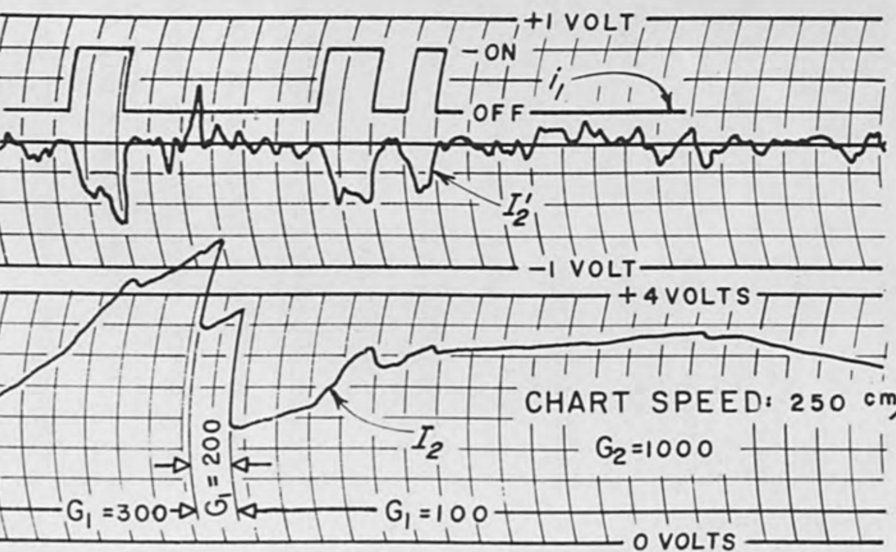

Fig. 9. Detection system output. Top trace is I_2' (demodulated); bottom trace is I_2.

5) Metastables generated in the first chamber may give rise to a spurious signal.

6) Noise due to the statistical nature of the ion beam may mask the signal.

The chopping of the second electron beam, the addition of synchronous detectors, and the incorporation of extensive shielding appear to have eliminated all but the last two of these effects. A block diagram of the detection system and its idealized wave forms are shown in Figs. 7 and 8.

The possible signal due to metastables is expected to be very small; though this has not been experimentally demonstrated, it has simply been assumed negligible.

The problem of noise is more significant. The signal-to-noise ratios obtained to date are very poor; that shown in the upper trace of Fig. 9 is only about 2:1 (measurements made on the Mg^{24+} peak). At least two orders of magnitude improvement could be achieved by increasing the atomic beam strength, the second electron beam current, the electron energies in both beams, and the transmission of the poorly designed spectrometer ion optics. The ratio can also be greatly improved by use of sharper filters and longer averaging times. Work is currently under way to effect these changes.

Uses of the Technique

The current disadvantages of the technique are its complexity and the fact that it is not yet fully developed. When it becomes possible to make transit-time measurements, for which equipment is yet to be built, and when Langmuir sources can be used, the method should be very useful in thin-film deposition, mass spectroscopy, flash desorption,

high-vacuum chemistry, the study of surface reactions, and other fields. In thin-film deposition it should be possible to feedback control the absolute mass flow from several evaporators simulatneously. Also, if a large number of cross sections are available for comparison, then cross sections measured by the MBC technique can be used as an additional means for identifying unknown peaks. In some cases it should be possible to distinguish between ions arising from electron collisions with atoms of the beam, and with those of the background gas. The modulation effect is greatly reduced for background-gas peaks since only a very small fraction of the background gas atoms go through both chambers in the proper direction. If this fraction could be calculated from geometry considerations, it would be possible, although extremely difficult, to make an absolutely calibrated background-gas pressure gauge.

At M.I.T. the technique will be used first to measure cross sections of the most common metal vapors.

REFERENCES

1) Crawford, C.K., Proceedings Fourth Symposium on Electron Beam Technology, Alloyd Electronics Corp., 1962, p. 59.

2) Crawford, C.K., and Woodward, C.E., Tech. Rep. 175, Lab. Ins. Res., Mass. Inst. Tech., November, 1962.

3) Paul, W., Z. Physik 152, 143 (1958).

4) Woodward, C.E., and Crawford, C.K., Tech. Rep. 176, Lab. Ins. Res., Mass. Inst. Tech., January, 1963.

FORMATION OF THIN POLYMER DIELECTRIC FILMS BY ULTRAVIOLET IRRADIATION OF SURFACES IN CONTACT WITH MONOMER VAPOR

by

L. V. Gregor and H. L. McGee

International Business Machines Corporation
Thomas J. Watson Research Center
Yorktown Heights, New York

FORMATION OF THIN POLYMER DIELECTRIC FILMS BY ULTRAVIOLET IRRADIATION OF SURFACES IN CONTACT WITH MONOMER VAPOR

ABSTRACT: Thin polymer films produced by electron bombardment of adsorbed organic molecules[1,2] or electrical discharges in organic vapors[3,4] have recently become useful in fabrication and study of thin-film phenomena and microelectronic circuits.[5] Ultraviolet irradiation of organic monomers in the gas phase is known to produce polymeric films on surfaces enclosing the gas.[6] Recently, it has been shown that direct surface irradiation results in films which have good electrical insulation properties.[7,8] This report summarizes the results of an investigation of this film process, particularly with respect to films derived from the monomers acrolein ($CH_2 = CH\text{-}CHO$), methyl methacrylate (CH_2 - $C(CH_3)$, $COOCH_3$), and divinylbenzene ($CH_2 = CH\text{-}C_6H_4\text{-}CH{=}CH_2$).

The experimental system consists of a conventional Veeco high-vacuum system and a steel bell jar equipped with sources for thermal evaporation films, a holder for substrates and evaporation masks, and a quartz window for admission of ultraviolet radiation from a mercury arc. The formation of the polymer film is studied by two methods:

1. After evaporation of a metallic film of suitable geometry onto a glass substrate, the surface is exposed to ultraviolet radiation in the presence of a suitable partial pressure of monomer in the bell jar. The illuminated region is defined by a conventional evaporation mask. Evaporation of a second metallic film onto

the polymer produces a set of capacitors. By combining direct physical measurement of polymer film thickness with capacitance measurements, the time average rate of film deposition and electrical properties of the film can be determined.

2. The polymer film is deposited on the illuminated surface of an oscillating quartz crystal, whose change in frequency is related to the mass of material being formed on its surface.[9] This method enables the instantaneous rate of deposition to be measured, and provides information concerning the mechanism of film formation.

The rate of film deposition is proportional to the partial pressure of monomer up to several mm Hg, and then approaches a constant value. The growth rate and surface temperature are related by the expression:

$$\text{Rate} = \text{Kexp}\left[\frac{\Delta\varepsilon}{kT}\right]$$

$\Delta\varepsilon$ is positive for all monomers investigated, i.e., the deposition rate increases with decreasing surface temperature. The rate of film growth is proportional to the square root of relative light intensity, and no "dark" growth was detected; the lifetime of "active" sites on the surface was found to be less than 10 milliseconds. By assuming a simple free radical addition polymerization mechanism, a rate law is derived:

$$\frac{dP}{dt} = k_2 \left(\frac{k_1}{k_3}\right)^{1/2} (I_o)^{1/2} [M]$$

which agrees with the data up to relatively high pressures of monomer.

The dielectric constant of the film is approximately that of the bulk polymer, but the dissipation factor is somewhat higher and tends to increase with increasing film thickness. The breakdown voltage is greater than 10^6 volts/cm, as is observed in films whose thickness is less than the average mean free path of an electron in the dielectric.[10] The bulk resistivity is between 10^{10} and 10^{14} ohm cm at low applied fields. For very thin films (below 500 Å), the conductivity increases nonlinearly at fields exceeding 10^6 volts/cm. The conduction mechanism is presumably field emission across the barrier.

The reliability of the dielectric films, defined as freedom from initial short-circuits due to "pinholes" or voids, is very good above 200 Å and approaches 100% above 500 Å. Thermal cycling between room temperature and 77°K does not appear to affect the capacitors nor does it introduce short-circuits. These qualities, plus long-term stability at room temperature, enable the films to be used as the insulation for complex thin-film circuits, such as thin-film triodes, cryotron loop circuits, and devices for studying tunnel emission, space-charge limited conductivity, and other phenomena in which an extremely thin dielectric barrier is required. The degree of "shadowing" or insulation creep beyond the borders of the illuminated area is less than 0.005" for mask-to-substrate spacing of 0.01" - 0.02", indicating that relatively high component densities per unit substrate area may be achieved.

TABLE I

Some Typical Electrical Properties of Polymer Dielectric Films

Monomer	Methyl Methacrylate	Acrolein	Divinyl benzene
Dielectric Constant at 1 kc and 25°C	3.5 ± 0.35	3.5 ± 0.3	3.2 ± 0.2
Dissipation Factor, avg., 500 Å	0.038	0.030	0.005
Dissipation Factor, avg., 4000 Å	0.11	0.09	0.012
Breakdown voltage, v/cm	2×10^6	3×10^6	5×10^6
% samples initially reliable	76% [1]	94%	98%
Stable on thermal cycling, 77° K-298°K	yes	yes	yes
Probable Cross-Linking	uncertain	yes [2]	yes

1 Reliable insulation produced only when a photoinitiator was used.

2 Polymer film insoluble in liquid monomer.

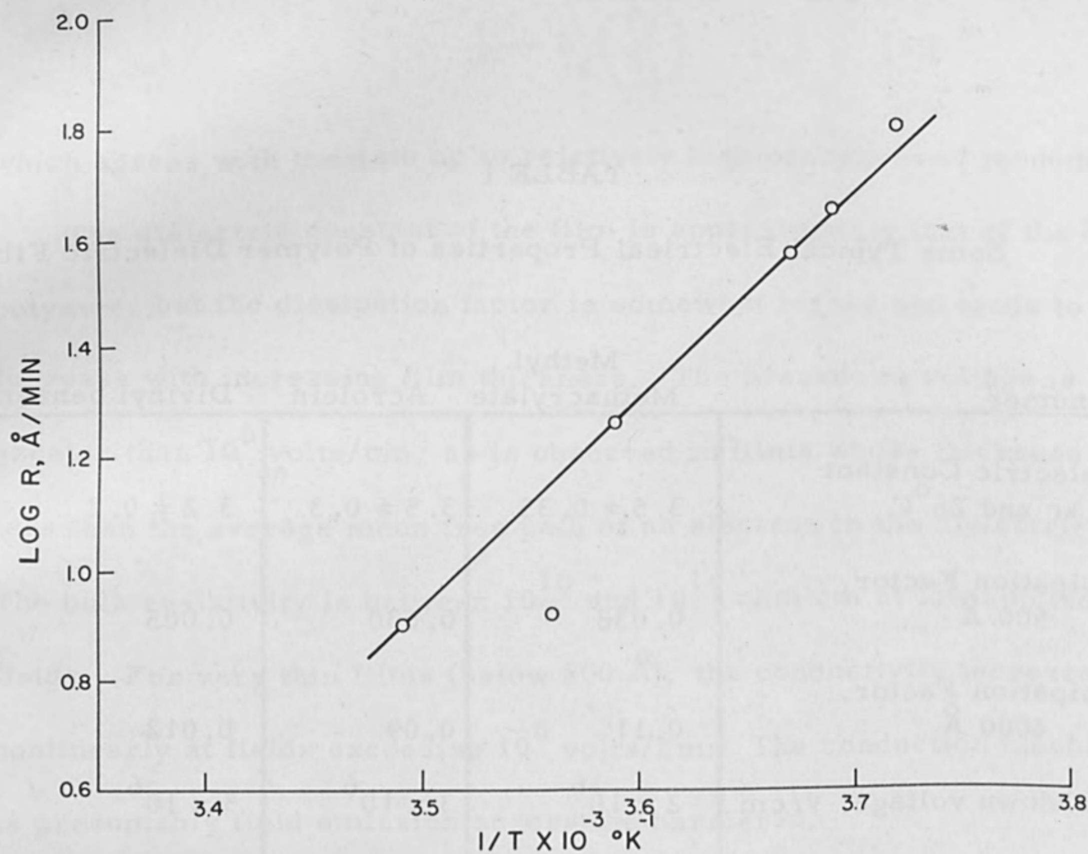

Fig. 1 Logarithm of polymer film growth rate versus reciprocal of absolute temperature of substrate. Monomer: acrolein.

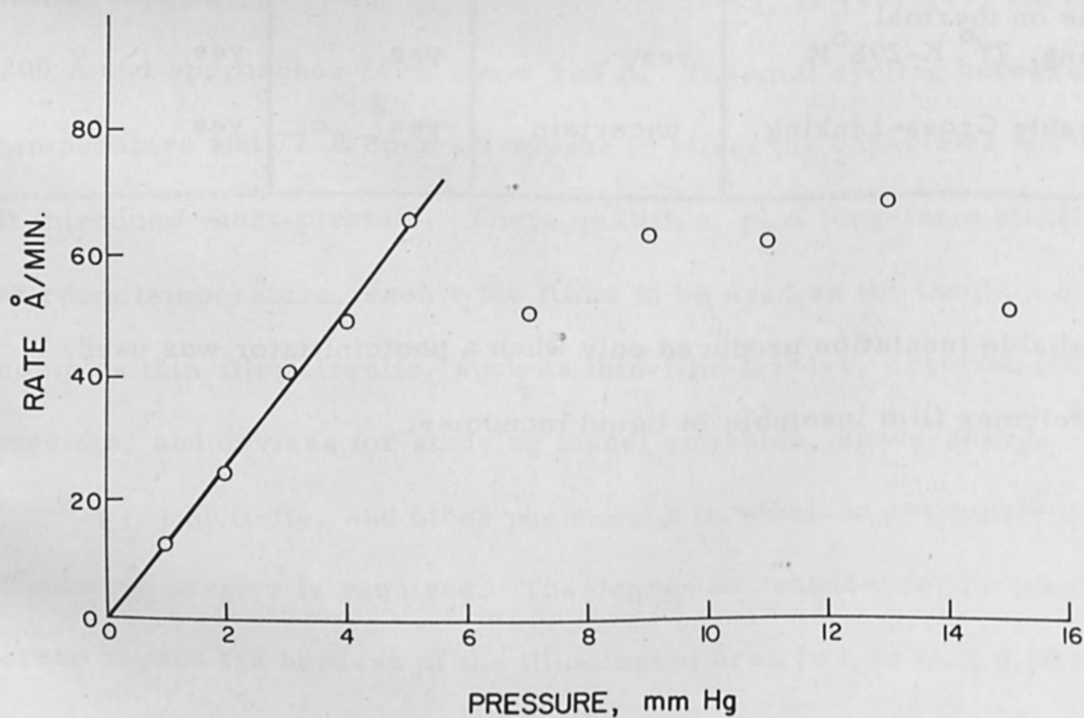

Fig. 2 Polymer film deposition rate versus partial pressure of monomer. Monomer: acrolein.

REFERENCES

1. Christy, R. W., J. Appl. Phys. 31, 1680 (1960).

2. Fotland, R. A. and Burkhard, W. J., 121st Meeting of the Electrochemical Society, Los Angeles, May 7, 1962.

3. Goodman, J., J. Polymer Sci., 44, 552 (1960).

4. Bradley, A., and Hammes, J. P., J. Electrochem. Soc. 110, 15 (1963).

5. See, for example, Schmidlin, F. W., (to Space Technology Laboratories, Inc.,), U. S. Patent 3,024,140 (March 6, 1962).

6. Melville, H. W., Proc. Roy. Soc. (London) A163, 511 (1937).

7. White, P., 31st NAS-NRC Conference on Electrical Insulation, Hershey, Pa., October 16, 1962.

8. Gregor, L. V., and McGee, H. L., Annual Report of NAS-NRC Conference on Electrical Insulation, Publication 1680, National Academy of Sciences-National Research Council, Washington, D.C. (1963).

9. Lostis, P., C.R. Acad. Sci. Paris 240, 2130 (1955); Rev. Opt. 38, 1 (1959).

10. Whitehead, S. "Dielectric Breakdown of Solids," Ch. II, Clarendon Press, Oxford (1951).

Electron Beam Welding of Refractory Materials for Ion Propulsion Systems

S. Robelotto
Member of the Technical Staff
Hughes Research Laboratories
Malibu, California

ELECTRON BEAM WELDING OF REFRACTORY MATERIALS FOR ION PROPULSION SYSTEMS*

Under contract from the National Aeronautics and Space Administration, the Hughes Research Laboratories is undertaking the design and construction of ion propulsion systems. The contact ion engine operates on the following principle: when vaporized cesium is passed through a high-work-function porous material which is above a critical temperature, contact ionization of the cesium occurs. By the use of suitable optics and accelerating potentials, a beam of ions is ejected, producing thrust. Although the thrust is limited to the millipound range, the ion engine is suited to interplanetary travel because of its ability to achieve a continuous thrust for periods up to one year. This paper is concerned with materials joining problems associated with the fabrication of ion propulsion systems, particularly the joining of refractory metals.

The primary fabrication problem was to join a porous tungsten emitter to a nonporous tungsten support with the following requirements: no fuel (cesium vapor) may leak through the joint, and neither the joint nor the porous tungsten may be degraded with long-term use. Early joining efforts utilized brazing, but it was believed that with extended operation the brazing alloy would migrate into the porous tungsten, resulting in degradation of both the joint and the porous tungsten. Consequently, an electron beam welding machine (see Fig. 1) was obtained to solve the specific problem of joining porous to non-porous tungsten. The unit has an accelerating voltage of 150 kV and a maximum beam current of 20 mA. At maximum power setting, the beam can be concentrated into a 0.010-in.-diameter spot. Linear weld travel speeds of 10 in./min to 120 in./min can be achieved. In addition, the beam can be oscillated at 60 cps or rotated by a circle generator.

*The work reported herein was supported by the National Aeronautics and Space Administration under Contract NAS 5-517.

Fig. 1. Electron beam welder

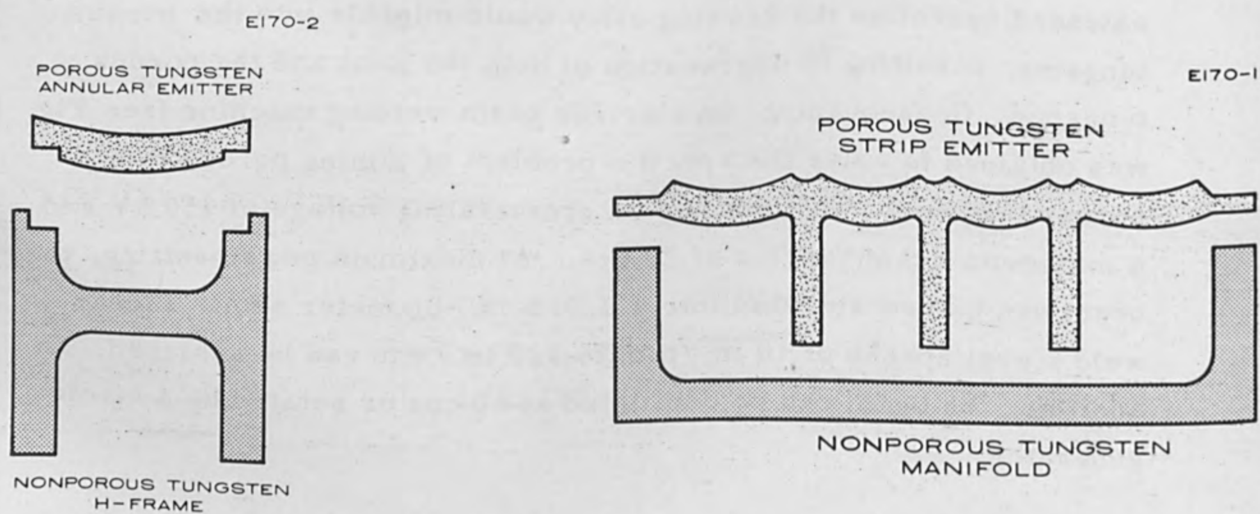

Fig. 3. Cross sectional view of multistrip ionizer

Fig. 2. Cross sectional view of annular ionizer

The two part configurations consist of an annular and a linear ionizer. A cross section of the annular ionizer is shown in Fig. 2. The porous tungsten annular emitter had a radiused contour and was approximately 0.050 in. thick, 0.25 in. wide, and 3 in. in diameter. The nonporous annular H-frame was slightly larger in diameter, 0.350 in. high, and had a wall thickness of 0.050 in. A seat 0.037 in. deep and 0.030 in. wide was machined in the H-frame for receiving and holding the porous ring. The cavity formed by the emitter and frame served as a reservoir for the cesium. The lower section of the H-frame was utilized as a cavity for a tungsten resistance heater which was used for heating the ionizer to operating temperature approaching $1000^{\circ}C$.

A cross section of the linear ionizer is shown in Fig. 3. The multistrip emitter was machined from a single plate of porous tungsten. The contoured sections were 0.050 in. thick, and the outside edge of the emitter was 0.030 in. thick. Equally spaced legs were machined on the emitter for support and heat transfer. Manifolds for the linear type engine were machined from a nonporous tungsten plate. The walls of the manifold were 0.080 in. thick and the overall dimensions of the strip ionizers were 1-1/4 x 4 in. and 2-5/8 x 4 in.

Preliminary studies were conducted with the 3-in. ionizer and a stainless steel holding jig. Three spring loaded adjusting screws were used to align the ionizer in the jig. While some progress was apparent, the following difficulties were encountered:

1. The high temperature reached during welding adversely affected the temper of the springs.
2. The jig imposed restraint on the H-frame.
3. The jig acted as a heat sink and prevented adequate preheating of the components.

The preliminary studies indicated that it would be necessary to design a special holding device to overcome these difficulties. The following requirements for the jig were determined:

1. The tool can impose little or no restraint on the part.
2. The tool must be thermally insulated from the part.

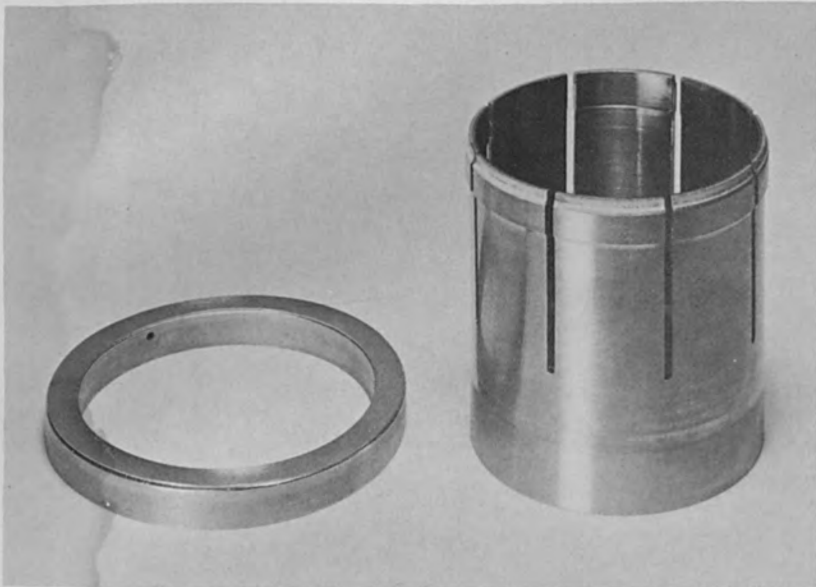

Fig. 4. Welded 3-in.-diameter ionizer and holding tool

Fig. 5. Ionizer positioned on holding tool

Fig. 6. Weld operation

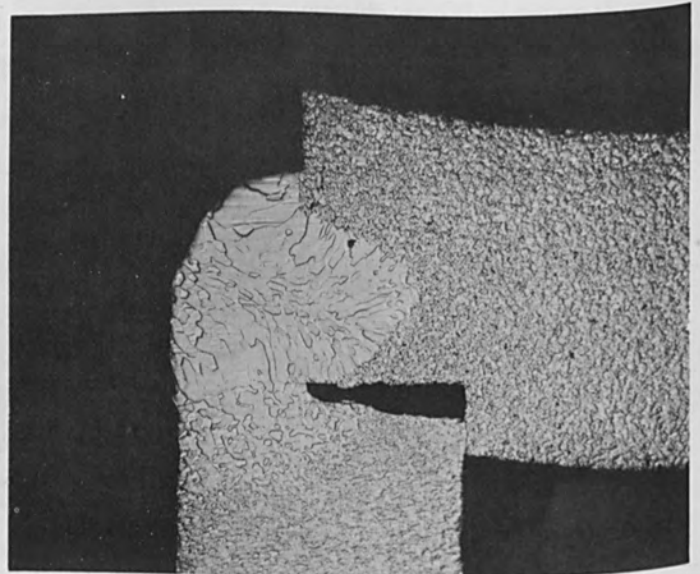

Fig. 7. Photomicrograph (75x) of weld cross section (3-in.-diameter annular ionizer)

3. The tool must follow the expansion and contraction of the part during the preheating, welding, and post-weld cooling thermal cycle.

4. The tool must maintain precise alignment of the joint with respect to the beam during welding.

With these criteria in mind, the holding tool shown in Fig. 4 was designed and fabricated. A welded 3-in. ionizer is also shown in the photograph. Because of the larger diameter of the jig, it was able to follow the expansion of the part during preheating and welding, and it allowed the part to contract with little restraint during cooling. With the jig action occurring concentrically, joint alignment during welding was accurately maintained. Figure 5 shows a welded ionizer positioned on the holding jig.

For welding, the part and jig were placed in the chamber so that the central axis of the part was approximately 15 to 20° from the horizontal. The part was then preheated by impinging a defocused beam (0.060-in. diameter) on the side of the H-frame. The beam current was slowly increased until the part attained the desired preheat temperature. At this time the beam was focused to a 0.020-in. diameter, and the weld was made at 110 kV, 10 mA, and a rotational speed of 12 rpm (approximately 100 in./min). Figure 6 shows the weld operation. Immediately following completion of the weld, the beam current was reduced and the beam was defocused. The beam was again impinged on the H-frame and the current was slowly reduced to provide slow, uniform cooling of the part to minimize thermal and weld stresses. Figure 7 is a photomicrograph (75x) showing the weld cross section.

The procedure produced parts without leaks or cracks, but distortion of the porous tungsten emitter occurred because of unequal thermal expansion between the emitter and H-frame. This unequal expansion resulted primarily from the difference in heat sink between the two details. Consequently, a jig was designed to hold the emitter in position during welding (see Fig. 8); the jig has the same features as the tool described above. Approximately 15 ionizers have been

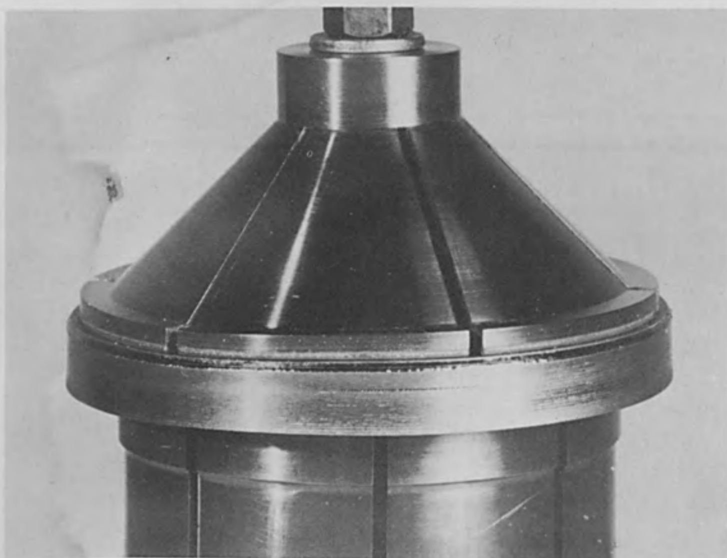

Fig. 8. Close view of emitter holding tool

Fig. 9. Segmented emitter

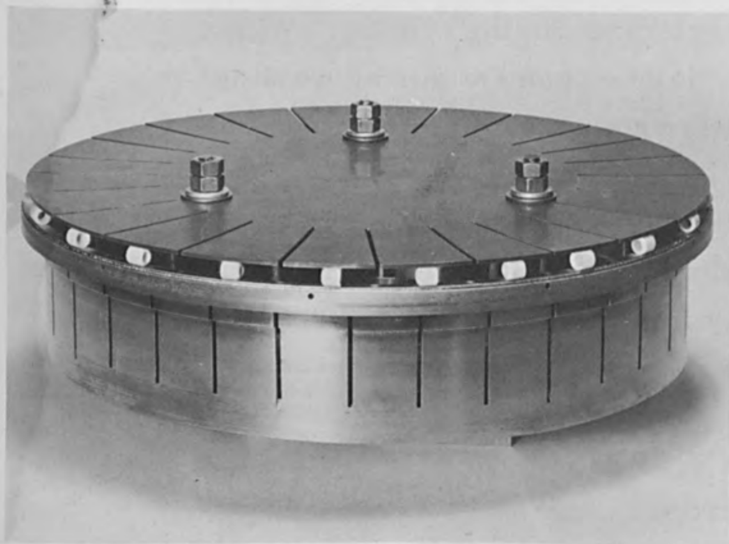

Fig. 10. Tooling for 10-in.-diameter ionizer

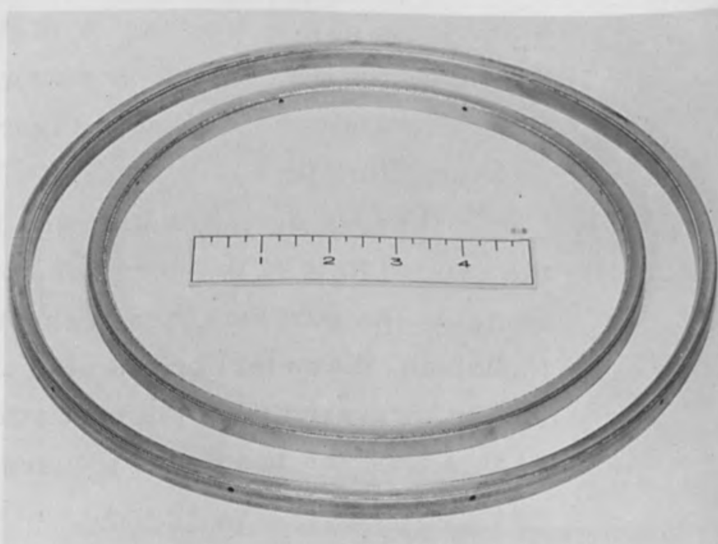

Fig. 11. Welded 8- and 10-in.-diameter ionizers

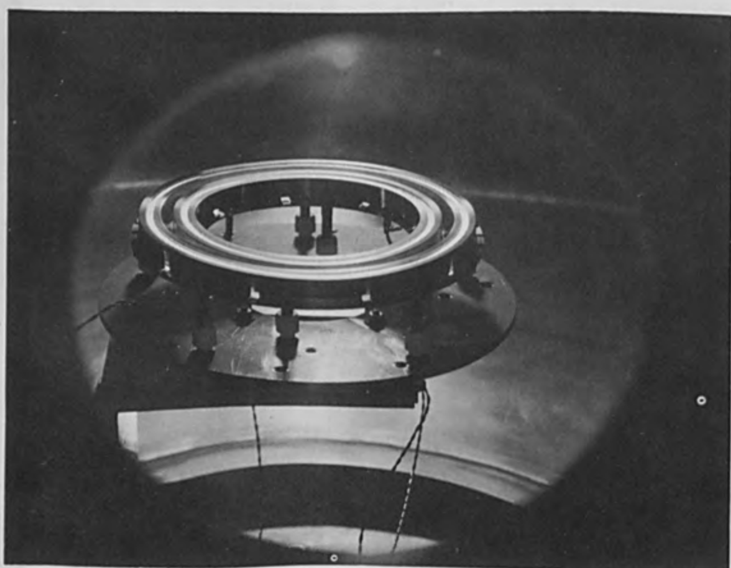

Fig. 12. Engine operation of 8- and 10-in.-diameter ionizers

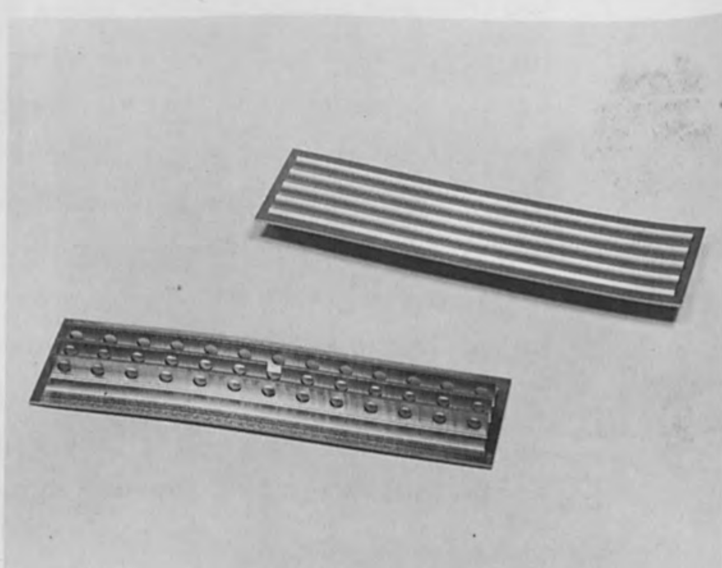

Fig. 13. Multistrip emitter

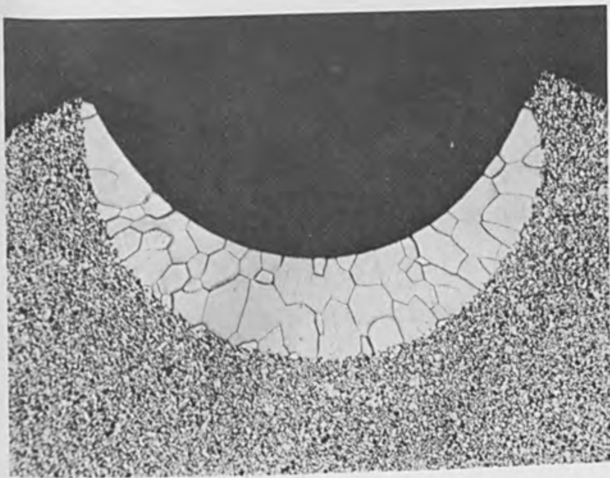

Fig. 14. Photomicrograph (150x) of sealed porous material

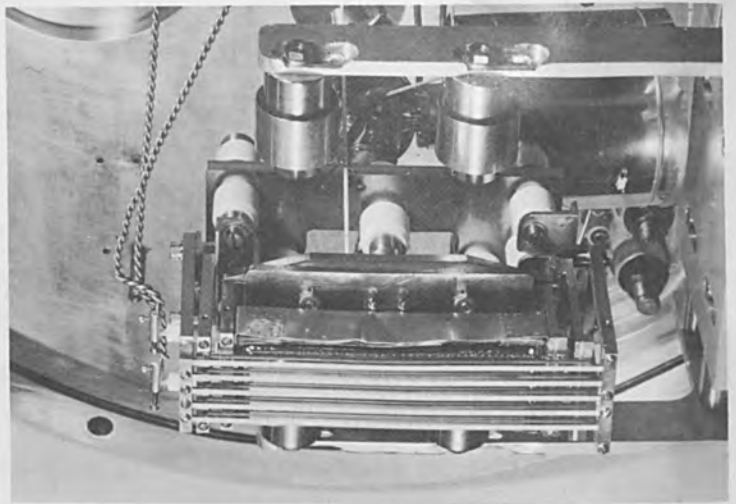

Fig. 17. Multistrip 1-1/4 x 4 in. ionizer assembled into an engine

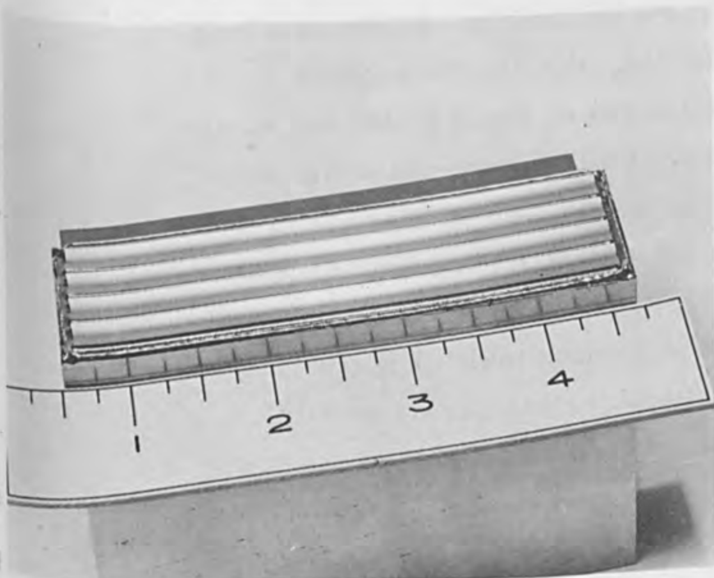

Fig. 15. Welded 1-1/4 x 4 in. multistrip ionizer

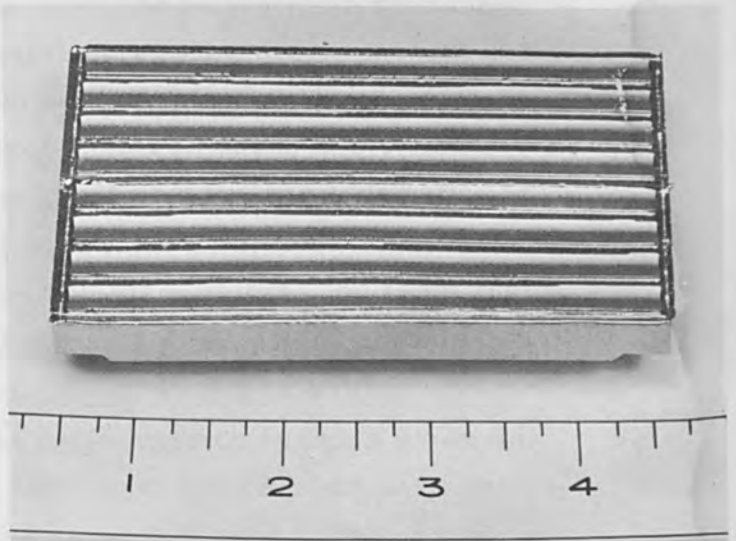

Fig. 18. Welded 2 5/8 x 4 in. multistrip ionizer

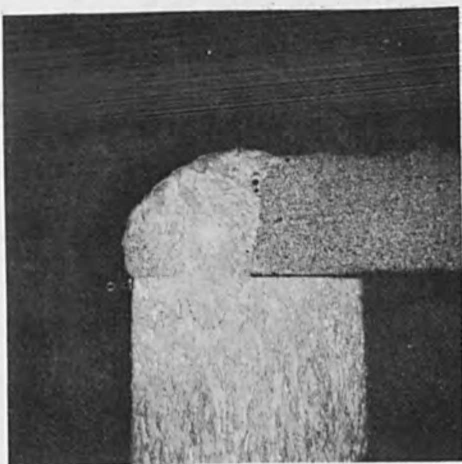

Fig. 16. Photomicrograph (50x) of emitter-to-manifold weld

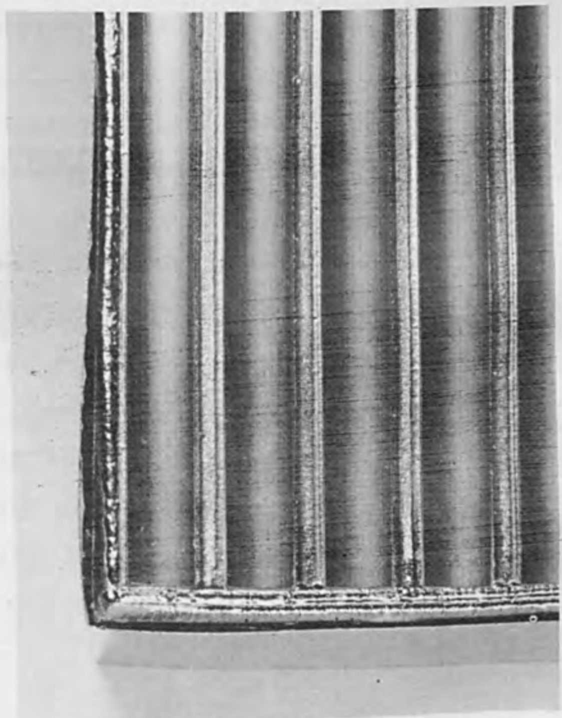

Fig. 19. Close view of sealed and welded 2-5/8 x 4 in. multistrip ionizer

fabricated with no cracks or leaks, using the two flexible jigs and the weld procedure described above. In addition, the ionizer face has been maintained flat within 0.002 in. in all instances.

Figure 9 shows an interesting modification of the annular ionizer. Instead of being made of a single piece, the porous tungsten consisted of eight segments in order to take advantage of the producer's capability for making smaller and more uniform porousity in a small section. The procedure for welding the segmented assembly was identical to that used for the one-piece porous tungsten, except that transverse welds were made by hand-tracking techniques after the peripheral welds were completed. No preheat was used for the transverse welds. It should also be noted that one segment weld was wider than the others because accumulative machining tolerance produced a gap of about 0.040 in. at that location. Filler material in the form of ribbon was placed in the gap and the joint was then welded.

Figure 10 shows tooling used for welding a 10-in. ionizer with the same general configuration as the 3-in. ionizer. Ceramic beads were used for thermal insulation under the holding tool. Figure 11 is a photograph of a welded 8- and 10-in.-diameter ionizer assembly, and Fig. 12 shows these assemblies in operation as an engine.

A 1-1/4 x 4 in. multistrip porous tungsten emitter is shown in Fig. 13. Because the strip emitter is machined from porous material and because no fuel (cesium) can be allowed to exit from the material except at the contoured areas, it was necessary to find a method for sealing the areas around and between the contoured sections. A procedure was developed which would melt only a small depth of metal on the surface of the emitter to make the area nonporous. This procedure has been termed "surface washing" or simply "washing." Figure 14 is a photomicrograph (150x) of a cross section of a washed area. The sealing must be accomplished within 0.005 in. or less of the knife edge of the emitter. Note that the pores have been retained immediately adjacent to the enlarged grains.

After washing, the emitter is placed in a nonporous tungsten manifold, positioned on a preheater, and welded into the manifold at 110 kV, 10 mA, and a travel speed of 55 in./min. Figure 15 is a photograph of a welded assembly and Fig. 16 is a photomicrograph (50x) of the emitter-to-manifold weld. Approximately ten assemblies of this type have been fabricated without cracks or leakage and, although 60 in. of wash and weld passes were required on each part, all assemblies were flat within 0.002 in. In addition, a tungsten feed tube was welded to the back of the manifold and a tantalum support leg was welded to each side of the manifold. Figure 17 shows an ionizer assembled in an engine ready for operation.

Figure 18 is a photograph of a welded 2-5/8 x 4 in. multistrip ionizer; a close view of the washed area and emitter-to-manifold weld is shown in Fig. 19. In two cases a corner of the emitter was broken off during machining. In both cases a chip of tungsten was placed in the defect and the assembly was repaired by hand tracking techniques. The chips were approximately 1/4 in. long and 1/8 in. wide.

Basic studies of ion physics were conducted with small porous buttons made from tungsten, rhenium, molybdenum, and tantalum. Each of these materials (with varying densities, pore sizes, and pore distribution) was successfully welded to a molybdenum support. The button and support were preheated with a defocused beam and then welded. Figure 20 shows a tungsten button welded to a molybdenum support. The wide weld was necessary to prevent fuel emission from areas outside the contoured section.

Figure 21 shows a molybdenum tube welded to a tungsten flange member. In order that the parts would be self jigging, the tungsten was machined so that a lap-butt joint occurred between the molybdenum tube and the tungsten flange. The design also gives support to the weld joint, resulting in higher load carrying ability. The tungsten lip on the near right-hand side in Fig. 21 was broken during machining and repaired by hand tracking techniques.

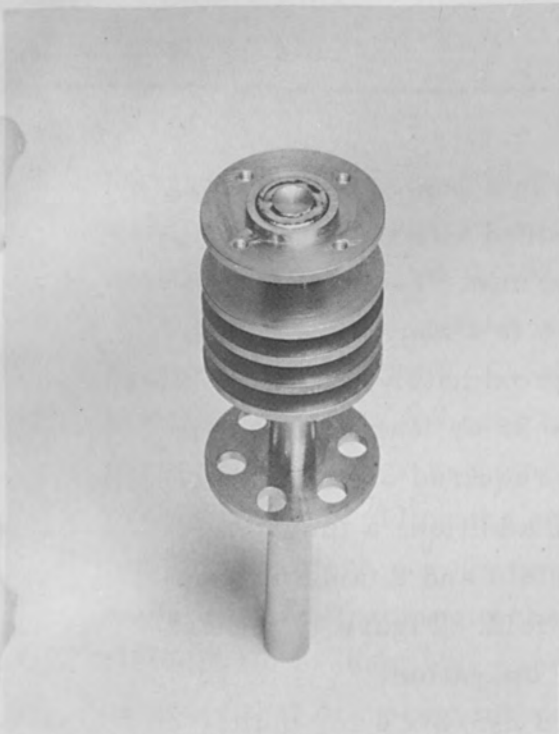

Fig. 20. Porous tungsten button welded to molybdenum support

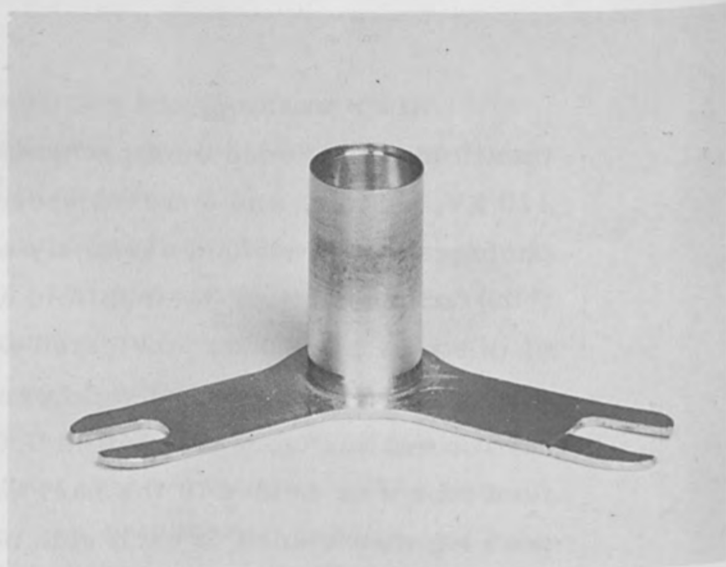

Fig. 21. Molybdenum tube welded to tungsten flange member

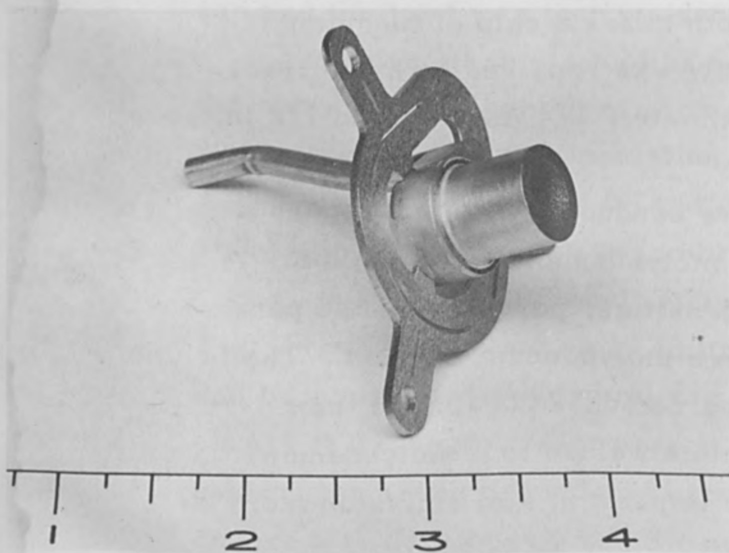

Fig. 22. Top view of contact ionizer

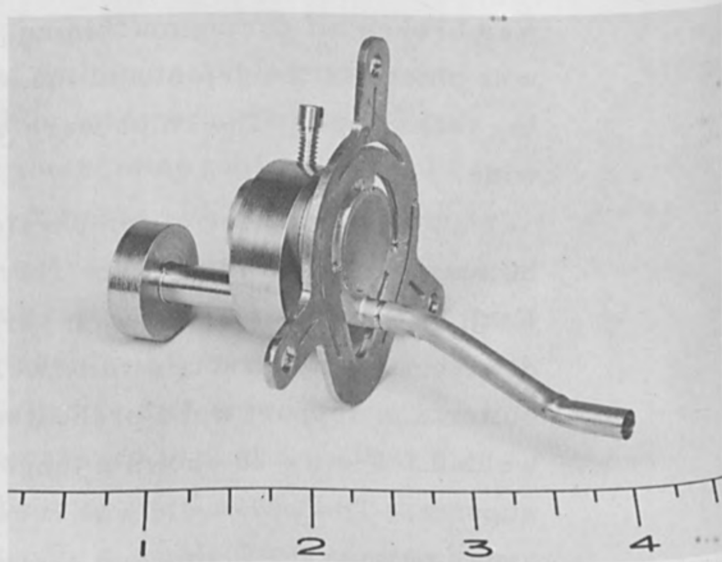

Fig. 23. Bottom view of contact ionizer and eccentric tail

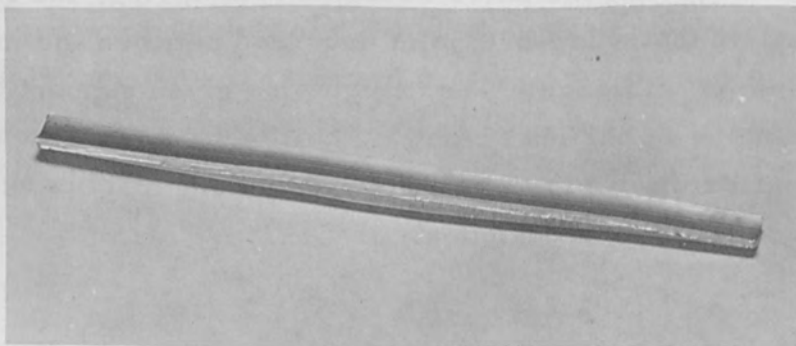

Fig. 24. Single strip ionizer with tantalum manifold

Figures 22 and 23 show a contact ionizer with a molybdenum jacket welded to a heavy walled tungsten cylinder. There were two circumferential welds between the tungsten cylinder and the molybdenum jacket. A tungsten support was welded to the jacket at three locations, and a molybdenum tube was welded to the jacket. The eccentric tool for rotating the part about the tube central axis may be seen in Fig. 23. The part was preheated with a defocused beam prior to welding and slow-cooled by a diffused beam after welding.

A single strip ionizer consisting of a porous tungsten emitter and a thin-walled (0.005-in.) tantalum manifold is shown in Fig. 24. The manifold was made by a forming operation; no preheat was required to make the weld.

In conclusion, it may be stated that electron beam welding is ideally suited for fabrication of ion propulsion systems which includes joining of not only similar refractory materials, but also dissimilar refractory materials. Complex, high-restraint configurations have been successfully welded without cracks or leaks; distortion was held to 0.002 in. although some cases required as much as 100 in. of welding for fabrication. Engine life tests have demonstrated that the weld and porous tungsten in the weld vicinity are capable of withstanding numerous thermal cycles and long usage without any evidence of failure or degradation.

MOLYBDENUM HONEYCOMB FOR AEROSPACE STRUCTURES

BY

Mel M. Schwartz
Research Specialist
Martin Company
Space Systems Division
Baltimore 3, Maryland

Molybdenum Honeycomb for Aerospace Structures

Introduction:

The advent of hypersonic and lifting re-entry vehicles has increased the desired operational temperature to where only refractory metals are feasible in the metals family. Two factors contributing to the slow development of these refractory metals were availability of the more promising alloys and welding (particularly in molybdenum). However, alloys of molybdenum are now available and the electron beam promises a solution to molybdenum welding problems.

Refractoriness of Molybdenum:

Good structural-type welds are difficult to achieve in molybdenum and its alloys by either resistance or fusion welding techniques. The development of cast weld zones produces brittle welds at room temperature due to high ductile-brittle transition temperatures and interstitial contamination through nitrogen, carbon and oxygen pickup in the molten weld metal during the welding process. Edge preparation prior to welding is also a problem, as shear cracks and laminations can cause excessive cracking.

Conventional fusion welding techniques of inert gas metal arc processes using carefully purged welding chambers are difficult to control for producing reliable joints. The optimum fusion welding process to date is by means of the electron beam welder, which has produced the best welded joints in foil and sheet gages of molybdenum and its alloys. A preliminary weld joint in foil gages of molybdenum is shown in Figure 1. The cast zone and recrystallized heat-affected area are kept to a minimum in electron beam welding. Work with molybdenum foil indicated that this process for fabricating honeycomb core is feasible.

Resistance welding of molybdenum and its alloys can produce fairly ductile welds using titanium or tantalum foil spacers between the molybdenum faces. This technique adds weight to the welded assembly and makes production processes more difficult. Electron beam welds make this technique unnecessary.

Pure molybdenum and the majority of its alloys rely primarily upon mechanical work for strengthening. In addition, cold working produces a metallurgical structure which imparts a greater ductility at lower temperatures than that of the recrystallized structure. For these reasons, the primary objective of molybdenum alloying is to increase the recrystallization temperature so that the cold work strengthening can be retained to higher temperatures. This increase in recrystallization temperature over pure molybdenum for comparable degrees of purity, strain hardening, time at temperature, and stress, ranges from 300°F for the Mo. - 0.5% Ti alloy to 450° for the TZC (Ti-Zr-C) alloy to 650°F for the TZM (Ti-Zr-Mo) alloy.

Description of Equipment:

The high accelerating voltages (150 KV maximum), and the advanced electron optics utilized in beam welding equipment produce a precisely controlled beam of exceptionally high power density. As the beam impinges on the work surface, the kinetic energy is transformed into thermal energy over a very localized area. This thermal energy provides sufficient heat to melt the material. The weld produced is dense and free of impurities and inclusions; also, because of the small heat affected area, minimum distortion and internal stresses result Figure 2.

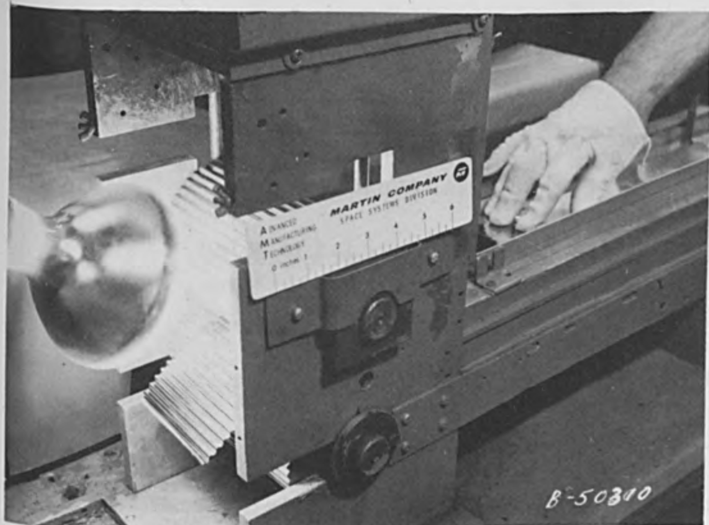

FIGURE 1

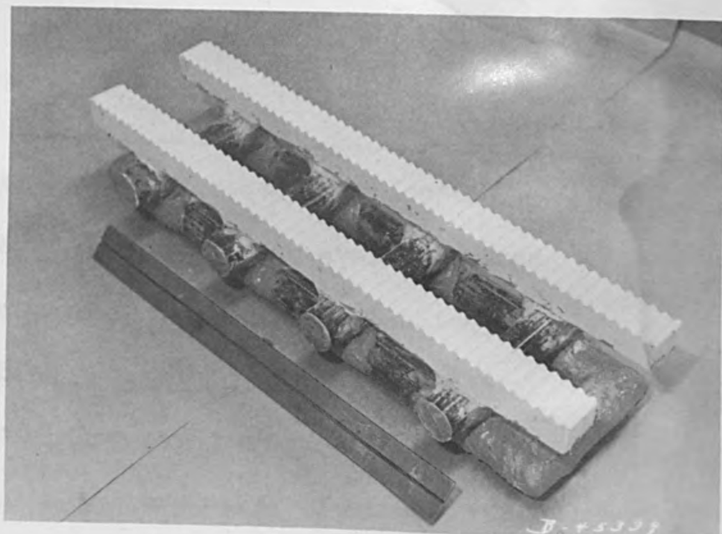

FIGURE 2

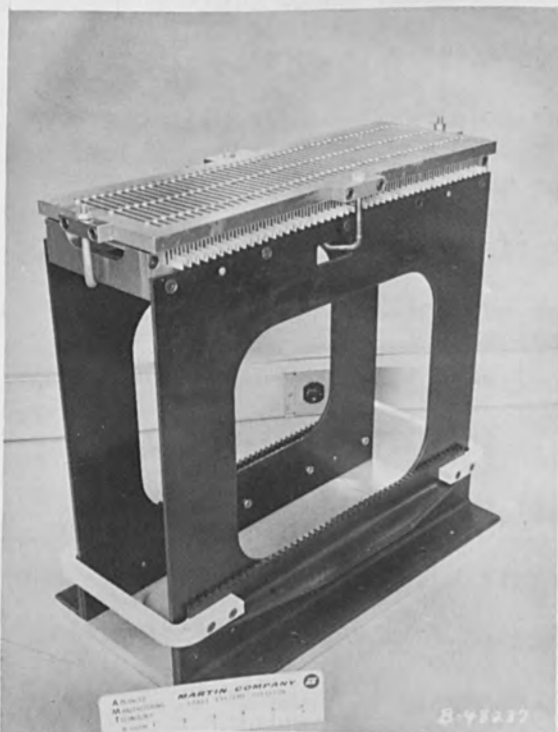

FIGURE 3

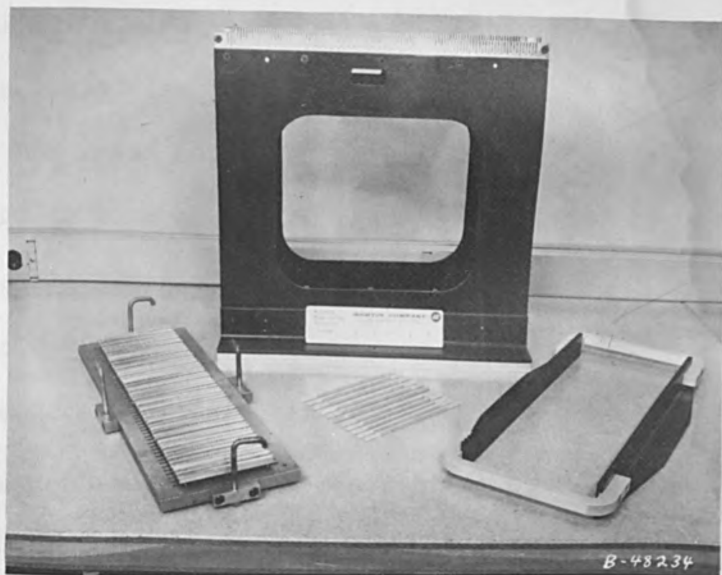

FIGURE 4

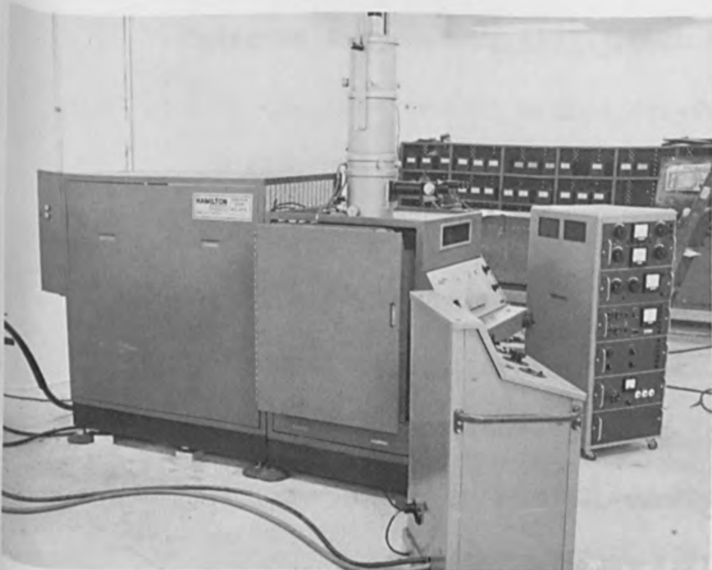

FIGURE 5

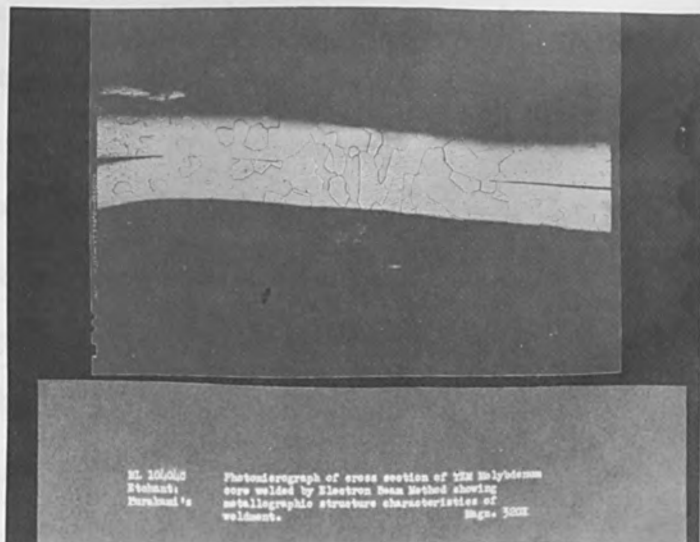

FIGURE 6

Tooling:

A tool was fabricated (Figures 3 & 4) to produce billets of TZM honeycomb core by electron beam welding techniques. This tool included two sets of mandrels which were used to hold the corrugated strips of foil in place for welding. A hold-down plate with localized pressure pins (approximately three pounds per pin) rested on the top of the upper set of mandrels which exerted a constant pressure on the foil to produce uniform nodal contact. The lower set of mandrels supported the nodes and reacted to the contact pressure of the upper set of mandrels. This contact was necessary to produce a continuous nodal weld. If continuous nodal contact was not maintained, no weld was made and the foil was severed by the electron beam. As each layer of corrugated foil was electron beam welded to make up the honeycomb core billet, a careful inspection was made to verify the soundness of each weld joint. If repair was necessary, this was accomplished by inserting additional 0.002 inch TZM foil material in the unwelded node of the core and the joint was rewelded.

After the welding of one layer of corrugated foil was completed, a special set of combs lifted the lower set of mandrels and placed them on top of the other set of mandrels. A new layer of corrugated foil was placed over the mandrels and nodal welds made. This process was repeated until welding of the billet was completed.

A renite template (Figure 5) was fabricated for use in inspecting the corrugated foil. A close check of the corrugated foil was necessary to assure that the axes of the corrugation were perpendicular to the edges of the foil. If the corrugations were not dimensionally correct, the nodes could become mismatched to such a degree that somewhere in fabrication of the core billet they could not be joined.

The TZM was cut into 18.5 inch lengths and corrugated in a special tool (Figure 6).

Properties of Welds:

Various welding parameters were evaluated to determine the optimum welding conditions for fabrication of the honeycomb core. These included voltage, amperage and welding speed. The best welds were produced with a machine setting of 90,000 volts and 0.85 milliamperes. Welding speeds of 27.5 to 58.0 inches per minute were evaluated and 40 inches per minute was selected as the optimum speed for honeycomb fabrication. The effect of welding speed on microstructure is shown in Figure 7 . Further studies are continuing to determine the beneficial effects of stress relieving the core after welding. (Figures 8 & 9). This subsequent stress relieving at 2100°F for 1 hour appears to increase room temperature ductility of the as-welded joint.

Preparation of Honeycomb Core:

After the honeycomb core was welded into a billet (14" x 14" x 4"), it was cut into slabs, which were then finished to the dimensions required. Three experimental methods were evaluated in an effort to establish the best method to slab and finish the honeycomb core. The three methods evaluated were:

1. A disc or mushroom-type cutter was used to cut the core. This technique of cutting was performed cold and caused tears in the core material and was abandoned.

2. The second method for cutting the honeycomb core billet was to use an electric discharge type machine. This method showed promise.

3. Finally the sawing and sanding of the core billet using heating lamps and blankets was tried and the results were excellent.

A honeycomb core billet and a slab finished by method 3 are shown in Figures 10 & 11. Both the second and third methods are capable of producing the required tolerances for honeycomb (± .003"). The third method is the more accurate of the two and requires only conventional shop equipment.

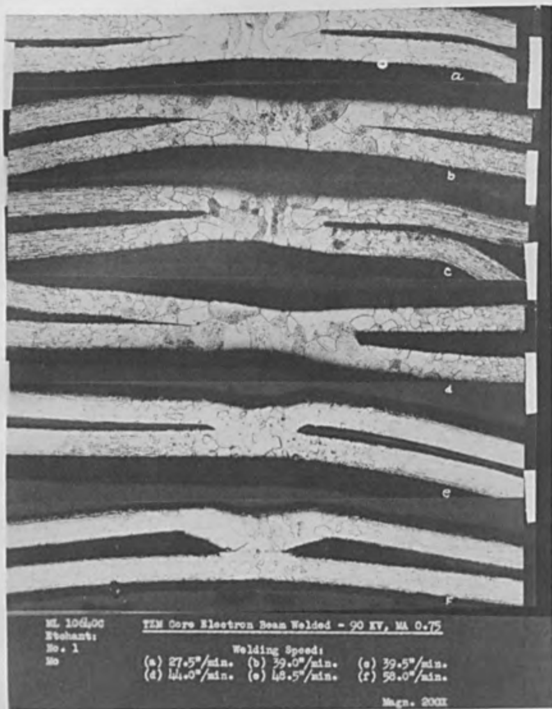

FIGURE 7

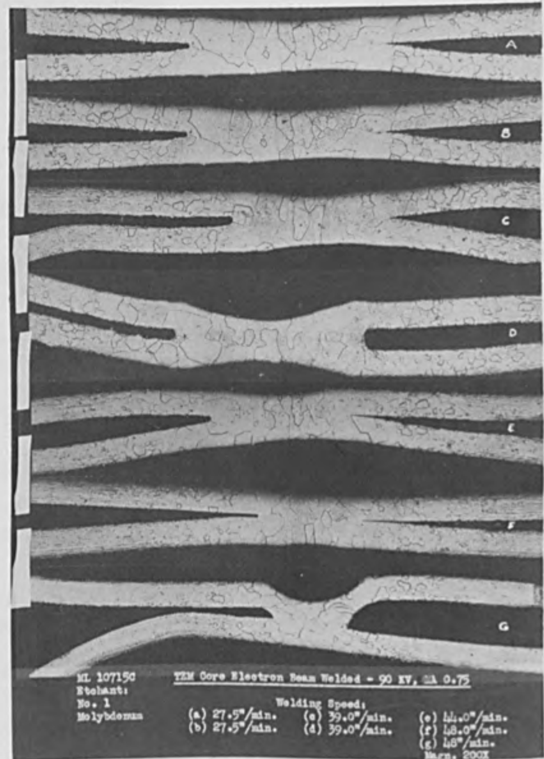

FIGURE 8

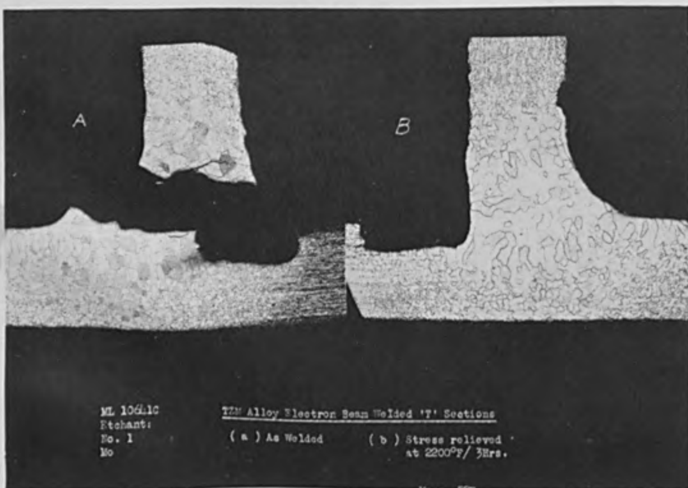

FIGURE 9

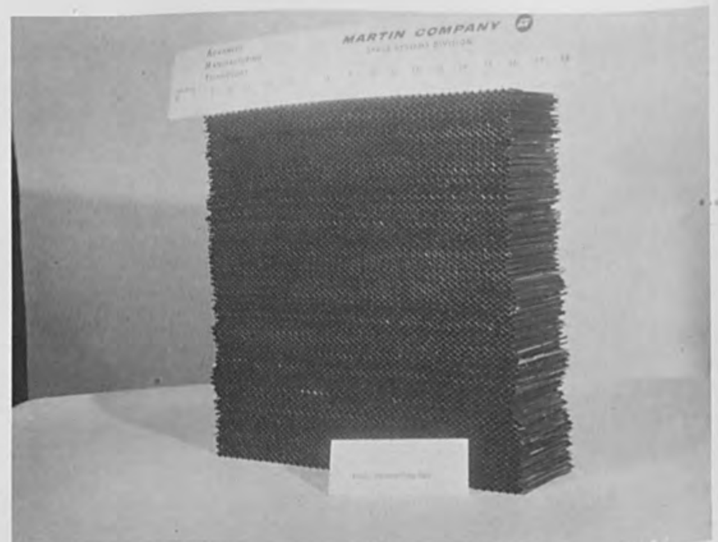

FIGURE 10

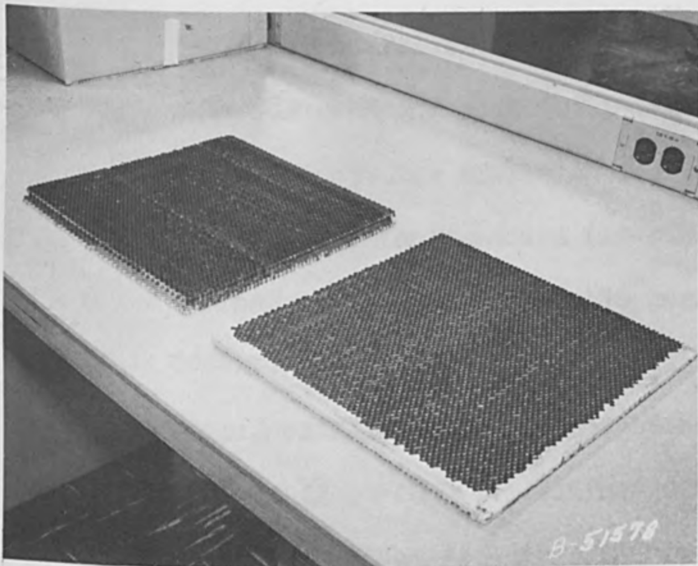

FIGURE 11

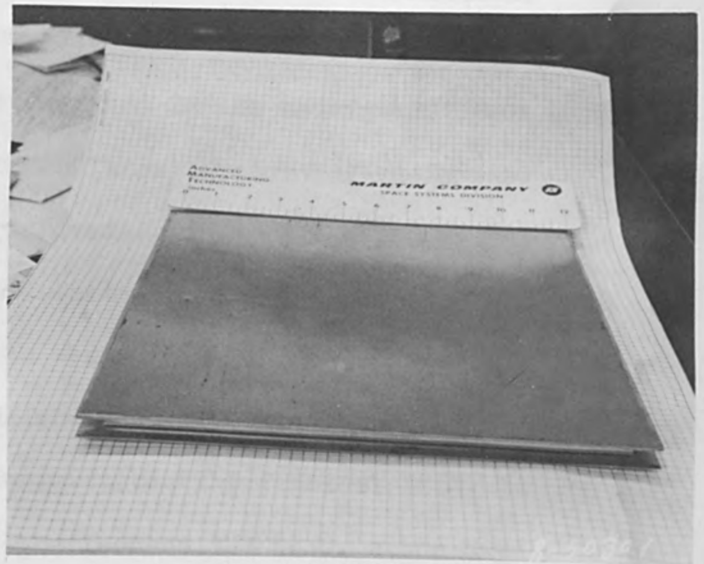

FIGURE 12

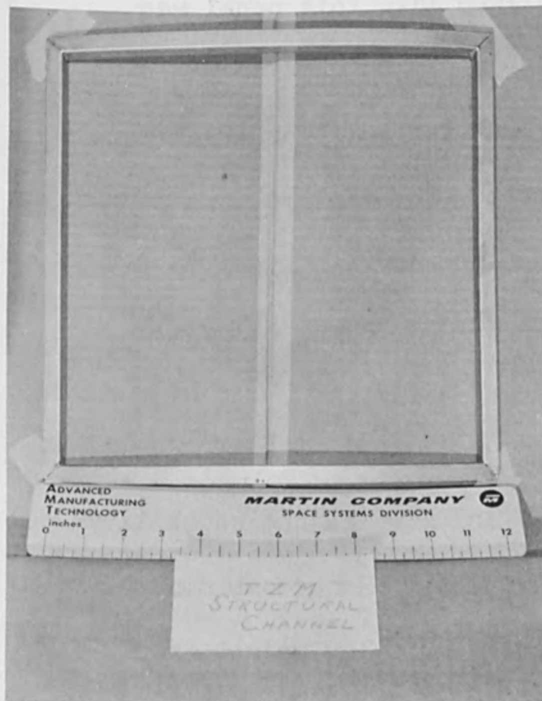

FIGURE 13

FIGURE 14

Application:

To illustrate how refractory metal alloys can be utilized in aerospace structures an R&D contract (AF33(657)-7276) from the Manufacturing Technology Laboratory (ASRCT) - Directorate, Materials and Processes and the Flight Dyanmics Laboratory (ASRMDS-21) Aeronautical Systems Division, Wright-Patterson Air Force Base, Ohio was recently awarded to the Martin Company.

A structural test panel is shown in Figure 12. The panel consists of .012" facings, 1/2" thick panels, 3/16" cell size, .002" foil honeycomb and a .025" "U" channel edge member. After the channels were formed the corners were mitered and electron beam welded to form a "picture frame" (Figure 13). The honeycomb core was then finished to fit the picture frame and then brazed.

A heat-shield test panel is shown in Figure 14. This panel was designed as a modular construction unit which could be used to build-up an entire vehicle surface. The panel has .008" facing, 3/8" thick panels and 3/16" cell .002" thick foil honeycomb core. The facings were formed into double stepped pans which were trimmed along certain lines to fit together as shown in Figure 14. The special stepped edges allow all the panel laps to be in the same direction.

Conclusions:

The key to success in the space vehicle industry is the capability to design and fabricate high efficiency structures. Honeycomb construction, developed to provide local stiffness at a low weight, represents such a structure. It has been highly developed and widely applied.

The ultimate uses of TZM and other refractory metal honeycomb structures hinge primarily on oxidation protection coatings which are undoubtedly the one most significant factor that has been responsible for the slow development of refractory metal structures. Recent developments in this field are encouraging, indicating that reliable coatings with adequate performance are highly dependent upon improved process control and inspection. In addition with the advent of the electron beam joining process the potentially difficult to handle materials such as molybdenum and its alloys now pose surmountable fabrication problems in aerospace applications.

THE INFLUENCE OF GAS CONTENT ON CRACK PROPAGATION ENERGY

By:

Sheldon S. White
Assistant to Technical Director

ALLOYD ELECTRONICS CORPORATION
35 Cambridge Parkway
Cambridge 42, Massachusetts

THE INFLUENCE OF GAS CONTENT ON CRACK PROPAGATION ENERGY

SYNOPSIS:

Several heats of H-11 hot-work die steel, having significantly different oxygen and nitrogen contents, have been tested for impact resistance. Constant tensile strength values were involved for both electron beam welded and unwelded specimens. Crack propagation energy values for both conditions were plotted against gas content on the same curves for various selected testing temperatures. The resulting smooth curves were reduced to linear functions on a longarithmic scale. The importance of vacuum method stock and the requirement of electron beam welding of clean surfaces is thereby shown, with high predictable impact resistance possible at high strength levels.

INTRODUCTION

Hot-work die steel of the H-11 type (5% Cr, 0.4%C) is one of the primary steel types presently being considered for airframe and missile fabrication. Such high strength steels are very competitive with titanium insofar as performance is concerned and considerably lower in price.

This steel is commonly designed for use in the 300,000 psi ultimate strength range. Standard arc welding techniques have, however, produced weldments which have had mechanical properties, expecially impact resistance and tensile strengths, considerably different from those of the base metal. Weldments in this steel have usually

produced required fusion zone strength levels since approximately 95% of the structure is quenched to untempered martensite. Impact values have been quite low due to interstitial contamination accompanying the gas cover. While maintaining these low impact values, the joints cannot utilize the high fusion zone strengths, but are forced to fracture in overheated and hence overly tempered and overly softened heat affected zones.

Because of these facts, a program to investigate the application of electron beam welding to this steel was instituted.[1] It was found that the very high heat concentration of a sharply focused electron beam caused very little heat affected zone softening, with joint efficiencies of 90-100% being reported.[1] It was felt that the atmospheric protection offered with such vacuum welding was of secondary importance. This was true despite the fact that some increase in impact resistance in fusion zones, as compared to unwelded stock, was noted for constant tensile strength conditions.[1]

To more thoroughly investigate the influence of gas content on impact resistance, further work involving the electron beam welding of air and vacuum melted heats of H-11 was initiated. The results of this program using 1/8" sheet material are discussed here.

EQUIPMENT

The equipment used in this program consisted of a 1' x 1' x 2' vacuum chamber specifically designed for the welding impact and flat tensile specimens in square butt weld configuration. The chamber was evacuated by mechanical and diffusion pumping and was capable of obtaining the operating pressure range of 10^{-4} to 10^{-5} mm. Hg pressure within 5 to 10 minutes from the beginning of the pump-down cycle. Copper chill bars and backing plate were used to aid in restricting the width of the heat affected zone and controlling fusion zone geometry.

Using a self-accelerated gun having a power density in the 200,000 KW/in^2 range, it was possible to accurately control weld width such that joints of 0.165" ± 0.010" could be made in a single pass utilizing 14,000 V, 250 m.a., and 10 i.p.m. travel rate.

To minimize friction, the carriage assembly rode on a three-point suspension utilizing linear ball bearings. A conventional electronic speed control driving a variable d-c motor was used. During all welding operations, no x-ray count significantly higher than that of background was observed.

EXPERIMENTAL PROCEEDURES

The steel heats were fully hardened by solutionizing at 1900°F for 1 hour, fan quenching, and tempering with 2 cycles at 600°F with 2 hours at temperature per cycle. This heat treatment was designed to give material a 300,000 p.s.i.

ultimate strength and was also found to correlate with the recommendations of Arnold[2] for realizing maximum ductility and toughness as well as high strength in H-11 steels. The hardened material was sand-blasted and solvent cleaned prior to welding.

The impact specimen used was a Charpy specimen in all dimensions except that of the thickness which is that of the sheet used. The specimen was further modified by introducing a natural fatigue crack at the base of the notch such a crack depth being controllable to within 0.050" ± 0.015". The specimens were impacted and the area through which the crack propagated was measured on each specimen.

The impact energy specimen used made it possible to measure essentially crack propagation energy only, since the crack proceeded from a pre-existing natural crack. This mode of fracture is also representative of that occurring in actual weldments where failures most often begin at existing stress raisers, without requiring significant energy for crack initiation. Since crack initiation energy is a function of specimen geometry and elastic strain energy, any true change in propagation values could be largely masked when utilizing specimens not having such a natural crack and, thereby, requiring significant imparted initiation energy. The crack propagation energies of fusion zones were determined by centering the notch on the fused centerline. Base metal impact values were determined utilizing unwelded material.

All gas analyses were determined by the vacuum fusion technique. Approximately a 1/16" cube was machined from plate or weldment center for analysis. In all cases hydrogen content was 1 ppm or below and is therefore not reported herein.

DISCUSSION OF RESULTS

The available results of vacuum fusion analyses are given in Table I. Vacuum melted stock had lower gas contents, as anticipated. It is interesting that gas content could be raised, as well as lowered, by electron beam melting. Presumably, this reflects absorbtion of the surface film.

Since both vacuum melted and air welded stock were tempered to 280,000 - 320,000 p.s.i. ultimate strength range and weldments in all heats fractured at 280,000 - 290,000 p.s.i. ultimate strength, the gaseous contents of all melts, whether of as-received stock or electron beam melted fusion zones could be directly compared on an equal strength basis. This was true even though weldments failed in high temperature heat affected zones, since these zones had essentially the same large grain size and structure as fusion zones, differing only in gas content. In this way, any evidence of a smooth relationship among these several data sources would indicate that grain size, and even structure, is of minor importance when compared to gas content for constant tensile strength.

TABLE I

Gas Content

	O, p.p.m.	N, p.p.m.	O+N, p.p.m.
Base Metal Heat No. 1 Air Melted	48	94	142
Weld Metal Heat No. 1	61	29	90
Base Metal Heat No. 2 Vacuum Melted	17	51	68
Weld Metal Heat No. 2	20	25	45
Base Metal Heat No. 3 Vacuum Melted	Not Available		
Weld Metal Heat No. 3	16	65	81
Base Metal Heat No. 4 Air Melted	67	122	189
Weld Metal Heat No. 4	90	130	220

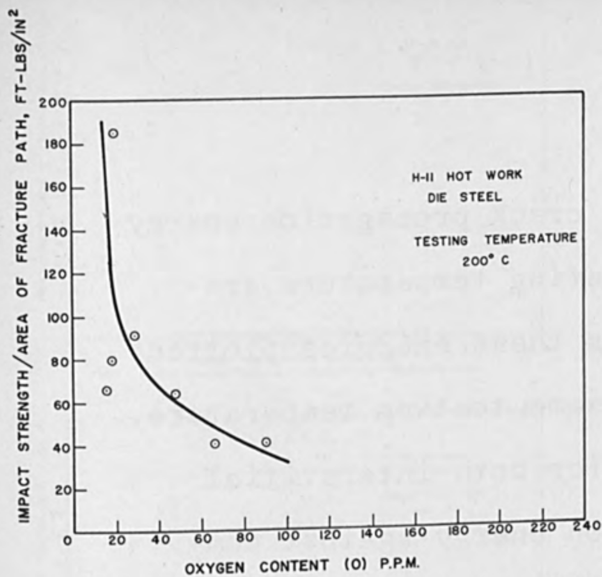

FIGURE 1 - Crack Propagation Energy as a Function of Oxygen Content

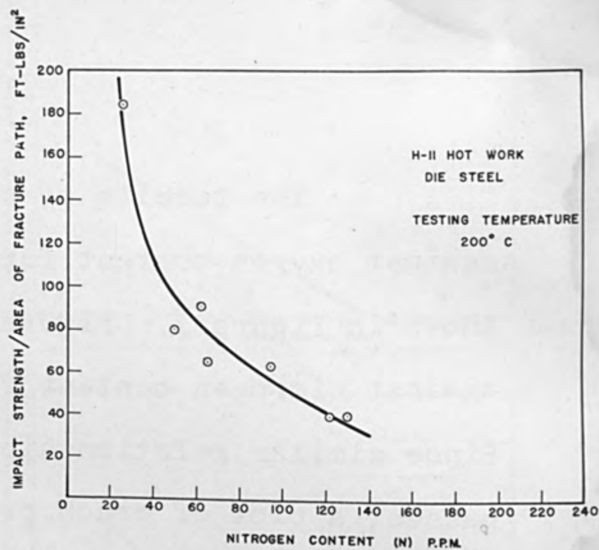

FIGURE 2 - Crack Propagation Energy as a Function of Nitrogen Content

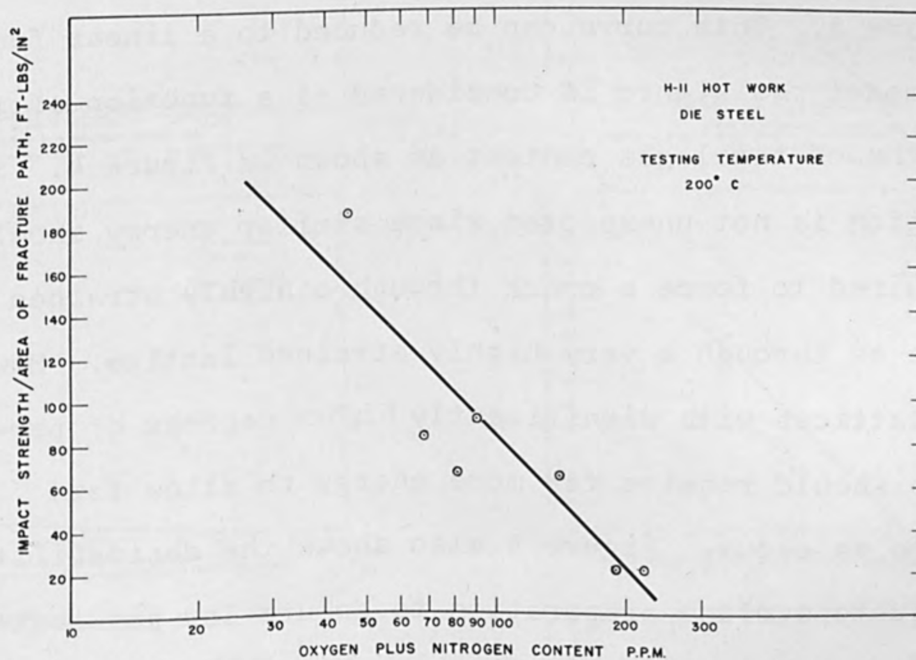

FIGURE 4 - Crack Propagation Energy as a Function of Oxygen Plus Nitrogen Content

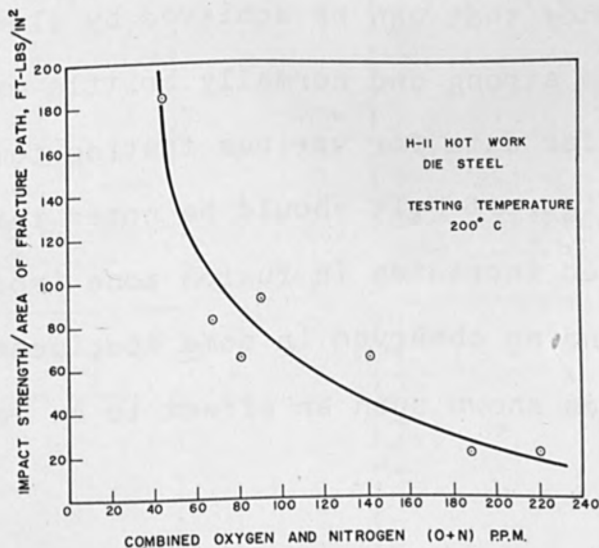

FIGURE 3 - Crack Propagation Energy as a Function of Oxygen Plus Nitrogen Content

The results of plotting crack propagation energy against oxygen content for one testing temperature are shown in Figure 1. Figure 2 shows these energies plotted against nitrogen content for the same testing temperature. Since similar relationships hold for both interstitial gasses, a plot of crack propagation energy against combined oxygen and nitrogen content is meaningful as shown in Figure 3. This curve can be reduced to a linear function when impact resistance is considered as a function of the logarithm of total gas content as shown in Figure 4. Such a relation is not unexpected since similar energy should be required to force a crack through a highly strained lattice as through a very highly strained lattice. However, lattices with significantly higher degrees of perfection should require far more energy to allow fast fracture to occur. Figure 4 also shows the desirability of adequate surface preparation to ensure low gas contents in fusion zones. These data also show the remarkably high impact resistance that can be achieved by electron beam welding of such strong and normally brittle material.

Similar data for various testing temperatures are presented in Figures 5-14. It should be noted that previous work[1] attributed increases in fusion zone impact resistance to erronous bending observed in some specimens. This further work has shown such an effect to be relatively uncommon.

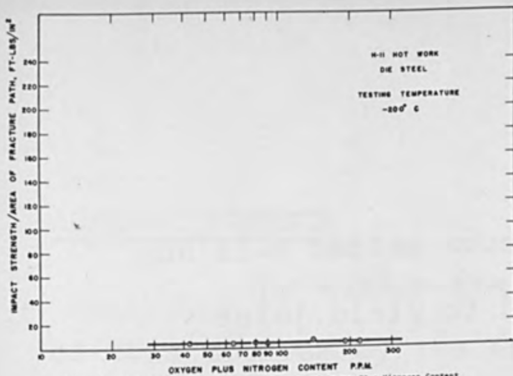

FIGURE 5 - Crack Propagation Energy as a Function of Oxygen Plus Nitrogen Content

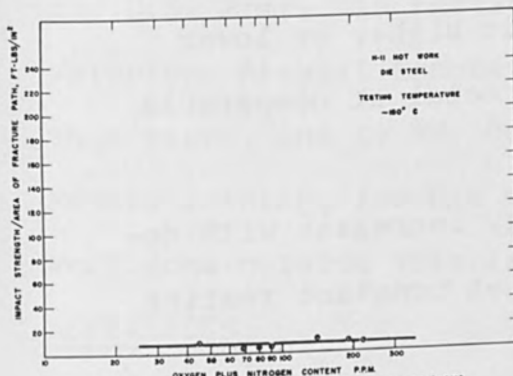

FIGURE 6 - Crack Propagation Energy as a Function of Oxygen Plus Nitrogen Content

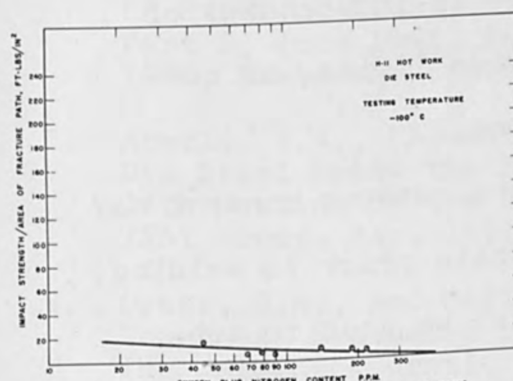

FIGURE 7 - Crack Propagation Energy as a Function of Oxygen Plus Nitrogen Content

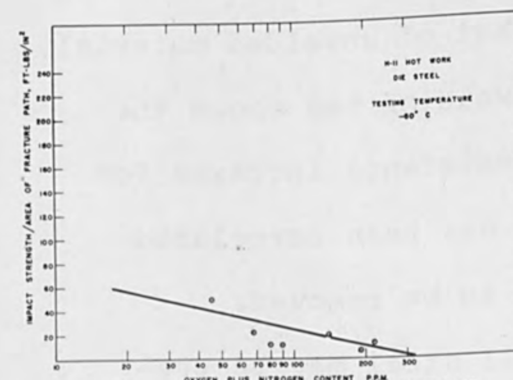

FIGURE 8 - Crack Propagation Energy as a Function of Oxygen Plus Nitrogen Content

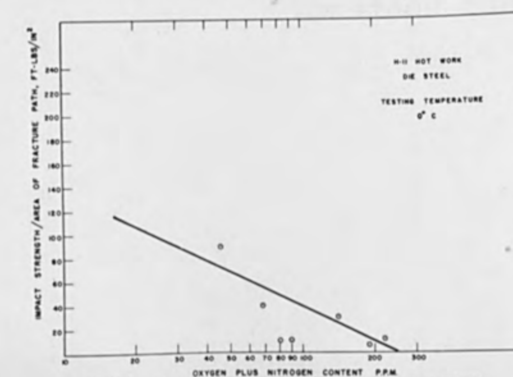

FIGURE 9 - Crack Propagation Energy as a Function of Oxygen Plus Nitrogen Content

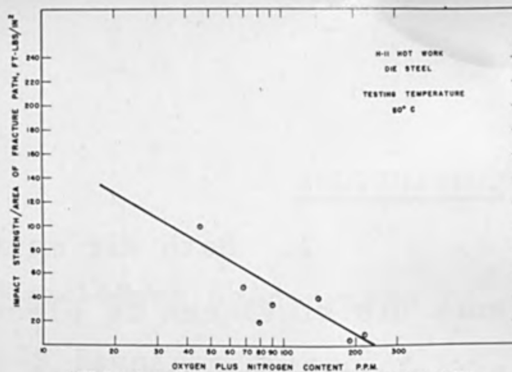

FIGURE 10 - Crack Propagation Energy as a Function of Oxygen Plus Nitrogen Content

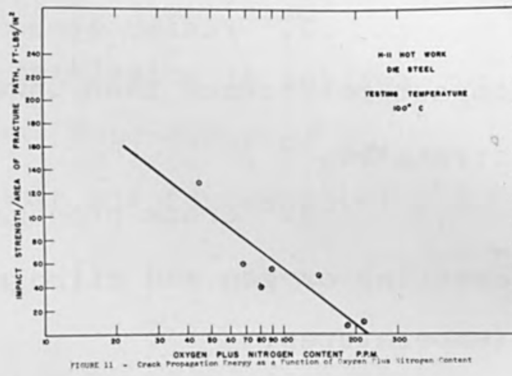

FIGURE 11 - Crack Propagation Energy as a Function of Oxygen Plus Nitrogen Content

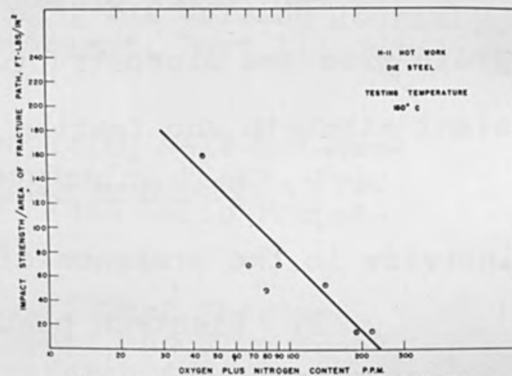

FIGURE 12 - Crack Propagation Energy as a Function of Oxygen Plus Nitrogen Content

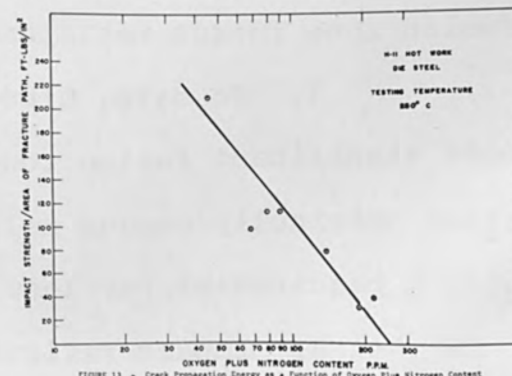

FIGURE 13 - Crack Propagation Energy as a Function of Oxygen Plus Nitrogen Content

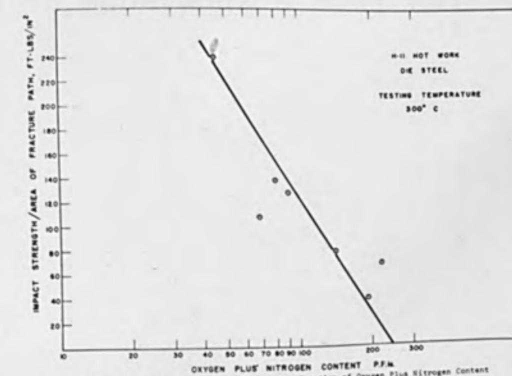

FIGURE 14 - Crack Propagation Energy as a Function of Oxygen Plus Nitrogen Content

CONCLUSIONS

1. Both air melted and vacuum melted H-11 hot work die steel can be electron welded to yield joint efficiencies of more than 90%.

2. Fusion zones may exhibit higher or lower impact resistance than unwelded base metal at comparable strengths.

3. Crack propagation energy increases with decreasing oxygen and nitrogen content at constant testing temperatures.

4. Crack propagation energy is independant of grain size and microstructure, over wide limits, at constant strength and testing temperatures.

5. Electron beam fusion zone gaseous content may increase in the presence of surface scale prior to welding.

6. Electron beam welding may be used to substantially lower fusion zone gaseous content, thereby raising fusion zone impact resistance above that of unwelded material.

7. To date, electron beam welding has shown the most significant fusion zone impact resistance increase for stock originally vacuum melted. This has been correlated with a requirement for less total gas to be removed.

8. Impact resistance of H-11 steel may be predicted from a knowledge of total gaseous content.

ACKNOWLEDGMENTS

The author gratefully acknowledges sponsorship of this program by the Army Materials Research Agency of the U.S. Army. In particular, I wish to thank the Watertown Arsenal Laboratories for permission to publish this paper, and to Mr. Donald Buffum, Supervisor of Metals Joining, for his technical help and for expiditing work done outside this laboratory.

REFERENCES

1. White, S.S., Lander, H.J., Hess, W.T., and Bakish, R., "A Study of Electron Beam Joining", The Welding Journal, Part I, June 1962, Research Supplement, Part II, July, 1962, Research Supplement.

2. Arnold, S.V., "Advantages of Tempering H-13 Hot-Work Die Steel below the Secondary Hardening Peak", Proc. 17th Meeting of the JANAF ARPA NASA Solid Propellant Group, May, 1961.

3. Orner, G.M., and Hartbower, C.E., "Sheet Fracture Toughness Evaluated by Charpy Impact and Slow Bend", The Welding Journal, 40, (9), Research Supplement, 405-S to 416-S (1961).

ELECTRON BEAM WELDING OF DISSIMILAR METALS

By

M.M. Schwartz

Research Specialist

Martin Company

Space Systems Division

Baltimore 3, Maryland

ELECTRON BEAM WELDING OF DISSIMILAR METALS

Man's advancing technology into space and the effectiveness of his space vehicles are paced by his progress in joining structures together.

Virtually every future design will involve operating environments including strength and temperatures far in excess of the capabilities of current structures and materials.

The success of every prime contractor, sub-contractor, and vendor will depend heavily on his knowledge of, and ability to work with current and upcoming materials and structures. Important among these are the refractory metals, with good structural strength in the 3000 and 4500°F range.

Manned spacecraft are being designed, however, for repeated flights from earth and back and will have to maintain their structural integrity and aerodynamic geometry under severe stresses at temperatures ranging to over 3000°F often cycled at rapid rates.

The chemical character of the various environments will extend from the extremes of oxidizing atmospheres to reducing ones and, in the case of rocket-motor exhausts, will include a great variety of reactive and erosive particles. Structural skins of spacecraft will be variously exposed to high thermal shock, thermal fatigue, high-velocity microparticle erosion, extreme mechanical shock, mechanical fatigue, chemical attack, ultraviolet, nuclear, and cosmic radiation, deep space vacuum and both

compressive and tensile stresses to the limit of the tolerances of the materials.

Of the several approaches to these problems, involving plastics, metals, ceramics, plastic-metal-ceramic composites, inorganic plymers, and so on, one of the most challenging and potentially one of the most requiring is current research in refractory metals.

The refractory metals are just emerging as important practical materials for high-temperature applications. Almost without exception, however, practically every order involves a heavy measure of development as well as straightforward production. Above, say, 2500°F there are no proper criteria for design specifications. There aren't even adequate testing procedures and facilities for developing such criteria. And as often as not a new operational requirement will necessitate a whole new look at both materials and fabrication techniques.

Materials used in the construction of the various types of reentry vehicles such as, lifting-body reentry rockets and glide reentry rockets are subjected to temperatures in excess of 2500°F.

A new generation of energy conversion devices (Thermionics) has also required and accelerated the need and fabrication techniques for metals capable of withstanding 3000 - 4000°F temperatures.

There has developed, therefore, an urgent need for joining dissimilar combinations of high-temperature metals capable of withstanding these severe temperatures. Refractory metals like columbium (niobium), tantalum, molybdenum, tungsten, and their alloys have been contemplated for use in the critical portions of such structures.

Fusion and resistance welding of these materials has presented numerous critical fabrication problems, attendant with metallurgical requirements such as recrystallization, heat effected zones of weldments, brittleness or ductility due to composition of metal alloy, and interstitials due to initial processing.

Fusion welding of the refractory metals is difficult because these materials absorb oxygen, nitrogen and hydrogen and become brittle. Electron-Beam welding in a vacuum of 1×10^{-4} mm Hg. reduces the volume of these gas contaminants to approximately 1% of the total impurities (including oxygen and nitrogen) that are found in the best welding process. Not only will the vacuum-melted metal not absorb large quantities of gas impurities, but often it will also give up contained gases as it is heated, thus producing vacuum-tight joints.

Brief Description of Equipment:

The high accelerating voltages (150 KV maximum), and the advanced electron optics utilized in electron beam welding equipment produce a precisely controlled beam of exceptionally high power density. As the beam impinges on

the work surface, the kinetic energy is transformed into thermal energy over a very localized area. This thermal energy provides sufficient heat to melt the material. The weld produced is dense and free of impurities and inclusions; also, because of the small heat affected area, minimum distortion and internal stresses result. Figure 1.

Applications by Martin:

The ability to produce reliable strong joints in materials is just about as important as the ability to make the materials in the first place. The first application of electron beam welding to nuclear components is a good example. Here, the requirements were leak tightness, corrosion resistance, and strength in that order. Figure 2. Applications like this have forced the development of a number of welding techniques: braze-welding, pressure welding, ultrasonic welding and electron beam welding. In many ways this last technique is the most versatile. Nevertheless, the basic metallurgy cannot be changed by any technique: any metal can be welded to any other, but the phase diagram of the two will dictate what phases are present in the weld. If brittle intermetallic phases occur in the system chosen, the weld may be brittle.

Assuming a favorable combination of metals is to be welded, what advantages does electron beam welding bring to the job? In addition to purity, there is the fact that a large amount of heat can be concentrated in a very small

area. This means the fused zone which forms the weld bead can be deep and narrow - with a depth-to-width ratio of from 4 to as high as 25, compared to about 1 for other fusion welding techniques. With much less molten metal to give off heat during cooling, there is less distortion of the weldment and, more important, the microstructure of the parent metal adjacent to the fusion zone is much less affected. And this "heat-affected zone" is very often the place where welds fail.

Another, more subtle advantage to the process is that the amount of heating can be varied smoothly by varying the voltage; this means pre-heating and post-heating are easily accomplished and spatter is seldom a problem.

Since the advent of commercially available electron beam equipment, many interesting applications have evolved. For example, Figures 3 and 4 demonstrate the capabilities of electron beam to effectively weld material varying in thickness from 0.002 to 1/8 inch. In addition, welding of materials which differ greatly in geometry or melting points is easily accomplished with a high energy density beam. This is made possible because the time interval required to raise each to its respective melting point is practically identical.

In engineering and constructing nuclear devices and structural components, the materials engineer has been confronted by a perplexing problem.

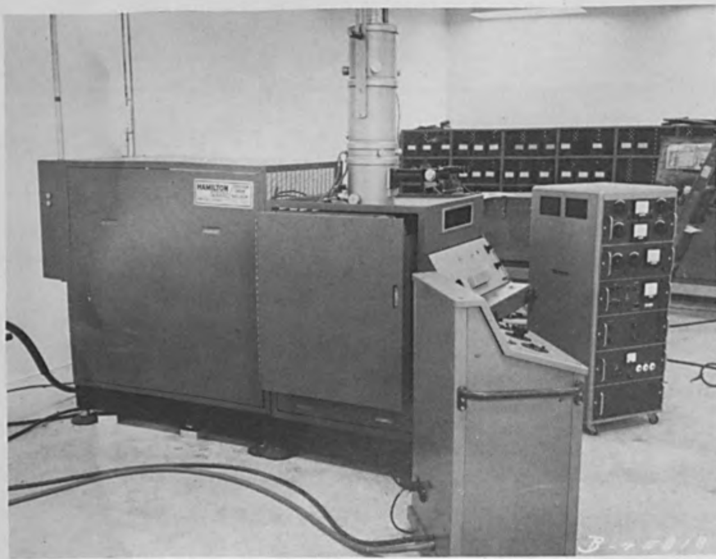

FIGURE 1

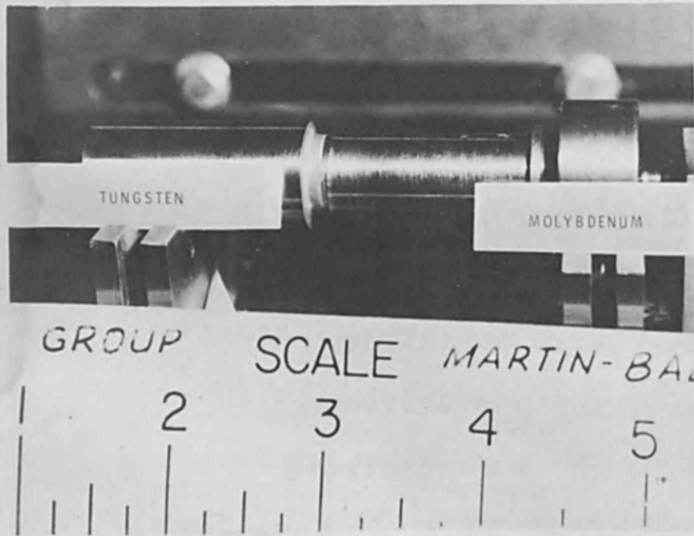

FIGURE 2

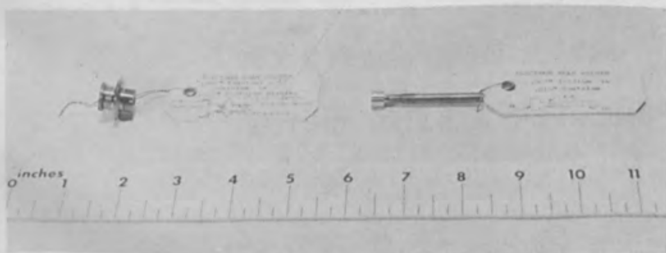

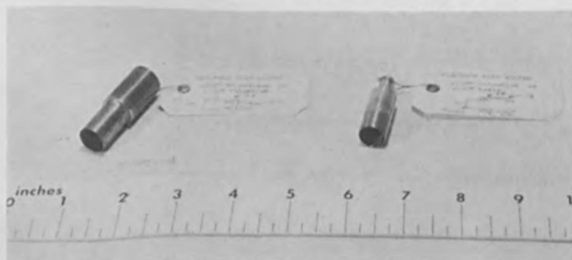

FIGURE 4

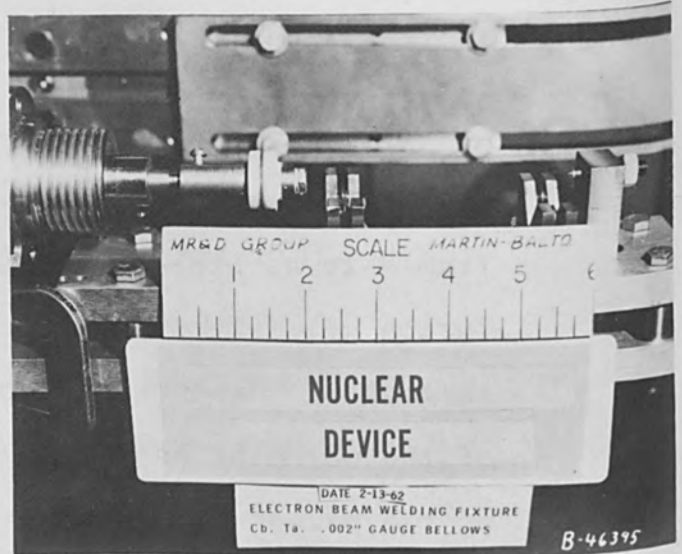

FIGURE 5

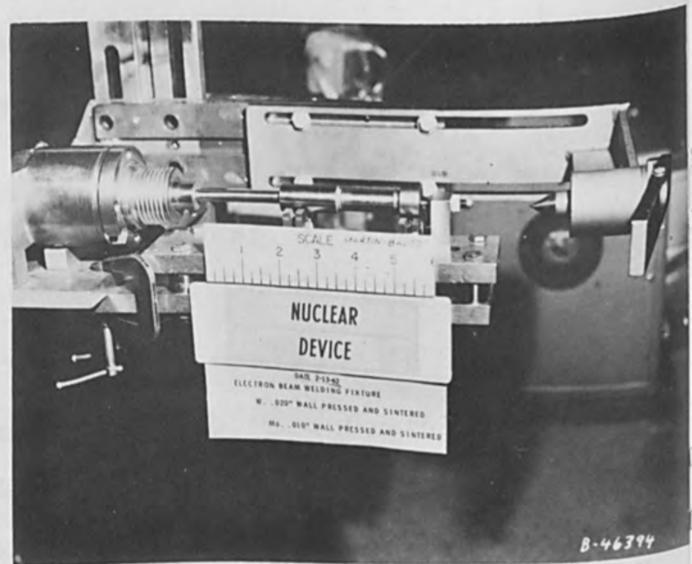

FIGURE 6

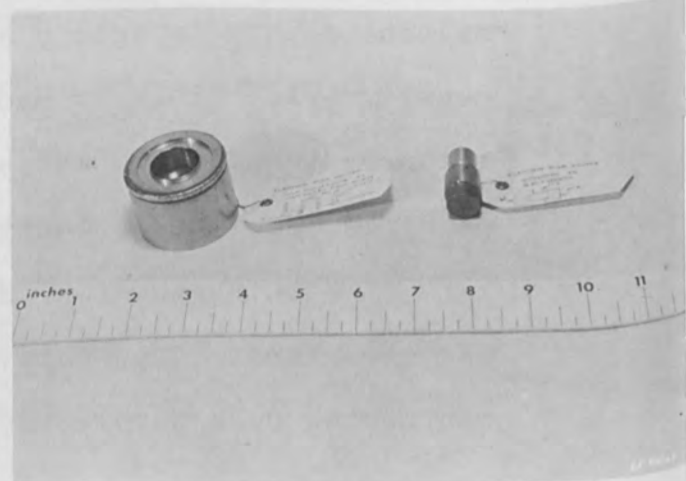

FIGURE 7

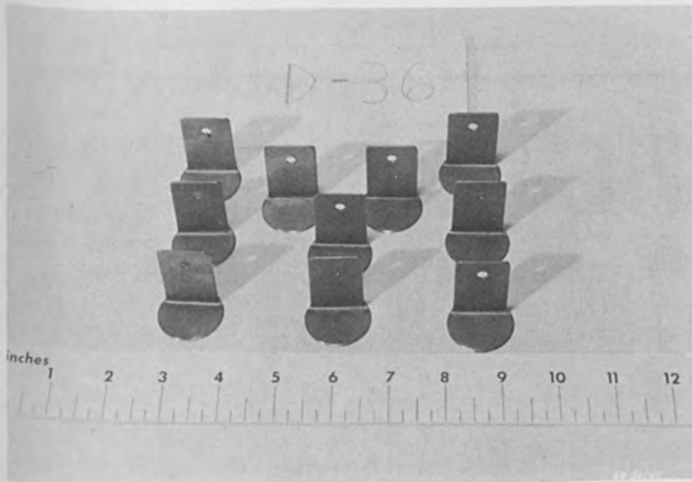

FIGURE 8

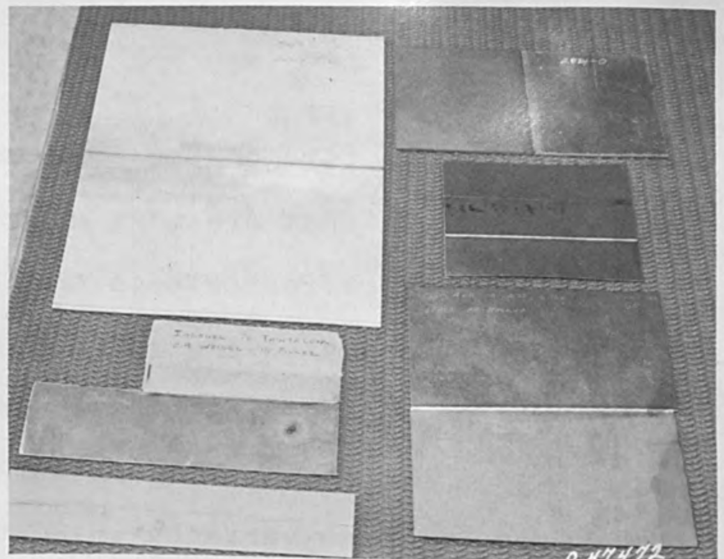

FIGURE 12

FIGURE 9

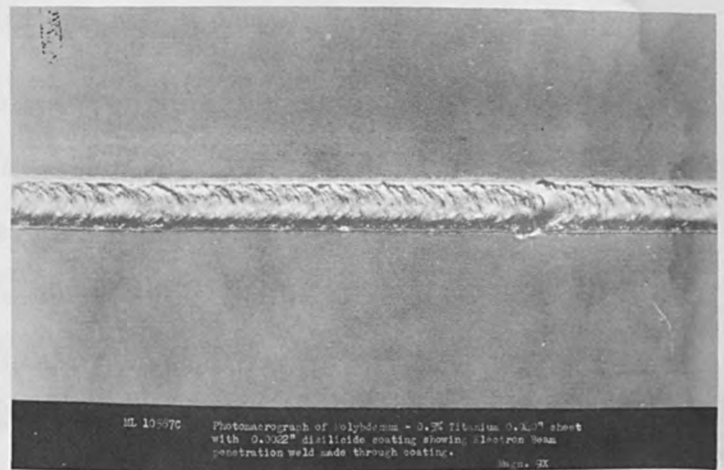

ML 10587C Photomacrograph of Molybdenum - 0.5% Titanium 0.040" sheet with 0.0022" disilicide coating showing Electron Beam penetration weld made through coating. Magn. 9X

FIGURE 13

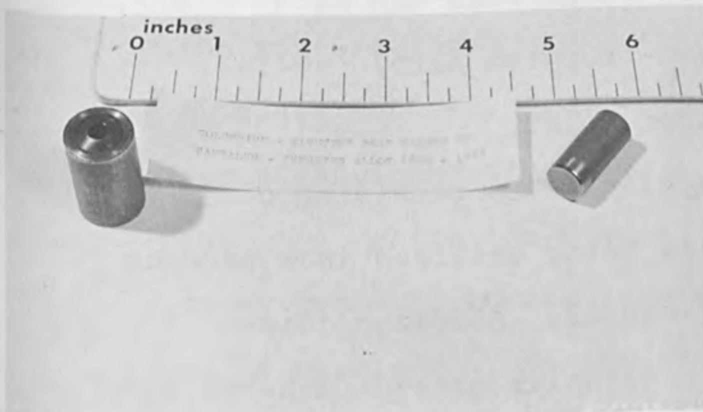

FIGURE 10

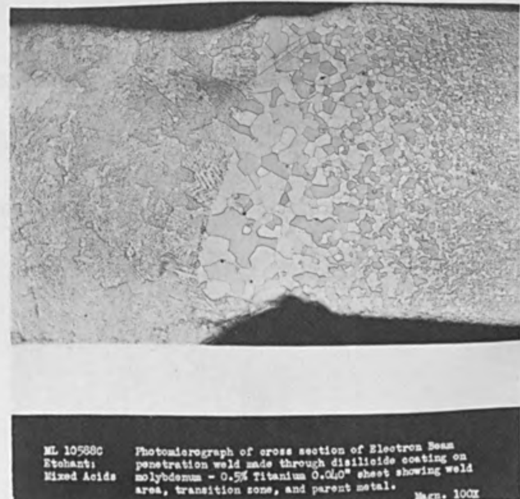

ML 10588C Etchant: Mixed Acids Photomicrograph of cross section of Electron Beam penetration weld made through disilicide coating on molybdenum - 0.5% Titanium 0.040" sheet showing weld area, transition zone, and parent metal. Magn. 100X

FIGURE 14

FIGURE 11

Some of the most promising combinations of materials are those that are most difficult to refine and to shape. The very refractoriness that makes some desirable has put them largely beyond reach as simple, economical choices in the engineering of spaceage devices.

The problem in working with these materials is not just the variance in melting points between the two materials (3000°F in some cases), but also the solubility of some with each other according to published literature on phase diagrams. Is a welded or brazed joint actually present?

The following series of photographs indicates the combinations of metals which Martin has joined by electron beam welding to produce nuclear generators and electronic devices. Figures 5,6,7, 8 and 9.

Recent work has shown that columbium can be successfully joined to the tantalum-tungsten alloy (90-10), and Figure 10 illustrates the welded joint.

Two other interesting applications receiving considerable interest but not actually being utilized in a product by Martin are shown in Figures 11 and 12. Aluminum joined to stainless steel and aluminum to titanium present answers to some of the propulsion engineers weight and joining problems, however, considerable mechanical property as well as corrosion tests must be performed to relay on this combination of materials.

Another interesting study which has been initiated is to investigate the use of electron beam welding thru a protective coating on refractory metals and then recoating the repaired surface. The initial results appear quite promising as shown in Figures 13 and 14.

Future of Electron Beam Joining:

The potential of electron beam welding has hardly been tapped.

With increasing emphasis on reliability, quality and reproducibility, electron beam welding techniques show promise of extended usage in even the most common commercial applications as well as in new highly specialized material joints.

Thus with the advent of new processing techniques, combinations of metals and alloys can be used to fabricate the required components for nuclear and electronic devices or space vehicles that will operate in what are to us abnormal environments.

While the cost of fabricating these exotic materials today seems high, the important thing is that processes are being developed. By the time spacecraft and nucleonics are commonplace these costs will be in line with the over-all price of the complete vehicle.

A CORRELATION OF WELDING VARIABLES

by M. H. Hablanian
Chief Development Engineer
NRC Equipment Corporation
A Subsidiary of the National Research Corp.

A CORRELATION OF WELDING VARIABLES

1. Introduction

When experimenting with electron beam welding in the laboratory it is desirable to have a method to predict the machine settings for welding a new and unfamiliar workpiece. At the previous meetings mention has been made of attempts to correlate the required machine settings with the thermal conductivity, or the thermal diffusivity or the product of the melting temperature and thermal diffusivity.

Here an attempt is made to find a better correlation using dimensional analysis of the most important variables pertaining to the electron beam process. The problem is handled as essentially a thermal one. The mechanism of cavity formation during high energy electron beam welding is not analyzed. It is assumed that the cavity is formed when a certain power density is reached. Thereafter as long as sufficient power is available to melt the material the beam will penetrate deeper. The radiation heat losses from the top (and at times the bottom) of the workpiece are neglected.

2. Dimensional Analysis

The most important variables governing the electron beam process disregarding the reasons for the deep penetration commonly obtained must be similar to those associated with general cases of moving sources of heat. They may be listed as follows:

a. Independent Variables:

- P - power input, in.lb./sec.
- d - beam spot diameter, in.
- k - thermal conductivity, in.lb./sec.°F
- ρc - volumetric specific heat, lb/in^2 °F
- V - welding speed, in/sec
- T_m - melting temperature, °F

b. Dependent Variables

b - depth of penetration, in.
t - average width of melted zone, in.

To be more precise, $T_m \rho c$ should represent the total energy required to melt a unit volume of the metal. Therefore T_m can be modified as follows:

$$T_m = (T_{melt} - T_{room}) + \frac{\text{Heat of fusion}}{\text{specific heat}}$$

According to the rules of dimensional analysis the selected dimensionless groups were Vt/κ, Vb/κ, Vd/κ and $T_m k^2/PV\rho c$ where $\kappa = k/\rho c$ = thermal diffusivity, in^2/sec.

Since t and b are the dependent variables we can write

$$\left(\frac{Vt}{\kappa} \text{ or } \frac{Vb}{\kappa}\right) = f\left(\frac{Vd}{\kappa}, \frac{T_m k^2}{PV\rho c}\right)$$

If the available experimental data are plotted in the form of such dimensionless groups the function f can be found. The problem can be further simplified by noting that the depth of penetration is usually proportional to power [1]. Since P and b occur only in the two terms of the above equation the relationship between those groups must be linear and then

$$\frac{Vb}{\kappa} = \frac{PV\rho c}{T_m k^2} f'\left(\frac{Vd}{\kappa}\right)$$

After cancelling and rearranging we obtain

$$\frac{bT_m k}{P} = f\left(\frac{Vd}{\kappa}\right)$$

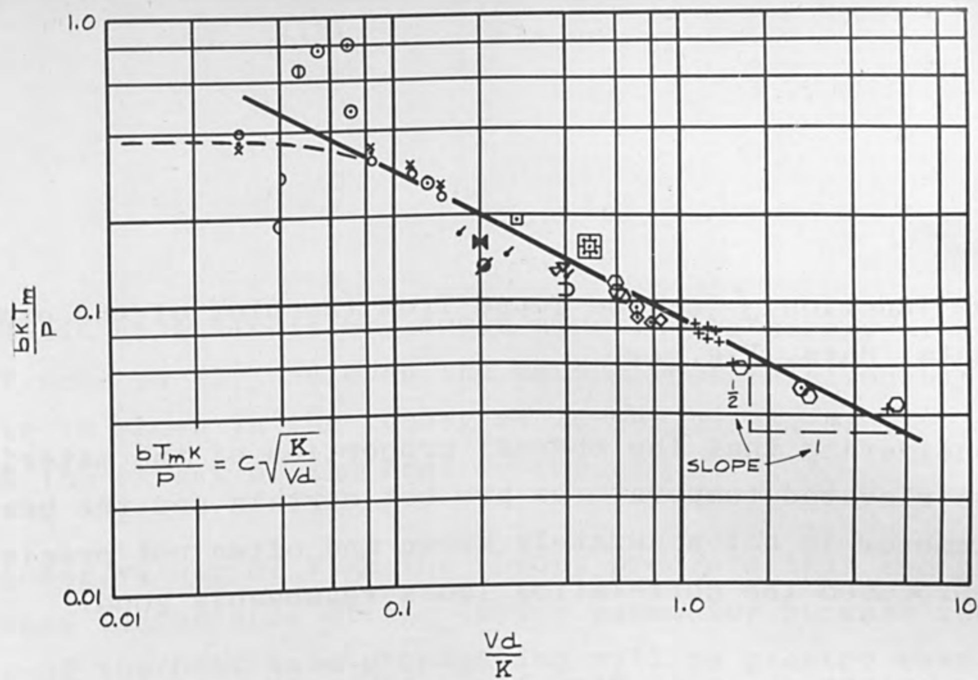

Fig. 1. Dimensionless Plot of Electron Beam Welding Data.

Symbol	Material	Power Watt	Speed in/min	Reference
ↄ	St. Steel	2300	6.3	3
⊕	Aluminum 2024	1450	10	4
⊡	St. Steel	1450	15	4
⊙	Beryllium	260	15	5
	Beryllium	275	15	5
	Beryllium	450	15	5
	Beryllium	840	80	5
•	4340	1950	27	1
○	4340	1250	27	1
x	4340	700	27	1
ϕ	Titanium	825	27	1
△	Titanium	780	27	1
⊡	St. Steel, 18-8	1350	27	1
	St. Steel, 18-8	1450	27	1
D	Aluminum	825	27	1
ɑ	Aluminum	780	27	1
O	St. Steel, 18-8	4750	50	NRC
⊙	St. Steel, 18-8	4750	25	NRC
+	St. Steel, 18-8	4750	15	NRC
◇	St. Steel, 18-8	4500	8	NRC
ϕ	Aluminum	3350	24	NRC
⋈	Aluminum	2100	24	NRC
✓	Zirconium	400	12	NRC
	Zirconium	3300	12	NRC
	Zirconium	4500	12	NRC
◬	St. Steel	5000	15.5	NRC
◈	Titanium	2000	17	NRC
	Titanium	2300	17	NRC

Table 1. Explanation of Symbols Used in Fig. 1.

The function f can be found from the plot of the experimental data, Fig. 1.

Considering that the thermal properties of the material at the elevated temperatures are not certain and the beam diameter is not accurately known and often not precisely reproduced the correlation looks reasonably good.

The points shown in Fig. 1 are taken from the previous Electron Beam Symposium proceedings and from the NRC laboratory records and the symbols used in Fig. 1 are explained in Table 1.

It seems clear that the experimental points fall near a line having a slope of minus 1/2 and hence

$$\frac{bTk}{P} = C\sqrt{\frac{\kappa}{Vd}}$$

where C is a constant (approx. 0.09 from Fig. 1)

Solving the last equation for P we obtain

$$P = \text{const.}\ bT_m \sqrt{k \rho c V d}$$

If we use the same thickness and the same machine settings, then, as far as thermal properties of the workpiece are concerned,

$$P \sim T_m \sqrt{k \rho c}$$

The value of the above discussion is not in the analysis itself but in the fact that the electron beam welding data appears to follow it. Actually the parameters used as a result of the

dimensional analysis are found also in the theory of moving heat sources (2) and even the square root relationship derived above is shown in the theory at larger values of Vl/κ, where l is the extent of the heat source.

At lower values of Vl/κ the theory predicts that the process becomes independent of the latter parameter because the velocity of the heat wave propagation will be greater than the moving velocity V. This is indicated in Fig. 1 by the dashed line.

If this is so, in this region the power needed to weld a certain piece should be proportional to bkT_m.

The experimental points in Fig. 1 above bkT_m/P values of 0.15 are obtained with the high voltage equipment, all the points below that line were obtained with various NRC welders, below 30 KV. The spot diameter, d, in the case of the high voltage equipment was taken to be 0.007 in. unless otherwise stated. In the case of the lower voltage welder the values of d range from 0.020 to 0.060 in.

The only points which deviate greatly from the straight line in Fig. 1 are those for aluminum and beryllium. In the case of aluminum most points are below the line. This may be explained by a higher temperature than the melting point obtained during welding, because of comparatively low melting point. In the case of beryllium the penetration deeper than predicted by the correlation could be associated with the unusually low density. However this aspect is probably associated with the mechanism of cavity formation which was not considered here.

A more refined analysis should take into account the density, the vapor pressure, the surface tension and perhaps some other variables.

Acknowledgment

The help of Prof. N. H. Cook (Massachusetts Institute of Technology) in reviewing the dimensional analysis is gratefully acknowledged.

References

1) Meier, J. W.
Proceedings, 3rd Symposium on Electron Beam Technology, 1961.

2) Jaeger, J. C.
Proceedings, Royal Society NSW Vol. 76, 1942.

3) Bas, E. B., Cremosnik, G., Lerch, H.
Transactions, 8th National Vacuum Symposium 1961, Pergamon Press.

4) Hoffman, H. H.
Proceedings, 3rd Symposium on Electron Beam Technology, 1961.

5) Hokanson, H. A., Rogers, S. L., & Kern, W. I.
Proceedings, 4th Symposium on Electron Beam Technology, 1962.

A MAGNETICALLY FOCUSED CRT GUN FOR ADVANCED DEVICE FABRICATION

By

Roger E. Peo
Associate Physicist
International Business Machines Corporation
Owego, New York

ABSTRACT

A low power, magnetically focused CRT electron gun system has been designed and built for advanced device fabrication. This was accomplished by modification of a standard CRT gun so that a minimum beam size of 0.010" diameter was attained with 5 milliamperes of beam current and accelerating voltages to 30 KV. The modifications, the system design, and the operating parameters are discussed in detail. Some of the reasons for this system design are presented.

A MAGNETICALLY FOCUSED CRT GUN FOR ADVANCED DEVICE FABRICATION

INTRODUCTION

As more and more advanced devices are developed, a need arises for new fabrication techniques. A recently developed technique is electron beam fabrication. To exploit this technique and apply it to advanced device fabrication, a system for investigation of electron beam techniques was developed. Such a system is described in this paper.

Electron beam applications may be divided into two broad categories: low power with small spot size, and high power with a corresponding increase in spot size. High power guns (greater than 300 watts total power) are commercially available from several manufacturers. However, because the requirements were initially in the direction of high resolution with low total power, the first effort was directed toward achieving a small beam spot size.

The only commercially available electron beam system capable of generating the required spot size (approx. 0. 005" dia.) operates at an accelerating voltage considerably above that specified by our over-all system requirements and applications. The lower voltage electron beam systems were not capable of attaining the desired beam diameter, at least not without extensive modification. Another choice was to investigate the type of gun found in cathode ray tubes and to modify the most suitable type to attain the appropriate parameters.

This appeared to be a desirable choice since there is an intermediate area wherein no low voltage, small beam diameter is available. The use of a cylindrical electrode type gun with magnetic focusing and deflection will provide a long focal length, small half angle beam at low accelerating voltages.

Penetration of electrons in various materials is given by the equation:[1]

$$X_m = A\phi_o^2/a\rho Z$$

where

- A = atomic weight of the material
- ϕ_o = accelerating voltage
- a = constant (use 6×10^{11})
- ρ = material density
- Z = atomic number of the material

Because most of our applications require working with very thin layers, examination of the above equation shows that it is desirable to keep the accelerating voltage as low as possible.

Using a cathode ray tube type gun is also an inexpensive solution to gun design, filament installation, and electrode spacing. Thus when the cathode emission falls below a usable value, the entire assembly can be discarded and a new one installed, and all the parameters in such a change will maintain the same values.

---

[1] "Electron Optics and the Electron Microscope", Zworkyn, Morton, Ramberg, Hillier and Vance, J. Wiley and Sons, N.Y., 1945.

A system designed around this type of electron gun is shown in figure 1. This system provides an electron beam with characteristics that are desirable for advanced device fabrication and cannot be found in commercially available electron beam equipment.

SYSTEM DESCRIPTION

Vacuum System

The vacuum system used for the evacuation of the work chamber consists of a liquid nitrogen trip, combination baffle and high vacuum valve, diffusion pump, and two mechanical pumps as shown in figure 2. The high vacuum valve, diffusion pump, roughing valve, mechanical pumps, vacuum lines, and other valves are commercially available. The liquid nitrogen trap was designed and built at IBM.

The foreline and roughing line pressures are measured by Pirani gauges. The high vacuum in the liquid nitrogen trap is measured by a cold cathode ionization gauge,and the vacuum in the chamber is measured by a Bayard-Alpert type ionization gauge. The cold trap pressure is monitored and recorded continuously by a 0 to 10 millivolt recorder to maintain a continuous record of system performance.

During the design and construction of the 19" wide by 19-7/8" high by 15-1/2" deep non-magnetic stainless steel chamber with a 12" diameter Lead glass viewing port, a 6" internal diameter, 4-arm Pyrex glass tee was used as a work chamber. With the gun operating and with liquid

Nitrogen in the trap, a chamber pressure of 1 to 5 x 10^{-6} torr is attained while the trap pressure is 5 x 10^{-7} to 1 x 10^{-6} torr. The glass tee can be evacuated to these pressures in about 30 minutes. An additional 10 minutes is required to bring the stainless steel chamber to the same pressure.

Electron Gun System

An electron gun capable of generating beam diameters of 0.010" to 0.020" with a beam current of about 2 milliamperes at 10 to 30 KV and a focal length of about 12 to 20" was obtained from a commercial supplier. This was a two anode, magnetically focused gun with a special high-emissivity cathode. The second anode had an aperture of 0.125" in diameter and a transmission in the neighborhood of 50% as originally supplied. By enlargement of the second anode aperture from 0.125 to 0.250" in diameter, the gun transmission was increased to about 90%. Complete removal of the aperture and spring finger assembly resulted in greater than 99% transmission. Neither of these modifications appeared detrimental to the system beam performance. Activation of the cathode as if it were to be operated at a filament voltage of 6.3 volts and then actually operating with 8 to 10 volts provides beam current of 2 ma as supplied by the manufacturer. Following the same procedure, but completely removing the second anode aperture results in a beam current of greater than 5 ma.

The gun in the upper portion of figure 3 shows the first modification. The gun in the lower portion of the figure shows the second modification

Figure 1. Electron Beam System for Advanced Device Fabrication

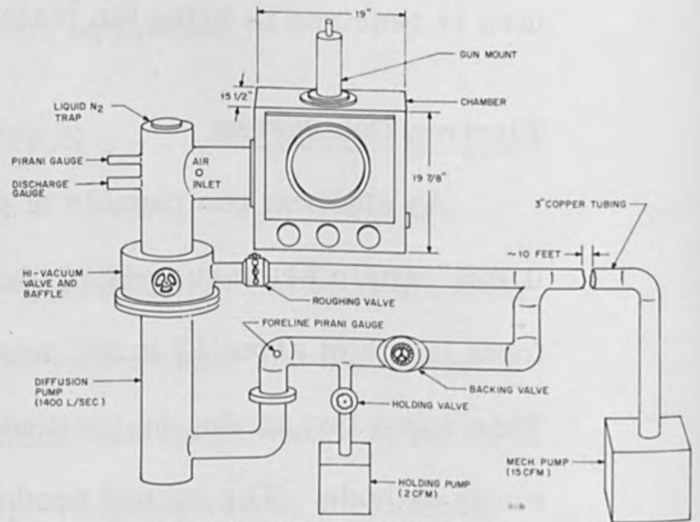

Figure 2. Electron Beam Vacuum System Layout

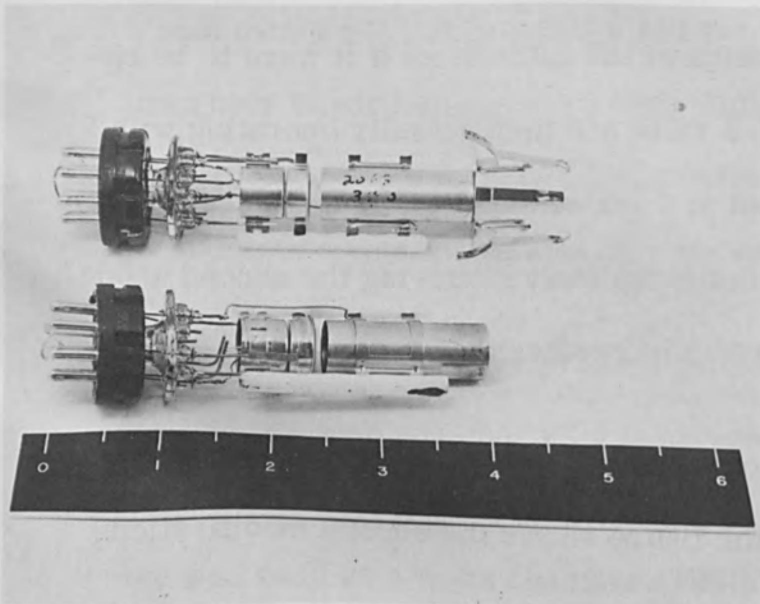

Figure 3. Modified Guns

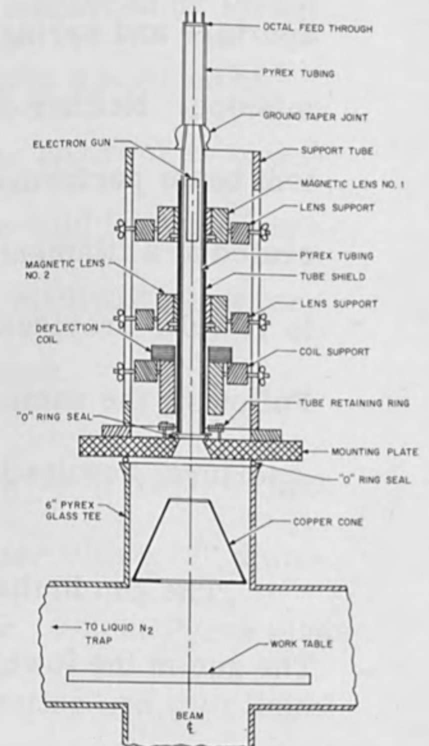

Figure 4. Electron Gun System

with the entire front assembly removed, leaving the second anode as a cylindrical lens.

Several standard types of electron guns, both magnetic and electrostatic focus types, were also tested. As this testing proceeded, the guns were also empirically modified. Because it appeared that an oxide coated, indirectly heated cathode would have a very short mean life under repeated cycling to atmosphere and exposure to contaminants in the system, this cathode was replaced by several types of Tungsten filaments. Due to the small and inconvenient volume in which the Tungsten filament had to be located, no satisfactory mounting method was devised. Rapid warping of the filament resulted, and this led to unsatisfactory gun operation. Testing was then resumed, using the oxide coated cathode. Using standard oxide coated cathodes, a mean useful life of about 7 to 8 hours was attained. With the specially supplied high emissivity gun, however, a cathode life of greater than 40 hours has been attained under the operating conditions previously described.

The electron gun mount assembly shown in figure 4 provides independent motion of two magnetic lenses and a deflection yoke, all mounted coaxially with the electron gun. The mount also allows the entire gun system to be attached to the work chamber. This mount was originally constructed entirely of non-magnetic metal materials. After initial testing, it was found that better over-all field conditions could be

attained by the use of plastic materials for the gun mounting plate, tube retaining ring, and the various coil mounts. Nylon screws were used for assembly in critical areas.

Installation of the gun in the gun mount is accomplished by heating the wax sealed ground glass taper joint and separating the two sections. The stub end having the female joint has a ceramic octal socket connected to an octal feed through. The electron gun, previously mounted on an octal plug, is simply inserted in the octal socket. The gun assembly is then inserted in the tube and the wax in the ground glass joint is reheated to make the vacuum seal. For the special cathode, activation requires 27.5 minutes. Realignment of the magnetic lenses to obtain proper concentricity with the new gun can be done in a few minutes using a motor driven reversing switch. The entire operation including evacuation of the system can be accomplished in approximately one hour.

Since the gun is operated in the post-accelerated mode, the target area is at the accelerating potential and, of necessity, the blank off-ports at the ends of the arms of the glass tee must be at ground potential. Using the gun in this manner elicited poor operation, probably due to the field gradients set up between the target and the various ground planes nearby. These field gradients produced non-uniform field conditions at the target surface and thus severely distorted the beam. To minimize this situation, a conic section was empirically constructed to provide a more uniform

field in the target volume. By operating this conic section at the accelerating voltage, the beam shape and control was significantly improved. This conic section was needed only for the glass tee work chamber, as no beam distortion was evident when the stainless steel chamber was used. This is probably due to greater uniformity of the ground planes.

Gun Control System

The electron gun control system was designed to be as flexible and versatile as possible. Since several types of guns were to be tested, the control system had to be capable of operating both magnetic and electrostatic focus type guns. The system devised is depicted in block diagram form in figure 5.

The filament control section operates, meters, and activates standard oxide coated cathodes as well as tungsten wire filaments. The electron gun control sections provide fusing, control, and metering for the various grids of the electron gun. In addition, two multi-range microammeters are provided for measurement of any grid current desired. The magnetic lens control panel operates two lenses, each capable of focusing a 25 KV beam at $2\frac{1}{2}$" with a coil current of 33 milliamperes.

The deflection amplifiers shown schematically in figure 6 were built at IBM. One of these amplifiers is used for horizontal deflection and one for vertical deflection. Briefly, this amplifier has an over-all frequency

response from DC to 20 KC with an over-all power gain of 30 db, and an input impedance of 11,000 ohms. There is a provision for DC positioning and AC signal level control in each amplifier. The power supplies to operate the amplifiers were also designed at IBM and built on the same chassis as the amplifier, but any DC supplies with good regulation that provide ±22 volts at 0.6 amps may be used. The deflection coils have a DC resistance of 160 ohms with an inductance of 25 mh per section. The waveform generators can be any type that will work into the deflection amplifier input impedance. A dual trace oscilloscope was used to monitor the deflection waveforms.

Two different high voltage supplies were used to provide the accelerating voltage. The first supply delivers 0 to 60 KV at 0 to 1 + milliampere, with a 1% ripple. An external milliammeter with a 0 to 1 milliampere movement and 1X - 2X multiplier was used to monitor beam current. The other supply delivers 0 to 30 KV at 0 to 20 milliamperes with less than 0.1% ripple. This supply has a built in multi-range milliammeter so the external meter is not used. The line voltage for either of these supplies is interlocked with a vacuum switch to prevent accidental turn-on when the chamber is open.

Operating Parameters

Accelerating Voltage . . . . 0 to 30 KV DC

Beam Current . . . . 0 to 5 ma

Filament Voltage . . . . 6 to 10 VAC

Filament Current . . . . 0.7 to .84 Amps

Cathode Voltage . . . . Grounded

Control Grid . . . . -30 to -140 VDC

First Anode . . . . 150 to 400 VDC

Tube Shield . . . . +200 VDC

Second Magnetic Lens . . . . approx. 12 ma

Conic Section (when used) . . . . same as accelerating voltage

	First Combination	Second Combination
Second Anode	25 to 150 VDC	250 to 560 VDC
First Magnetic Lens	0 to 12 ma	12 to 35 ma

The general set-up procedure for the last two parameters was to choose a second anode voltage by observation of spot size and beam current, and then to adjust the first magnetic lens current for final beam control. Specific values must be determined for all parameters, depending on the desired beam configuration. The minimum spot size observed was about 0.010" in diameter. This size was ascertained by comparison of the beam with objects of known size using a 20X stereo microscope. An "effective" beam size of 0.010" diameter has been noted by measurement of the beam path in various materials. As of this writing no precise measurements have been made to determine the energy density distribution in the beam.

Operation

While using the first high voltage supply, a "halo" was always present around the main spot. It was estimated that this "halo" could easily contain more than 10% of the indicated beam current. Substitution of the second high voltage supply virtually eliminated the "halo". In addition, over-all beam control was improved, the beam was less erratic, and variation of the parametric controls evoked a more uniform beam variation. These improvements are credited to the lower ripple, better regulation, and higher power handling capability of the second supply.

The deflection system is capable of moving the beam linearly anywhere within a solid angle of 22°, which allows a total working area of 4" x 4" at a distance of 10" from the end of the gun mount. The major limitation to a larger working area is the gun mounting tube construction, the base of which intercepts the beam, preventing further deflection. The work-to-gun distance can be varied from 14" to 8" to accommodate various mounting fixtures.

Since the maximum accelerating voltage used is 30 KV and the maximum current available is 5×10^{-3} amperes, the total power delivered to the target is 150 watts. The assumption of an average spot diameter of 0.015" at this power input results in a beam power density of 8.5×10^{5} watts per square inch or 1.24×10^{5} watts per square centimeter. Variation of any of these parameters alters the beam power density and, for

the bulk of the work done, the power input was considerably lower than this maximum figure.

Some beam instability has been noted during operation, especially momentary jitters at high power inputs due to the work outgassing. There was also some jitter at very low power inputs which was attributed to charge build-up on various insulating surfaces of the work. This latter instability was virtually eliminated by careful work fixturing.

SYSTEM APPLICATIONS

Solder Reflow

One area of investigation centered around attaching circuit modules to printed circuit boards. This is accomplished by simultaneously heating pre-tinned wrap around lands on the module and pre-tinned land areas on the board so that the available solder flows between the land areas and creates a mechanical and electrical bond. This type of joint is referred to as a solder reflowed fillet or simply solder fillet. Since the electron beam operates in a vacuum and has a localized heating effect, the beam creates fluxless solder fillets without excessive heat transfer to the components mounted on the module. The fixture used for electron beam investigation of this application is shown in figure 7. The strip below the blocks is a phosphor screen used for initial beam positioning. The board and blocks shown are dummys for test purposes.

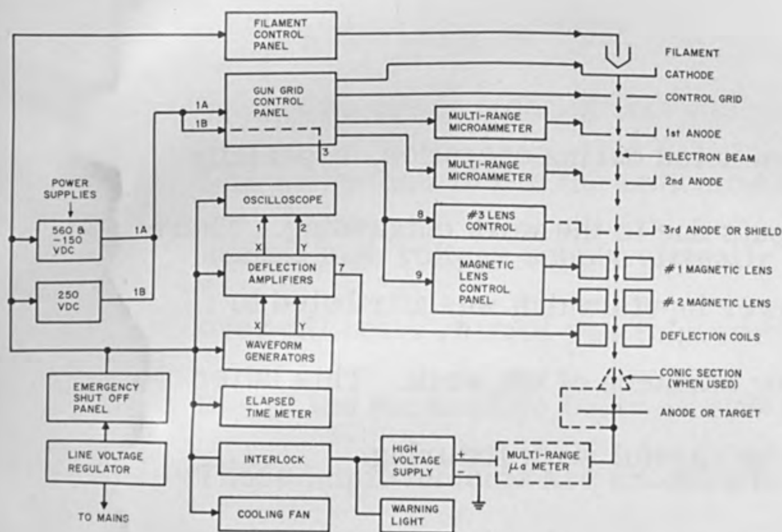

Figure 5. Electron Beam System Block Diagram

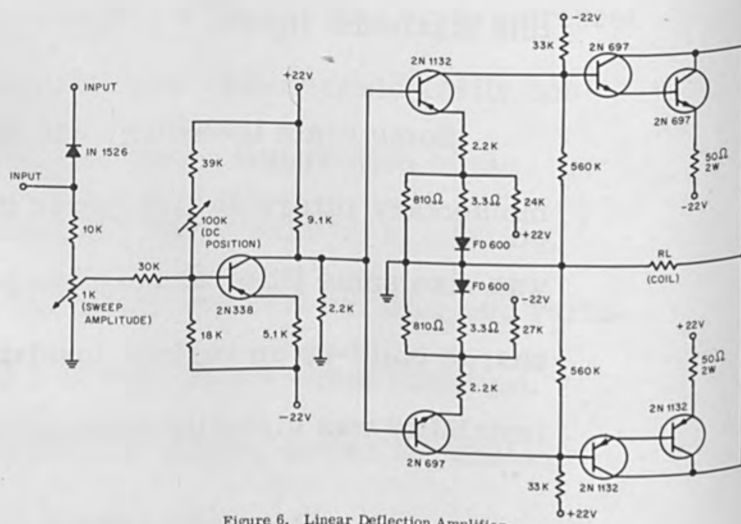

Figure 6. Linear Deflection Amplifier

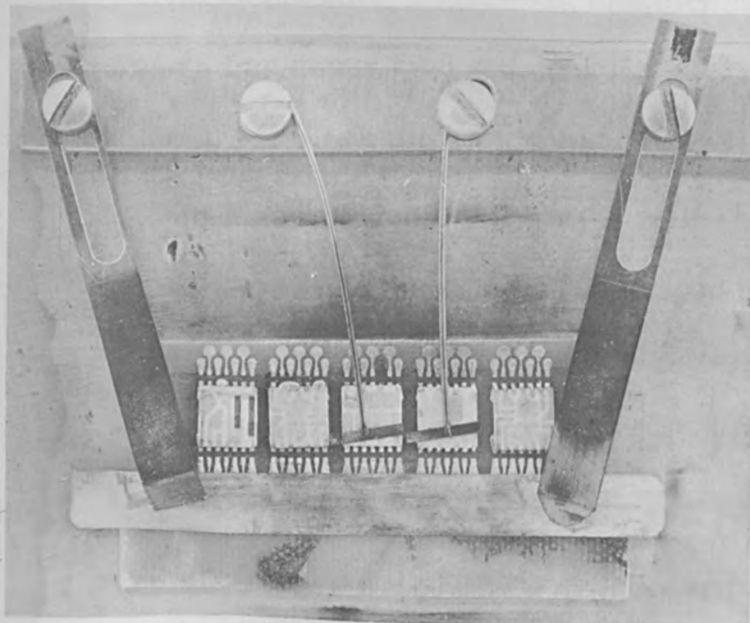

Figure 7. Mounting Fixture

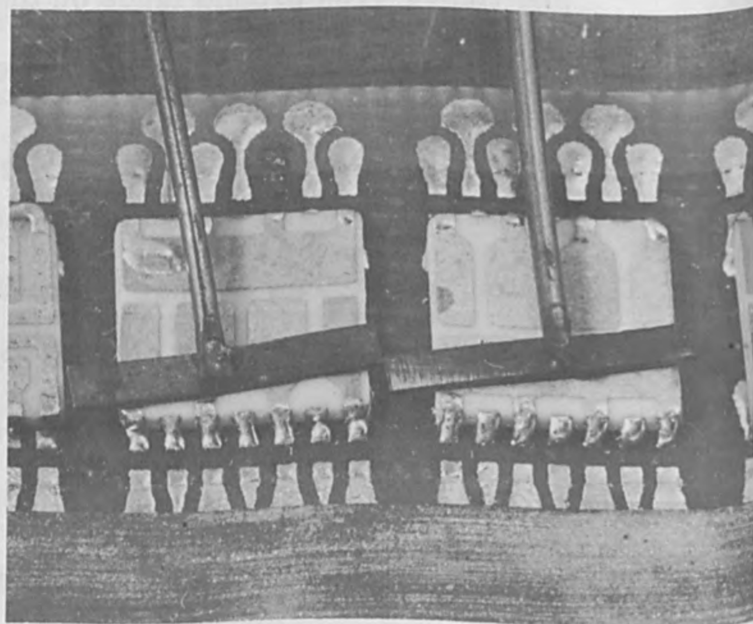

Figure 8. Electron Beam Solder Reflow Fillets

The advantages of electron beam solder fillets can be summarized as follows:

1. No flux is necessary, which eliminates the potential problem of entrapped residual matter in the joint and a resulting high resistance interface.
2. Ease of programming beam location to close tolerances, thus heating only the fillet area(s).
3. Low power input and high speed heating, which prevents excessive module heating and consequent damage due to heating sensitive components. This also prevents excessive digestion of noble metal conductor material by the solder compositions, especially when thin films and tin-bearing solders are required for device applications.

The solders used were a 903 eutectic solder which is a tin-lead alloy, bearing 2% silver with a melting point of 354°F, and a standard 60-40 tin-lead solder with a melting point of 361°F. A problem was experienced with the poor wetting of the 903 solder, but no problem was encountered with the wetting of 60-40 solder. The lands on the printed circuit board were copper tinned with the appropriate solder. The lands on the dummy block were platinum gold tinned with solder. The experimental printed circuit board was a glass filled epoxy board with land areas on both sides but no laminations. This board withstands temperatures to 356°F. The final printed circuit board is a B-stage epoxy laminate and

withstands temperatures to 212°F. These figures are for atmospheric pressure and normal heating techniques. Some change is to be expected for vacuum environment and electron beam heating.

Initial efforts to obtain solder reflowed fillets between dummy blocks and printed circuit board lands by making one fillet at a time met with failure. This was attributed to the other six fillets holding up the block and preventing the desired wetting and subsequent flow of the solder to create the fillet. The next step was to feed a 100 cycle per second sawtooth wave into the horizontal (x-axis) deflection amplifier and adjust the amplitude to obtain a line sweep the width of the block. This sweep heats all seven fillet areas simultaneously, eliminating six cold fillets and the resultant block support from these fillets. Proper adjustment of the beam size and power input did result in fillet formation. The major difficulty occurred when the beam energy was sufficiently high to melt the solder adequately, then the board areas between the lands became damaged. Examination of the various temperatures involved with the materials used indicated that the high intensity beam must not impinge on the board. Suitable sweep and grid control circuitry was designed so that the beam was "on" only directly over the fillet. This technique resulted in good solder fillets with no damage to the printed circuit board as shown in figure 8.

The beam was first set up on a phosphor screen. Over-all sweep length was controlled by setting the sawtooth wave amplitude. After the

desired beam pattern was observed on the fluorescent target, the Y axis (vertical deflection) DC level was changed to move the pattern to the land area and create the solder fillets. This step was observed through a stereo microscope. When all fillets were made as indicated visually, the beam was moved back to the target, repositioned, and the next series of fillets were made in the same manner.

The balance of the gun control system parameters could be varied over broad ranges without detriment to the solder fillets. For best results, these parameters were adjusted to give a 0.010 to 0.020" diameter beam at the work. It was found that lower accelerating voltages gave the best operating range; thus an accelerating voltage of 14 KV was used. The beam current varied from 100-400 microamperes; the magnitude depended upon spot size in order to keep the current density nearly constant. For the majority of the tests 200 microamperes at 14 KV was used with an approximately 0.016" diameter spot which is equivalent to 2.8 watts total power input, or a power density of 43×10^3 watts per square inch.

It requires about 10 seconds to make 14 solder fillets with the electron beam, or about 1.4 watt-seconds per fillet. An infrared method, however, for creating these fillets requires 140 watts input for 10 seconds or 100 watt-seconds per fillet. The use of the electron beam reduces the power input to an individual block by a factor of as much as 70.

Thin Film Scribing

Thin films are used in many types of advanced devices. Many times, a certain film configuration is desired which is either impractical or impossible to achieve by masking techniques. Furthermore,it is often undesirable to use chemical etching techniques on the film because of side effects in this process. The electron beam by-passes many of these problems. An extremely high temperature can be generated in a very small area, vaporizing any known material. Suitable programming of beam location on a continuous film then selectively removes the film and generates any desired pattern. The system described in this paper has been used in a feasibility investigation of the fabrication of a thin film memory.

CONCLUSION

This electron beam system has been run for more than 120 hours as described above. During this period, work was performed for projects in advanced development with the results of these efforts indicating the feasibility of electron beam techniques. The equipment has proven to be stable during operation and is easy to operate,and satisfactory beam operation can be obtained over a broad range of parameter settings.

In addition to the specific applications mentioned above, the electron beam offers a host of other possibilities for advanced device work. Some

of these presently under study are semiconductor device fabrication, surface preparation, annealing of materials, evaporation of materials, and welding. Because all of these applications are carried out in high or ultra high vacuum, the purity and repeatability of the results are more nearly assured.

Use of this type of system has shown that low power electron beam fabrication techniques are feasible for advanced development applications. As future applications are investigated, the over-all value of such a system will be even more explicitly demonstrated.

ACKNOWLEDGMENTS

The author wishes to acknowledge the assistance of the following people: D. D. Metzger for many helpful discussions; P. L. Baron who did much of the laboratory work; and B. W. Merkle for design of the deflection amplifier.

A PIERCE ELECTRON GUN OF HIGH POWER

By:

Y.J. Langlet

Societe General d'Applications Electro-Thermiques
Boulogne sur Seine
France

CANON DE PIERCE DE GRANDE PUISSANCE

Pour construire un canon à électrons industriel à haute puissance, disons de l'ordre de 300 à 500 kW et plus, la principale difficulté à surmonter est l'élimination des calories apportées sur les électrodes, soit par les électrons perdus, soit par le rayonnement de la cathode portée à haute température.

Cette puissance calorifique est difficile à extraire car elle se dégage sur des surfaces très petites.

Par ailleurs, il faut les extraire à des températures aussi basses que possible pour éviter les déformations des électrodes du canon car la précision de leur forme est une condition importante du rendement du canon et de sa durée de vie.

Pour résoudre ces problèmes, nous avons dessiné un canon en appliquant trois principes :

- 1/ Dessiner des électrodes telles que les pertes électroniques soient les plus faibles possible et les dessiner de façon à ce que leur surface soit maximum pour éliminer la chaleur qu'elles reçoivent.
- 2/ Eloigner la source de chauffage de la cathode pour augmenter les surfaces de liaison qui permettent de refroidir cette partie du canon.
- 3/ Refroidir par convection forcée d'un liquide circulant à grande vitesse les pièces du canon, même lorsqu'elles sont portées à haute tension.

La figure 1 montre la vue générale des formes et la disposition des pièces du canon que nous avons été conduits à définir en fonction de ces impératifs.

1/ Dessin de la cathode et de l'anode

La cathode (1) est une pièce massive en tantale que l'on porte à une température de l'ordre de 2.500° K. Nous limitons son taux d'émission à environ 0, 3 A/cm2 qui lui confère une durée de vie très grande, près de 500 heures.

Cette condition fixe sa dimension.

Le calcul de ces électrodes devrait d'abord être très précis. Un rendement électronique de 98 % a pour conséquence que : 2 % des électrons émis perdent leur énergie sur l'anode, soit 300 kW x 0,02 = 6 kW.

D'autre part, l'anode reçoit un flux de chaleur par rayonnement de la cathode qui est de l'ordre de 4 à 5 kW lorsque le courant électronique émis est, par exemple, de 6 A.

Pour réduire les pertes électroniques sur l'anode, ces électrodes ont été calculées à la cuve rhéographique au Centre de Calcul Analogique du C.N.R.S.* dont l'équipement électronique permet d'atteindre une grande précision.

Parmi l'infinité des solutions admissibles, nous avons choisi une anode dont l'élément central, qui reçoit la plus grande densité d'énergie, a la forme d'un cylindre de grande surface en vue d'évacuer plus facilement la chaleur apportée.

Cette solution entraine d'ailleurs des difficultés de construction technologique que l'on pourra facilement observer sur la figure.

2/ <u>Source de chauffage de la cathode</u>

Pour éloigner la source de chauffage de la cathode, nous avons choisi de chauffer celle-ci par un véritable canon à électrons dont les formes ont été étudiées avec autant de précision que celles du canon principal.

C'est un canon de Pierce à cathode épaisse d'une dizaine de kiloWatts, chauffée indirectement par le bombardement d'électrons produit par un filament chauffé.

Ce canon spécial a été calculé au C.N.R.S. et sa mise au point a été faite sur maquette vraie grandeur pour obtenir une température uniforme de la cathode.

3/ <u>Refroidissement</u>

a/ <u>Refroidissement des supports de la cathode</u>

La figure 2 en donne le principe.

La pièce qui réunit le canon auxiliaire à la cathode principale est un cylindre dont les dimensions ont été calculées en fonction d'un refroidissement par liquide.

La paroi latérale du cylindre est une double chambre où l'on établit une circulation méthodique du fluide qui emmène les calories.

* Centre National de la Recherche Scientifique à CHATILLON S/S BAGNEUX (France)

En particulier, l'épaisseur du film fluide qui refroidit la paroi intérieure a été soigneusement calculée pour assurer une vitesse de convection telle que la température du support de cathode ne dépasse pas 300° C.

Cette partie du canon est portée à un potentiel négatif élevé, de l'ordre de 20.000 à 40.000 Volts, par rapport à l'anode qui est à la masse.

Comme il faut refroidir le fluide qui emmène les calories dans un échangeur qui est au potentiel de la masse, le liquide refroidisseur doit être un bon diélectrique.

Notons que par suite de la vitesse de convection élevée, le débit de ce fluide est grand et sa température ne s'élève que de quelques degrés dans le canon.

b/ <u>Refroidissement de l'anode</u>

Il est basé sur les mêmes principes.

La partie centrale de l'anode est une double chambre cylindrique où l'on établit une circulation méthodique du fluide refroidisseur.

On réduit l'épaisseur de la veine liquide aux endroits qui reçoivent une forte densité d'énergie pour qu'en ces points le coefficient de convection forcée soit grand afin de limiter la température de l'anode à 300 ou 400° C.

Le plateau de l'anode est refroidit lui aussi par une lame mince de liquide qui circule à grande vitesse.

4/ <u>Régulation de puissance du canon</u>

Pour terminer cet exposé, nous citerons un nouvel avantage de ce dispositif.

Pour commander la puissance du canon, on laisse constante la tension d'accélération entre cathode et anode.

On modifie seulement l'intensité électronique émise par la cathode en imposant la température de celle-ci par règlage de la puissance de bombardement qu'elle reçoit du canon auxiliaire, mais ce même canon auxiliaire, d'une puissance d'une dizaine de kiloWatts est lui-même commandé par la puissance de bombardement fournie à la cathode auxiliaire par le filament, ce qui s'obtient en règlant la tension d'accélération entre filament et cathode auxiliaire.

Le canon est donc commandé par une source d'énergie de faible valeur. Elle est très facile à règler à partir d'un régulateur sur lequel on affiche la puissance désirée.

Fig. 1

Fig. 2

ULTRA HIGH VACUUM ELECTRON BOMBARDMENT FURNACE

A. W. Sweet

Manufacturing Engineer-Processing Systems

General Electric Company
600 Main Street
Johnson City, New York

ULTRA HIGH VACUUM ELECTRON BOMBARDMENT FURNACE

A Manufacturing Engineering organization generally supports the engineering effort on new products in the areas of materials, processes, and equipment so that these new products can be manufactured on schedule with quality, economy, and reliability. In the advance engineering of inertial guidance devices it became increasingly apparent that higher temperatures and lower pressures were required in all material and process areas. For example, cryogenic and electrostatic gyros required material purification and outgassing, heat treating, and metal joining by such processes as electron beam welding, vacuum brazing and diffusion bonding. One application required that niobium be annealed in the cleanest possible environment and the metallurgists indicated that 2200 degrees Centigrade for four hours at 10^{-12} Torr would be most desirable.

Furnace Requirements

To achieve the rigorous requirements for extremely low pressures and high furnace temperatures the following basic equipment specifications were conceived:

1. Heating - electron bombardment
2. Pressure - 10^{-9} to 10^{-12} Torr

3. Temperature - 1,000 to 2,500 degrees Centigrade

4. Working space - cylindrical, 5 inch diameter by 7 inches

5. Pumping - Cascaded mercury diffusion pumps

Cryogenic wall

Ion pumping.

The resulting furnace installation is shown in figure 1, with the power supply in figure 2, and the furnace and bakeout oven in figure 3.

Design Concepts

Electron bombardment heating was envisioned as the basic concept because it has many advantages over resistance heating although the problem of control was anticipated. Large, water cooled, high current carrying conductors which would be required for resistance heating could be eliminated. This minimized the electrical feedthrough problem since high voltage, bakeable, ultra high vacuum feedthrough terminals could be easily provided for electron bombardment heating.

Filaments for electron bombardment heating were preferrred over resistance heating elements for several reasons. Filaments are of open construction and facilitate the pumping of desorbed gases to a far greater degree than

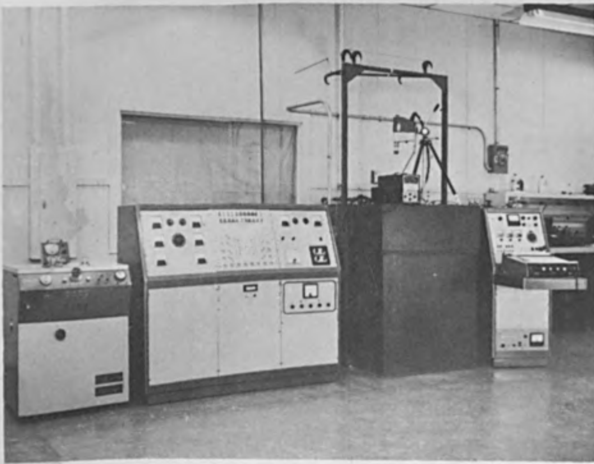

Figure 1. Furnace Installation

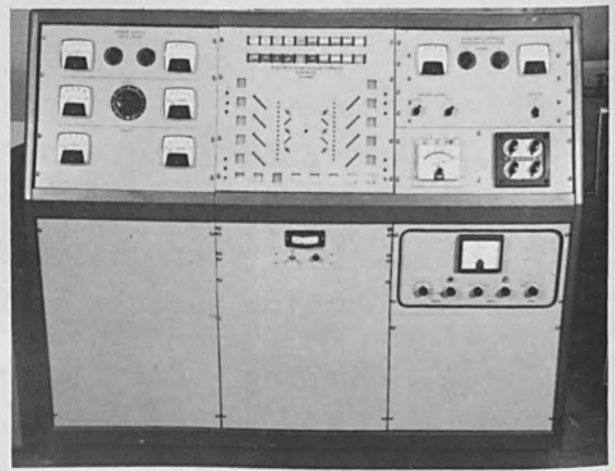

Figure 2. Power Supply and Control Console

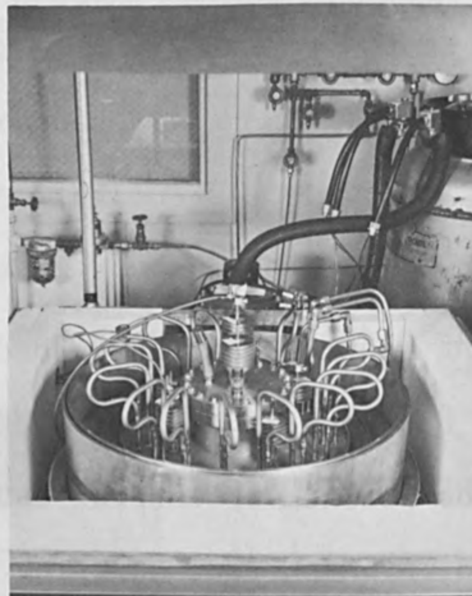

Figure 3. E/B Furnace in Bakeout Oven

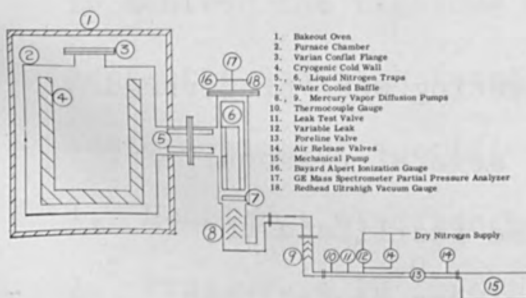

Figure 4. Vacuum System Schematic

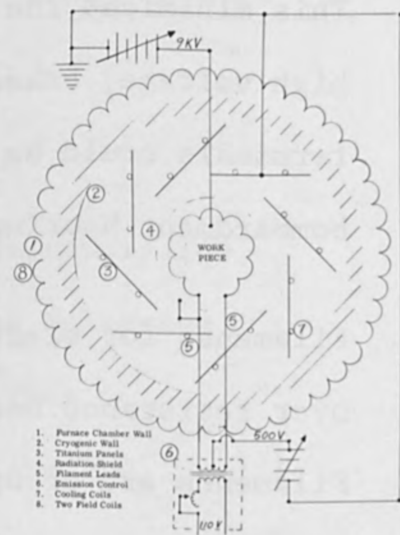

Figure 5. Schematic of Horizontal Section

could be attained if the work were surrounded by conventional high temperature resistance elements. The filament volume and surface area are diminutive in comparison and outgassing is minimized and accomplished faster. The filament is also more easily supported, more easily replaced and much less expensive. It can be operated at a lower temperature than a resistance element in achieving workpiece temperatures above 2,200 degrees Centigrade. Vaporization and resulting condensation on view ports, electrical feedthrough terminals and the work itself is minimized. Bakeout time can be decreased. Initial cost and maintenance costs are lower.

Most important, electron bombardment generates heat in the work where it is desired, and higher temperatures can be reached with far greater speed than can be attained with radiated heat from resistance heating elements. Radiation shielding can therefore be decreased. This lowers the surface area to be outgassed, increases pumping conductance and lowers material cost. Power and water consumption are also lower.

Initially, the major disadvantage of electron bombardment heating appeared to be control. The thermionic emission

(or amount of current produced) from the surface of the filament might not be easily controlled. This current, i.e., the number of electrons emitted per second, depends on the chemical and physical nature of the filament emitter, and on its absolute temperature. The basic problem was then to control the temperature of the filament since the other parameters (material, size, and configuration) could be fixed by selection.

The filament emission current at a selected filament temperature can be calculated from Richardson's equation.

$$I_s = AT^2 e^{\frac{-b_o}{KT}} \quad \text{or} \quad \log I = \log A + 2 \log T \quad \frac{-b_o}{2.303T}$$

where: I_s - emission current (amp/sq cm)

A - constant characteristic of the emitter

K - Boltzmann's constant

T - absolute temperature in degrees Kelvin

b_o - work function potential of the emitter

e - base 2.718+ of natural logarithms.

Full current will not flow from the filament unless demanded by the space potential surrounding the filament.

From a practical point of view, the filament (cathode or emitter) must be reasonably strong at the operating temperature and have a high vapor pressure. The material

should be workable with little tendency to sag and yet not be too brittle. The work function of emitter materials with these characteristics is usually high but this is not of great importance in this application. Filaments of tungsten, tantalum, and niobium were considered.

It is preferable in certain furnace processing operations to use a specific filament material. For example, in the stress relief or annealing of niobium for cryogenic applications a niobium filament promotes purity by minimizing contamination from condensed vapors. If a dissimilar material such as tungsten or tantalum were used, vaporized filament material could deposit on and contaminate the niobium workpiece.

To design the furnace filament one must first select the filament material, filament temperature, type of configuration and total emission desired; this total emission and the accelerating voltage determine furnace power. Filament area and power can then be determined. This filament power must be compatible with the filament power supply. Two simultaneous equations can then be solved for the filament length and radius.

$R = p \frac{l}{nr} (1+at)$ where: R = filament resistance

$A = 2\ nrl$ p = resistivity

l & r = filament length and radius

a = temp. coef. of resistivity

t = temperature - Centigrade

A = filament area.

Some trial and error is involved in the selection of filament heater current and voltage to arrive at a desired filament length, diameter and configuration. Experience then indicates desirable changes and these can be made quickly and easily.

Calculations and decisions resulted in the following:

1. Maximum filament emission current - 1.5 amp
2. Filament materials - niobium, tungsten, tantalum
3. Filament design - cage
4. Filament temperature - 2200 degrees Centigrade
5. Filament power - 250 watts maximum
6. Accelerating voltage - 9 KV
7. Furnace power - 13.5 KW
8. Filament operation - emission limited.

The major problem was to control filament temperature and thereby control emission which could vary with heat radiated from the work and the radiation shield.

This was particularly important in the high temperature range above 2200 degrees Centigrade. The filament had to be operated in the emission limited mode to prevent temperature fluctuations and any possible runaway condition. Our Research Laboratory supplied an emission regulator power supply to control the filament temperature and the resulting emission current.

Vacuum System

The vacuum pumping system, figure 4, consisted of cascaded mercury vapor diffusion pumps, water baffle traps and a cryogenic cold wall seventeen square feet in surface area. The system can be operated automatically or manually. The entire system is capable of bakeout at 450 degrees Centigrade. Pressure can be measured by ionization, magnetron ionization and mass spectrometer equipment. The fore line is operated in the viscous flow region (500 microns) to prevent backstraming of mechanical pump fluid.

Ion Pumping

Electron bombardment heating offered an opportunity to incorporate ion pumping. Bakeable electrical coils were located to create a magnetic field. This field increases

the electron paths and also increases the probability of collision with gas molecules to form gas ions. Water cooled titanium panels for sputtering were placed as shown schematically in figure 5 which also shows the various power supply inputs.

Operating Results

Limited operating experience has been gained since the furnace was completed. Temperatures have been measured by a two-color optical pyrometer in excess of 2500 degrees Centigrade. Pressures have been achieved at 10^{-8} - 10^{-9} Torr without bakeout. The field coils and ion pumping have not been fully tested and evaluated. Temperatures of 1800 degrees Centigrade have been achieved at 10^{-7} Torr.

Work In Progress

As soon as initial tests have been completed and additional filament designs have been evaluated, the one large viton O-ring seal will be removed from the large top flange shown in figures 6 and 7. This flange will then be welded to the chamber with access to the furnace through the top flange assembly shown in figure 8.

Conclusions

Ultra high vacuum electron bombardment furnaces are feasible. They can be scaled up. Heating is rapid, controllable and economical.

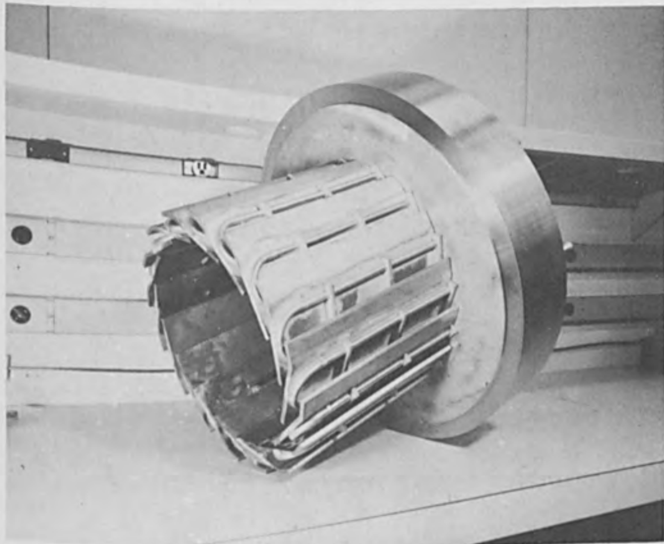

Figure 6. Top Flange and Water Cooled Titanium Panel Assembly

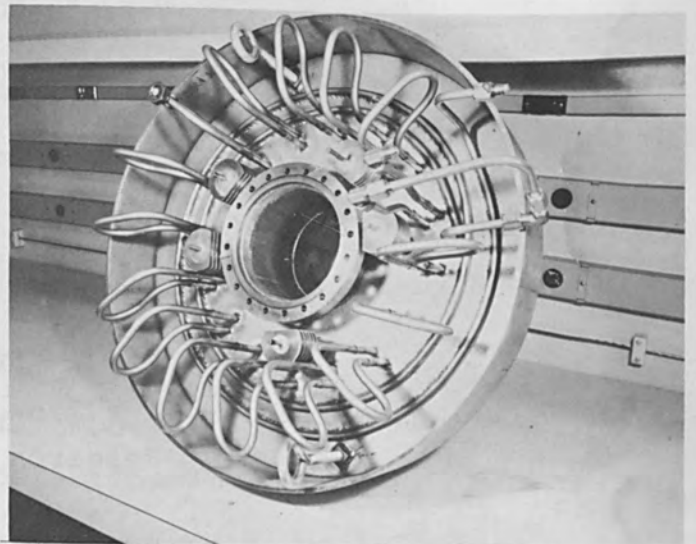

Figure 7. Top Flange and Entry Port

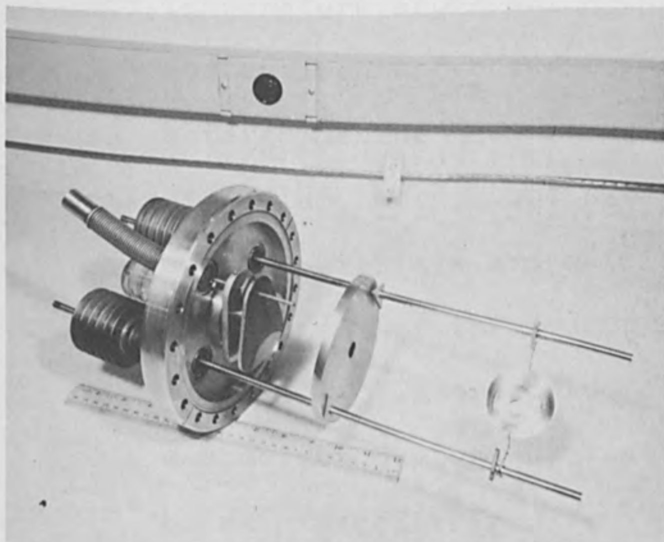

Figure 8. Entry Port Flange Assembly

Figure 9. Viewport and High Voltage Terminal

A BAKEABLE U.H.V. ELECTRON MICROSCOPE
FOR
METALLURGICAL USE

By:

J.W. Griffith
Research Director

J.C. Mutton
Electronic Supervisor

W.Mason
Physicist

ELECTRO-GLASS LABORATORIES, INC.
BEAVERTON, OREGON

A BAKEABLE U.H.V. ELECTRON MICROSCOPE FOR METALLURGICAL USE

The justification for wanting a bakeable electron microscope can be laid at the door of our modern technological age--the space and nuclear age. In both of these fields, the strength of materials at elevated temperature is a severe requirement, as is known by those in the electron beam field. To these parameters is added the unfortunate condition that most useful refractory materials are readily attacked by gases in high temperature environments.

The examination of reactive materials, especially at elevated temperatures, requires a vacuum far greater than those in available microscopes. As an example, at 10^{-6} Torr, a monolayer of gas is adsorbed on a surface in approximately one microsecond. Several layers are built upon a sample during the examination period. If the material is at a temperature above which the chemical action with materials in the environment occurs, the structure of the sample is altered making the micrograph meaningless. Such materials as cesium, potassium, phosphorus as well as other very reactive materials are difficult to examine in the vacuum environment of the ordinary electron microscope.

In order to reduce the probability for destroying a specimen during examination, an extremely clean system must be maintained (Fig. 1). Vacuum pumps with extremely low vapor

pressure possibilities must be used. Cryostatic roughing of the microscope as well as ion pumping techniques are necessary. Fortunately, the state of vacuum art has produced commercial equipment capable of producing pressures better than existing microscopes by a factor of about 10^5. Such pumps have very low outgassing characteristics, are reliable in operation and are provided with accessories, such as flanges etc., to facilitate their use.

A necessary procedure in obtaining ultrahigh vacuum is the removal of gas producing materials from the walls of the microscope column. Since this gaseous material is volatile at elevated temperatures, a "bake-out," in the standard ultrahigh vacuum parlance, reduces the wall contamination appreciably. The "bake-out" is particularly useful at pressures of the order of 10^{-9} to 10^{-10} Torr and makes an extremely clean specimen environment possible.

Fortunately for us, not many electron microscopes are bakeable to 400°C. There are several reasons involved. Presently available electron microscopes use magnetic lenses--usually of an electromagnetic nature (Fig. 2). The lenses are composed of precision machined pole pieces, of special magnetic material, surrounded by multiple turns of magnet wire carrying a precisely regulated current. 400°C is above the charring temperature of insulation on wire used in electromagnetic lenses. With present lens design, it is virtually impossible to remove the wire during a "bake-out" cycle. In

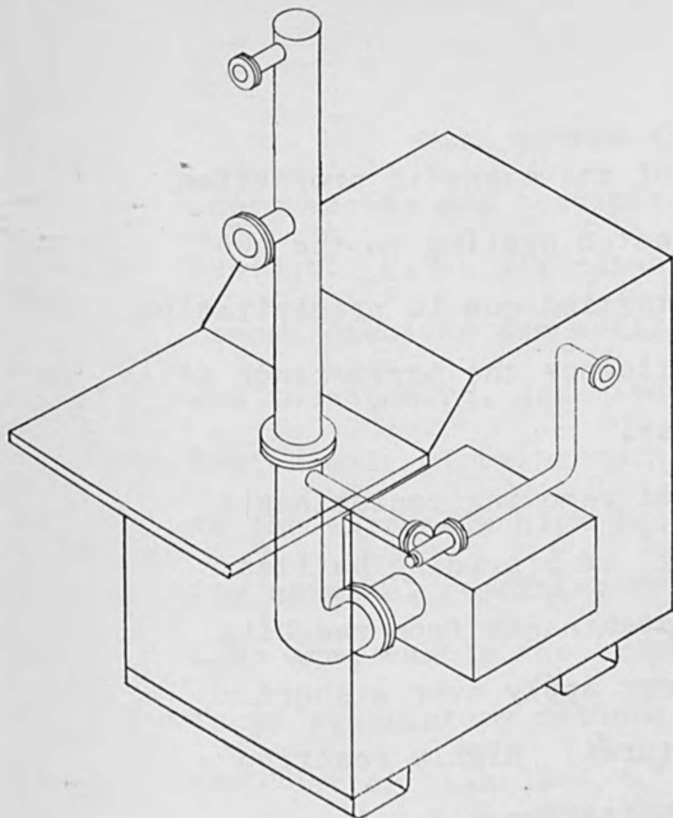

Figure I Vacuum Pumping System

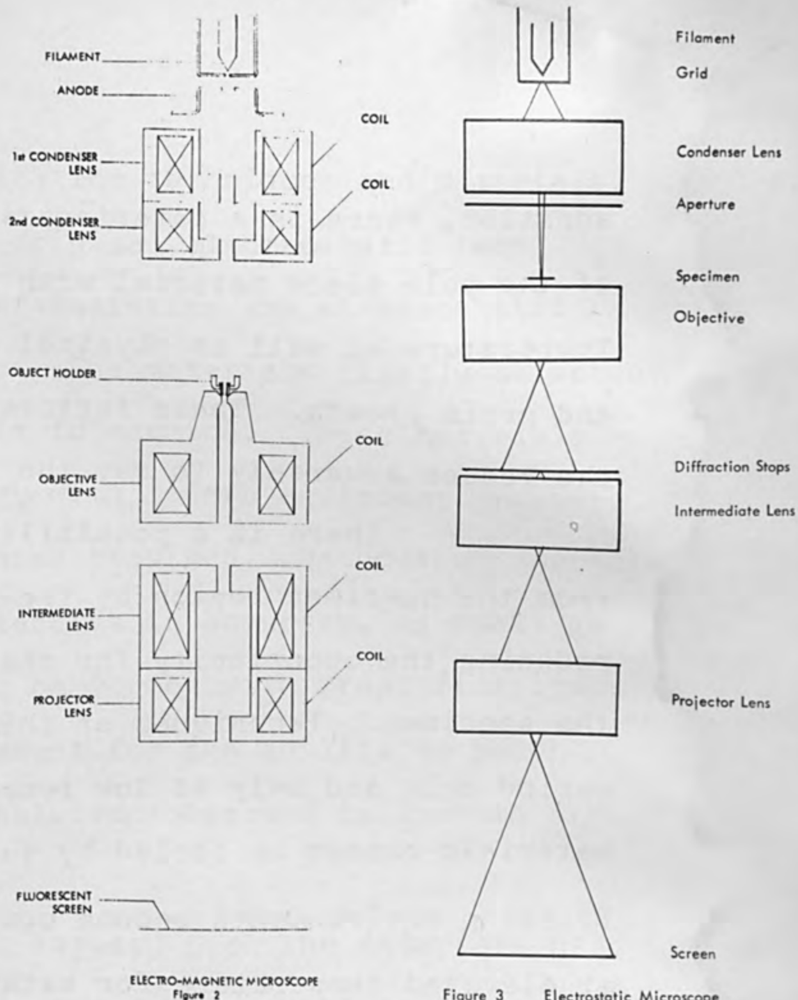

ELECTRO-MAGNETIC MICROSCOPE Figure 2

Figure 3 Electrostatic Microscope

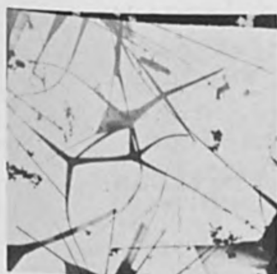

a. zinc smoke 30,000X

b. magnesium smoke 30,000X

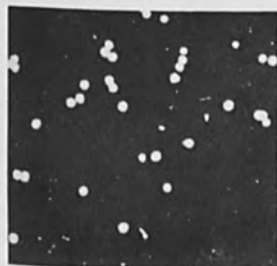

c. colloidal gold 160,000X

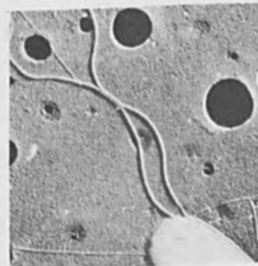

d. gold shadowed bacterium 50,000X

Figure 4 Electron Micrographs

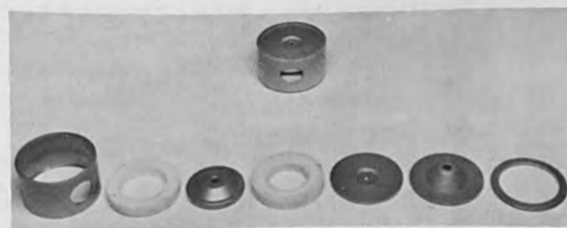

Assembly and Parts

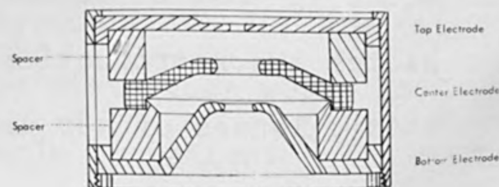

Electrostatic

FIGURE 5 Lens Cell

addition, there is a deterioration of the magnetic properties of the pole piece material with repeated cycling to the 400°C temperature as well as physical distortion due to precipitation and grain growth. These factors influence the performance of the lenses adversely to say the least.

There is a possibility of removing contaminants from the specimen region by freezing[1] or providing baffles reducing the opportunity for the contaminants from reaching the specimen. Techniques of this sort apply over a short period only and only at low temperatures. Highly reactive materials cannot be fooled by such subterfuges for long. Freezing environments become costly if specimens are maintained at elevated temperature for extended periods.

There is no real substitute for an ultrahigh vacuum system and clean environmental conditions. Since it is impractical to overcome the problems in baking a magnetic lens microscope, electrostatic optical systems are used. Previous objections to electrostatic systems[2] disappear with the work of Dr. Gertrude Rempfer. Electrostatic optical systems (Figure 3) designed by Dr. Rempfer have produced images equal to the best available at present. Theoretical and practical limit of resolution by the electrostatic optical systems is equal to that of magnetic optical systems. The following plates are reproductions of images taken with the electrostatic lenses of her design (Figs. 4a, 4b, 4c, 4d).

With modern fabrication techniques and materials, improvements are possible on original electrostatic lens systems. Materials capable of resisting the electrostatic forces involved are available. The materials finally selected are tough, hard, and miserable to machine. These materials are capable of being machined, with modern equipment however, to the extremely high tolerances required. Methods of correcting original remaining deficiencies in accuracy, as small as they are, enable the image to be formed with great fidelity. These proprietary methods account for the ability to reach the "better than 15 A.U." resolution observed in systems of Dr. Rempfer's design.

Another condition imposed upon the materials used in this bakeable microscope is that of extremely low dimensional hysterisis. All materials change physical size with changes in temperature (Fig. 5). These changes are not necessarily uniform nor symmetrical. Such non-uniform changes are due to rolling or forging directions, crystal orientation as well as physical shape of the part subjected to such treatment. Since it is somewhat impractical to operate the microscope at the 400°C temperature, any changes made in the physical dimensions during "bake-out" must be cancelled upon return to operating temperature. Any deviation between dimensions is considered dimensional hysterisis. The greater the nonsymmetrical hysterisis, the more distortion would be accrued in the microscope--an intolerable situation.

Many metallurgical considerations must also be evaluated, but these are beyond the scope of this paper. Let it be sufficient that the materials had to be compatible in a high temperature vacuum environment. The insulators must not only endure the voltage requirements but be of low vapor pressure material, be machinable to extremely close tolerances and be compatible with the metal parts. The metal parts must possess the electrical, as well as dimensional, characteristics but also refrain from adhering or galling. The metals must also be of a non-magnetic nature (Fig. 5b).

Very few materials were able to fulfill these requirements. One combination selected was Haynes 25 for the lens elements, a high alumina ceramic for insulators and an austenitic steel for lens support, with high carbon content, proved superior to most others. Repeated heat cycling indicated the desired dimensional stability was maintained.

Since most of the dimensional changes are microscopic in nature, normal measuring techniques were unsuited as quality controls on parts. The only method capable of answering the "will they, won't they work" question was actual use as a microscope. One of the most useful tests was that of making a series of exposures inside of, at and outside of focus. One view showing an outside of focus condition is shown (Fig. 6) for it is difficult to reproduce the inside of focus condition. This slide is an uncorrected objective lens cell at approximately 50,000 diameters magnification. The

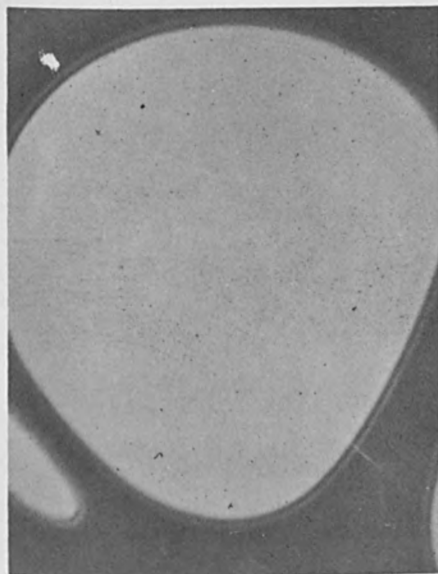

Figure 6 Outside of Focus

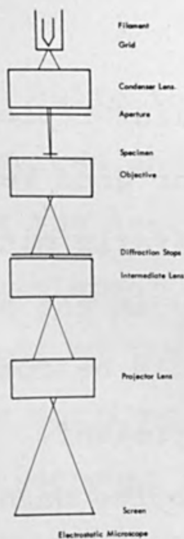

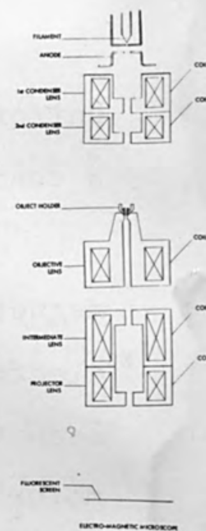

Figure 7 Comparison of Microscopes

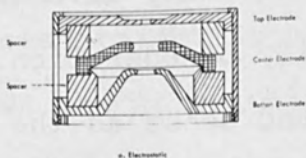

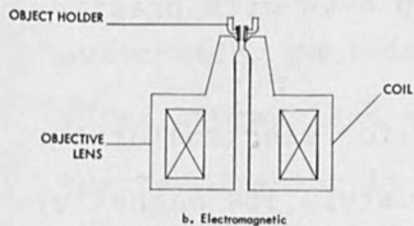

Figure 8 Comparison of Lens Cells

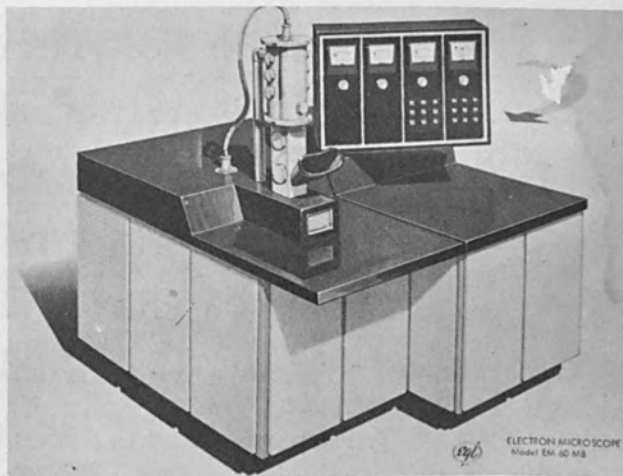

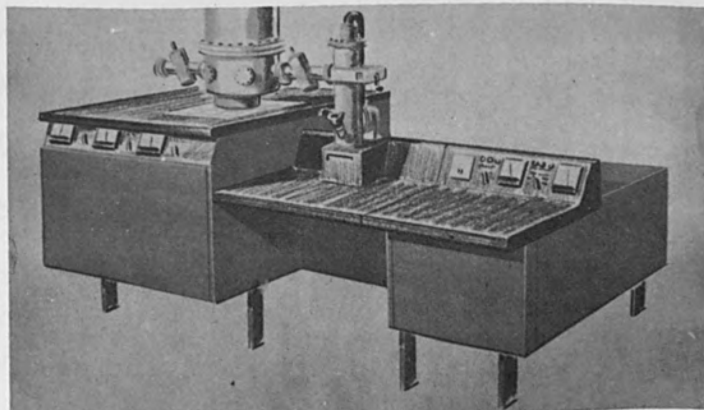

Figure 9 EGL Microscopes

uniform spacing of the line indicates fairly low astigmatism--a condition necessary for good resolution.

The electrostatic microscope differs from the magnetic microscope only in the medium used to refract the electrons. Fig. 7a should be compared with Fig. 7b. It is seen that no coils are present. Instead of following the motor rule applicable to the magnetic lenses, the electron trajectories are bent by shaped fields involving negatively charged electrodes. Since electrons carry a negative charge, they can be repelled by electrodes which also carry a negative charge. By making the electrode the proper shape and surrounded by other electrodes with correct geometry, electrons can be made to follow desired trajectories just as light rays are made to follow desired trajectories in glass lenses.

Electrostatic optical systems have many advantages over magnetic optics[3]. Aside from simplicity of operation, images are oriented in the same direction and sense as the object--no rotational trajectories. Power supply regulation requirements are greatly reduced since voltage fluctuations applied to all elements proportionally provide images of the same magnification--the image remains sharp even with drastic changes in potential applied.

Object area is also simplified for electrostatic optics (Fig. 8). In order to provide adequately low magnetic reluctance, the thickness of magnetic material, for shaping the delicate magnetic field for the objective lens, must be substantial. The object end of the electrostatic objective

lens can be a flat disc with quite thin dimensions. It is necessary to immerse the specimen and holder into the pole piece of a magnetic lens but the specimen and holder can remain above the entire lens element to be in the same relative position with respect to the refracting region. This makes it possible to provide specimen manipulation over wide ranges as well as providing improved region for heating and cooling equipment, stereo manipulators, an ability to rotate the sample from a transmission study position to a reflection study postion with plenty of space for beam deflection equipment.

High intensity of illumination is a highly touted feature of electron microscopes. For equal illumination, the angle of illumination is slightly larger for magnetic lenses if the aberration coefficient is smaller. This necessitates the use of a post objective aperture to keep down the spherical aberration. This means that a smaller percentage of the beam hitting the specimen is used than in the case where the initial illumination angle is small. The larger current hitting the sample causes additional heating resulting in possible movement of the image as well as evaporating material. This material collects upon the surfaces of the lens and accumulates charges further distorting the beam making it necessary to use stigmators and other beam distortion correcting devices. The field shaping electrodes,

in the electrostatic microscope, are shielded from such build up of charge collecting materials.

In order to provide a microscope (Fig. 9) capable of enabling a research worker to examine reactive materials, an electrostatic microscope with ultrahigh vacuum capabilities has been designed. Although it has extremely good resolving capabilities, its image quality is not affected by the necessary "bake-out" at high temperature to insure ultraclean specimen environment.

Appreciation is expressed for the work of Y.S. Lee, C. Haase and Charlot Benedict. The patient consideration and aid of E.G. Burroughs and W. Liebon of Ft. Belvoir is also appreciated. The help and guidance of Dr. Gertrude Rempfer was of inestimable value.

REFERENCES

1. Japanese Electron Microscope Co., Bulletin (1962)
2. Zworykin, Morton, etal, "Electron Optics and the Electron Microscope," John Wiley & Sons, N.Y., 1948, p. 98.
3. Rempfer, Gertrude, Private Communication

General

4. Electron Microscope, 5th International Congress (1962).
5. Thomas, Gareth, "Transmission Electron Microscopy of Metals," J.Wiley & Sons, N.Y., 1962.

THE USE OF LASER BEAM FOR WELDING

R.H. Fairbanks, Sr.

TRG, Inc., Syosset, N.Y.

THE USE OF LASER BEAM FOR WELDING*

Laser beam welding is a new fabrication technique that is currently under development. Most laser welders under construction are based upon using the coherent output energy of the pulsed ruby laser. Ruby has been chosen for the welding application because of its mechanical and thermal durability, availability, low cost, power output potential, and thermal characteristics. Other materials, such as neodymium doped calcium tungstate or fluoride, will eventually prove useful as their durability and quality improve. Continuous solid state or gaseous lasers are not now of interest in welding because they lack the average power required of the heat source.

This paper will be confined to (1) the application of a first-order theory of ruby output[1] developed by Dr. R.L. Martin formerly of our laboratory** to the design of a laser beam fusion system, (2) certain metallurgical characteristics of laser melts, and (3) advantages, applications, and limitations of the laser as a heat source.

Experimentally, the characterization of the quality of performance of the ruby crystal with respect to the output energy E_o, is given roughly by slope of the curve

---

* Supported under Contract AF33(657)-8799, Manufacturing Technology Laboratory, Fabrication Branch, Aeronautical System Division, USAF.

** Formerly of TRG, now affiliated with Argonne National Laboratories, Particle Accelerator Division, Argonne, Ill.

(1) Fairbanks, Sr., R.H. & Daly, R.T., "Laser (Optical Maser) Beam Fusion Welding," IR-7-985(I) ASD Project Number 7-985. October 1962.

$$\epsilon_o = K \left(\frac{E_{in}}{E_{th}} - 1\right) \qquad (1)$$

where **K** is the normalized output slope, E_{in} is the energy into the lamp, and E_{th} is the energy into the lamp at threshold.

We will now proceed to derive this expression by using our previously published "Theory of Normal Pulse Ruby Laser Output"[2] and to apply the results in a semi-qualitative manner to the problem of the design of a laser beam welding system.

The laser oscillation is at equilibrium when the oscillating fields are neither building up nor decaying with time. Except for effects which cause spiking in the ruby output, the time required for the field to reach equilibrium with the population inversion density will be of the order of 1 μsec. Since the variation of lamp intensity during this time is small, we can treat the oscillation as being at equilibrium. The conservation of energy requires that the rate of loss of energy input to the oscillation be equal to the losses caused by residual absorption in ruby, scattering, absorption in the reflecting films, and energy transmitted in the output beam. An output efficiency ϵ_o can be defined as the ratio of the output power to the power input into the laser oscillations

$$\epsilon_o = \frac{P_o}{P_{osc}} \qquad (2)$$

---

(2) Reference 1 and Fairbanks, Sr., R.H. & Daly, R.T., "Laser (Optical Maser) Beam Fusion Welding," IR-7-985(II) ASD Project Number 7-985. December 1962

where P_o is the output power/cm^3 and P_{osc} is the power/cm^3 into the laser oscillation.

Except for a common time factor, $e^{-i\omega t}$, the fields within the laser cavity--represented as a Fabry-Perot resonator--are shown in Figure 1. In the following discussion A, B and C are field amplitudes, γ is the complex amplitude propagation constant, r_1 and r_2 are the complex amplitude reflection coefficients, t_1 is the complex amplitude transmission coefficient, and ℓ is the length of the cavity. The propagation constant is given by

$$\gamma = \frac{\alpha}{2} + i\beta \tag{3}$$

where α is the overall power gain coefficient (we use the convention of positive values of α to imply gain), and β is the phase propagation constant.

For the steady-state condition at the reference planes (1) and (2) we have the following relations:

$$B = r_1 A \tag{4}$$

$$r_2 B e^{\gamma \ell} = A e^{-\gamma \ell} \tag{5}$$

$$C = t_1 A \quad . \tag{6}$$

The solution of these equations yields the steady-state condition

$$r_1 r_2 e^{2\gamma \ell} = 1 \tag{7}$$

This equation is complex and yields the familiar phase

condition for oscillation,

$$2\beta\ell + \phi_1 + \phi_2 = 2n\pi \quad (8)$$

where we define the complex reflectivities as

$$r_1 = R_1 e^{i\phi_1}, \quad (9)$$

$$r_2 = R_2 e^{i\phi_2}, \quad (10)$$

where R_1 and R_2 are the power reflection coefficients of the resonator and ϕ_1 and ϕ_2 are the power propagation constants. The magnitude part of the steady-state expression (7) yields the gain condition

$$R_1 R_2 e^{\alpha_t \ell} = 1 \ * \quad (11)$$

Neither of the steady-state conditions determines the field amplitudes A, B, and C. These can be determined by the application of the principle of the conservation of energy.

First consider the losses at the reflecting films: at r_1 the power loss is

$$A^2 - B^2 \quad (12)$$

at r_2 the power loss is

$$B^2 e^{\alpha_t \ell} - A^2 e^{-\alpha_t \ell} \quad (13)$$

Combining these losses with the steady-state requirements of (4), (5), and (6), the total power loss at both films is

---

* This subscript t is used to signify threshold.

$$P_{L(ref)} = A^2 \left[(1-R_1{}^2) + \frac{R_1}{R_2}(1-R_2{}^2)\right] \qquad (14)$$

The power loss is not symmetrical with respect to R_1 and R_2, because the intensity incident on each of the two films is different unless $R_1 = R_2$ (this would not be the case in a laser oscillator).

The power loss due to a distributed loss coefficient, α_ℓ, within the medium can be readily computed. With an increment of length dx, the variation of intensity across this increment in either direction is

$$dI(x) = I(x)\alpha dx = I(x)(\alpha_g - \alpha_\ell) \qquad (15)$$

where α_g is the material gain coefficient. The differential loss in any increment dx is, therefore,

$$dI_\ell(x) = B^2 e^{\alpha x}(-\alpha_\gamma)dx + A^2 e^{-\alpha x}(-\alpha_\ell)dx. \qquad (16)$$

Integrating (16) from $x = 0$ to $x = \ell$ we have

$$I_\ell = \frac{\alpha_\ell}{\alpha}\left[B^2(e^{\alpha\ell} - 1) + A^2(1 - e^{-\alpha\ell})\right] \qquad (17)$$

which, when combined with our expressions for the steady-state (4,5,6,9, and 10), gives

$$I_\ell = A^2 \frac{\alpha_\ell}{\alpha_t}\left[(1 - R_1{}^2) + \frac{R_1}{R_2}(1 - R_2{}^2)\right] \qquad (18)$$

The total loss to the oscillator is equal to the sum of this expression and (14) is equivalent to the input power to the oscillation in the steady-state. Making use of the relation

$$\alpha_t = \alpha_g - \alpha_\ell \qquad (19)$$

this becomes

$$P_{osc} = A^2 \frac{\alpha_g}{\alpha_t} \left[(1 - R_1^2) + \frac{R_1}{R_2}(1 - R_2^2) \right] . \quad (20)$$

The output power is the square of the absolute magnitude of C or (with $|t_1| = T_1$)

$$P_o = T_1^2 A^2 \quad (21)$$

Thus, the output efficiency given by the ratio of (21) and (20) is

$$\epsilon_o = \frac{\alpha_t}{\alpha_g} \left[\frac{T_1^2}{(1-R_1^2) + \frac{R_1}{R_2}(1-R_2^2)} \right] \quad (22)$$

We have assumed that the medium gain was uniform throughout the length of the cavity. Actually the amplitude of the electric fields is not uniform. The fields are weakest near the end with the highly reflecting mirror so that the rate of induced emission will be least at this end. The population inversion and medium gain would therefore be greatest near this end, making the formulas not strictly accurate.

We will assume that the thermal relaxation between the R_1 and R_2 levels is infinitely fast so that their populations are given by the Boltzmann ratio at all times--that is,

$$\frac{N_2}{N_1} = a = e^{-\Delta E/kT} \quad (23)$$

where ΔE is their energy difference, k is the Boltzmann constant, and T is the absolute temperature. We will further assume that the decay rates from the absorption bands to the R levels are infinitely fast and ignore the effect on population

densities of reabsorption or induced emission of the R light emitted spontaneously.

At equilibrium a portion of the power which is absorbed into the R levels (P_a) is lost by spontaneous emission (P_s). The remainder is added to the oscillating field by induced emission. The basic equations are then

$$P_{osc} = P_a - P_s \tag{24}$$

$$P_o = \epsilon_o P_{osc} \tag{25}$$

Equation (25) was presented previously (2). Below threshold the equilibrium populations are such that $P_a = P_s$. At threshold which is defined by

$$r_1 r_2 e^{\alpha_t \ell} = 1 \tag{26}$$

the populations clamp and the value of P_s remains at its threshold value P_{st} for high input powers. Thus, Equation (24) becomes

$$P_{osc} = P_{st} \left(\frac{P_a}{P_{at}} - 1\right). \tag{27}$$

Since the populations are clamped above threshold, the absorption efficiency is given by its value at threshold. Provided that the lamp brightness is a linear function of input power

$$\frac{P_a}{P_{at}} = \frac{P_L}{P_{Lt}} \quad . \tag{28}$$

This expression assumes that the quantum efficiency of excitation is independent of pumping power. Equation (27) becomes

$$P_{osc} = P_{st} \left(\frac{P_L}{P_{Lt}} - 1\right), \tag{29}$$

therefore,

$$P_o = \epsilon_o P_{st} \left(\frac{P_L}{P_{Lt}} - 1\right) . \tag{30}$$

If we assume that the laser is pumped with a square-shaped lamp pulse at levels significantly greater than threshold and that the time over which oscillation occurs is large compared with the time required to achieve threshold, we can integrate (30) to give

$$E_o \approx \epsilon_o E_{st} \left(\frac{E_{in}}{E_{th}} - 1\right) \tag{31}$$

where E_o is the energy output per pulse per unit volume, ϵ_o is the output efficiency defined previously, E_{st} is the energy emitted by spontaneous emission per unit volume with the population densities equal to the threshold value, E_{in} is the electrical energy input into the lamp, and E_{th} is its value at threshold for the onset of oscillation.

The energy spontaneously emitted with the population density equal to threshold is

$$E_{st} = h\nu N_o A\tau \left(\frac{1 + a}{3 + a}\right) \left(\frac{\alpha_g}{\alpha_o} + 1\right) . \tag{32}$$

Where N_o is the total chromium ion concentration, A is now the rate of spontaneous emission, τ is the duration of rectangular lamp pulse, a is the Boltzmann ratio of population of the R_2 level to that of the R_1 level, and α_o is the absorption coefficient of the unexcited ruby. The term α_{gt} was defined previously; therefore,

$$E_o = h\nu N_o A\tau \frac{\alpha_t}{\alpha_{gt}} \left[\frac{T_1^{\;2}}{(1-R_1^{\;2}) + \frac{R_1}{R_2}(1-R_2^{\;2})} \right] \left[\left(\frac{1+a}{3+a}\right) \left(\frac{\alpha_{gt}}{\alpha_o} + 1\right) \right] \left(\frac{E_{in}}{E_{th}} - 1\right). \qquad (33)$$

Within the limits of the exactness of its derivation, this expression relates the oscillator parameters to the energy output of the ruby. The expression does not treat losses that occur at the totally reflecting or transmitting end other than transmission and absorption losses. The expression also does not consider losses caused by diffraction and the divergence of the laser beam. The latter could be of importance in applications of lasers where long rods or external reflectors are to be used.

The normalized output slope of Equation (1) is

$$K = h\nu N_o A\tau \frac{\alpha_t}{\alpha_{gt}} \left[\frac{T_1^{\;2}}{(1-R_1^{\;2}) + \frac{R_1}{R_2}(1-R_2^{\;2})} \right] \left(\frac{1+a}{3+a}\right) \left(\frac{\alpha_{gt}}{\alpha_o} + 1\right). \qquad (34)$$

The factors A, a, and α_o are independent variables and are a function of the average temperature of the crystal. Obviously, N_o is also an independent variable, its limits being characterized by the solubility range of the chromium oxide in sapphire. In practice one tries to achieve

$$\frac{T_1^{\;2}}{(1 - R_1^{\;2}) + \frac{R_1}{R_2}(1 - R_2^{\;2})} = 1. \qquad (35)$$

This would be the case if $R_2 \approx 1$ and where the output end is non-absorbing (so that $T_1^{\;2} = 1 - R_1^{\;2}$). To approach these

idealized conditions one would have to carefully control the quality of the optical reflectors that are used with the resonator. Therefore the normalized slope under certain idealized conditions becomes

$$K = k \left(\frac{\alpha_t}{\alpha_o} + \frac{\alpha_t}{\alpha_{gt}}\right) \tag{36}$$

where k and α_o are constants.

As mentioned previously the gain coefficient necessary to achieve threshold is

$$\alpha_{gt} = \alpha_t + \alpha_\ell \; . \tag{37}$$

In so far as α_t is constant, the slope of the curve is somewhat dependent upon the distributed medium losses, α_ℓ. The gain coefficient to achieve threshold is therefore a crystal quality parameter. Poor crystal quality also leads to local variations of N_o.

The overall gain coefficient at threshold was defined by the condition for oscillation of a Fabry-Perot resonator as

$$R_1 R_2 e^{\alpha_t \ell} = 1. \tag{38}$$

In the present discussion, we have set $R_2 = 1$, so that

$$\alpha_t \approx \frac{1}{\ell} \; \ell n \; \frac{1}{R_1} \; . \tag{39}$$

Thus, if one increases the length of the rod, the output reflection-transmission properties must be adjusted to achieve the optimum normalized output slope K. An increase of length must also be accompanied by an increase in lamp power.

An artist's concept of the laser welding head and table is shown in Figure 2, where the laser head, complete with optical system, microscope, and laser cavity (pump lamp and ruby), is mounted over a standard milling table. The overall welding system is shown in Figure 3. The laser must be pumped to a highly energized state before oscillation and hence usable power output can be achieved. This is accomplished using a pulse-forming network that is charged by a power supply. The power supply must deliver 12.5 kilowatts continuously to the network and will be operated from a 220 volt, 3 phase line. The pulse-forming network stores energy over a relatively long period and transfers it in a short burst of controlled shape to the pump lamps in the laser head. This network will produce 0.45 to 18 millisecond pulses. Its energy storage will be variable from 2,000 to 60,000 joules at a maximum voltage of 8,000 volts.

The laser head houses the optical train, ruby laser, pump lamps, and ruby lamp cooling cavities. The minimum power output rating of the laser welder will be 10 watts, and the optical working distances will be 2.5 and 5 inches. The output beam is in the form of a spot or line--the spot diameter can be varied from 0.005 to 0.040 inch and the line can be varied from 0.005 to 0.040 inch in width and 0.060 to 0.640 inch in length. The system uses a pulsed mode of operation. A line weld is produced by automatically overlapping spots or lines. The welder will also have drilling and cutting capabilities.

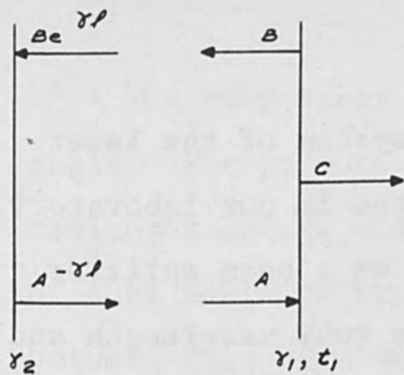

Figure 1.

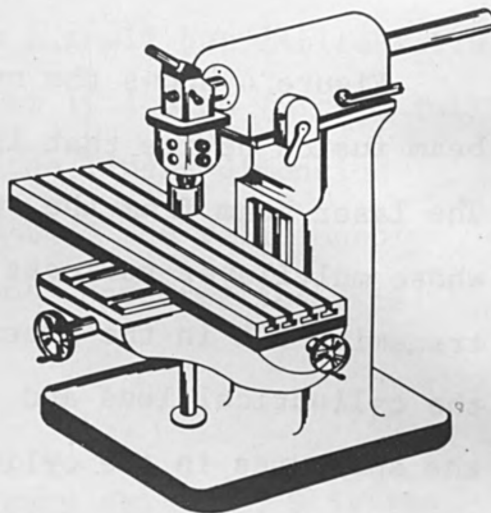

Figure 2.

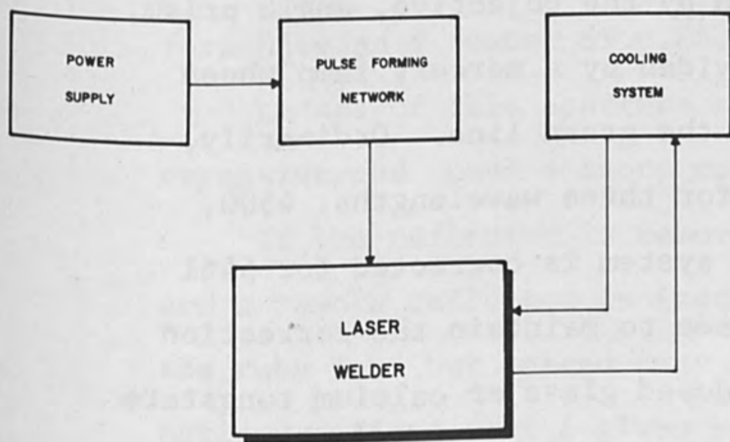

Figure 3.

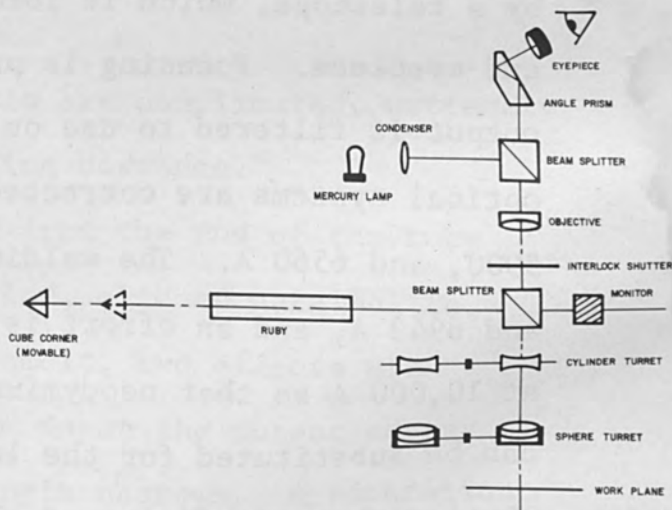

Figure 4.

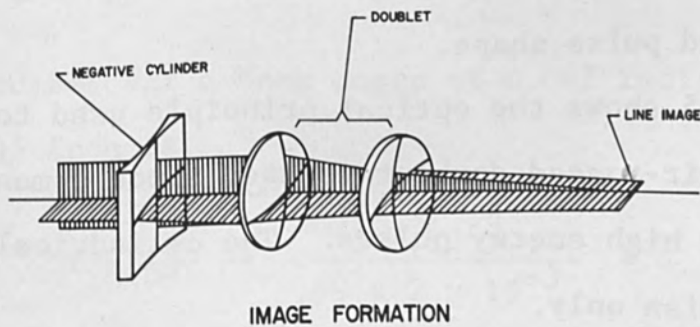

Figure 5.

Figure 4 shows the overall optical system of the laser beam fusion device that is being fabricated in our laboratory. The laser beam from the ruby is incident on a beam splitter whose multilayer reflects over 95% of the ruby wavelength and transmits 90% in the green. The ruby light then goes through the cylindrical lens and sphere turrets to the work. One of the apertures in the cylinder turret contains no lens to provide for spot welding and focusing. The work plane must lie in the focal plane of the sphere; therefore, an image of the work plane is formed at infinity. This image can be examined by a telescope, which is formed by the objective, angle prism, and eyepiece. Focusing is provided by a mercury lamp whose output is filtered to use only the green line. Ordinarily, optical systems are corrected for three wavelengths: 4500, 5900, and 6560 Å. The welding system is corrected for 5461 and 6943 Å, and an effort is made to maintain the correction at 10,000 Å so that neodymium doped glass or calcium tungstate can be substituted for the laser crystal. An interlock shutter prevents firing of the laser during focusing. The 5% of the laser light that is transmitted by the first beam splitter is used for monitoring the output energy, pulse duration, and pulse shape.

Figure 5 shows the optical principle used to form a line image. An air-spaced doublet is used since cements are destroyed by high energy pulses. The cylindrical lens focuses in one meridian only.

The ruby laser emits energy in a small but finite solid angle. For an output in the order of 10 joules (with a full reflector on one end of the ruby), the linear dimension of this angle is typically 0.01 radian. The relationship between this beam divergence and lens characteristics is given by:

$$s = D\theta f, \tag{40}$$

where s is the spot size, D is the ruby diameter, θ is the divergence and f is the number of the lens. In present laser welders, the smallest spot size will be 0.005 inch; with a ruby 0.59 inch in diameter, the required lens would therefore have an f number of 0.85.

Lenses of this aperture ratio are complicated, extremely expensive, and have a short working distance.

If the reflector is removed from the end of the ruby and a remote reflector is installed, aligned parallel to the ruby face but spaced away from it, two effects are noticed. First, for a given pump input the output energy decreases and second, the beam angle narrows. A separation of 20 inches will reduce the beam angle to about 0.002 radian accompanied by an output energy decrease of less than a factor of two.

The f number for a beam angle of 0.002 radian and a spot of 0.005 inch is:

$$f = \frac{s}{D\theta} = \frac{5 \times 10^{-3}}{.59 \times 2 \times 10^{-3}} = 4.24, \tag{41}$$

this requirement can easily be met by a doublet with a working distance of 2.5 inches.

Ordinarily, the remote reflector would have to be parallel to the ruby face to about 10 seconds of arc, which is a difficult requirement. However, the plane reflector can be replaced by a glass cube corner, which, because of its retroreflective properties, has no tilt alignment restrictions. Reflection is of the total internal type, the only losses being that of Fresnel reflection at the front face when this face is unaligned. This reflector can be used only with a 0° oriented ruby because it produces a circularly or elliptically polarized output beam that is not affected by the cube corner. A standard or a 90° ruby, however, produces linearly polarized light, and the reflection in a cube corner converts this to elliptically polarized light, thus reducing the effective gain of the ruby.

The change of beam angle with reflector separation is predictable, so that the spot size can be changed by about a factor of four by changing the location of the cube corner.

The ability of light to penetrate metals is limited, so that the mechanism of the heating effect must be related to surface heating. There are three requirements for the laser beam to perform fusion welding in a single pulse:

a) The intensity per unit area must be adequate to melt the surface of the metal.

b) The intensity per unit area must be less than a given maximum which will vaporize the surface.

c) The duration of the pulse must be sufficient to

allow penetration of the molten zone by conduction through the metals.

Each of these requirements depends upon the metal, its thickness, and its reflectivity. The reflectivity of the refractory metals for light at 6943 Å is about 60%, so that 40% of the incident light is absorbed.

Consider a continuous laser source and assume that a molten cylinder is formed whose diameter is one-half its depth. Assume further that this cylinder is moved across the metal sheet at a welding speed of 8 inches per minute, then Table I lists the minimum intensity required for this CW laser for two thicknesses of representative metals. It is obvious that present CW lasers cannot be used for fusion welding because they are limited to an output of the order of 1 mw.

Table II contains an estimate of pulsed laser power, E_m, and pulse duration, τ required to penetrate the metal thickness by thermal conductivity. It was assumed that the initial temperature of the metal sheet was 0°C and for $T > 0$ heat was added to the upper surface only to hold it at the vaporization temperature. The heat of fusion for the high temperature metals is smaller than the heat required to raise the temperatures to the melting point. It was, therefore, added to the specific heat for this calculation. The results show that for present practical pulse durations of the high-power ruby laser, thin sheets of metal can be butt- or lap-welded. If a 10-joule laser output is used for

TABLE I

CW Power Requirements, Watts

at w = 8 ipm

	.005"	.125"
Molybdenum	78	1,900
Stainless 321	10	250
Titanium	3.8	96
Aluminum	88	2,200
Tungsten	180	4,500
Niobium (Columbium)	46	1,100

Depth: Width 2:1

TABLE II

Pulsed LASER Welding

	.005"		.125"		.005"
	E_m Joules	τ_m sec	E_m Joules	τ	W_{ipm} at 10 w av
Molybdenum	14×10^{-3}	.19	220	120	110
Stainless 321	14×10^{-3}	1.4	210	890	110
Titanium	5.6×10^{-3}	1.5	88	940	270
Aluminum	10×10^{-3}	.12	160	74	150
Tungsten	22×10^{-3}	.13	340	80	68
Niobium (Columbium)	17×10^{-3}	.37	260	240	88

Depth: Wdith 2:1

welding, assuming suitable optics are available for shaping the beam, practical welding speeds (inches/minute in Table II) are realized with up to 0.025 inch metal sheets. The possibility exists of fusion-welding sheets of thicknesses up to 0.125 inch by surface melting in a V-groove of a butt joint. Experience with electron beam welding indicates that with a proper opening of the groove, the molten material puts the metal under tension as it solidifies and fills the void without added filler. Preliminary experience suggests that this is also true for laser welding. We have assumed (in Tables I and II) that the focused laser beam was rectangular along the seam to be welded. The preset width of the beam is dependent upon material thickness, and its length corresponds to that required for achieving complete fusion of the metal in the incident beam with a single laser pulse.

In the figures showing metallurgical preparations, samples were obtained as follows. A single pulse of the laser was focused onto unbroken surfaces of a metal sheet. The intensity for a unit area of the laser beam was varied by adjusting the focusing. The metal samples were then cross-sectioned, etched and polished.

With laser beam fusion, the usual welding problems exist that are associated with evaporation and expulsion of metal. This is particularily serious in titanium (Figure 6 c and d) and will also become a problem with tantalum alloys (Figure 7 c).

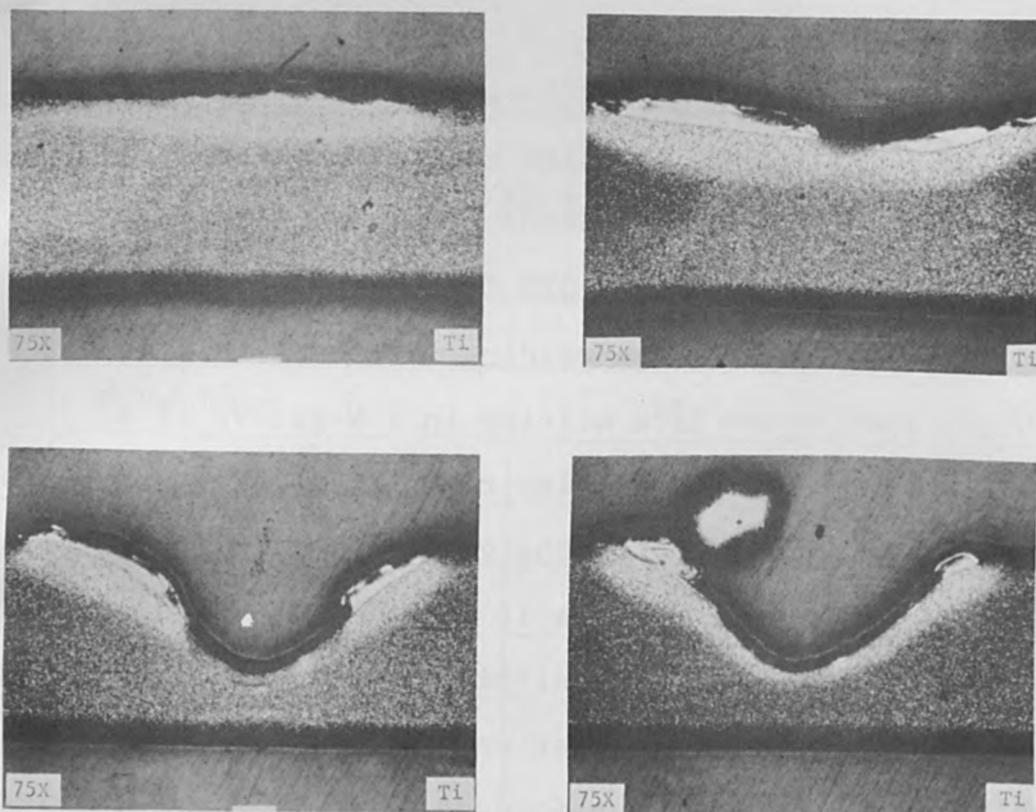

Figure 6.

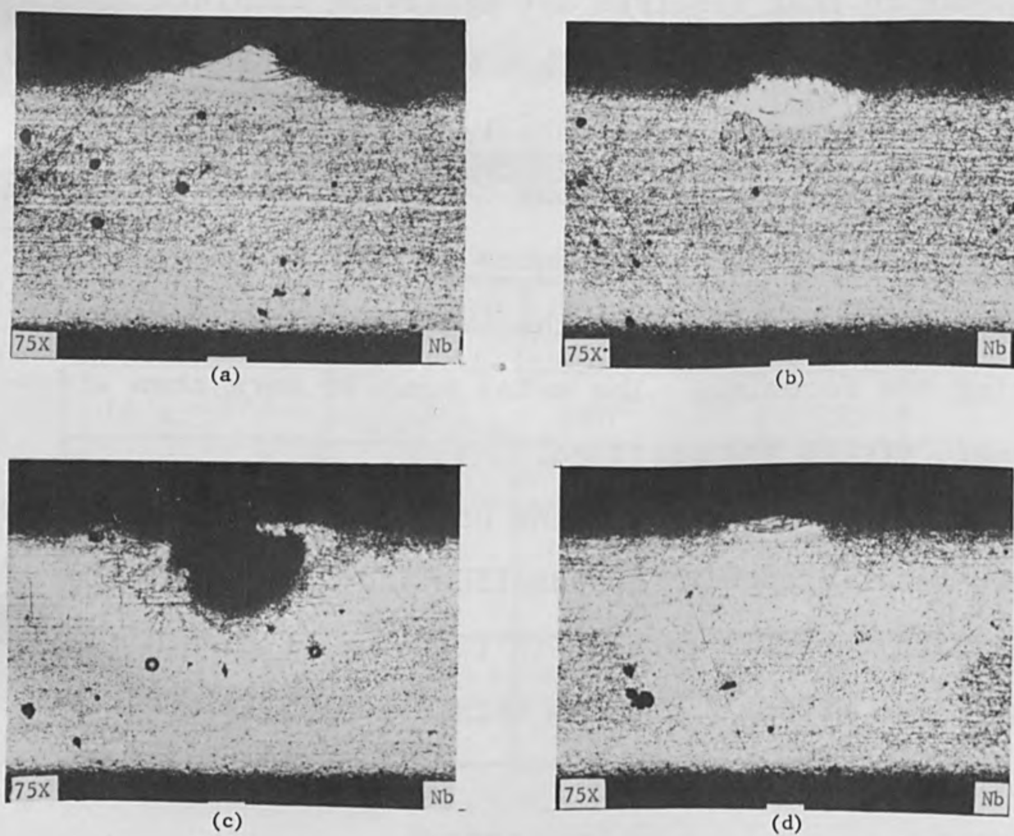

(a) (b)

(c) (d)

Figure 7.

Based upon experimental evidence (electron beam) that metals cannot stand instantaneous heat fluxes greater than about 10,000,000 watts/in^2, it is possible to discuss this problem* in a semiquantitative manner.

Consider the problem of pulsed heat delivery through a circular region on the surface of a thin sheet, where the object is to accomplish melting with the minimum required heat, Q. Assuming no losses, Q is given by:

$$Q = \frac{\pi d^2 t \rho H'}{4} \tag{42}$$

where d is the diameter of the spot, t is the thickness of the sheet, ρ is the density of the solid metal, and H' is the heat per unit **mass** required to accomplish melting (including the heat of fusion).

The heat requirement per unit area is then

$$Q/A = t\rho H' \tag{43}$$

If the pulse time is too long, much of the heat will be conducted away--that is, the process becomes inefficient, and the total energy required is larger than the minimum value indicated above. If the pulse time is too short, excessive evaporation takes place. The maximum time, Θ_{max}, for efficient melting depends on the diameter of the spot and the thermal diffusivity, α.

---

* Professor C.M. Adams, Jr., M.I.T., Personal communication.

$$\theta_{max} = \frac{d^2}{16\alpha} \qquad (44)$$

Equation (44) is of interest only with relatively thick materials which challenge the capacity of the laser beam from a total energy standpoint, and which therefore demand efficient utilization of heat. For light gauge materials, the total energy requirements are so low that inefficient operation can deliberately be tolerated, and the problem becomes exclusively one of ensuring that the pulse is of sufficiently low instantaneous intensity that evaporation and expulsion of liquid metal do not constitute a problem.

The minimum pulse time, θ_{min}, is related to the maximum tolerable intensity as follows:

$$\theta_{min} = \frac{t\rho H'}{f_{max}} \qquad (45)$$

where, f_{max}, is the maximum permissible heat flux. This expression is based on the assumption that the heat flux during the pulse is uniform (a) over the surface of the spot and (b) over the time period of the pulse. Neither of these assumptions is actually true, and it is expected that these non-uniformities of energy delivery will increase the minimum time, because it is the instantaneous intensity that is the criterion of whether evaporation will be a problem. This will be determined by the hottest region in the spot at the moment of maximum intensity. Spatial non-uniformity also aggravates the evaporation problem in another way. If the intensity of the spot varies from point to point on the

surface, local temperatures and vapor pressures will also vary, and the mechanism by which liquid metal is expelled is favored by gradients in the local vapor pressure. Thus, if the spot is hot at the center, a definite lateral thrust will be exerted in the liquid that causes cratering. There is no question that the maximum tolerable intensity and, therefore, the minimum pulse time varies with the material. The figure of merit appears to be the vapor pressure of the metal at its melting point.

With laser beam fusion, undercutting of the metal may also be a problem. This can be seen in Figure 8 a, where undercutting is observed in the right-hand base-metal weld interface.

One of the advantages of pulsed laser beam fusion is associated with the extremely high solidification rates observed.

The cooling rate as a function of temperature, T, can be expressed by*

$$\frac{dT}{d\theta} = 4\pi k \left(\frac{t}{Q}\right)(T - T_o)^2 \qquad (46)$$

where $d\theta$ is the differential time, T is the maximum temperature of the system, T_o is the ambient bulk temperature, k is the thermal conductivity, t is the thickness of the sample, and Q is the heat supplied. With this approach, we have observed a cooling rate with tungsten of 10 million

---

* Professor C.M. Adams, M.I.T., Personal communication.

(a)

(b)

(c)

Figure 8.

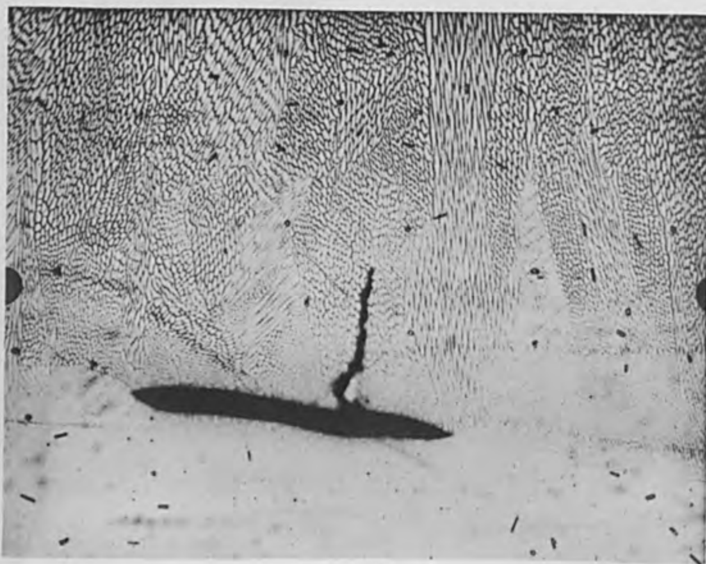
Figure 9.

Figure 10.

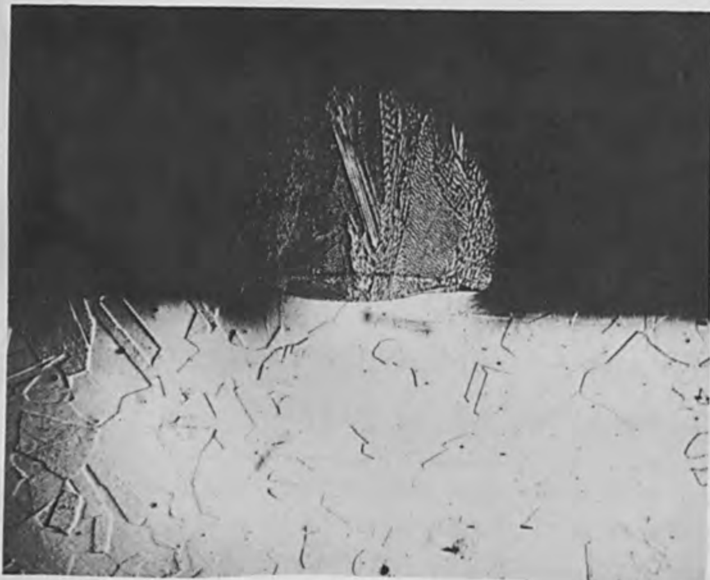
Figure 11.

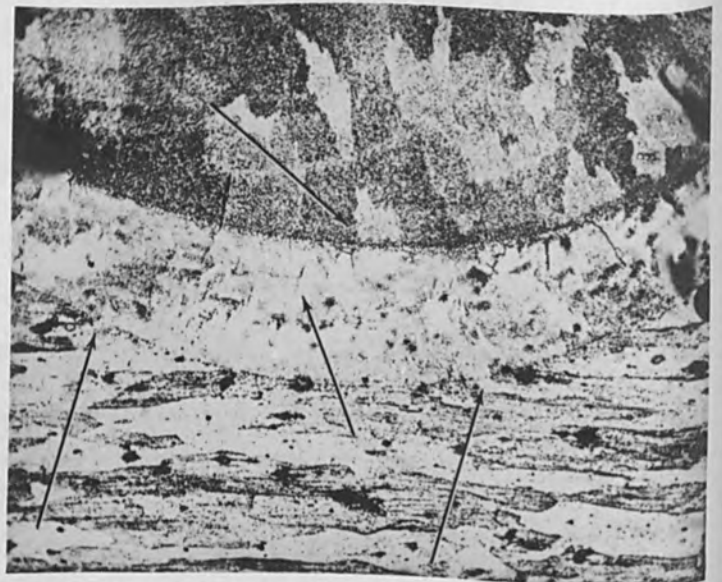
Figure 12.

degrees K/sec. This rate is greater than any other previously used in a laboratory or commercial fusion process with this metal. Similar results have been observed with other metals.

In welding, the metallurgical structures of weldments are of interest from the standpoint of how they affect the mechanical properties. A typical stainless-steel laser weldment is shown in Figure 9 at 500 X. We observe a high dispersion of alloy elements and impurities in the fusion area; this degree of dispersion is not seen in the parent metal (lower portion of picture). High dispersion is metallurgically associated with high strength and toughness. In addition to welding, it may be possible to use the laser for converting entire components into the desirable type of metallurgical structure shown here.

The remarkable grain continuity observed across fusion boundaries may lead to another area of application. Figures 10 and 11 show how laser-melted metal crystallizes as an extension of the underlying structure. This phenomenon is sometimes referred to, especially in the electronics industry, as epitaxial growth. It may have important applications in the production of crystals, solid-state electronic devices, and other metallurgical structures in which the crystallographic texture plays an important role. Epitaxy is also important in laser welding because it favors continuity of mechanical structure. Preliminary studies by one of our

consultants* have indicated that pulsed electron beam fusion of stainless-steel (304 or 316) also appear to cause epitaxial growth. We do not yet know if all laser melts will show epitaxial growth.

Other advantages of laser beam fusion are numerous, some of these are:

a) Standoff welding is possible
b) No charge problem exists
c) High intensity can be achieved
d) No vacuum is required
e) Momentum associated with beam is negligible
f) Speed of thermal cycle minimizes the inert gas shielding problem.

Other features of some of these melts that are of interest are double fusion boundaries. This is seen at 500 X with aluminum 52-S1/2 in Figure 12. We have also noted this type of boundary in some of our stainless-steel metals. The reason for the double fusion boundaries is currently under study. With this aluminum alloy, a micro-cracking problem may exist; the quantitative aspects of this defect have not yet been fully established.

In general, the outlook for laser beam welding is good. Because of the unique nature of the laser as a high-intensity pulsed heat source, its application is expected to lead to other novel structural effects. These plus the inherent advantages of the technique will assure the laser a place in

---

* Mr. J. Kennedy, Grumman Aircraft Engineering Corp., Welding Section, Bethpage, N.Y., Personal communication.

welding. Much fundamental metallurgical knowledge will be gained from studies of structural features of laser melts.

GRID CONTROLLED PLASMA ELECTRON BEAM

by

M. A. Cocca, Metallurgical Engineer
Research Laboratory
General Electric Company, Schenectady, N.Y.

and

L. H. Stauffer, Physicist
Advanced Technology Laboratories
General Electric Company, Schenectady, N.Y.

SUMMARY

An experimental development for producing controlled electron beams of high intensity in low pressure gases is described. A hollow cylindrical cathode with perforated walls is provided with a concentric internal grid and a beam forming aperture at one end of the cathode. The unheated cathode emits a collimated electron beam ranging in energy from 3 to 20 kilovolts depending on the adjustment of gas pressure and cathode potential. Electron beam currents of 2 amperes or more are readily produced at beam power levels of over 30 kilowatts.

Continuous adjustment of the beam intensity, without affecting its focus, is accomplished by applying a small bias voltage between a control grid and the cathode. Since the grid controls the flow of low energy electrons from the internal walls of the cathode, beam response is fast and continuous.

Because the cathode is rugged and simple and operates unheated in a gas at low pressure, it has important advantages for electron beam thermal processing applications. As a process tool it provides the inherent advantages of hot cathode electron beam devices without the limitations imposed by the sophisticated gun and auxiliary equipment designs required in hot cathode equipment. Experiments have demonstrated the ability of the plasma electron beam to perform

melting and refining operations in a controlled atmosphere. These experiments give an indication of the degree to which the device can be employed in melting, welding, sintering and heat treating processes. Other possible applications include beam power tube amplifiers and oscillators, microwave power generation by plasma interaction, and electron beam irradiation of materials.

GRID CONTROLLED PLASMA ELECTRON BEAM

L.H. Stauffer and M.A. Cocca

Introduction

Electron beams having energies of 10 to 100 kilovolts, or more, are finding increasing applications where very high power densities are needed. For the melting, refining and heat treating of refractory metals in vacuum, electron beams can deliver kilowatts of highly concentrated beam power under precise control. In electron beam welding several tens of thousands of kilowatts per square inch[1] may be concentrated at a focal spot a few mils in diameter to weld or cut such metals as titanium, tantalum and tungsten. Such beams are usually generated by electron guns employing heated cathodes of tungsten or some other good thermionic emitter. Hot cathode guns use electrostatic lens systems for forming the electron beam and may employ magnetic lenses to further concentrate it into a small focal spot.

In these highly concentrated electron beams space charge spreading becomes a problem, and mutual repulsion of the electrons in the beam tends to limit the current density which can be achieved in the normal high vacuum environment.

In addition, the hot cathode and other components (such as filaments in indirectly heated cathodes) are susceptible to oxidation

and contamination and possible total failure if pressure bursts occur in the system. In most processing operations the latter are frequently encountered due to removal of gaseous impurities from the material being treated. Generally hot cathode guns are limited to operation at pressures of 10^{-4} Torr or less. These pressure requirements give rise to further process limitations such as the need for more complex systems and notable vaporization loss of higher vapor pressure materials.

Within the past year the General Electric Company and the Martin Company independently announced developments in the field of cold cathode electron guns which have wide applications in science and industry[2,3]. These electron beam sources use a cold cathode in the form of a hollow perforated cylinder or sphere with a small circular hole from which the beam emerges. They do not operate in a high vacuum as does a hot cathode. Instead an inert gas such as argon or helium is employed at low pressure (1 to 10 microns or higher). On application of a high D-C potential a well-collimated electron beam is formed in the low pressure gas atmosphere. A proper, though not critical, range of adjustment of gas pressure and cathode voltage is required to maintain collimation and stability in the beam. Depending on cathode design, beam currents may range from milliamperes to amperes with cathode potentials of 10 to 20 kilovolts or more.

Beam Formation

Formation of the plasma electron beam is associated with the interaction of ionized regions inside and outside the cathode with electric fields between its perforated surface and the plasma boundaries. Positive ions formed in the beam path by electron collisions with gas atoms play an important role in beam collimation by neutralizing the negative space charge which would otherwise cause beam spreading.

Figure 1 shows a cathode made of 40 mesh 10 mil stainless steel screening emitting a self-collimating electron beam in helium at approximately 15 microns pressure. This cylindrical cathode measures 1-1/8" x 1-1/2" and has a 1/4" beam exit aperture. A stainless steel stem extending through an insulating bushing supports the cathode from an aluminum cover plate which acts as the anode. This cover plate together with a large glass cylinder form a bell jar to which selected gases can be admitted at pressures in the micron range. An oil diffusion pumping system is used to evacuate the chamber.

When the gas pressure and cathode voltage are adjusted properly the beam mode of operation sets in and the electron beam path is marked by the luminousity of excited atoms in its path. Ordinarily, the gas density is too low to cause appreciable scattering of the beam. Beams up to 30" in length have been produced by this method with little spreading. The focussing effect of positive ions in

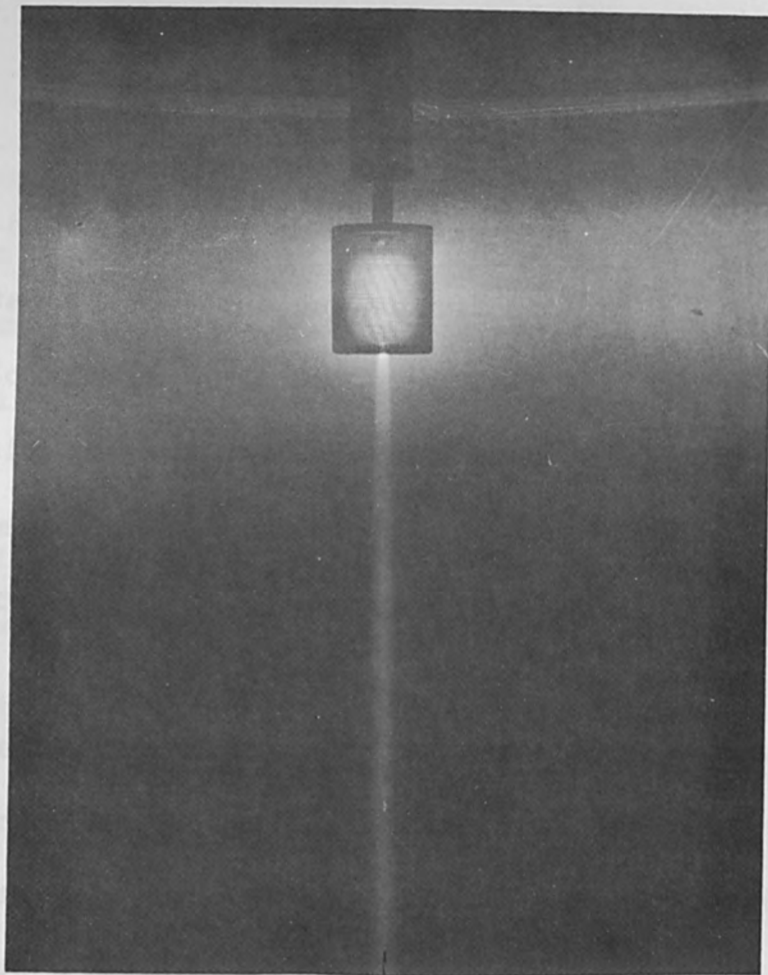

Figure 1

Electron beam emerging
from the cold-cathode electron gun
with no additional focusing.

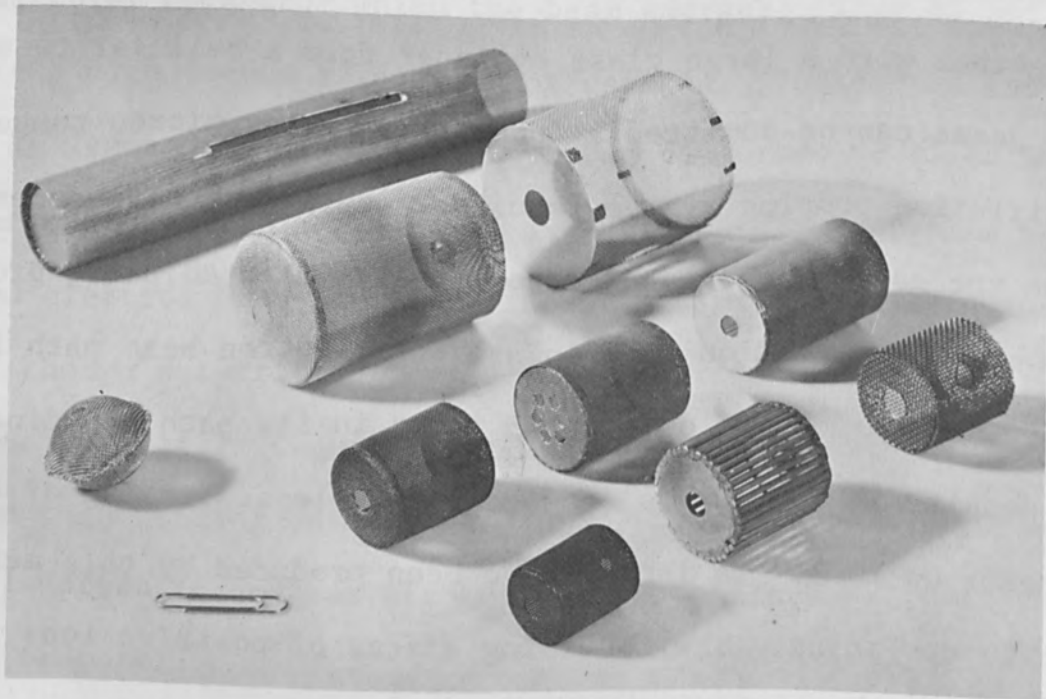

Fig. 2 CATHODES MADE OF WIRE MESH AND THIN PERFORATED SHEET METAL

the beam path is an important factor in maintaining collimation.[4] Typically, the beam cross section is about the size of the exit aperture, though it can be made smaller by adjustment of pressure and cathode voltage.

At pressures and voltages outside the range of the beam mode a more or less diffuse glow discharge is obtained. In argon the beam mode is most easily supported at pressures from 3 to 10 microns with applied voltages from 5 to 10 kilovolts depending on gas pressure and cathode characteristics. In lighter gases such as hydrogen and helium the beam mode is obtained at higher pressures (10 to 100 microns). Beam currents range up to 2 amperes for a 3-inch cathode in argon with 20 kilovolts applied. Divergent or convergent beams may be obtained by adjusting the gas pressure or cathode voltage.

Measurements of beam power delivered to a shielded cup have shown that from 75 to 95 per cent of the input power resides in the electron beam. Presumably, the power not accounted for in the beam is consumed in maintaining the positive glow region surrounding the cathode and the plasma inside it. Some power is, of course, dissipated as heat in the cathode, but thermionic emission does not normally contribute electrons to the beam.

Cathode Construction

Several different cathode designs have been used successfully. Some of them are shown in Figure 2. For power levels of 2 kilowatts

or less a cylindrical cathode made from perforated stainless steel sheet has been found convenient. Construction is very simple, the parts being cut to shape and assembled by spot welding. Cathodes are supported by a coaxially shielded lead as shown in Figure 3 in order to prevent a discharge from the supporting high voltage rod. High power cathodes are usually made from molybdenum wire mesh using solid sheet molybdenum end plates. Assembly is by means of spot welding, using thin tantalum foil between the molybdenum parts to facilitate the welding. Two interesting variations are shown in Figure 2, a long, slotted cylinder, and a squirrel-cage type. The cylinder was used to produce a sheet beam for use in a plasma ionization experiment, while the squirrel cage construction was a prototype for a water cooled cathode for extremely high power operation, using tubing instead of rods.

Basic Experiments

Preliminary experiments were carried out with a demountable apparatus, schematically illustrated in Figure 4. Cathodes of various sizes, made of perforated sheet or wire mesh have been tested. Copper, aluminum, stainless steel and molybdenum cathodes have been tried in several inert gases. Collimated electron beams can be readily produced with all of these metals in helium or argon. For very high beam currents stainless steel or molybdenum mesh are preferred because they can better withstand the heating due to positive ion bombardment.

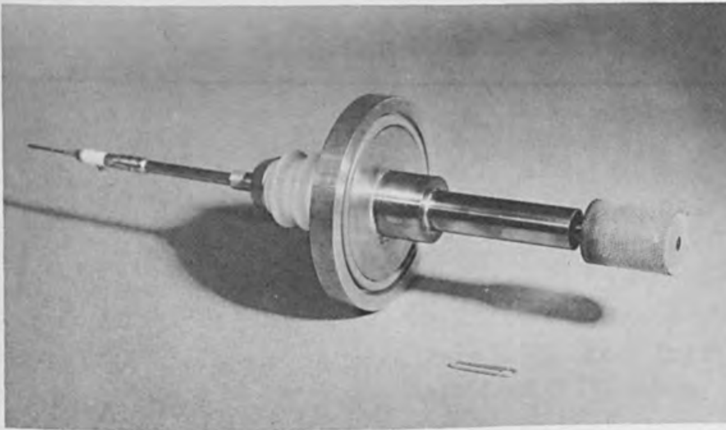

Fig. 3 CATHODE ASSEMBLY WITH SEALING FLANGE AND BUSHINGS

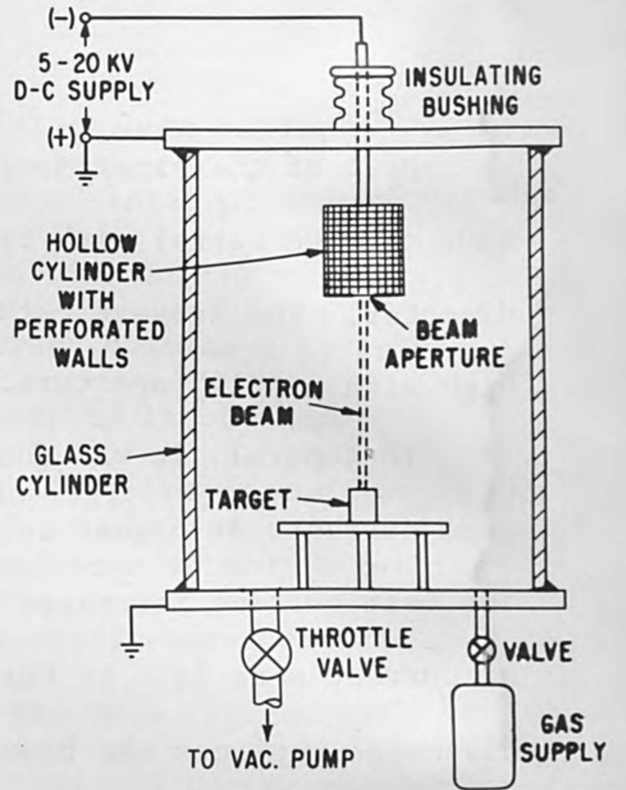

Fig. 4. Schematic of Experimental Assembly

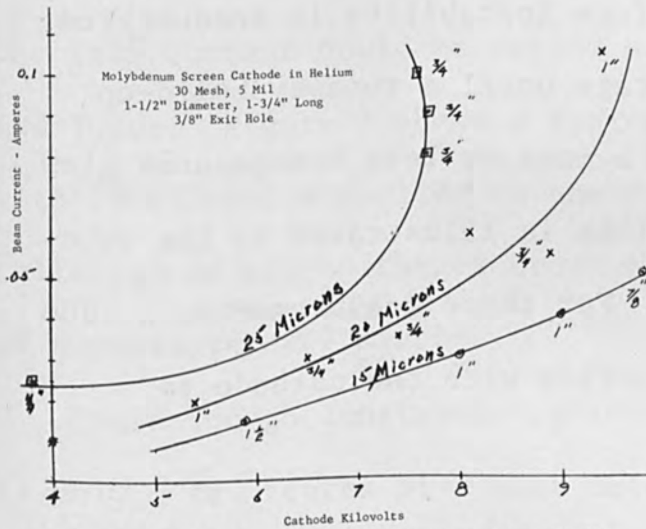

FIG. 5 CURRENT-VOLTAGE CHARACTERISTICS FOR THE BEAM MODE AT VARIOUS PRESSURES
ATTACHED NUMBERS GIVE HELIUM PRESSURES IN MICRONS

Fig. 6 EXPLODED VIEW OF GRID CONTROLLED CATHODE ASSEMBLY

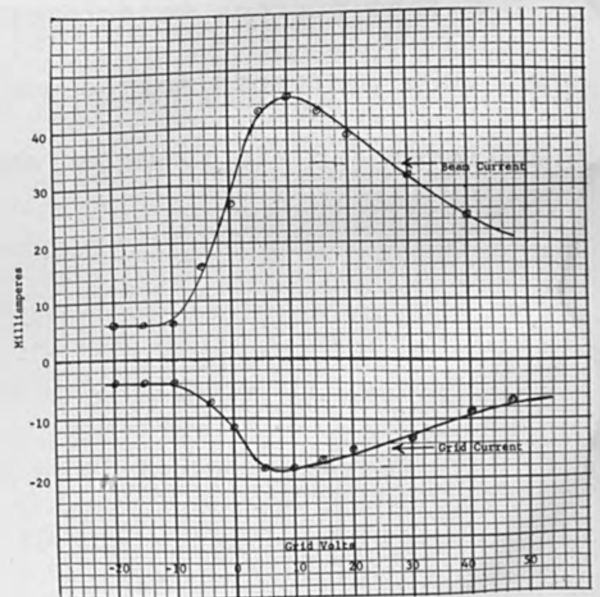

FIG. 7

GRID CONTROL CHARACTERISTICS IN ARGON AT 7 MICRONS PRESSURE

Most of the experiments were done at moderate power inputs (500 to 1000 watts) with cylindrical cathodes about one inch in diameter. The largest cathode tested was 3" in diameter and 4" high with a 5/16" aperture.

In general, it was found that larger cathodes can produce higher beam currents at higher voltages before instability is encountered. The beam current increases with voltage until a runaway build-up of current sets in. At this point, a more or less homogeneous glow discharge replaces the beam mode. This is illustrated by the volt-ampere characteristics of Figure 5. For these measurements, a 5800 ohm ballast resistor was placed in series with the cathode to stabilize the discharge.

Grid Control

Beam current measurements were taken with an internal grid made of .005", 32 mesh molybdenum wire in the form of an open ended cylinder 7/8" in diameter and 1-1/8" long. This was supported

inside of a finely perforated stainless steel cathode having a transmission factor of about 30 per cent and an internal diameter of about 1-1/8". Figure 6 shows an exploded view of the assembly.

It was found that the floating grid always assumes a positive potential (several hundred volts) with respect to the cathode. When a variable D-C bias was applied from an isolated potentiometer the beam current could be varied over a wide range without affecting its focus. Figure 7 shows a typical grid control characteristic with 10 kilovolts applied to the cathode. The beam current was collected in a deep target cup. Argon was supplied to the chamber at a pressure of 7 microns.

Even though substantial grid current is drawn the grid power is only a few tenths of a watt because of the low grid potentials employed for beam control. It should also be pointed out that the direction of current flow, in the conventional sense, is always observed to be from grid to cathode in the external circuit. This indicates a net loss of electrons from the grid to the plasma. A grid biasing resistor can be used to generate positive grid potentials if desired.

Certain features of the grid control curve (Figure 7) are of interest in interpreting the action of the grid on the external beam. At negative grid potentials beyond 10 volts the beam current

remains at a minimum, indicating cutoff of electrons from the inner cathode walls. At less negative potentials electrons from the inner cathode walls are admitted to the internal plasma and are drawn out into the beam. Finally at a grid potential above +10 volts the potential difference between grid and cathode tends to retain electrons within the region enclosed by the grid. This retarding action slowly reduces the beam current as the grid potential is increased.

Experiments with other gases such as helium and nitrogen show similar grid control characteristics though the controlling action is less pronounced then with argon.

Beam Focussing

With no auxilliary focussing the spot size of the electron beam can be varied from less than 1/8" to as large as desired by adjusting the cathode potential over a range of a few per cent at any given pressure. The self focussing property of the plasma electron beam is due to the combined action of positive ion space charge near the aperture, and in the beam path, and the electrostatic lensing property of an aperture separating regions of different potential gradients. A region of high potential gradient surrounding the cathode accelerates electrons from the aperture and collects the relatively slow moving positive ions which, enroute,

form a positive space charge concentration augmenting the extraction field at the exit aperture. The focal length f of such an aperture lens is approximately given by

$$f = \frac{4V}{E_2 - E_1}$$

where E_2 and E_1 are the external and internal field strengths respectively and V is the cathode potential. This accounts for the voltage dependence of the beam focus. Since the thickness of the sheaths separating the internal and external plasma boundaries from the cathode walls diminishes with increasing gas pressure, E_2 and E_1 also vary with gas pressure and thereby influence beam focussing.

To achieve adjustable beam focussing without the necessity of changing the cathode voltage, and hence the electron velocity, a simple magnetic lens may be used. Because the beam is already collimated, or slightly divergent, the lens need not be a strong one. Only a few hundred ampere turns are needed to focus the beam. Spot sizes approximately 10 mils in diameter have been achieved with a short solenoid supported a few inches below the cathode.

Origin of Electrons

Because the cathode operates at temperatures too low for appreciable thermionic emission other mechanisms must be looked for to explain the origin of the beam. While the plasma body inside

the cathode may supply a small fraction of the electrons most of them must come from the inner cathode surface. This is borne out by the observed suppression of the beam current on application of a negative grid potential. Most of the electrons from the inside of the cathode are suppressed when a negative bias of 8 volts is applied. This suggests that low energy secondary electrons produced by high energy ion bombardment or photoelectrons (or both) make up the bulk of the beam current. Since the grid is open ended it cannot exercise complete cut-off of the beam. However, more complete cut-off could be obtained if the end were closed with a sheet of mesh having an exit aperture for the beam.

Cathodes with oxide films or other deposits become clean after a few minutes of operation. This indicates that positive ions drawn out of the surrounding sheath are accelerated to high velocities and, by entering the perforations and the aperture, bombard both the inside and outside surfaces of the cathode. Foreign surface layers are, thus, quickly removed from the cathode surfaces by the impact of ions from the discharge. More important, however, is the possibility for a single energetic ion to remove one or more electrons from metals such as molybdenum[5]. This together with photoelectrons ejected by the spectrum of ultraviolet light emitted by the discharge may well account for the entire cold emission from the cathode. Also it should be pointed

out that the cathode is subject to a flux of soft X-rays from the target which could account for considerable photo-emission.

Even though the combined areas of all of the perforations or mesh openings totals many times the area of the beam aperture only a small fraction of the cathode current is accounted for by electrons escaping from these small openings. These electrons are accelerated outward from the cathode and, by collisions, ionize the surrounding gas. A continuous supply of positive ions is thus maintained. A large portion of the electrons are not stopped by gas collisions and these strike the walls. This is evidenced by fluorescence and slight heating of the glass walls.

Experiments with apertures of different sizes and with multiple apertures in a single cathode, have shown that the beam seeks out the largest aperture and that emission from other apertures is suppressed. Once the external beam is established its space charge constricts the boundaries of the cathode dark space near the aperture and enhances the field strength to extract electrons from the internal plasma. While there is a continuous replenishment of electrons to the internal plasma from the cathode walls the space charge balance remains on the positive side when the beam mode predominates.

Applications

Certain unique advantages possessed by this type of electron gun should be kept in mind in considering possible applications. They are:

1. Insensitivity to contamination.
2. Ability to operate in a partial vacuum (pressure up to one hundred microns in hydrogen or helium).
3. Grid control of beam intensity.
4. Self-focussing properties.
5. Good depth of focus.
6. Ruggedness and simplicity.
7. Design flexibility to provide various beam configurations.

Some of its characteristics may also be listed as disadvantages:

1. Gas pressure and cathode voltage must be regulated.
2. Chamber walls must be spaced several cathode diameters from the cathode.

Among the obvious applications are electron beam welding, melting and refining of refractory materials and chemical processing. Other possible applications such as microwave generation by plasma interaction, light source excitation and ionization of gases are being explored.

Control of the electron beam intensity by an internal grid has opened new circuitry applications. It offers the possibility for developing new types of amplifiers, oscillators and control circuits. Since the grid does not initiate or extinguish the glow discharge but controls electron flow the response time should be limited only by interelectrode capacitance and electron transit time. In sealed-off

beam type power tubes mercury or other metallic vapors could be employed to provide the required ionization in the cathode region.

While the more obvious applications are being developed, others, possibly more important, await a better understanding of the basic mechanism of this type of electron beam formation.

For welding the plasma electron gun offers the advantage of a long beam with a small angle of convergence which can be focussed on remote parts of the work with less interference than would be encountered with a highly convergent beam with less depth of focus. Beam control by biasing the grid in combination with a variable focus magnetic lens provides for independent adjustment of total beam power and power density at the focal spot. By operating at voltages below 25 kilovolts only soft X-rays are generated which are absorbed by relatively thin metal or glass walls.

To provide additional flexibility for the cathode in applications where large gas pressure fluctuations occur or where different gases are used over the work, a differential pumping arrangement may be employed. Figure 8 shows one possible arrangement in which the beam passes through 2 small apertures which have higher impedance to gas flow than the pumping outlets. Gas, sufficient to sustain the discharge, is admitted into the upper chamber in which the cathode is located. This arrangement would be equally useful for melting, zone refining or sintering operations.

Melting Experiments

To determine feasibility of using the plasma electron beam for metallurgical process applications requiring higher power levels, a number of melting experiments were conducted. A conventional electron beam melting furnace in use at the Research Laboratory was temporarily converted to accomodate the plasma cathode. As shown in Figure 9, the conventional gun was removed from the water-cooled furnace chamber. A cover plate in the top of the chamber was fitted with a porcelain bushing which supported a 3" D x 4" L cathode, similar to that shown in Figure 3. The beam exit hole was approxi- 1/4" D and the top end of the cathode was fastened to a plate cooled by water carried by copper tubes sealed through the insulating bushing. Cooling water was supplied through about 10 feet of Tygon tubing to isolate the high voltage.

The bottom of the furnace was equipped with a water-cooled copper crucible, 2" D and about 1" deep, and located approximately 14" below the cathode. At this distance no magnetic focussing was required to form a beam ranging from 1/4" to 3/4" D on the material in the crucible.

The furnace chamber was pumped by a 4100 l/sec pumping system. After initial pumpdown (about .001 microns) argon gas was supplied through a high impedance leak and regulating valve to maintain a

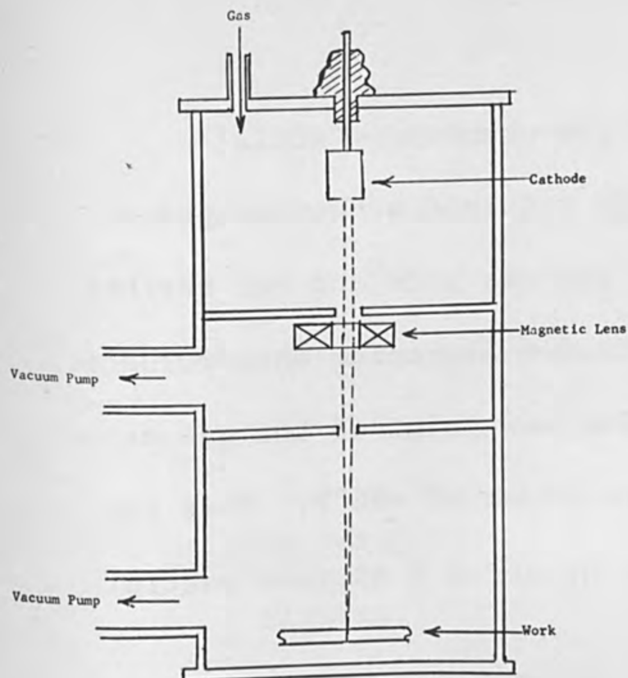

FIG. 8

PRESSURE STABILIZATION BY DIFFERENTIAL PUMPING

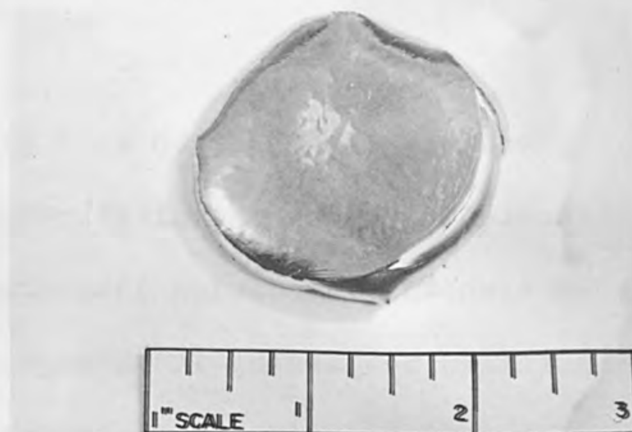

Figure 10 - Plasma electron beam melted columbium button.

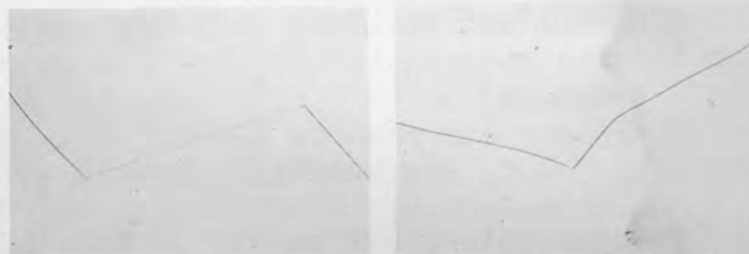

Figure 11 - EB-59, columbium, as-cast. 100X

Figure 12 - CC-1, columbium, as-cast. 100X

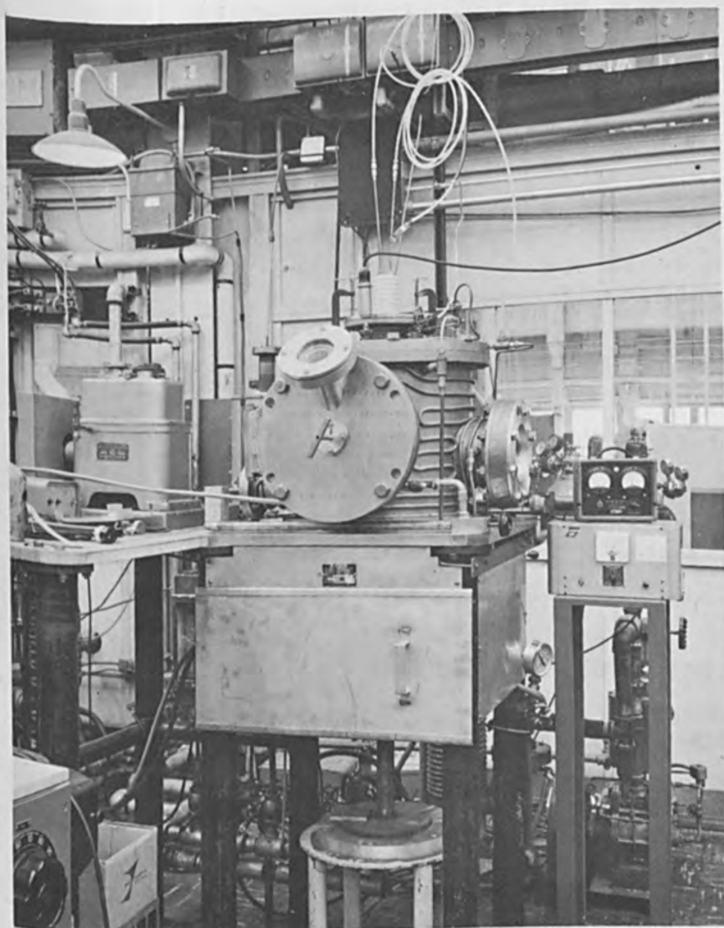

Figure 9 - Electron beam melting furnace chamber equipped with plasma cathode.

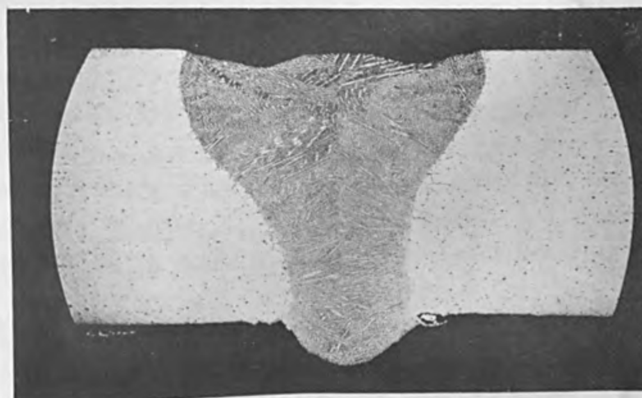

Figure 13 - Rene 41 sheet - conventional E.B. weld. 50X

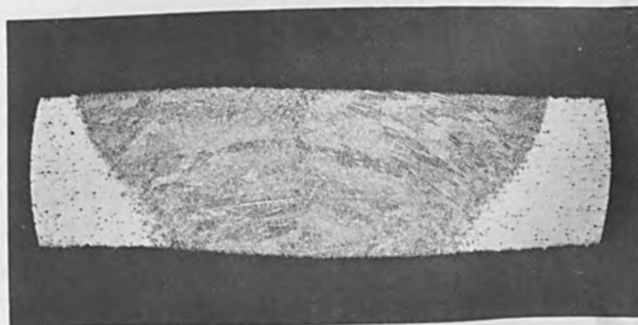

Figure 14 - Rene 41 sheet - plasma E.B. weld. 50X

a dynamic pressure of 3 to 5 microns in the chamber. Partial throttling of the pumping system was also required to attain pressure control. Bottled lamp grade argon gas was used and was further purified by passing it through a hot titanium-zirconium chip furnace, before introducing it to the chamber. The dew point of the gas as it is introduced to the chamber is of the order of -96°F. This is equivalent to about 5-10 PPM water vapor or about 5 microns partial pressure[6].

D.C. was supplied through a 1200 ohm ballast resistor from an adjustable power supply capable of 3 amperes at 20 kilovolts. After making initial adjustments stable currents up to 2 amperes at 15-17 kilovolts were maintained on the starting material until melting was completed. A single melt cycle in the case of buttons such as that shown in Figure 10 was actually composed of two melts, i.e., the starting material was melted and partially consolidated. It was turned over and power again applied to consolidate the other half. The buttons are approximately 200-300 grams in weight and at power levels up to 30 kilowatts, required only a few minutes for each half cycle. An evaluation and comparison of the conventional (hot cathode) and plasma (cold cathode) electron beam melted columbium buttons was made to obtain some measure of the relative ability of the plasma cathode to consolidate and/or refine. Buttons melted by the conventional E.B. process are identified with prefix "EB" whereas those melted by the plasma (cold cathode) beam are designated by the prefix "CC". These results are discussed in the next section.

It should be noted that under the conditions described above, ion bombardment of the cathode was sufficient to raise it to a dull red heat. After removal from the furnace the cathode surface was found to be bright and clean with no signs of erosion or other physical damage.

Melting Results

Figures 11 and 12 are photomicrographs of two as-cast columbium buttons, EB-59 and CC-1 respectively. As is evident the two structures are comparable, both being fairly clean in appearance and having quite large grains. In order to better appraise the differences between as-cast materials, analyses were obtained for the interstitials, oxygen, nitrogen, hydrogen and carbon. These results are given in Table I. It should be pointed out that the starting material used for EB-59 and CC-1 was the same, and its analysis as given by the supplier is listed in the Table. Both of these buttons had been subjected to a number of low pressure melt cycles in the conventional electron beam apparatus. Melting pressures of the order of .005 to .050 microns (5×10^{-6} to 5×10^{-5} Torr) were the norm. CC-1, however, was then further remelted (on both sides) by the plasma electron beam technique.

EB-69 and CC-2 represent a condition where both buttons were only subjected to a single melt cycle. Here again the starting material analysis is given in the Table for comparison and it is seen that although EB-69 was refined to a small extent, CC-2 has

increased in oxygen and nitrogen content as well as in DPN hardness values. This can be explained on the basis that the argon used for this particular melt was not passed over hot Ti-Zr chip retort, as was the case for CC-1, and was also introduced to the furnace through an intermediate chamber which had not been purged for any length of time prior to its use in the gas control and delivery system. Nevertheless, in either case, it is evident that with a purified gas as the plasma medium, the plasma electron beam is capable of providing process purity conditions which are more than adequate for a wide variety of applications. At the levels of interstitials shown, it is not necessarily conclusive that the plasma electron beam process is capable of refining conditions comparable to those available at extremely low pressures in hot cathode equipment. Rather, besides purity of the gas employed, the degree of refinement attainable is as much a function of the type and amount of the impurities (e.g. relative levels of carbon and oxygen), the amount of superheat applied, time at temperature, and the nature and pressure of the gas used in the process.[7,8] The process actually provides an additional degree of flexibility in that various process conditions (other than that of basic refining) are attainable, since any one of a variety of gases may be used as the plasma medium.

Very recently, some welds were made in a relatively low power plasma electron beam device on René 51. There was not time to obtain any extensive data on these welds but properties measurements

are currently being conducted. As evidence of the capability of the plasma electron beam to effect a sound weld, photomicrographs of a conventional electron beam weld and a plasma electron beam weld on Rene-41 are shown in Figures 13 and 14. Samples were supplied by R. Kutchera, General Electric Company, Cincinnati, Ohio.

Conclusions and Future Developments

This development has demonstrated that the perforated hollow cathode, when provided with an internal control grid, can generate well collimated and precisely controlled electron beams of high intensity. Because a high vacuum environment is not required and because the cathode is simple and rugged and operates at low temperature it is well suited to applications requiring a concentrated heat input. On the basis of the data presented and observations of the beam in operation, it is apparent that the device can readily be applied to a variety of metallurgical process applications. It has demonstrated the capability of performing these functions and at the same time providing an atmosphere condition which is conducive to maintaining or effecting high purity in the material being processed. In operations where the evolution of gaseous reaction products is considerable or different gases from those used as ionized mediums are desired, compartmenting and separate pumping arrangements can be provided. In all instances because of the operational pressures employed, the equipment necessary to do this can be of relatively unsophisticated design.

Also, other applications are opened by the addition of grid control of the beam. Circuitry applications such as new types of oscillators, amplifiers and control circuits are definitely possible. While the more obvious applications are being developed, others, possibly more important, await a better understanding of the basic mechanisms of this type of electron beam formation.

TABLE I

SAMPLE NO.	MELTING MODE	INTERSTITIALS O	N	H	C	HARDNESS DPN*
EB - 59	CONVENTIONAL	6	12	0	18	56-60
EB - 69	CONVENTIONAL	34	23	0	<10	61-65
CC - 1	COLD CATHODE	37	25	0	<16	54-58
CC - 2	COLD CATHODE	123	70	0	10	80-89
STARTING MATERIAL	EB-59 AND CC-1	<50	50	5	<30	69-64
STARTING MATERIAL	EB-69 AND CC-2	38	41	<10	60	NA

*ALL HARDNESSES ARE RESULT OF SIX OR MORE READINGS PER SAMPLE.

REFERENCES

1. Solomon, J. L., "New Developments in Electron Beam Welding Machines," Welding Journal, p. 719-727, August 1962.

2. Stauffer, L. H., and Boring, K. L., "Hollow Cathode Enhances Plasma Electron Gun," Electronics 35, no. 49, p. 60, (December 7, 1962).

3. Van Paassen, H. L. L., and Allen, R. J., "High Impedance Gas Discharge Production of Collimated Electron Beams," Bul. Am. Phys. Soc. 7, p. 69, January 1962.

4. Linder, E. G., and Hernquist, K. G., "Electron Space Charge Neutralization by Positive Ions," J. App. Phys. 21, 1088, November 1958.

5. Massey and Burhop, "Electronic and Ionic Impact Phenomena," pp. 547-549, Oxford Press.

6. DMIC Report 174, "Electron Beam Processes", September 15, 1962; DMIC, Battelle Memorial Inst.

7. Bakish, R., "Introduction to Electron Beam Technology", pps. 145-167, John Wiley & Sons, 1962.

8. Noesen, S. J., "Removal of Gaseous Impurities by Vacuum Arc Melting", Vacuum Symposium Transactions, American Vacuum Society, p. 150, Pergamon Press, 1950.

THE HOLLOW CATHODE DISCHARGE

By:

John R. Morley
Director of Applied Physics
and Engineering Manager

ALLOYD ELECTRONICS CORPORATION
35 Cambridge Parkway
Cambridge 42, Massachusetts

ABSTRACT

A high current, low voltage magnetically confined electron beam is discussed in terms of its operation and performance. A low pressure gas plasma cathode supplies up to 1000 amperes of electron emission. The beam is operated at 30 to 50 volts providing approximately 40KW of power. Chamber pressures between 10^{-4} to 10^{-2} Torr of an inert gas are maintained. Various shapes of electron beam are reported upon. Some information on strip annealing of copper and of casting steel ingots is presented.

THE HOLLOW CATHODE DISCHARGE

INTRODUCTION

The generation of heat or of a heat source under vacuum was conventionally carried out by using resistive or inductive heating, or for very high temperatures, by the utilization of electron beams. Typical electron guns which produce these beams operate at relatively low currents and high voltages, generally below an ampere and above 10 kilovolts. It is also desirable to operate at as low a pressure as possible and preferably not higher than 10^{-4} torr. Most of the operational difficulties associated with these guns occur because of high voltage breakdown, either due to an avalanche type of discharge, triggered by an increase of background gas pressure, or due to insulating surfaces becoming coated with conductive material. One technique for reducing this arcing was described yesterday by M. Doctoroff[1]; alternately, a larger pumping system, or a differentially pumped electron gun may be used to improve reliability, but eventually voltage breakdown will occur. During such voltage breakdown the potential across the arc itself drops to a few volts only, for an arc has a characteristically low impedance. However this arcing need not be regarded as a transient phenomena, but a very stable process as can be witnessed in a heli-arc welder.

If therefore it were possible to devise a cathode capable of emitting a thousand or so amperes and of operating

1. See these proceedings

the electron beam at a few volts potential, then this vacuum 'arc' would produce the same useful power that can be generated in the case of the high voltage gun, but without the shortcoming of voltage breakdown. In the hollow cathode discharge this is precisely what has been achieved by the use of a low pressure plasma cathode.

THE HOLLOW CATHODE PROCESS

A plasma may be simply defined as a region of gas at very high temperatures which is either fully or partially ionized and contains approximately equal numbers of negatively and positively charged particles. When the gas is in this excited state either electrons or positive ions may be extracted from it by applying an electric field of the correct polarity.

There are many techniques which may be used for the generation of these plasmas and the simplest is radio frequency excitation of a gas which may occur at any pressure ranging from near vacuum to many atmospheres. Energy given to the gas by the coupling of the radio frequency power to the gasatoms will produce and maintain the required ionization.

The hollow cathode process itself uses such a plasma cathode as the source of electrons. In its present form, it is capable of delivering up to 1000 amperes of current. Acceleration of the electrons to the workpiece is carried out somewhere between 30 and 50 volts potential,

thus giving rise in this particular unit to an electron beam with a total power of approximately 40 kilowatts.

Located within a vacuum chamber is a water cooled refractory metal tube with one end blocked by a tantalum plug with a small orifice drilled through it. (See Figure 1). Argon gas passes down the tube and flows through the orifice as a fine jet expanding into the vacuum chamber which is continuously pumped to maintain a background pressure between 10^{-2} and 10^{-4} torr. A D.C. low voltage high current power supply is connected between cathode and anode, the cathode being negative. When radio frequency power is coupled into the gas, ionization occurs and a low pressure plasma is generated within the hollow cathode. Electrons are removed from the plasma by the applied voltage gradient and are accelerated to the anode or workpiece. An axial magnetic field of 200-300 gauss prevents the beam spreading by space charge forces.

Since plasmas are essentially neutral in total charge, removal of electrons will tend to leave the plasma with an excess of positive ions. These excess ions will be accelerated to the cathode where they provide sufficient power to raise the cathode temperature so that thermionic emission occurs. The electrons emitted from the hot cathode, itself, supplement the number of electrons which are available from the plasma. By operating the cathode at approximately 2400°Kelvin then not only can a reasonable cathode life be obtained but the process can be made 70 to 80%

efficient, that is the ratio of the power supply output to the power received at the work. The very nature of the discharge itself, that is very high currents at very low voltage, tends to stabilize the system, and although the power delivered to the workpiece is a function of gas pressure, for a given pressure the power delivered over a wide range of current is remarkably constant and this can be seen in Figures 2 and 3. A photograph of the apparatus, Figure 4, with the beam turned on shows the intense blue column of light which is due to the ionization of argon, the gas being used in this particular operation.

An electron starting from the cathode will spiral about a particular magnetic field line until it reaches the target. This phenomena can be taken advantage of and many different shapes and sizes of cathodes can be used and the image of these will be faithfully reproduced at the target, providing that an axial parallel magnetic field is used between the cathode and the anode. Figure 5, shows an elongated cathode which is a tube with a number of small holes drilled along its length. In operation it will be noticed that the beam does not now form in the shape of a cylinder but is a strip beam 6 or 8 inches long and approximately 1/4" in thickness.

The gas in a typical half-inch diameter tantalum cathode will be about 30% ionized, and will deliver up to 600 amperes of current, at a current densities in the order

HOLLOW CATHODE DISCHARGE

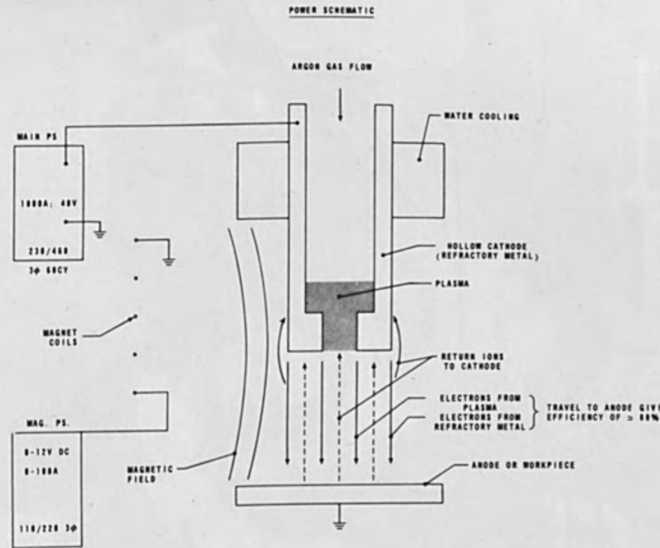

FIGURE 1

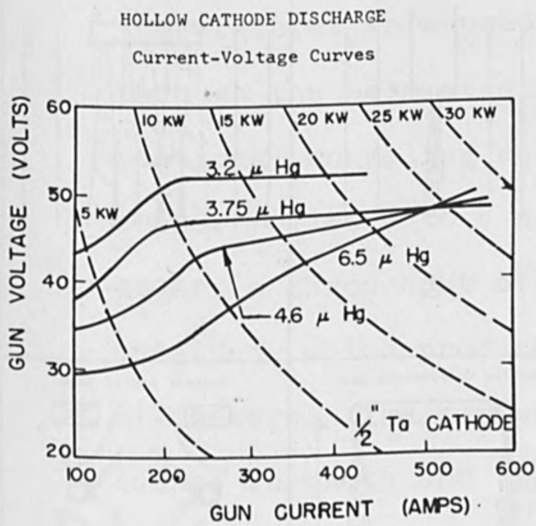

FIGURE 2

HOLLOW CATHODE DISCHARGE

Power Curves

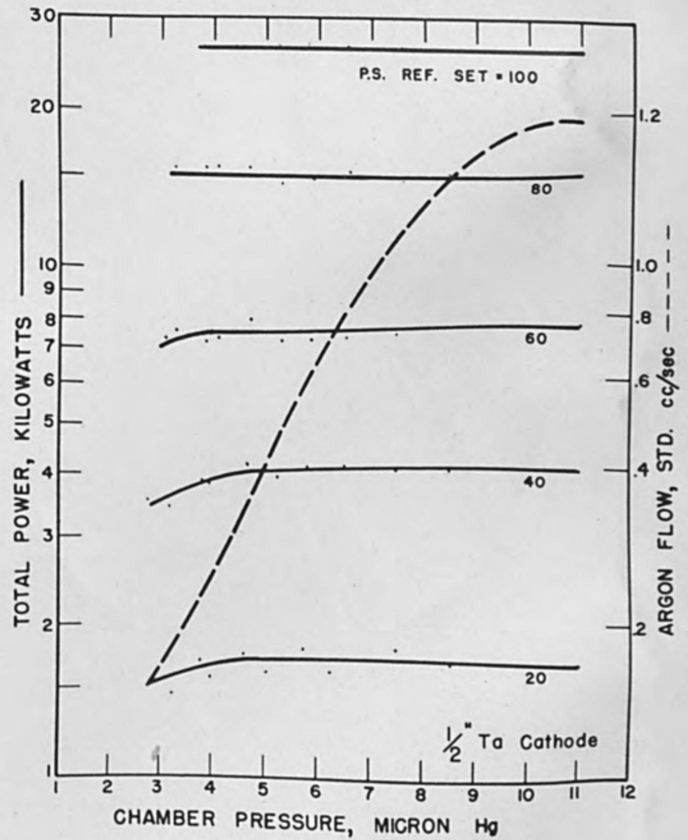

FIGURE 3

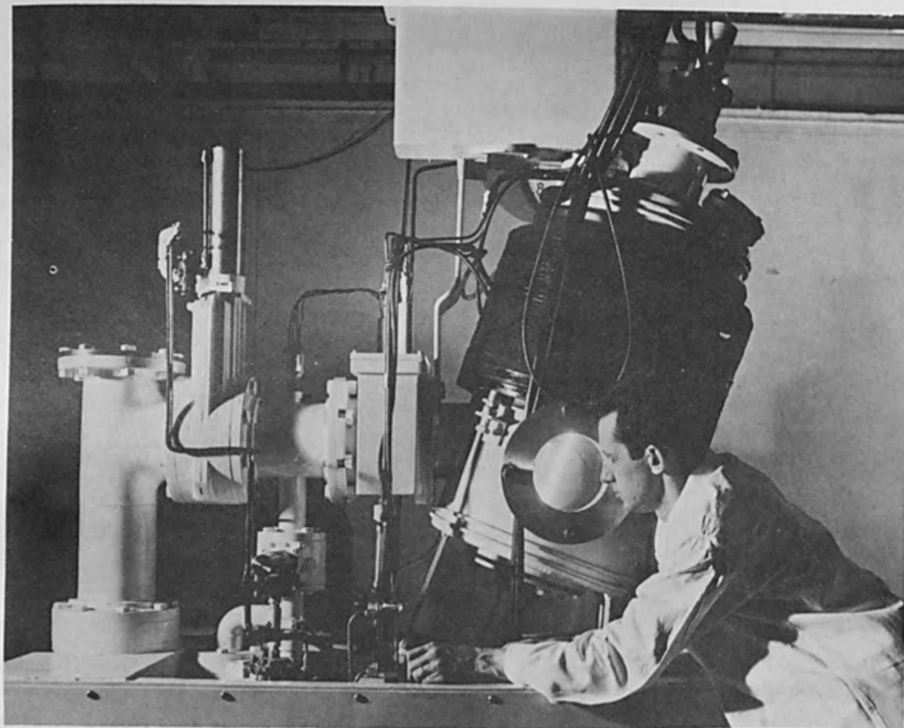

FIGURE 4

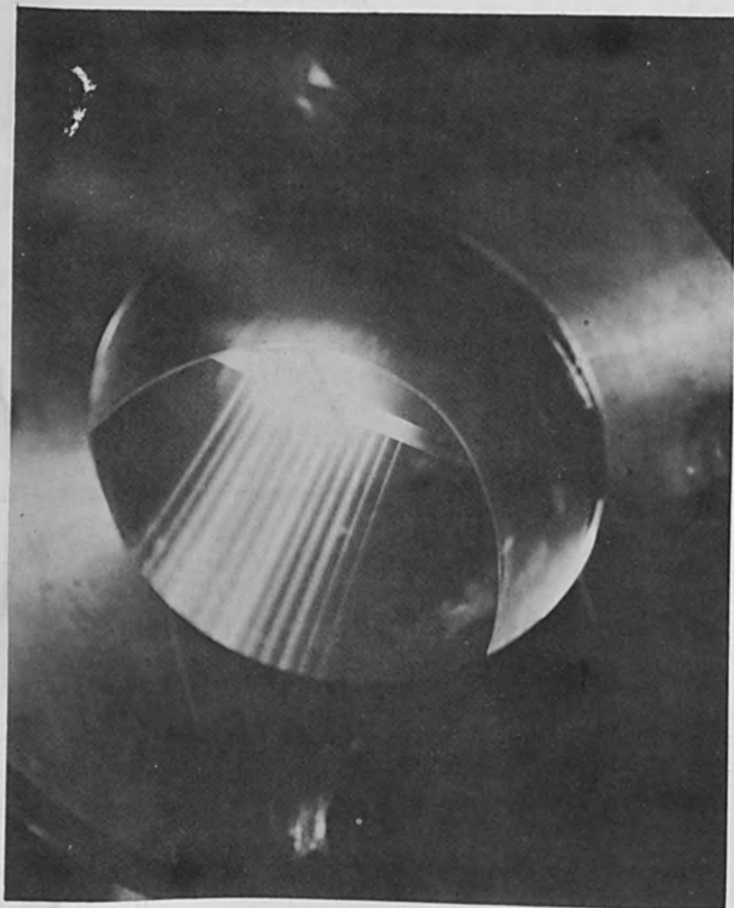

FIGURE 5

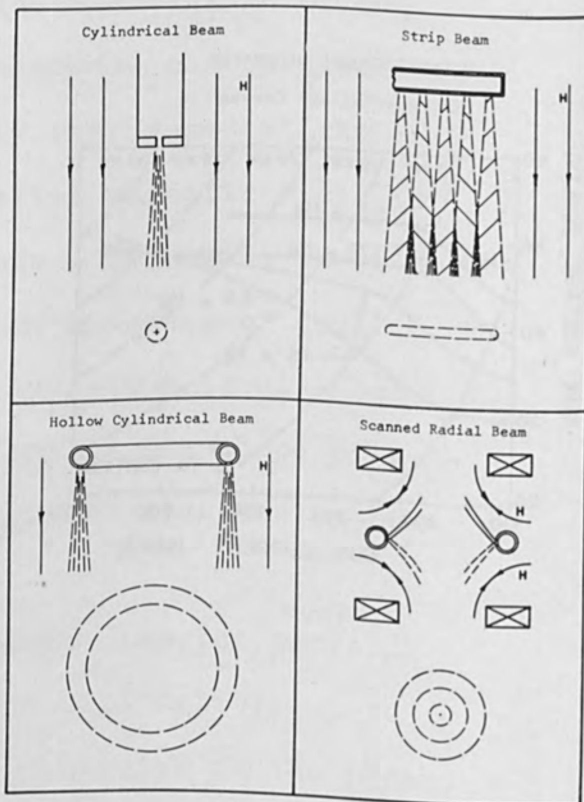

FIGURE 6

cathode would be of the order of 40 hours. With some of the more sophisticated designs, lives of several hundred hours are possible.

The few of the applications with the variety of shaped beams that are possible from such a peice of equipment will now be described. A variety of cathodes are shown in Figure 6. One of the first experiments carried out within the machine was the annealing of copper and tantalum strip using a batch process. For this, the extended source cathode was used which gives a strip beam several inches long and metal was run through this beam so that the melting point of the particular material was approached within 100°C or so. Making use of the fact that annealing is a time-temperature function, these high temperatures were used to enable the strip to be passed through the beam at a much higher speed than with conventional annealing equipment. Using a silver bearing copper rolled 4 to 6 numbers hard and 30 kilowatts of power, a throughput of 350 pounds/per hour of copper was obtained, which produced a grain size of from 0.15 to 0.25 milimeters. The strips processed ranged from one to five inches in width and from 5 mils to 20 mils in thickness. Excellent uniformity of grain size both across the width and along the length of the strip was obtained.

An obvious extension to this idea is the continuous processing of strip by passing it in one side of the vacuum chamber, through a differently pumped system,

and removing it from the other side by a similar system. It is interesting to note that the operating costs of annealing, including labor and depreciation, are estimated to be approximately the same as conventional gas annealing by the continuous process.

Using the cylindrical cathode, some continuous ingot casting has been performed with this machine and material usually in the form of chunk, chip, or flake was fed into a continuous casting mold. Using a 2" diameter water-cooled mold, casting of stainless steel has been performed at the rate of approximately 100 pounds per hour for this particular 30 kilowatt unit. Very high temperatures can be obtained with the machine and tungsten and tantalum have been melted with ease.

Other applications of this process which have yet to be developed include the manufacture of a tube furnace; using a spiral type of cathode for very high temperature tensile testing; the adaption of the unit to carry out the brazing operations under vacuum; focusing the beam by a conical magnetic field so the power density of the beam is increased to carry out welding operations;and the utilization of the plasma cathode itself as a source of electrons for a high current medium voltage gun.

It is not necessary to use the self-accelerated principle only; that is, the connection of the power supply

between the cathode and the workpiece. For being an electron beam it is very possible to interpose an anode with a hole in it and the beam will pass through the anode to the workpiece in field free space.

ELECTRON BEAM WELDING AT ATMOSPHERIC PRESSURE

By: L.H. Leonard
Project Engineer
Alloyd Electronics Corporation

Abstract

Electron beam welding of aero-space metal in a non-vacuum environment is feasible if the electron beam has sufficient initial power density that after being degraded by scattering, the residual power density is adequate to accomplish joining.

The minimum power-density required for the joining is approximately 0.5 Megawatt per square centimeter. To obtain these power densities in the non-vacuum environment, the beam, brought out from a region of high vacuum through a series of three differentially pumped aperatures, must have an initial power density slightly in excess of 0.5 Mw/cm^2 when using helium gas as the controlled environment.

The work reported here was sponsored in part by the Fabrication Branch, Manufacturing Technology Laboratory, AFSC Aeronautical Systems Division of the U.S. Air Force.

ELECTRON BEAM WELDING AT ATMOSPHERIC PRESSURE

INTRODUCTION

The early work of Stohr (1) and his co-workers at the French Atomic energy establishment introduced to welding technology a new and exciting system for metals joining. His application of a high energy focused electron beam to the problem of welding reactive metals was the first radical departure in this field since the advent of TIG welding. Since that period, around 1953, a great level of interest has been aroused in exploring the full potential of electron beam welding systems.

One aspect which appears more and more frequently is that of the size limitation of the process. The use of high vacuum chambers is practical for the electron beam processing of small specialized parts, but this becomes prohibitive when really large structures are considered. Recently, attention has turned to the concept of electron beam welding in air, or in a controlled gas atmosphere, to avoid the use of large vacuum chambers. The end results hoped for would be an ability to achieve under these more flexible conditions, welds exhibiting the general characteristics of the electron beam vacuum process. These characteristics are, broadly, a high depth-to-width ratio, a minimum heat affected or recrystallized zone, and a minimum of deleterious impurity contamination.

Statement of Problem

The problem of developing an electron beam welding system for operation in a non-vacuum environment involves a series of theoretical and practical problems. The problems may be broadly divided into three groupings:

1. Electron Scatter: The electron beam will be degraded by scatter as it transverses the regions at near-atmospheric pressures.
2. Beam Transfer Unit: The electron beam must be generated under high vacuum and made to impinge on a workpiece at atmospheric pressure. Some mechanism is required to allow the transfer of the beam through that pressure difference.
3. Electron Beam Generation: An electron beam must be generated which can transverse the beam transfer unit, undergo degradation by scattering, and yet arrive at the workpiece with adequate residual power density to accomplish welding. Once the requirements have been established, the design of the gun is relatively straightforward.

These problems are, of course, all inter-related, and in order to solve any one completely, they must all have been solved. The sequence in which the groupings are presented appears to be the logical one in which to discuss the problems involved.

ELECTRON SCATTER

Calculations were performed to estimate the sum of the unscattered fraction of the incident beam and the useful portion of the scattered fraction that reaches the weld surface. A detailed explanation of the calculations of scattered intensities is given in another report. (2) Relative intensity curves were drawn for several gases at different values of gas density and two levels of accelerating voltage, 100 KV and 150 KV. Only the 100 KV electron beam in helium calculations will be discussed.

Interactions Between Swift Electrons and Atoms

Classical scatter theory predicts an alteration of the beam in traversing gaseous matter. The degree of alteration is dependent on the gas atomic number, the gas density and the distance traversed in the gas.

For an electron beam in the low relativistic range, two types of interactions with the gas predominate:

1) inelastic scattering; electrons are scattered from the incident beam with loss of energy,
2) elastic scattering; incident electrons are scattered without loss of energy.

Inelastic scattering results in a transfer of energy to the atom, either by excitation or ionization. The angle of scatter will generally be small, since the interactions are predominantly that of an incident electron with an atomic electron rather than with the relatively massive nucleus. On the other

hand, when the scattering is elastic, the interaction is most often one with the coulomb field of the nucleus and will generally result in a larger scatter angle.

As an electron passes through the gas, it may experience several such interactions in succession. The average distance traversed by an incident electron before an interaction occurs is defined as the mean free path. This distance is a function of the parameters gas atomic number and gas density, as well as the momentum of the incident electrons. It is a statistical average for many electrons. The free path length of individual electrons will vary in a random way, but in general it will be close to the mean.

Mean free paths were calculated after Goudsmit and Saunderson (3), using the Born approximation to represent the atomic field. The gas is assumed to be at standard pressure and room temperature (760 Torr; 30°C).

Figure 1 shows the ratio of the unscattered power density, ρ , to the initial power density, ρ_o, as a function of the gas thickness, t, for several values of the gas pressure.

Scatter Distribution

Besides the classification by types of interaction, scatter theory is traditionally categorized by the number of interactions:

1) single scattering - one mean free path or less,

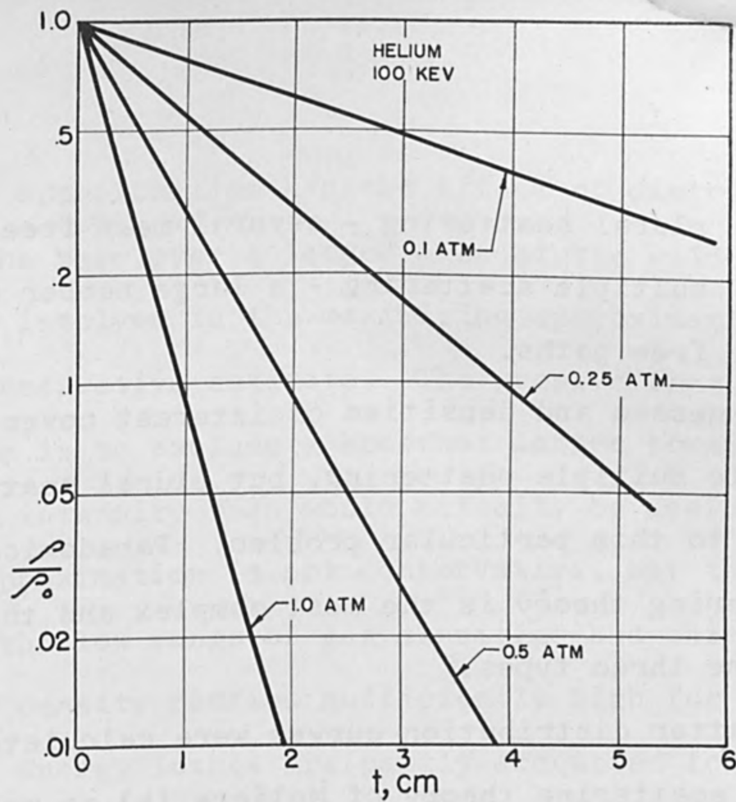

Ratio of unscattered intensity to initial electron intensity

FIGURE 1

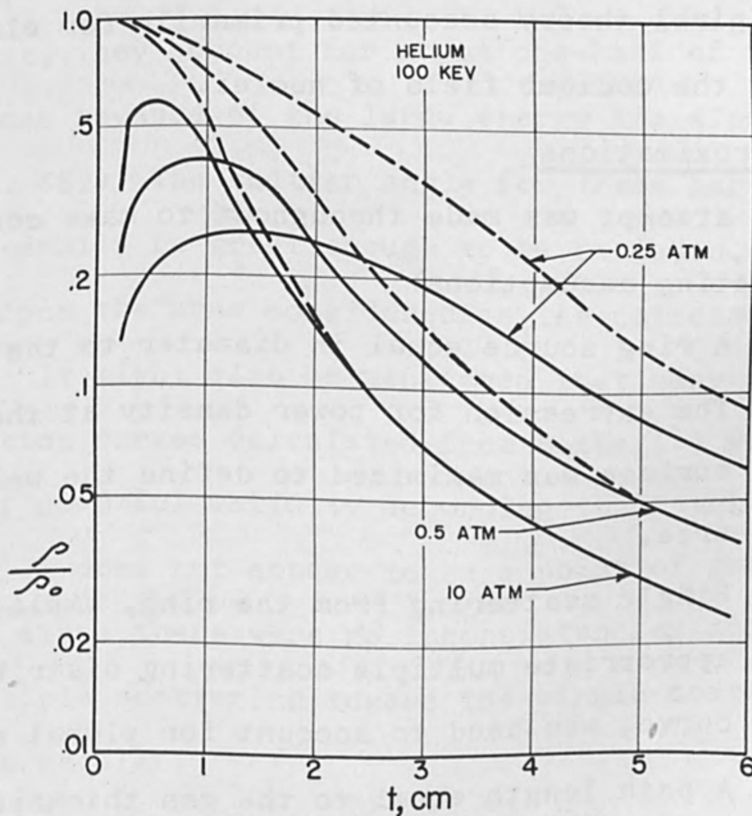

Ratio of scattered and total power density to the initial power density in the weld area.

FIGURE 2

2) plural scattering - several mean free paths,

3) multiple scattering - a large number of mean free paths.

The gas thicknesses and densities of interest cover the range from single to multiple scattering, but plural scattering applies most to this particular problem. Paradoxically, plural scattering theory is the most complex and the least studied of the three types.

Scatter distribution curves were calculated using the multiple scattering theory of Moliere (4) as modified by Bethe. (5) Bethe's modification was to include a term which accounts for inelastic scattering by atomic electrons. Moliere's original theory accounted primarily for elastic scattering by the coulomb field of nuclei.

Approximations

The attempt was made throughout to make conservative approximating assumptions:

1. A ring source equal in diameter to the beam.
2. The expression for power density at the weld surface was maximized to define the welding area.
3. Single scattering from the ring, employing the appropriate multiple scattering distribution curve, was used to account for plural scattering.
4. A path length equal to the gas thickness was assumed.
5. Accounting for energy losses is incomplete.

The first approximation has the effect of distributing the peak of the beam over a larger area at the weld surface. The error involved in the maximizing approximation can cause only a conservative estimate. The gross effect of the third assumption is to exclude a somewhat larger portion of the scattered intensity than would actually be useful. The fourth listed approximation is not conservative, but the error is least in the low range of gas densities and thicknesses where the power density remains sufficiently high for welding.

Energy losses are partly accounted for since Bethe (5) includes an approximation for inelastic scattering by the atomic electrons. Evans (6) states that, although the hard collisions between incident and atomic electrons are infrequent, they account for about one-half of the total energy loss because of the large energy transfer. (see Evans, p. 582) The scatter angle for these hard collisions would generally be great enough to be excluded, by scatter theory, from the area considered in the calculations.

It might also be mentioned that many of the scatter distribution curves calculated from Bethe (5) were in the region of doubtful validity according to restrictions on the theory. It does not appear to be a point of great concern, however, since there were no inconsistencies and the trend from multiple scattering toward the single scattering curve was quite regular.

The curves of Figure 2 illustrate the results of the calculations. The ratio of final-to-initial power density is plotted as a function of thickness for several gas densities. The solid curves represent the contribution to the area of maximum power density of the scattered electrons. The broken lines represent the total power arriving in that area, including both the scattered and unscattered electron contributions.

BEAM TRANSFER

Since the pieces to be welded are to be in a gaseous environment at or near atmospheric pressure, some connecting link must be found between the high vacuum of the gun chamber and the weld environment through which the beam must pass. Very high energy beams are normally brought out to atmosphere through thin aluminum or beryllium foils stretched across an aperture in the chamber wall. Such foils are not satisfactory in this application because they cause dispersion of the beam, and the resultant heating effect on the foil severely limits the possible power density. An alternative method of bringing a beam from the vacuum chamber into the atmosphere is to provide differentially pumped aperatures. Such a system limits the flow of gas into the high vacuum region by small orifices which restrict gaseous effusion, and by the use of the secondary vacuum pumping system. A schematic of such an arrangement is shown in

Figure 3. The pressures to be expected are derived with the aid of the nomograph shown as Figure 4. (after (7)) A limitation to such a system lies in the fact that the beam must traverse in the differential chamber a distance which is large compared with the beam diameter. Since the dispersion of an electron beam is a function of gas density times the distance it travels through such a gas, excessive energy loss and scatter will occur if the traverse distance is too long. The limitation in reducing this traverse distance arises from the fact that the cross sectional area between apertures must be sufficiently large to allow a high conductance path for efficient vacuum pumping in the differential chamber. The dispersion can also be reduced by lowering the gas density along the path length. In particular, the first chamber should be operated at the lowest pressure consistent with the integrated vacuum system.

The design of the nozzles and apertures must include provision for cooling since there is some dispersion of the beam in transit, with a resultant heating effect. Since the alignment of such a system must be extremely accurate, heat distortion must be minimized.

Controlled Atmosphere Unit

A controlled atmosphere unit must be incorporated which is external to the differential pumping system proper. This is required for both the beam and the weld.

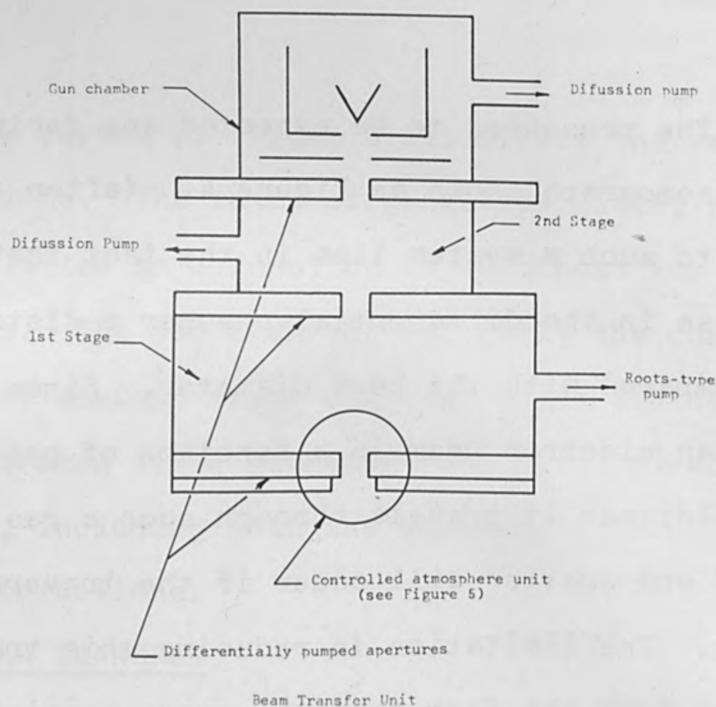

Beam Transfer Unit

FIGURE 3

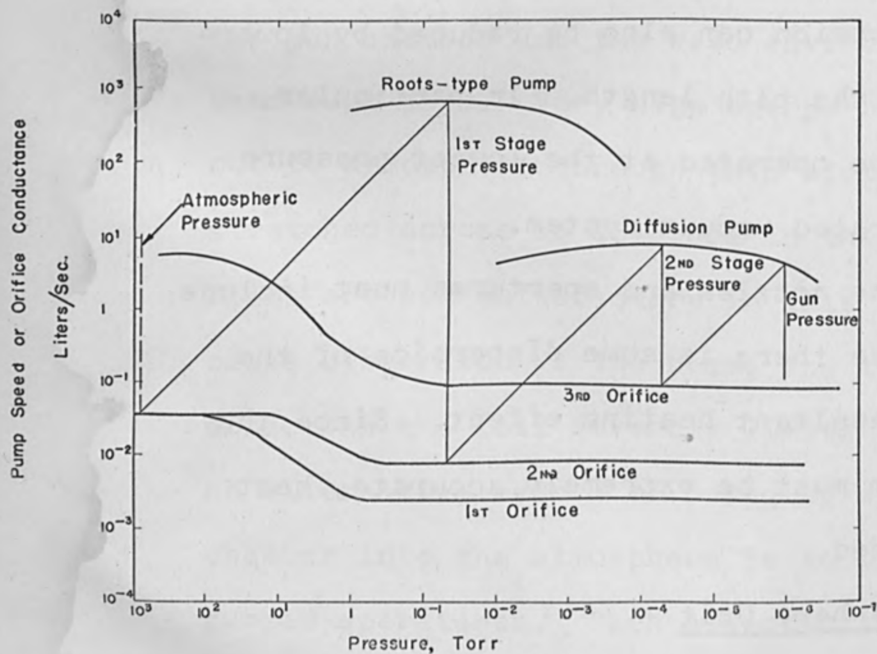

FIGURE 4

DIFFERENTIAL PUMPING NOMOGRAPH

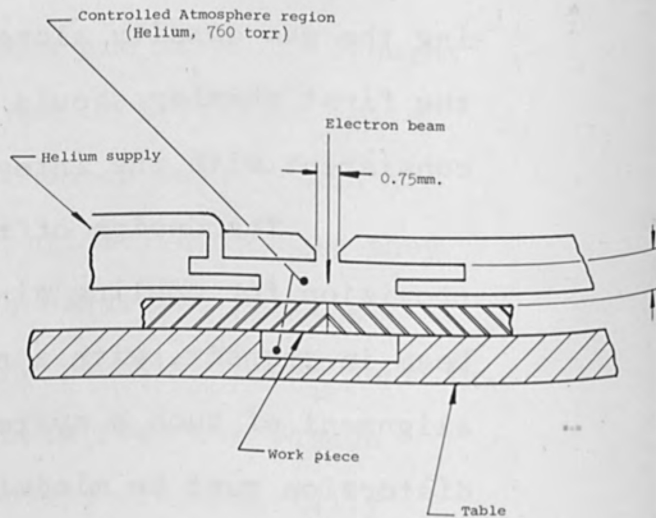

Detail of the controlled atmosphere chamber, showing also the work piece, table and back up channel.

Figure 5

From the point of view of the beam, the unit is required if the maximum attainable power density is to be achieved. Gas scatter is the governing factor, and this can be minimized if the gas through which the beam passes is exclusively helium. In order to obtain such a helium environment, other gases must be excluded by the unit. On the other hand, certain of the materials to be welded require an inert gas seal if their properties are not to be radically altered by the process.

If the gas content of the area in the vicinity of the weld is to be controlled, it is necessary that a chamber be intergrated with the first orifice of the differential pumping chamber, one wall of which is formed or completed by the work pieces. If gas scatter is to be minimized, the length along the beam axis must be kept short.

In the system shown in Figure 5, the controlled atmosphere chamber is maintained at a slight positive pressure with respect to the surrounding atmosphere. The chamber has been made shallow to reduce the probability of electron scattering, and the diameter has been reduced to lower the total gas consumption. Although a smaller diameter would decrease gas consumption even further, care must be taken that the solidous material in the weld is not exposed to the possibly contaminated atmosphere outside the area covered by the chamber. Further, the materials comprising the unit should not be directly exposed to molten work material if thermal distortions are to be avoided.

WELD CRITERIA

The data available on the power and power density needed for welding various materials is scant. At this time, the effects of these two parameters on such factors as the ability to accomplish a weld, the depth-to-width ratio of the weld geometry, and the depth or penetration of the weld, have not been separated.

As a working hypothesis, it is assumed that the power density determines the ability to achieve a weld. That is, there is a threshold value of power density below which melting and hence joining, will not take place in a particular material. At the threshold level, joining will take place with a depth-to-width ratio of unity or less. As the power density is increased above the threshold value, the depth-to-width ratio also increases, and finally, the point will be reached at which machining or vaporization, rather than welding, will occur.

The power available will then determine the depth of penetration which can be achieved with the depth-to-width ratio given by the power density (i.e. for the same pentration, less actual power will be required if the power density can be increased).

These assumptions are concurred by such references as are available. The data in Table I for example, may be considered illustrative of this. This data also suggestes upper limits on the power density threshold needed to achieve welding.

TABLE I

Beam Power Parameters for Welding Various Materials

Material	Sample Thickness	Power	Power Density	Weld Geometry	Source
	Inch	Kilowatts	$\frac{\text{Megawatts}}{\text{cm}^2}$	$\frac{\text{Depth}}{\text{Width}}$	
Tungsten	0.125	5.0 2.25	0.62 3.5	1 6	8 9
Molybdenum	0.125	3.8 2.1	0.48 4.3	1 6	8 9
Titanium	0.125	3.2	0.40	1	8
Stainless Steel	0.125 0.500	3.5 3	.45 0.60	1 8	8 10

The external shield will have a thickness of about 0.2 cm. allowing 0.3 cm effective thickness within the beam transfer unit, the total gas thickness equivalent becomes 0.5 cm at atmospheric pressure. (If the pressure drop were linear with distance through the first chamber, the contribution would amount to 0.25 cm).

Assuming a gas thickness of 0.5 cm, the ratio of welding-surface-to-incident power density may be estimated by reference to Figure 2. The threshold power density for welding is estimated to be about 0.5 Mw/cm^2 as indicated in Table I. Combining this information, the requisite initial power density, ρ_o, for welding is seen to be 0.505 Mw/cm^2.

PRELIMINARY EXPERIMENTAL RESULTS

A laboratory system has been constructed to verify the feasibility of E.B.I.G. (Electron Beam Inert Gas) welding. Figure 6 is a photograph of the system. A beam has been brought into atmosphere (Figure 7 is a 100KV, 8 ma emergent beam) and it has fused metal (Figure 8).

At the present time, we are learning to control the E.B.I.G. welder. The metallurgical properties obtainable, and the future of the process are yet to be determined.

Acknowledgements: The author wishes to acknowledge the contributions and suggestions of J.R. Morley, S.S. White, L.Dunn and H. Yopp during the course of this project.

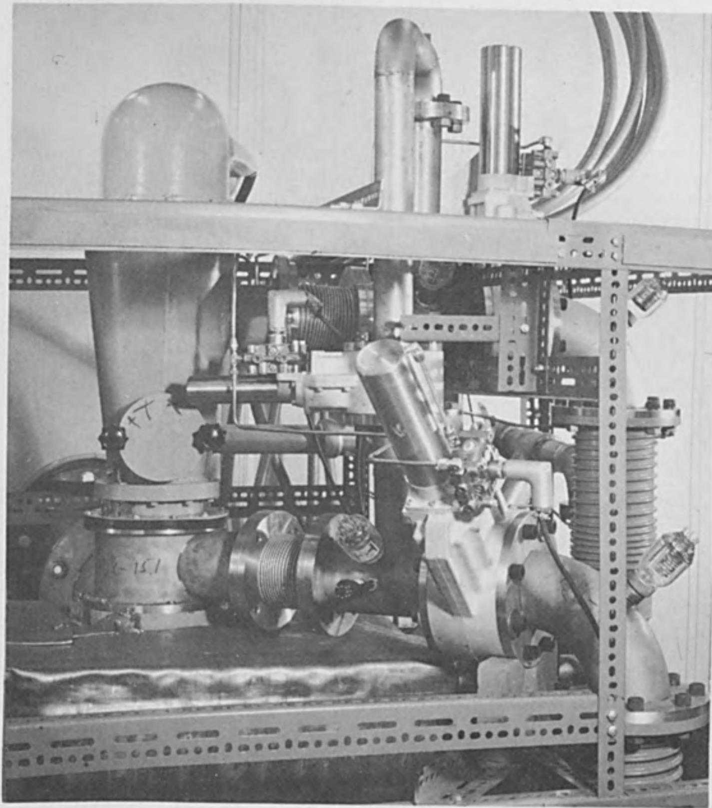

Figure 6
Non-Vacuum Electron Beam Welder
side view

FIGURE 7

Emergent Electron Beam

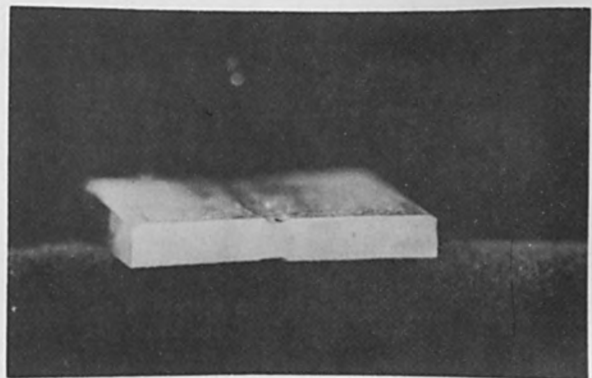

FIGURE 8

Butt weld: 1/8" thick stainless steel
108KV, 6 ma work current, 6ipm pass speed

BIBLIOGRAPHY

1. Stohr, J.A., Reports of the French Atomic Energy Commission, Saclay, 1954.

2. Leonard, L.H., et al, Development of Non Vacuum Electron Beam Welding, final report on contract AF 33(657)-7237, Alloyd Electronics, 1963.

3. Goudsmit, S. and Saunderson, J.L., Phys. Rev. 57, 24 (1940).

4. Moliere, G., Z. Naturforsch, 32, 78 (1948).

5. Bethe, H.A., Phys. Rev. 89, 1256 (1953).

6. Evans, R.D., The Atomic Nucleus, McGraw-Hill, N.Y., 1955.

7. Schumaker, B.W., The Designing of Dynamic Pressure Stages for High Pressure/High Vacuum Systems, USTIA Report No. 78, University of Toronto, 1961.

8. White, S.,private communication.

9. White, S., et. al., Tech. Report, No. WAL 401.54/2-1, S.T. Inf. Agency.

10. Hablanian, H., Proceedings IIIrd Symposium on Electron Beam Technology, R. Bakish, Editor, Boston, 1961.

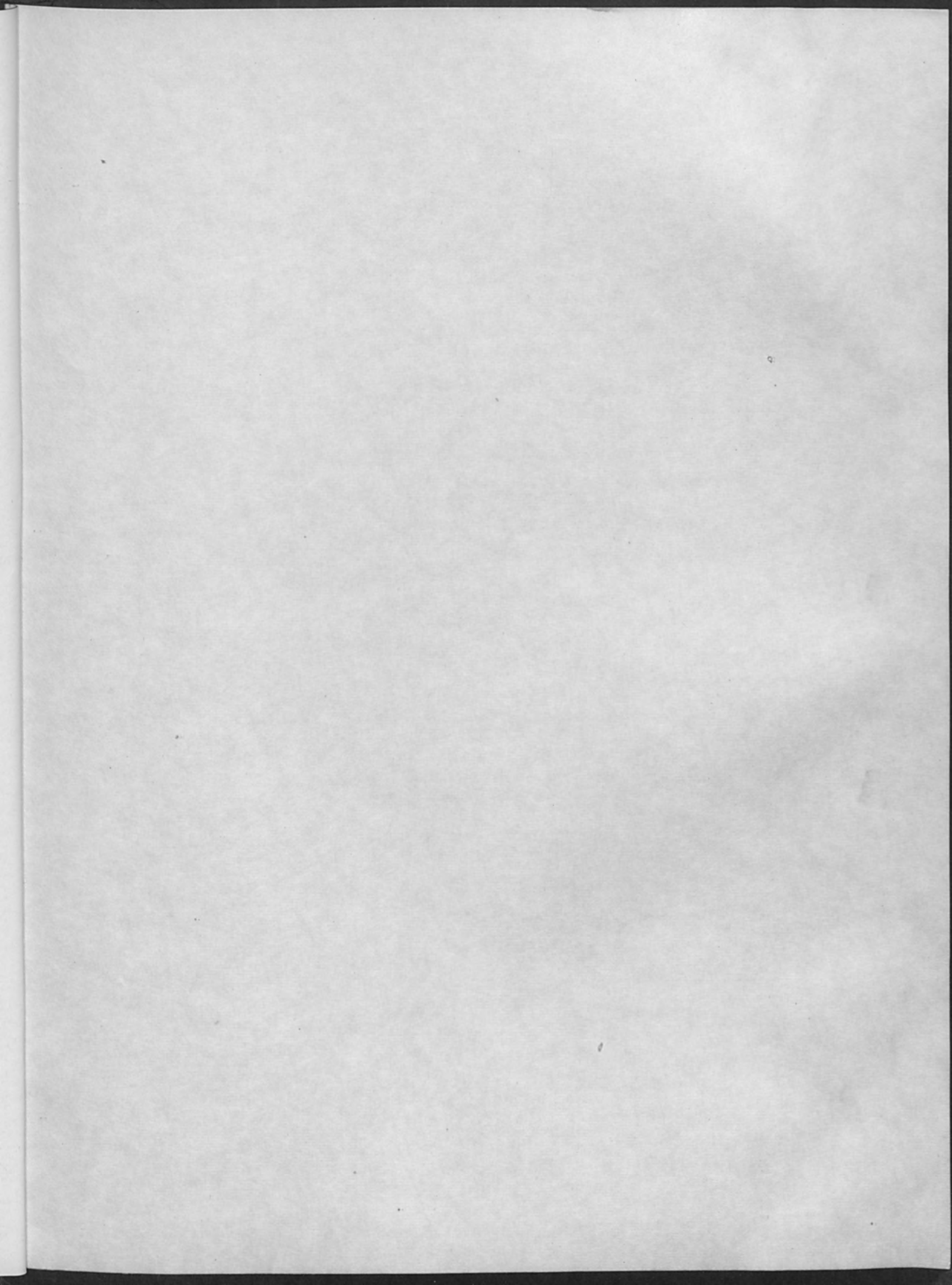

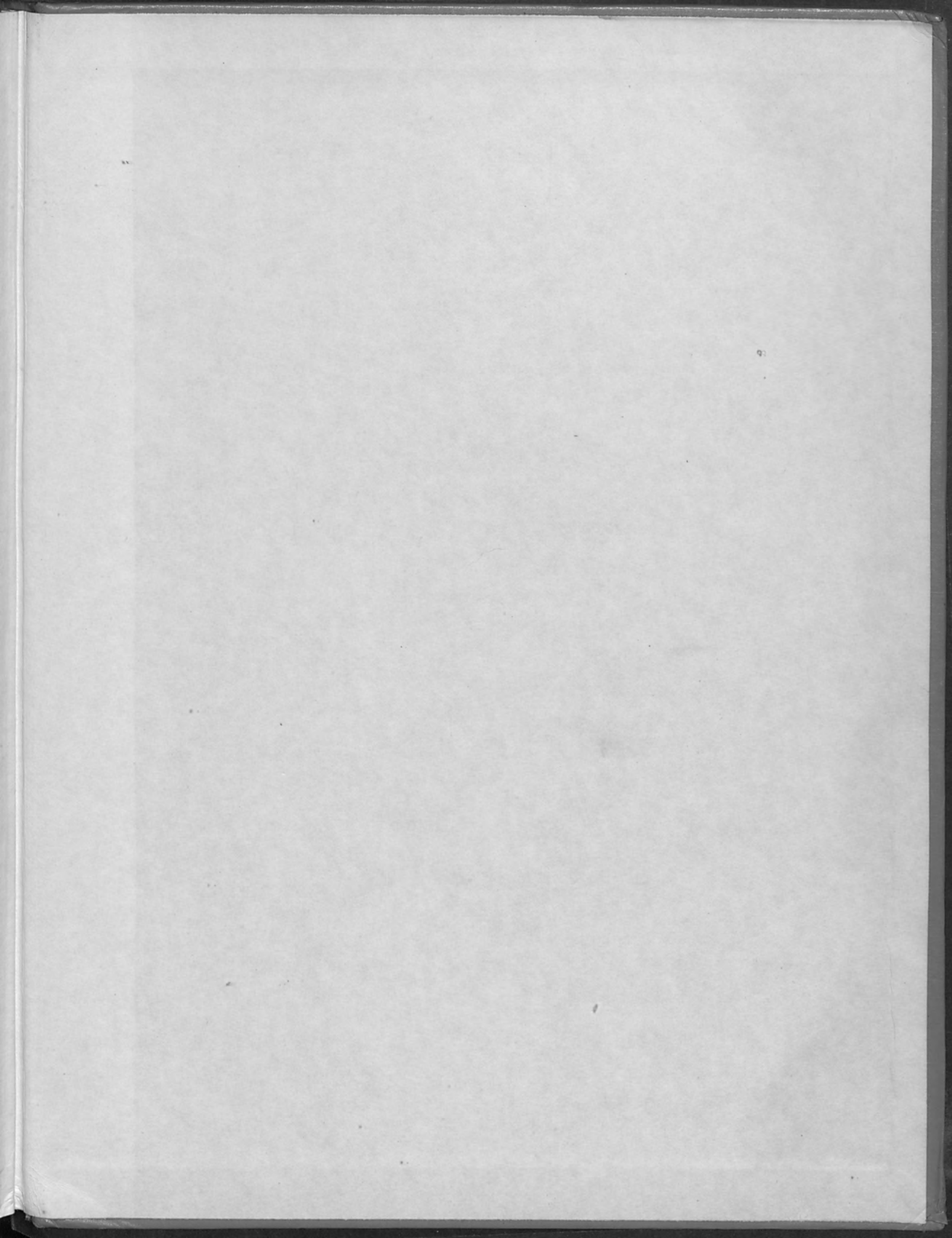

alloyd electronics corporation
CAMBRIDGE 42, MASSACHUSETTS